論文 / 著書情報
Article / Book Information

題目(和文)	
Title(English)	A comprehensive assessment of terrestrial water and groundwater storage using multisource datasets
著者(和文)	ABHISHEK
Author(English)	Abhishek
出典(和文)	学位:博士(学術), 学位授与機関:東京工業大学, 報告番号:甲第12258号, 授与年月日:2022年9月22日, 学位の種別:課程博士, 審査員:木内 豪,鼎 信次郎,中村 恭志,中村 隆志,VARQUEZ ALVIN CHRIST,市井 和仁
Citation(English)	Degree:Doctor (Academic), Conferring organization: Tokyo Institute of Technology, Report number:甲第12258号, Conferred date:2022/9/22, Degree Type:Course doctor, Examiner:,,,,,
学位種別(和文)	博士論文
Type(English)	Doctoral Thesis

A comprehensive assessment of terrestrial water and groundwater storage using multisource datasets

ABHISHEK

A dissertation submitted for the Degree of

Doctor of Philosophy

Global Engineering for Development, Environment and Society (GEDES)

School of Environment and Society

Tokyo Institute of Technology

Japan

August 2022

Acknowledgment

Dedicated to my lovely sister(s)

Firstly, I would like to express my sincere gratitude to my advisor Prof. Tsuyoshi Kinouchi for his invaluable contribution in continually advocating for and handling everything with utmost perseverance, enabling perfect maneuvering of my career path and ensuring a smooth transition to limited dependence in the course of merely two and half years. His water resource engineering knowledge has inspired me to enjoy and learn every bit of what I have been doing. Combined with the intellectual freedom and his decisive suggestions, which I am grateful for, it was an amazing stay here. Flexibility in his schedule and personalized and dedicated care have synergized well-being, productivity, and growth, especially during the pandemic and post-pandemic era. I am thankful to him, along with my motherland and almighty, for giving me an opportunity to experience the learning and absorb and appreciate the culture at one of the world's best institutes, the Tokyo Institute of Technology (TokyoTech), one of the best experiences that are yet to evolve more with the future associations within the laboratory and beyond.

I am indebted to Nakamura sensei and Itsukushima sensei, dissertation committee members (Alvin sensei, Ichii sensei, Nakamura sensei: thank you so much for joining the committee and taking the time to review my thesis), Kanae sensei, collaborators, including Prof. Sayama, Jinghua, and others for rendering their earnest academic, scientific, and/or moral support/contribution. Previous mentors from other universities, whose early guidance has helped in a profound base, have made remarkable contributions to achieving the current feat. I recognize the support provided by all the TokyoTech, MEXT, and other associated units, institutions, and communities that have been an integral part of my journey, directly or indirectly. Special mention to Yamaoka san for making our lives easy at the office.

I am also grateful to all the members of Kinouchi lab, Nakamura lab, and all my friends and colleagues for all the good times together. Their extreme compassion, continued friendship, and instrumental contributions have added to my personal and professional experiences. My sincere thanks to Kexin for always being there for all the academic and non-academic discussions with the highest affection and persistence, which will benefit both of us in the future. Last but not least, I would thank Dr. Deepika, whose presence and unconditional care and devotion have inevitably made our lives beautiful for the previous eleven years. Thanks to our parents and all (extended) family members whose role has been pivotal in our academic and personal pursuits.

Contents

List of acronyms and abbreviations

NASA: National Aeronautics and Space Administration

GLDAS: Global Land Data Assimilation System

GRACE: Gravity Recovery and Climate Experiment

GRACE-FO: GRACE Follow On

TWS(A): Terrestrial Water Storage (Anomaly)

LWS(A): Land Water Storage (Anomaly)

SMS(A): Soil Moisture (Anomaly)

RS: Reservoir Storage

GWS(A): Groundwater Storage (Anomaly)

GRB: Godavari River Basin

KRB: Krishna River Basin

MRB: Mahanadi River Basin

CPRB: Chao Phraya River Basin

P: Precipitation

ET: Evaporation

T: Temperature

FAOSTAT: Food and Agriculture Organization Corporate Statistical Database

PCR-GLOBWB: PCRaster Global Water Balance

LSMs: Land Surface Models

GHMs: Global Hydrological Models

WSDI: Water storage deficit index

$\mathrm{WSDI_m}$: Modelled WSDI

$\mathrm{WSDI_g}$: GRCAE-based WSDI

SPI: Standard Precipitation Index

sc-PDSI: self-Calibrating Palmer Drought Severity Index

SSMI: Standardized soil moisture index

WSC: Water storage components

Water storage deficits (WSD)

Abstract

Terrestrial water storage (TWS), including all surface and subsurface water, is generally the prime source of livelihood, especially in countries like India and Thailand, where agriculture dominates the economies. Owing to the inherent limitations of spatiotemporal discontinuity of the conventional in-situ data, the holistic quantification of the dynamics of TWS remains limited, thus hindering the effective and efficient planning and subsequent implementation of water management strategies. However, with the remote sensing advancements, there has been an unprecedented improvement in mapping these variables, which are utilized in this thesis to develop new methods for a comprehensively assessing water resources over study basins, namely, Godavari, Krishna, and Mahanadi river basins located in Peninsular India during 1980-2017 and the Chao Phraya river basin (CPRB) of Thailand during 2002-2020.

Newly developed artificial neural network method coupled with the genetic algorithms successfully filled the gaps in and between GRACE and GRACE-Follow On data, ensuring a comprehensive understanding of the long-term trends and variability in the TWS and its constituent components. All four study basins are revealed to suffer from over-reliance on groundwater, which generally cannot be visually confirmed in advance or contemporarily, imposing dire consequences if left unattended. The reduced surface water availability due to decreased precipitation and the absence of stringent regulations on pumping are inferred to aggravate the groundwater storage vulnerability to uncontrolled extraction. Moreover, an increasing trend in the novel drought potential index based on the antecedent TWS and the current precipitation amount reveals the CPRB's tendency toward a drought-prone region, highlighting a quick and urgent intervention in reservoir management and groundwater recharge projects in the area. The proposed methodological framework and the improved understanding of regional water cycle dynamics by the enforced water budget closure have the potential to benchmark regional hydroclimate models with broad applicability in the global river basins.

List of Tables

List of Figures

Chapter 1

Introduction

1. Introduction

1.1. Significance of Terrestrial water storage

Terrestrial water, comprised of biomass, snow cover, surface water, canopy water, and soil moisture, and groundwater (Figure 1.1), is a vital source of industrial, agricultural, and domestic water demands and is crucial for sustaining many auxiliary sectors, including ecosystem and economy (Tiwari et al., 2009). The increasing stress on terrestrial aquatic systems has threatened nearly 2/3rd of the prevailing habitats, with over five billion people currently living in the regions prone to water scarcity. This number is most likely to increase in the future due to climate change, population growth, and human activities like groundwater extractions, urbanization, and land use and land cover changes (Rodell et al., 2018; Vörösmarty et al., 2010). Apart from compromising food production, reduced water availability will lead to the increasing cost of infrastructure (e.g., groundwater pumping), land subsidence in karst aquifer systems, altering water demand and supply, ultimately affecting the economy with more pronounced and severe impact on the developing countries (Döll et al., 2014; Long et al., 2016). In agrarian economies like India and Thailand, where the dependency on surface and subsurface water resources have tremendously enhanced during the past decade leading to, e.g., 28% area of India vulnerable and 33% already affected with the water deficit conditions at various levels, sustainable management ensuring the equitable availability of the prevailing water resources becomes crucial (CGWB, 2017; Mishra and Singh, 2009).

Apart from the societal and economic importance, terrestrial water plays a vital role in Earth system processes, including climate, weather, and biogeochemical cycles (Abhishek et al., 2021; Seyoum and Milewski, 2017). Thus, understanding the TWS dynamics is not only essential for human life but also crucial for assessing the water cycle, planning, policymaking, and other management strategies for water resources in a changing climate and for a continuously increasing population (Papa et al., 2015; Scanlon et al., 2018; Wada et al., 2014). TWS is a decisive component of the hydrologic cycle and therefore its improved quantification is pivotal in understanding the regional water cycle, which ultimately helps to allocate, govern, and manage the basin-scale water resources efficiently and effectively (Ndehedehe et al., 2016). Need for a holistic quantification of TWS and its segregated components and their spatiotemporal dynamics and variability is crucial in the river basins of

India and Thailand, where there is growing concern of vulnerability of water extremes (droughts and floods), to efficiently mitigate the multitude of direct and indirect impacts on regional and the global economies, latter of which face perturbations through supply-chain disruptions. In the coupled human-natural systems, where the synergistic impacts of natural and anthropogenic drivers are challenging to disentangle, an integrated representation of the land systems is of paramount importance for policymakers (Abhishek et al., 2021).

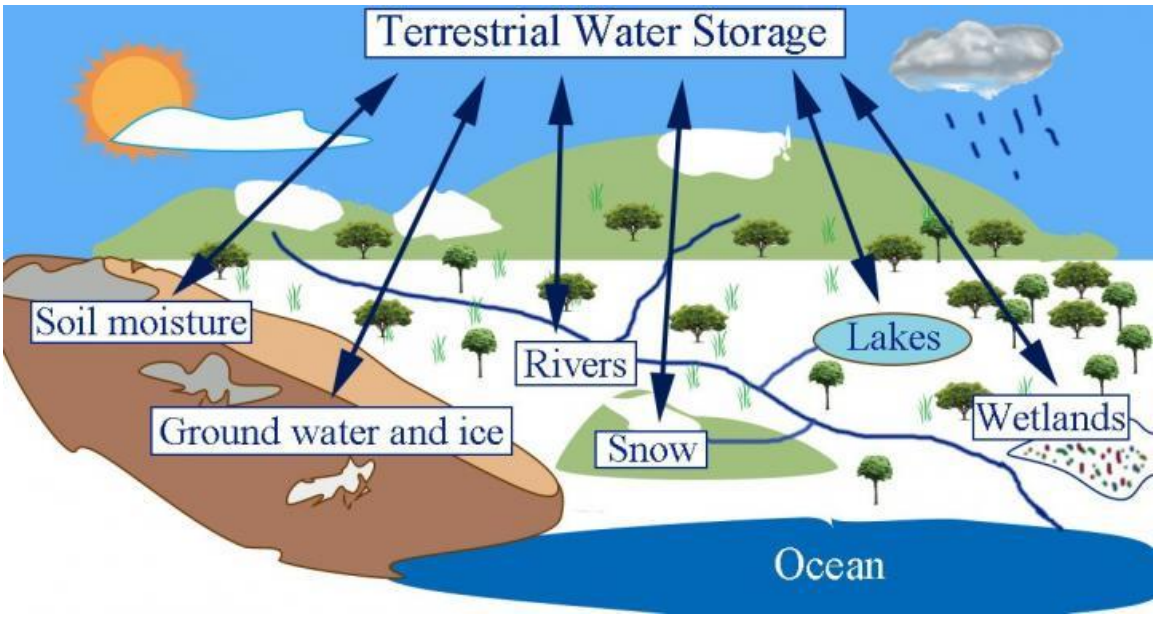

Figure 1.1. Illustration of Terrestrial water storage in a region. TWS includes all of the water storage components and can physically provide integrated information about the overall status of the land. (Credit: Enda Zhu)

Traditionally, ground-based data of various meteorological (e.g., precipitation), hydrological (e.g., reservoir storage, river runoff), and geological (e.g., aquifer properties) parameters have been used for understanding the various earth systems processes. However, the inherent limitations of in-situ data, including high installation and maintenance costs, inadequate spatiotemporal representation, recorded data gaps, lack of proper documentation, unfavorable topography, and restrictive data-sharing, have usually hindered a holistic investigation of various processes. However, with the beginning of remote sensing, there has been an unprecedented improvement in mapping these variables on required spatiotemporal scales, which are utilized, in this Thesis, to develop new methods for a comprehensive assessment of water resources over the study regions of India and Thailand.

1.2. Traditional and recent methods to quantify water storage dynamics

Traditional assessment of the water resources systems utilizes data from the groundwater observation wells and water level gauges in rivers and reservoirs (Abhishek and Kinouchi, 2022, 2021). However, the limited availability of the in-situ data, their inability to represent the required spatial domain, recorded data gaps, and their subsequent interpolation, the lack of digitization, and restricted data access policies limit the holistic quantification and make a forecast of the freshwater availability exceedingly difficult over almost all the major aquifer systems (Famiglietti et al., 2011; Rodell et al., 2018). Therefore, as an alternative, the remotely sensed hydro-meteorological fields from the satellite observation are integrated into the hydrological models as boundary conditions for a consistent assessment of the aquifer systems and the related water storage estimation (Bonan et al., 2002). However, the heterogeneity of aquifers, spatial variability in climatic variables, and anthropogenic impacts on hydrological fluxes, including reservoir impoundment, groundwater extraction, etc., deviate the model outputs from exactly mimicking the real field subjected to their operational scales (Abhishek et al., 2021; Abhishek and Kinouchi, 2022, 2021).

Notwithstanding a large variety and number of hydrological models using satellite data for quantifying the water resources trends, the joint mission by the National Aeronautics and Space Administration (NASA), USA, and Deutsches Zentrum für Luft-und Raumfahrt (DLR), Germany, known as Gravity Recovery and Climate Experiment (GRACE), has been collecting and archiving the Earth's gravity anomalies since March 2002, which can be further processed to the terrestrial water storage anomaly (TWSA) series with unprecedented accuracy (Famiglietti et al., 2015). After decommissioning of GRACE mission, its follow on (GRACE-FO), launched in May 2018, has continued the GRACE legacy till date. GRACE (and GRACE-FO) is a tandem satellite mission that detects changes in Earth's gravity field by monitoring the changes in distance between the two satellites as they orbit Earth (Chen et al., 2020, Tapley et al., 2019), as shown schematically in Figure 1.2. Outperforming a variety of remotely sensed data that primarily focus on few components of water storage, GRACE-(FO)-derived TWS has the least uncertainties on a basin size of > 100,000 km^2 (that has been shown currently ~63,000 km^2 with an error level of 2 cm in terms of equivalent water height) at the current processing level and thus provides a big picture of the water storage (Famiglietti et al., 2015; Vishwakarma et al., 2018).

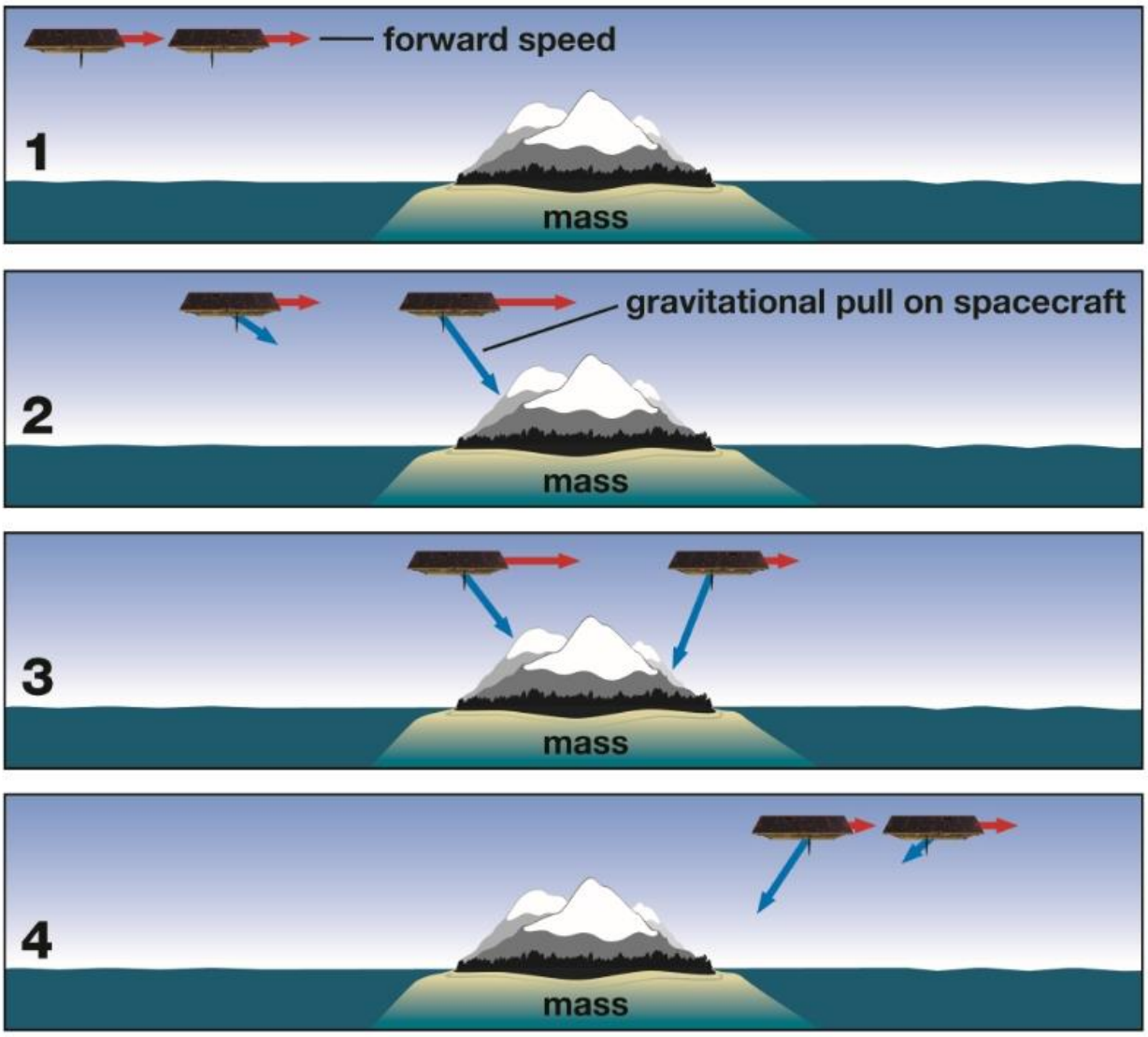

Figure 1.2. A schematic showing the various stages of the gravity measurement by the GRACE twin satellite system. (1) normal configuration of relatively constant velocity of the twin satellite separated by a distance of about 220 km and orbiting the earth at around 450 km, (2) the leading satellite experiences the enhanced gravitational pull attributed to the positive mass anomaly, leading increased acceleration and pulling away from the trailing satellite, (3) the trailing satellite also experiences the similar gravitational pull, thus catching up to the leading satellite, (4) the leading satellite comes to normal while there is still slight pull on the trailing satellite, before going back to the normal configuration (1). This acceleration-deacceleration of the two satellites is being recorded and then possessed as the gravity change and ultimately as the TWSA. (Credit: NASA)

Some studies have used GRACE based TWS for assessing the impact of anthropogenic disturbances (e.g., Scanlon et al., 2012), climate change (e.g., Rodell et al., 2018), and events of droughts (e.g., Liu et al., 2020), and floods (e.g., Chen et al., 2010) in various regions globally. To the best of my knowledge, however, no work has been done utilizing the GRACE-(FO) to analyze the dynamics of the terrestrial water storage (TWS) and segregated constituent components in the Peninsular Indian river basins and Chao Phraya River Basin, where frequent floods and droughts have been affecting various human activities. Moreover, the sparse and infrequent measurement of groundwater (GW), in addition to overreliance on GW by registered and unregistered wells, especially during dry periods, potentially limit appropriate monitoring and assessment of GW resources, leading to the continuous unsustainable abstraction, which eventually may lead to significant depletion of the commonly invisible GW. In this thesis, therefore, GRACE satellite data and the land surface and global hydrological models' output data are jointly used to disaggregate the constituent components of TWS, quantify the linkage and interaction among water fluxes (e.g., runoff, evapotranspiration), assess the hydroclimatic extremes that occurred in the basin, and analyze the effect of the policy change for water management essentially among GW and surface water.

The ancillary data from hydrological models further compliment the GRACE data for validation purposes and for isolating the individual components (e.g., groundwater storage (GWS), soil moisture storage (SMS)) from the integrated mass column of TWS (Long et al., 2016; Scanlon et al., 2018). For this purpose, researchers have been shifting to the global hydrology and water resources models (e.g., PCR-GLOBWB model; Sutanudjaja et al., 2018) from the conventional Land Surface Models (LSMs) to consider the human interventions and exclusively incorporate the water storage components. PCR-GLOBWB 2.0 model, which is a conceptual and process-based global (except Greenland and Antarctica) hydrology and water resources model (GHWRM) with a computational grid of 5 arcmins (0.1°×0.1°) and simulates the hydrological fluxes at a daily time step (Sutanudjaja et al., 2018). The model integrates human water use with the dynamic water balance between surface and subsurface water storage in two vertically stacked soil layers (soil zone depth of 1.5 meters) using the five-module setup, namely 'irrigation and water use module', 'meteorological forcing module', 'land surface module', 'groundwater module' and the 'surface water routing module' (Sutanudjaja et al., 2018; Wada et al., 2014), as shown in Figure 1.3.

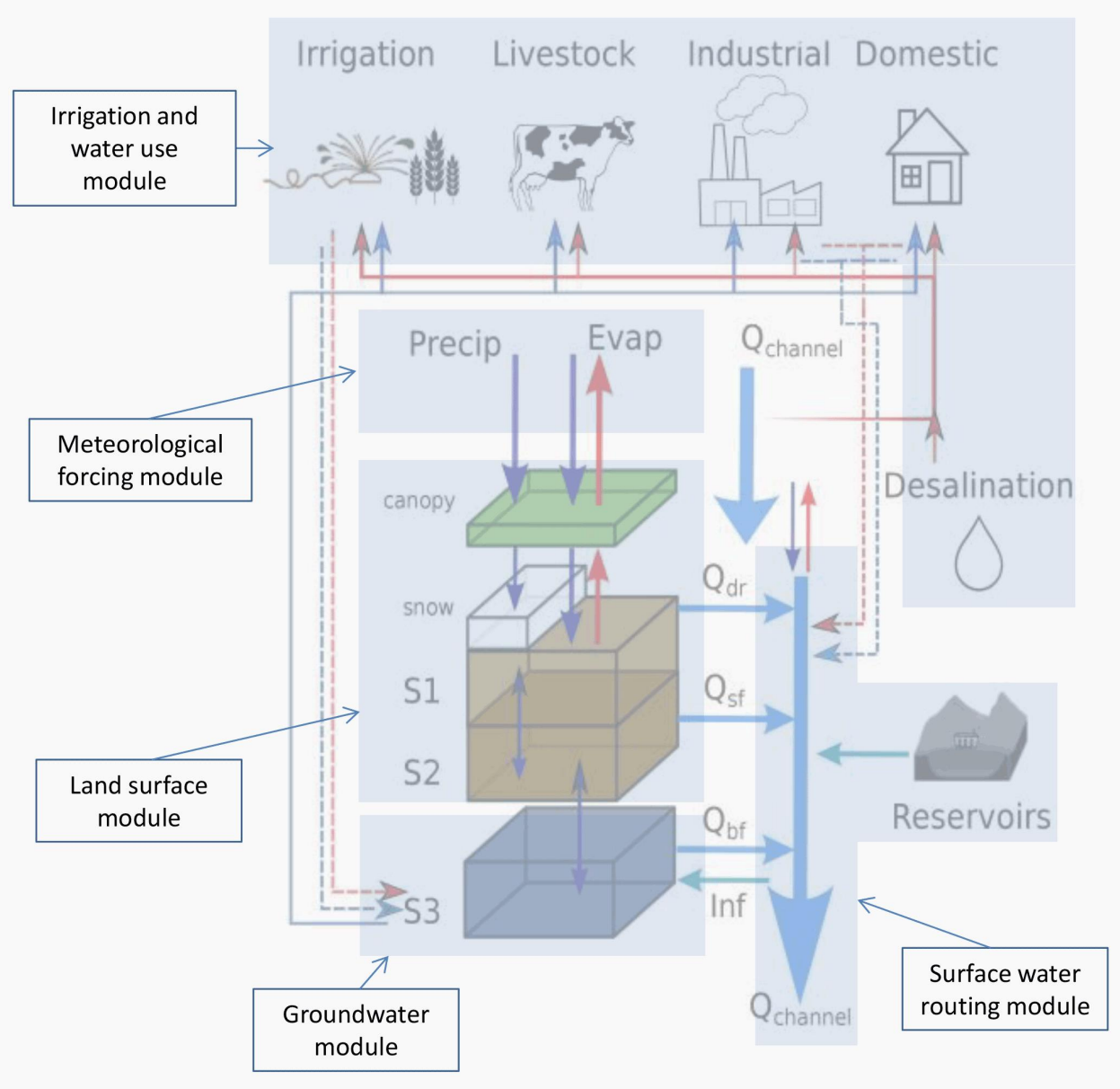

Figure 1.3. Schematic of the PCR-GLOBWB 2 model configuration. Various modules (surface water routing model, irrigation ad water use module, meteorological forcing module, land surface module, and groundwater module) incorporated in the model structure for simulating the various water storage components are also shown. Arrows indicate the movement of the fluxes within the land mass and for various sectorial water usages. Actual water consumption for any given sector is calculated as the difference between the withdrawals and the return flows. For detailed descriptions of various notations, readers are referred to (Sutanudjaja et al., 2018). (Credit: Sutanudjaja et al., 2018)

This combination of two datasets (GRACE based TWS and model various GHM based TWS componets) has been proven as a reliable and robust method for monitoring spatiotemporal variations of terrestrial water and its constituent components over global, continental, subcontinental, regional, and basin scales (Scanlon et al., 2018); a strategy which have been utilized in this thesis for varying applications.

1.3. Rationale of employing deficit-based drought characterization

The conventional approach of drought quantification solely depends on the limited accuracy of the ground-based hydro-meteorological data. In-situ data stations and their records suffer from many limitations, including inhomogeneous and inadequate distribution of monitoring network, data gaps, unavailability at the required spatiotemporal scale, associated high installation and maintenance cost, measurement limits within near-surface zones, and need for high human resources (Abhishek and Kinouchi, 2021, 2022; Creutzfeldt et al., 2012; Z. Sun et al., 2018). Furthermore, the drought characterization imposes a difficulty because it must take a multitude of dimensions, viz., drought magnitude, duration, type, frequency, and severity, into account (Z. Sun et al., 2018). Conventional methods for assessing drought severity include many subjective and objective information, including hydro-meteorological data and drought impact reports (Thomas et al., 2014). Additionally, the lack of a comprehensive universal definition and poor understanding of its precursors lead to drought classification in various categories. The most popular drought indices among a total of more than 150 and around 74 operational indices are the Standardized Runoff Index (SRI), Standardized Precipitation Index (SPI), and Palmer Drought Severity Index (PDSI) (Z. Sun et al., 2018; Zargar et al., 2011). SRI, SPI, and PDSI are used to determine the seasonal loss in streamflow, monitor short- and long-term regional precipitation dynamics, and characterize agro-climatological droughts, respectively (Bloomfield and Marchant, 2013; Mishra and Singh, 2010; Thomas et al., 2014; Wilhite et al., 2007). All of these physically-based drought indices rely solely upon one or more of the meteorological parameters surface or subsurface water storage components and do not consider a combined effect of all these parameters (Heim, 2002; Z. Sun et al., 2018). Moreover, there is no mechanism in all these indices to incorporate the variability in all water storage components, and hence, they lack in providing the integrated water storage deficit information over the target area.

Amid the inherent drawbacks of traditional drought indices, researchers have recently sought integrated and hybrid drought indices based on remotely sensed water storage data (Z. Sun

et al., 2018; Thomas et al., 2014). Drought indices should represent the overall state of water resources, thus providing a comprehensive view of droughts for more practical, accurate, and viable management and decision-making. Satellite observations followed by the postprocessing techniques have proven quite useful for adequate drought characterization and monitoring on the required spatial and temporal scales in the past decades, especially after the launch of GRACE satellites (Niemeyer, 2008). Drought characterization based on the remotely sensed data of land water storage (LWS) outperforms the traditional methods because it represents the integrated deficits in surface water, soil moisture, and groundwater over the region of interest and thus depicts the real picture of bulk water dynamics (Cao et al., 2015; Z. Sun et al., 2018). Many integrated drought indices, primarily GRACE based, have been introduced and employed to assess the droughts globally, including the hydrological drought index (GHDI) (Yi and Wen, 2016) applied for the continental United States, total storage deficit index (TSDI) for Northwestern China (Cao et al., 2015) and the Saskatchewan River Basin in Canada (Yirdaw et al., 2008), terrestrial water storage (TWS) anomaly index (TWSI) (J. Wang et al., 2014) for the Haihe River Basin, China at various spatiotemporal scales. However, these studies depend on limited data sources covering a short duration equal to that of GRACE records, thus lacking a robust global framework for long-term drought characterization. This data brevity issue with the GRACE data limits our ability to get insights into the water resources dynamics far beyond the GRACE records.

1.4. Goals and objectives

This thesis is motivated to fill the aforementioned gaps (i.e., lack of understanding of the earth system process before GRACE era, limited studies on integrated and segregated TWS in the agrarian economies like India and Thailand, ambiguities in quantifying the hydroclimate extremes, and unclosed water budgets) in previous research by addressing the following core questions, 1) what is the multidecadal variability of deficits based on the TWS and GWS in the Peninsular Indian river basins. 2) how well the GRACE derived GWS is compared with the in-situ data? 3) how much do state-of-the-art multisource data vary among themselves, and how well does an ensemble mean represent the regional water balance and the hydroclimate extremes in the Chao Phraya River basin in Thailand? 4) what are the closure constraints and biases in various water cycle components and how can the multisource data be used for reference for future hydrological applications?

These questions are answered by reconciling GRACE derived TWS, various hydrologic data products from LSMs and GHMs, in-situ rain gauge data and groundwater data. A novel artificial neural network method is employed to ensure the continuity in the GRACE based TWSA data and a novel drought index is proposed to holistically quantify the drought conditions. The long-term implications of the altered water cycle and dwindling water storage in the study basins are further discussed in the context of efficient and effective water management as a pathway for future research.

After discussing the significance of TWs and recent advancement in the regional water storage dynamics, in the second chapter, the droughts in land water and groundwater over three Peninsular Indian river basins are characterized during past 35 years from 1980 to 2014. Various drought features including, the severity and recovery time, are presented.

In the third chapter, the surface- and subsurface- water resources dynamics over the Indian river basins are holistically quantified during the more recent time period, i.e., July 2002 to June 2017, and with refined methodology (e.g., using distributed aquifer properties) for converting the in-situ groundwater well data to the regional GWS. Two distinct periods of variable trends are identified with explicit attribution of the governing factors.

In the fourth chapter, assessment of water related extremes, floods and droughts, is presented with the evaluation by the novel drought index in the Chao Phraya river basin, Thailand. Drought propagation from meteorology to the soil moisture and terrestrial water storage is also analyzed and the inferences for the policymakers and water managers are discussed for an likely institutional interventions for an efficient water availability in the basin.

In the fifth Chapter, a case study is presented focusing on the quantification, attribution and correction of the water budget closure errors employing three different closure techniques. The basin-scale assessment focuses on the upper Chao Phraya river basin where the observed runoff gauge data is available. Improved insights into the multi scalar (monthly, seasonal, and annual) time series of raw and corrected water cycle components provide a physically consistent reference point for further hydrological studies in the region and methodological implications in other river basins.

Lastly, summary of the thesis is presented with an outline of the future research.

Chapter 2

Multidecadal Land water and Groundwater Drought Evaluation in India

This chapter has been adapted from Abhishek and Kinouchi, 2022.

Abhishek, Kinouchi, T., 2022. Multidecadal Land Water and Groundwater Drought Evaluation in Peninsular India. Remote Sens. 14, 1486. https://doi.org/10.3390/rs14061486

2. Multidecadal Land water and Groundwater Drought Evaluation in India

2.1. Motivation

2.1.1. Increasing water scarcity in Peninsular India

With a global increase in drought frequency and severity, the drought assessment has become of paramount importance in India's temperate climate, which predominantly governs crop productivity (Dai, 2013, 2011; Tripathi et al., 2015). Unsustainable extraction by anthropogenic activities in conjunction with the climate shift to warmer temperature has reduced groundwater availability and impaired its quality, making it vulnerable to projected climate change and population growth (Famiglietti and Rodell, 2013; Taylor et al., 2013). The water scarcity in India has recently been expanded to the agriculturally important Peninsular India, where overexploitation of groundwater (GW) and fluctuations in monsoon rainfall may further magnify the prevailing GW stress and impose subsequent food security risks (Sharma and Goyal, 2018). Some of the river basins located in Peninsular India are moderate to severely non-resilient to the hydrological disturbances and have experienced seasonal to long-term water shortages (Sharma and Goyal, 2018). However, droughts in India are mostly reported based on the percentile of rainfall and sometimes even by visual drying of the land surface (Sinha et al., 2017), highlighting a need for quantitative and robust drought characterization based on integrated water storage deficits (WSD). Under these circumstances, understanding the basin-scale hydrological fluxes becomes vital for better monitoring and characterizing droughts and subsequent water resources management under the prevailing conditions. In the absence of a real-time integrated drought monitoring platform in India, timely and reliable identification and classification of the drought events are in urgent need.

Although India receives an annual rainfall of 1200 mm (highest amongst countries of comparable size) (Rodell et al., 2009), due to the highly uneven distribution in spatial and temporal scales, about half of the country is either already affected or vulnerable to the water deficit conditions at various levels of water scarcity (Kumar et al., 2005; Mishra et al., 2009; Samra, 2004). This water scarcity situation in India, and in the study basins in Peninsular India, is expected to worsen due to the combined impact of natural (climatic shifts to warmer

temperatures) and anthropogenic factors (the high water demand from the growing population). Since most of the water demands in the basins are met by the groundwater withdrawals, which are highly dependent on the fluctuating monsoon precipitation, understanding various factors governing the groundwater availability in the region becomes of paramount importance. As per the assessment by the Central Groundwater Board, the ratio of groundwater consumption to recharge is over 100% (i.e., consumption>recharge) in some parts of North-West India, implying the unsustainable use of the GW in the region (GoI, 2017). Moreover, out of 6584 GW assessment units, 1034 are already over-exploited, and 253 are critical, and another 681 are semi-critical (GoI, 2017), affecting 33% area of India already and making another 28% area vulnerable to the water deficit conditions at various levels of water scarcity (Kumar et al., 2005; Mishra et al., 2009; Samra, 2004). Apart from the dependence of livelihood, variabilities of the prevailing groundwater resources limit crop production and hamper economic development in the region. Therefore, there is a clear need for the basin-wise assessment of the GW resources, which will further assist in efficiently dealing with the storage fluctuations and consequences resulting from the monsoon variabilities and lead to effective irrigation scheduling in the agriculture dominant study region.

Although there have been several studies focusing on the North-West Indian region (Chinnasamy et al., 2013; Dasgupta et al., 2014; Long et al., 2016a; Panda and Wahr, 2016; Rodell et al., 2009; Tiwari et al., 2009), the Peninsular Indian region remains largely unexplored, with only a few recent studies those too concentrate only on a short period (e.g., for 2002-2016 (Satish Kumar et al., 2020)). Moreover, no study has been carried out to assess the basin-scale integrated and segregated water storage dynamics, holistic drought characterization, and assessment of various drought indices focusing on groundwater beyond the GRACE period. Therefore, in this chapter, the water storage dynamics for a period of 35 years (1980-2014) and its implications on the intermittent in-situ groundwater observations in the three river basins in Peninsular India, which comprise a total of ~22% geographical area of the country, is investigated.

2.1.2. Status and importance of groundwater in India

Droughts, primarily a form of the water deficit conditions, cause significant impacts on various sectors, including food security, public health, ecosystems' stability, freshwater availability,

and socio-economic development in a region (Du et al., 2013; Z. Sun et al., 2018). The impacts of droughts are evident in almost every region and climate, spanning from the tropical parts of Asia to the historic cities of Europe, with varying meaning and significance (Abhishek et al., 2021; Jacobi et al., 2013; Schreiner-McGraw and Ajami, 2021). The joint influence of the population growth-induced water demands and climate change, which is expected to increase the areal extent, intensity, duration, and frequency of droughts globally in the near future (Dai, 2013; Trenberth et al., 2014), has drawn the attention of the researchers in hydrology and associated disciplines (Mishra and Singh, 2010). The cascade of drought, i.e., the propagation of water deficit, from precipitation (meteorological) to soil moisture (agricultural) and streamflow (hydrological), ultimately affects the groundwater storage leading to a distinctive class of drought termed as groundwater drought (Bloomfield et al., 2015; Mishra and Singh, 2010; Thomas et al., 2017). However, compared to the (near)-surface water storage components (surface water and soil moisture), an accurate assessment of the groundwater (GW) dynamics and the embedded water deficit conditions, which are not commonly visible, is still challenging, especially at the regional scales and for multidecadal time scales.

Groundwater accounts for about 98% of the global freshwater resources, excluding glaciers and ice-caps, making it a vital source for meeting environmental and human-induced water demands (Li et al., 2019). However, there has been unprecedented stress on the groundwater resources due to overexploitation, which has resulted in, for example, depletion of ~330 km^3 GW in the High Plains Aquifer in the U.S. (from 1950 to 2007) (Bridget R. Scanlon et al., 2012) and ~140 km^3 over the California Central Valley (from 1860s to 2003) (Famiglietti et al., 2011). This stress is not limited only to the dry regions where a limited amount of surface water is available but also extends to the areas with abundant rainfall where multiple attributing factors exist, such as the spatiotemporal heterogeneity in precipitation, poor management, and pollution of surface water resources, and population growth, cause over-reliance on the GW (Thomas et al., 2017). Further, the existing low resiliency makes quantification of the multidecadal groundwater resources dynamics of prime importance for the (semi)-arid regions, such as Peninsular India, where the GW abstractions primarily govern the regional food security and socio-economic stability (Famiglietti, 2014; Richey et al., 2015).

India is the world's largest user of groundwater at an annual rate of 230 km^3, which is over a quarter of the global total, 90% (much higher than the global average of 40%) of which is

used for ~60% (global value: 38%) of the total irrigated land in the country. The remaining 10% is used in meeting ~80-85% of the water demands of ~90 million rural households (Siebert et al., 2010; Worldbank, 2012; Zaveri et al., 2016). This high dependence on GW resources in India has resulted in half of the country's area already suffering from water stress conditions with a meager per capita share of water storage (Chindarkar and Grafton, 2019). Assessment of the in-situ groundwater data collected by India's agency Central Ground Water Board has revealed that 42% of GW wells experienced a decrease in water level, with 7% showing a decline of as high as 2-4 m between 2001 and 2011 (CGWB, 2014a). Furthermore, the ratio of groundwater consumption to recharge increased to 62% in 2011 from 58% in 2004 in the country (Chindarkar and Grafton, 2019; Suhag, 2016).

Several inherent hindrances in in-situ data comprehension, mainly caused by the inadequacy of the monitoring network, recorded data gaps, discrete spatial representation, among others, limit the holistic characterization of the groundwater storage solely based on the actual field observations (Li and Rodell, 2015). Notwithstanding these hindrances, satellite observation (especially, Gravity Recovery and Climate Experiment, i.e., GRACE) jointly assimilated with auxiliary data from the global hydrological models (e.g., PCR-GLOBWB) has proven quite promising to quantify the hydrological cycle components on the required spatial and temporal scales globally in the past decade (Abhishek and Kinouchi, 2021; Andrew et al., 2017; Chen et al., 2020; Jing et al., 2020; Long et al., 2016b; Rodell et al., 2018; Satish Kumar et al., 2020; Scanlon et al., 2018, 2015). However, all of these studies focus on the brief observational records coinciding with the GRACE, i.e., from Apr 2002 onwards, and the water storage dynamics with an explicit focus on groundwater, to the best of my knowledge, remains largely unexplored beyond the GRACE records. Therefore, in this chapter, the multidecadal (1980-2014) water storage deficits in both land water storage (LWS) and groundwater storage (GWS) are characterized and subsequently the droughts in terms of magnitude, duration, severity, and recovery time in Peninsular India are analyzed where the water scarcity is recently increasing (Figure 2.1).

The major contribution of the current chapter is as follows. Firstly, the multidecadal study period (35 years) provides insights into the long-term slow systemic changes in the hydrological system of a cumulative catchment area of 709151 km^2 (~22% of the geographical area of India), providing a blueprint for future climate change studies. Secondly, the applicability of the PCR-GLOBWB model, with embedded model uncertainties, to simulate

the integrated and segregated water storage components beyond the GRACE satellite is demonstrated and subsequently the superiority of the LWS-based deficit index over traditional indices is shown. Thirdly, to address the challenge for a real-time monitoring framework imposed by the irregular groundwater measurements, the water storage deficit index (WSDI) is proposed as a potential proxy near-real-time indicator of the groundwater drought index (GWDI) and for its subsequent usage for early GW drought warning systems. Given the robust but straightforward approach, the current basin-scale decadal drought characterization framework can be employed globally in various data-scarce or data-limited river basins.

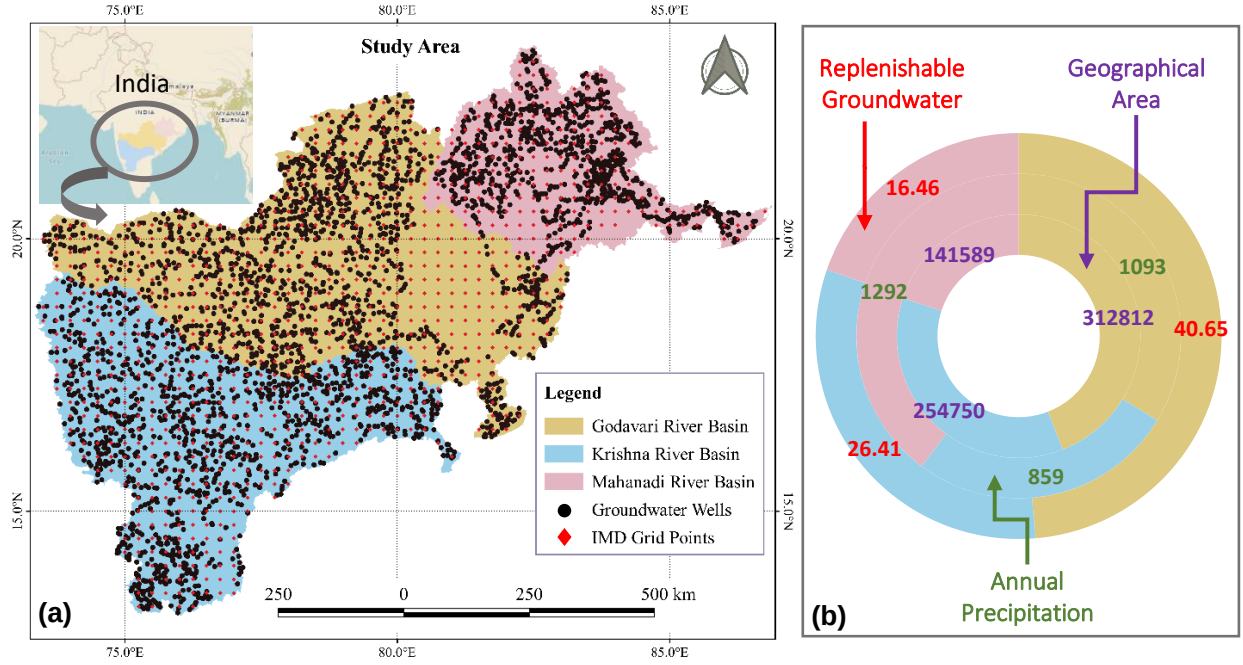

Figure 2.1. Specifications of the Peninsular Indian river basins. (a) Godavari, Krishna, and Mahanadi river basins (GRB, KRB, and MRB, respectively) selected for the current study. The grid points corresponding to the IMD (India Meteorological Department) gridded precipitation data, and the groundwater well locations are also shown by filled red diamonds and filled black circles, respectively. (b) Basin-wide estimates of total replenishable groundwater resources (km^3), geographical area (km^2), and annual precipitation (mm) from Jan 1980 to Dec 2014. Further specifications of the study basins are listed in Table 1. After (Abhishek and Kinouchi, 2022).

2.2. Materials and Methods

Study Area

Three river basins, namely, the Godavari, Krishna, and Mahanadi river basins (abbreviated as GRB, KRB, and MRB, respectively), were selected for the study (Figure 2.1, Table 2.1). Compared to the national mean annual rainfall (1200 mm), these basins receive a limited amount (for the GRB and KRB) or a fair amount (for the MRB) of rainfall. The dependency of water supply on the groundwater in all three basins is more than 70%, which is likely to be increased in the future due to the continuously rising groundwater consumption (Census of India, 2011; GoI, 2017). Moreover, inadequate public water supply systems and advanced pumping and drilling technologies may further intensify the unsustainable groundwater extraction, often through unregistered wells, in the area.

Table 2.1. Salient features of the three study basins in Peninsular India. Three river basins selected in the study and their geographical area, basin averaged precipitation for Jan 1980 to Dec 2014 (CWC, 2019), population statistics (Census of India, 2011), water scarcity situation (CWC, 2019), and the maximum groundwater level (GWL) depth as per the observational wells used in this study. After (Abhishek and Kinouchi, 2022).

River Basin	**Geographical Area (km^2)**	**Mean Annual Rainfall (mm)**	**Variability (min.-max.) in rainfall (mm)**	**Estimated population (million)**		**Estimated per capita water availability (m^3)**		**Current category***	**No. of wells†**	**GWL depth (m)**
				2025	2050	2025	2050			
Godavari (GRB)	312812	1093	400-2500	89.18	104.92	1320.25	1122.19	Water stressed	430	33.6
Krishna (KRB)	254750	859	100-4000	100.41	118.13	886.76	753.75	Water scarce	515	47.8
Mahanadi (MRB)	141589	1292	1080-1653	43.93	51.68	1661.73	1412.54	Water stressed	135	34.4

* The estimated per capita water availability is below 1700 m^3 in the GRB and MRB, which are under water-stressed conditions, and below 1000 m^3 in the KRB, which is in water-scarcity condition (CWC, 2019).

† represents the total number of wells after filtering for each basin.

2.2.1. Water Storage Components and Climate Data

The high resolution (0.25°x0.25°) daily gridded precipitation data, which has been developed by using a network of 6955 rain gauge stations pan-India, was accessed from the India Meteorological Department for the study duration (https://www.imdpune.gov.in/;(Pai et al., 2014)). This precipitation data, along with the standard dataset for other hydro-meteorological variables, was further used for forcing PCR-GLOBWB 2.0 model. Time series of various water storage components (WSCs), i.e., soil moisture, groundwater, and routed surface runoff, were simulated using the model from Jan 1980 to Dec 2014. All these components were then summed up to get the modeled LWS ($\mathrm{LWS_m}$). For convenience, all the model outputs are named as modeled WSCs (e.g., modeled soil moisture storage; $\mathrm{SMS_m}$, similarly $\mathrm{GWS_m}$ and $\mathrm{LWS_m}$).

Further, an arithmetic mean of the two GRACE mascon solutions represented as basin-averaged equivalent water depth (mm) was used to compare the model performance in simulating LWS. Mass Concentration blocks (mascons) are another form of gravity field which compared to other GRACE products (e.g., conventional spherical harmonic solutions), do not need spatial (e.g., smoothing) or spectral (e.g., de-striping) filtering or other empirical scaling and therefore have higher signal-to-noise ratio, higher spatial resolutions, and eventually reduced errors (Save et al., 2016; Watkins et al., 2015). GRACE-derived LWS represents the integrated sum of canopy water, surface water, soil moisture, groundwater and has been used in several studies for varying purposes of water budget and water storage dynamics (Abhishek et al., 2022, 2021; Rodell et al., 2018; Scanlon et al., 2015). Overall, an inter-comparison of GRACE LWS shows strong agreement between all products with the variance among different GRACE products ranging within error bounds of the GRACE data with no significant biases, which is consistent with previous studies (Sakumura et al., 2014). Since there is minimal signal loss attributed to the regularization and post-fit residual analysis, no signal restoration procedures are required for GRACE Mascon (mass concentration) solutions (Abhishek et al., 2022; Scanlon et al., 2015). Further details of the two datasets (GRACE-derived and PCR-GLOBWB model based) are explained in details as below.

Regarding the PCR-GLOBWB, due to the non-availability of continuous ground data for model calibration, similar to the previous studies (Abhishek et al., 2021; Bhanja et al., 2017a; Scanlon et al., 2018; Sutanudjaja et al., 2018; Wang et al., 2021; Yin et al., 2021), the model

was not calibrated, and the standard parameterization settings were used. Since precipitation has been shown the most critical parameter in model output rather than the model parameters' uncertainties (Felfelani et al., 2017; Sperna Weiland et al., 2015; Tangdamrongsub et al., 2017), the high quality regional daily precipitation data (0.25°x0.25°) from the India Meteorological Department are used for the study duration (https://www.imdpune.gov.in/;(Pai et al., 2014)). A spin-up period of 50 years using the hydro-meteorological data of the year 1901-1950 (IMD precipitation data is available for 118 years, 1901 to 2018; https://www.imdpune.gov.in/) was used to enable the groundwater volumes to be in equilibrium with the study's current climatic settings. Daily outputs of individual water storage components for each grid cell were converted to the basin averaged monthly time series (for consistency in comparison with GRACE-based estimates of GWS: $\mathrm{GWS_g}$) and summed to get the modeled land water storage ($\mathrm{LWS_m} = \mathrm{SMS_m} + \mathrm{SWS_m} + \mathrm{GWS_m}$). Although the modeled surface water storage ($\mathrm{SWS_m}$) was used in calculating $\mathrm{LWS_m}$, it is not explicitly analyzed in the study because of its negligible contribution to $\mathrm{LWS_m}$ and subsequent insignificant decadal trends compared to other components. The long-term mean of $\mathrm{LWS_m}$ from 04/2002 to 12/2014 (consistent with $\mathrm{LWS_g}$ baseline time) was subtracted from $\mathrm{LWS_m}$ time-series to get the monthly anomaly series of $\mathrm{LWS_m}$.

Please note that the PCR-GLOBWB model is not being endorsed over other global hydrological and water resource models (GHWRMs) such as WGHM (WaterGAP Global Hydrology Model, which also includes coupling of human water use and reservoir management although with different mechanisms of water abstraction, groundwater availability, among others, compared to PCR-GLOBWB) (Alcamo et al., 2003; Döll et al., 2014, 2003; Sutanudjaja et al., 2018), among others (Telteu et al., 2021), which have also been used for analyzing the land water storage at various global (Scanlon et al., 2018) or regional scales (Abhishek and Kinouchi, 2021). One global model is chosen just for the demonstration purposes of how well we can understand the dynamics and variability of land storage and its constituent components beyond the GRACE time period and subsequently assess the capability of land water storage (whether $\mathrm{LWS_g}$ or $\mathrm{LWS_m}$) to depict the near-real-time groundwater situation in the region.

Regarding the model calibration and validation, it should be calibrated with the ground data, wherever available (e.g., soil moisture (López et al., 2017) discharge data (Sutanudjaja et al.,

2014), (López et al., 2017; Sutanudjaja et al., 2014)(López et al., 2017; Sutanudjaja et al., 2014)and the performance should be further analyzed statistically for the study region into consideration. Also, the applicability of the model as an auxiliary data source for GRACE-based water storage estimation can further be characterized either using more recent satellite datasets of soil moisture (e.g., SMAP; Soil Moisture Active Passive), land water storage (e.g., Swarm (Richter et al., 2021)), among others. Additionally, wherever available, the in-situ data records can also be used to further evaluate the model's performance to simulate the individual water storage components. Advancements towards hyper-resolution global water resource modeling and improved methods of satellite gravimetry will further enhance our understanding of the various regional and global hydrological systems.

In this context, given the ability of the PCR-GLOBWB 2.0 model (taken as an example for demonstration purpose in this thesis) to simulate the various water storage components, it is hypothesized that the model output can be used for a robust but straightforward basin-scale decadal drought assessment in terms of the water storage deficits and subsequent characterization of droughts (magnitude, duration, severity, and recovery time), beyond the GRACE satellite observations. Further, the water storage deficit index (WSDI) is compared with various conventional indices like, SPI, self-Calibrating PDSI (sc-PDSI) and standardized soil moisture index (SSMI). WSDI (whether PCR-GLOBWB based: modelled WSDI ($\mathrm{WSDI_m}$) or GRACE based: $\mathrm{WSDI_g}$) accounts for both the natural processes (rain, infiltration, evaporation, storage, etc.) and anthropogenic activities (groundwater abstraction, supply, irrigation, etc.) in the terrestrial hydrologic system, and therefore provide holistic assessment of the bulk water storage dynamics in the region. Moreover, unlike $\mathrm{WSDI_m}$, $\mathrm{WSDI_g}$ is free from the impact of the uncertainties arising from the water balance models or from the hydrometeorological forcing. The outperformance of deficit-based (below normal conditions) drought characterization over traditional assessment is shown in terms of capturing the holistic picture of the water storage and at the same time, free from influence of different calculation methods and inadequate representation of the terrestrial water storage in a region.

Regarding the GRACE data, the most recently released Level-06 (RL06M v02) monthly GRACE mascon (mass concentration) solutions from two processing centers, namely, the Jet Propulsion Laboratory and Centre for Space Research (JPL-M and CSR-M, respectively, thereafter) were used for characterizing the dynamics of land water storage ($\mathrm{LWS_g}$) over the study region (Save, 2020; Save et al., 2016; Watkins et al., 2015; Wiese et al., 2018). This

newest data has been corrected in several aspects compared to the previous versions, such as representation on ellipsoidal Earth applied separately to land and ocean to minimize signal leakage, application of the Coastline Resolution Improvement filter leading to the reduced leakage errors across coastlines, the inclusion of the realistic geophysical information during the solution inversion to intrinsically remove correlated errors, among others. Additionally, unlike the conventional spherical harmonic approach, given their regularization process (and hence reduced systematic errors), mascons do not need any additional postprocessing in terms of signal restoration (Li et al., 2019; Scanlon et al., 2016, 2015). Data from April 2002 through December 2014 were used to minimize the uncertainties in GRACE estimates, especially at the seasonal time scales, which might have been induced due to the operational issues towards the end of the mission (Chen et al., 2020). Since the ensemble mean of the two independent gravity products is found effective in reducing the uncertainty errors in the gravity fields (e.g., (Sakumura, 2013; Sakumura et al., 2014; Xie et al., 2019), an arithmetic average of $\mathrm{LWS_g}$ derived from the two mascon solutions was used for further analysis. The basin-wide $\mathrm{LWS_g}$ are presented in terms of the basin-wide equivalent water depth (mm) or equivalent water volume (km^3) anomalies relative to the long-term mean of 04/2002 to 12/2014. The missing values in the data series since early 2011 due to the active battery management were filled by the linear interpolation of the two bounding values (Andrew et al., 2017; Xie et al., 2019).

Linear and Non-linear Trend Analysis: Although the linear trend analysis gives the long-term change in the basin, the existing non-linearity in the data has motivated us to use the non-linear non-parametric trend analysis, namely the Hodrick-Prescott (HP) filter. For a doubly infinite series, the cyclic component was estimated in the given data time series $\mathrm{y_t}$, by the high pass filter (Hodrick and Prescott, 1997):

$$\tilde{c_t} = \tilde{H}(L)y_t \tag{2.1}$$

where $\tilde{H}(L)$ is the weight function with L as the loss parameter. $\tilde{H}(L)$ is given by

$$\tilde{H}(L) = \frac{\lambda (1-L)^2 (1-L^{-1})^2}{1+\lambda (1-L)^2 (1-L^{-1})^2} = \frac{\lambda L^{-2}(1-L)^4}{1+\lambda L^{-2}(1-L)^4} \tag{2.2}$$

where, λ (=1600, as most commonly used (Ravn and Uhlig, 2002)) is the user-defined smoothing parameter. The trend component is then separated by the low pass filter;

$$T_t = \left(1 - \tilde{H}\,(L)\right) y_t = \left(1 + \lambda\,(1 - L)^2\,(1 - L^{-1})^2\right)^{-1} y_t \quad (2.3)$$

where T_t is the HP trend in the respective time series. This method has recently been used in similar hydrological applications (Bhanja et al., 2019, 2016; Sun, 2013) dealing with the monthly water storage data. The HP filter algorithm was employed using the MATLAB and Statistics Toolbox Release 2019a.

2.2.2. Drought Severity and Recovery Time

The monthly events of water storage deficits in both LWS_m and GWS_m were calculated by removing their respective climatology and further calculated and inter-compared the event severity and recovery times. An approach by (Thomas et al., 2014) is extended for calculating the deviations (surplus or deficit) from the average conditions, as below (example of GWS_m):

$$GWSD_i = GWSA_i - GWSA_i^c \quad (2.4)$$

where $GWSD_i$ is the GWS deficit, $GWSA_i$ is the GWS anomaly based on GWS_m, and $GWSA_i^c$ is the climatology of GWSA for the ith month. The monthly climatology was calculated as the average monthly GWSA over the study period.

Land water or groundwater storage deficits (LWSD or GWSD), i.e., deseasonalized LWS_m or GWS_m (monthly climatology removed from the original anomaly time series), quantify the instantaneous drought conditions in the land water or groundwater by the departures from the normal circumstances in the particular region but do not depict the severity during the whole period of the event. Moreover, LWSD/GWSD does not provide any information of the time elapsed before the water storage conditions return to normal, which is imperative for basin-scale water management and policymaking. Therefore, the event severity (S_t), which represents the cumulative water storage deficit (WSD) for a particular drought event (during the period of negative WSD) and thus highlights the overall water loss during the event, corresponding to each water deficit event (which primarily represents the cumulative GWS_m deficit from the onset of the deficit) was calculated as:

$$S_t = \bar{M}_t * D_t \quad (2.5)$$

where S_t is the event severity (mm months), $\bar{M}_t$ (mm) and D_t (months) are the average water deficit in GWS_m and duration since the onset of the deficit period, respectively. The subscript t signifies that all the parameters are a function of time. S_t characterizes the accumulated

influence of deficiency associated with a particular drought event. The same procedure was applied for $\mathrm{LWS_m}$ based calculations. For understanding the drought recovery, the time to recover from below-normal storage conditions was calculated corresponding to monthly storage deficits (both LWSD and GWSD), that is explained in details below.

Firstly, the rate of change in the monthly water storage deficit was calculated as below:

$$\frac{\mathrm{d(WSD)}}{\mathrm{dt}} = \frac{\mathrm{WSD_i - WSD_{i-1}}}{\Delta \mathrm{t}} \text{ for } \mathrm{i} = 1 \sim \mathrm{n} \quad (2.6)$$

where $\frac{\mathrm{d(WSD)}}{\mathrm{dt}}$ is the rate of change in LWSD or GWSD (evaluated only for the drought events), $\Delta \mathrm{t}$ is unity since the change was calculated during the consecutive months $i-1$ and i, and n is the length of $\mathrm{LWS_m}$ data record. For estimating the recovery time for each month's deficit, which is defined as the time to recover to the average storage conditions, the empirical cumulative distribution function (eCDF) of the $\frac{\mathrm{d(WSD)}}{\mathrm{dt}}$ series was calculated for three basins, all of which follow the normal distribution according to the Kolmogorov-Smirnov (K-S) test for the whole time series (see Figure 2.2 below). The 95th percentile (two-sigma) of the normally distributed eCDF represents the maximum positive rate of change of LWSD/GWSD, and hence the minimum recovery time was obtained by dividing the LWSD/GWSD for the particular month (in mm or km^3) with 2σ value of eCDF (in mm month^{-1} or km^3 month^{-1} corresponding to figures 2.2b and 2.2d, for GWSD and LWSD, respectively). Thus derived recovery time (in months) provides a physical time scale to get back to the normal storage conditions during each drought event.

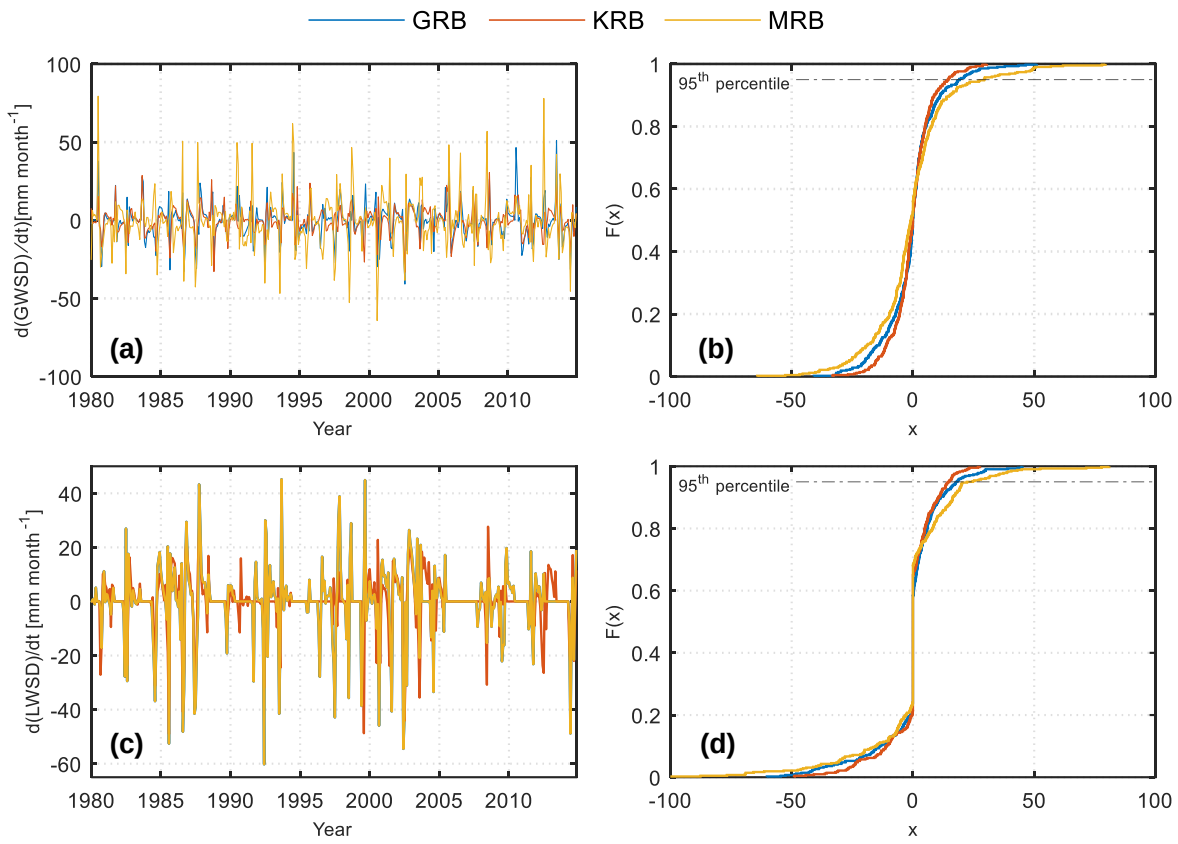

Figure 2.2. Recovery time calculation for the drought events. Left: The time derivative of monthly WSD (GWSD and LWSD) considering both positive and negative deficits. Right: empirical cumulative distribution (eCDF) of d(WSD)/dt and 95th percentile used to determine the minimum time to recovery, all for 35 years. After (Abhishek and Kinouchi, 2022).

2.2.3. Standardized Indices

A total of four types of standardized indices were utilized to assess the temporal extent and variability of the basin-scale droughts in multiple water storage or hydro-meteorological components and assess the model's potential to simulate individual WSCs. These indices include self-calibrating Palmer Drought Severity Index (sc-PDSI) (Dai et al., 2004), 12-month Standardized Precipitation Index (SPI12) (Mckee et al., 1993), normalized water storage deficit index (Abhishek et al., 2021) (WSDI; $\mathrm{WSDI_m}$ based on $\mathrm{LWS_m}$ and $\mathrm{WSDI_g}$ based on $\mathrm{LWS_g}$), and normalized groundwater drought index (Thomas et al., 2017) (GWDI; $\mathrm{GWDI_m}$, $\mathrm{GWDI_g}$, $\mathrm{GWDI_o}$). Since the contribution of the surface water component to LWS is negligible in the study area In India, SRI was not included in the analysis. Please note that the subscripts

m, g, and o represent the indices derived from the modeled, GRACE-derived, and observed in-situ data, respectively. For all WSDIs and GWDIs, the zero-mean normalization procedure was followed as below (example of GWDI):

$$\mathrm{GWDI}_{j,k} = \frac{\mathrm{GWSD}_{j,k} - \mu}{\sigma} \quad (2.7)$$

where $\mathrm{GWDI}_{j,k}$ is the normalized GW deficit index for the j^{th} year and k^{th} month, μ and σ represent the mean and standard deviation of the respective time series, respectively. Statistical parameters of Pearson correlation and Spearman's rho are calculated to analyze the linear relationships and monotonicity between various indices (Abhishek et al., 2021; Abhishek and Kinouchi, 2021).

Further details of the derivation and significance of various standardized indices are provided below.

2.2.5.1. Self-calibrating Palmer Drought Severity Index (sc-PDSI)

The self-calibrating Palmer Drought Severity Index (sc-PDSI) was used for evaluating the long-term droughts in the basins and for quantifying their association with climate change. The sc-PDSI was evaluated using the regional level water balance incorporating four inputs, namely, precipitation, air temperature, latitude, and field capacity of the underlying soil, following the open access MATLAB tool developed by (Jacobi et al., 2013). This method incorporates the two-bucket system-based water balance equation as below:

$$\mathrm{L_U} = \frac{[(\mathrm{ET} - \mathrm{P}) - \mathrm{L_S}]\mathrm{S_U}}{\mathrm{FC}} \quad (2.8)$$

where $\mathrm{L_U}$ and $\mathrm{L_S}$ are the water loss from the underlying and surface layers, respectively, ET is the average potential evapotranspiration using the Thornthwaite and Hamon PET methods (applied for avoiding any bias associated with a particular method), P and $\mathrm{S_U}$ are the precipitation and the water amount in the underlying layer, FC is the field capacity of the combined soil layers. Monthly Z-values were calculated using the water balance output and the full record as the calibration period. This method is based on the assumptions and definitions by (Alley, 1984). Firstly, a monthly water balance is calculated, followed by the calculation of the z-index and finally, the PDSI. Ls is the loss due to the evapotranspiration from the surface layer, which occurs when ET>P (evapotranspiration > precipitation) for a particular month and is assumed to be at a potential rate. $\mathrm{S_U}$ is the amount of water available

in the underlying soil layer, which determines the water loss from the layer (L_U). FC, i.e., field capacity or the available moisture capacity, is the total moisture capacity of the system. All of these parameters were calculated by the MATLAB tool, details of which can be found in (Jacobi et al., 2013). This method outperforms the traditional PDSI calculation methods in terms of sensitivity to the potential evapotranspiration (PET), computational simplicity, and transparency (Jacobi et al., 2013).

2.2.5.2. 12-month Standardized Precipitation Index (SPI12)

For the Standardized Precipitation Index, 12-months SPI (SPI12) was used for comparing the inter-and intra-basin drought conditions since shorter time SPIs are highly sensitive to the short-term precipitation fluctuations and do not reflect the multiyear droughts robustly (WMO, 2012). SPI quantifies the standardized departure of precipitation from the long-term mean using the normal distribution (transformed from gamma distribution using equal probability function) (Mckee et al., 1993). Since the short time-scaled precipitation anomalies are reflected only in the soil moisture dynamics, SPI12 was used to effectively incorporate its reflection on the integrated land water storage dynamics on the basin scale. Detailed reasoning of selecting SPI12 over other shorter time period SPI's is as below,

The 3-month (or shorter) SPIs reflect short- and medium-term moisture conditions and provide a seasonal precipitation estimation. These SPIs may lead to misinterpretation of the droughts when a temporary wet or dry period occurs (WMO, 2012). Continuous and persistent drought monitoring is imperative to accurately determine when droughts begin and end. Large negative or positive in 3-month (or shorter) SPIs may be associated with precipitation totals that are not very different from the long-term mean. This behavior becomes much more critical in the Peninsular Indian region, experiencing the high variability of the precipitation extremes due to the south Asia monsoon.

The 6-month SPI indicates seasonal to medium-term trends in precipitation and is still considered to be sensitive to the short-term extreme precipitation conditions. The 9-month SPI indicates inter-seasonal precipitation patterns over a medium timescale duration. Droughts usually take a season or more to develop (WMO, 2012), and hence may not be accurately represented by these short SPIs.

The 12-month SPI reflects long-term precipitation patterns and tends to gravitate toward zero unless a distinctive wet or dry trend is taking place. Also, the multiyear droughts resulting

from the various water storage components (even including the groundwater storage) are evident in the 12-month SPI. Moreover, the PDSI is more closely related to the 12-month SPI than the short-term SPIs (WMO, 2012). Since the main focus was to determine the long-term droughts based on the total water storage and their comparison with the other indices, keeping the above points into consideration and similar to the previous studies (e.g., (Scanlon et al., 2015), the 12-month SPI was selected for the comparison purposes.

2.2.5.3. Normalized land water storage index (WSDI)

First, water storage deficit (WSD) based drought indices for both $\mathrm{LWS_m}$ and $\mathrm{LWS_g}$ were calculated. The long-term mean of monthly $\mathrm{LWS_m}$/$\mathrm{LWS_g}$ was calculated for each month by averaging the monthly values of the $\mathrm{LWS_m}$/$\mathrm{LWS_g}$ anomaly. This climatology was then subtracted from the original time series of $\mathrm{LWS_m}$/$\mathrm{LWS_g}$ anomaly to give the water storage deficit amount in a particular month as,

$$\mathrm{WSD_{j,k}} = \mathrm{LWSA_{j,k}} - \overline{\mathrm{LWSA_k}} \quad (2.9)$$

where WSD is the water storage deficit, subscripts j and k depict the year and month, respectively, $\mathrm{LWSA_{j,k}}$ is the land water storage anomaly (based on $\mathrm{LWS_m}$ or $\mathrm{LWS_g}$) for the jth year and kth month, $\overline{\mathrm{LWSA_k}}$ represents the average monthly $\mathrm{LWS_m}$ anomaly over 35 years or $\mathrm{LWS_g}$ anomaly over 12 years. Monthly deficits (i.e., deseasonalized time series) in other modeled WS components, i.e., $\mathrm{SMS_m}$ and $\mathrm{GWS_m}$, were also calculated using Eq. 2.9.

Since the water storage deficits represented as volumetric water storage may sometimes be ambiguous in interpretation since for a given deficit volume, a smaller area will have a higher intensity of the drought than the larger area. Therefore, to eliminate the effect of the geographical area on the analyses, the volumetric WSD was further calculated as basin-wide equivalent water depth. Also, for suitability of comparative assessment and inter-comparison among the other traditional indices, WSD was normalized to get the water storage deficit index (WSDI) following zero-mean normalization procedure (Z. Sun et al., 2018);

$$\mathrm{WSDI_{j,k}} = \frac{\mathrm{WSD_{j,k}} - \mu}{\sigma} \quad (2.10)$$

where $\mathrm{WSDI_{j,k}}$ is the normalized water storage deficiency index (WSDI; $\mathrm{WSDI_m}$ based on $\mathrm{LWS_m}$ and $\mathrm{WSDI_g}$ based on $\mathrm{LWS_g}$) for the jth year and kth month, μ and σ represent the mean and standard deviation of the time series of WSD, respectively.

2.2.5.4. In-situ groundwater level data

India's Central Ground Water Board (CGWB) has been maintaining and monitoring a dense network of operational groundwater wells (>15000 in total during 2014, the study duration, which is continually increasing) in India ((Bhanja et al., 2017b; CGWB, 2017, 2014b; India-WRIS, 2012). The in-situ groundwater level is measured seasonally, i.e., four times a year during January (post-monsoon), May (pre-monsoon), August (monsoon-time), and November (post-monsoon) (Bhanja et al., 2017b). After screening the wells for temporal continuity (wells having two or more continuous gaps were precluded from the analysis) and applying the inter Interquartile range (IQR) filter (essentially for reducing outliers and partly the impact of confined aquifers) (Bhanja and Mukherjee, 2019; Davis, 2002; Long et al., 2016b), data of 1080 wells distributed in the three study basins was further used (Figure 2.1, Table 2.1). These wells comprise about 32% of piezometers and 68% of the observation/monitoring wells, and the majority (~70%) of the wells are dug wells (CGWB, 2017). Most (~88%) of the wells in the study area are located in the unconfined shallow aquifer (CGWB, 2014b).

Further, for individual wells, the long-time (from May 2002 to Nov 2014) of the groundwater level is subtracted from the time series, and then the sign is reversed for depth conversion and multiplied with the S_y value to get the groundwater storage anomaly (GWSA) associated with the particular well. The individual GWSA calculated per well was further converted to the basin-wide GWSA time series using the simple Thiessen polygon method as below,

$$\mathrm{GWSA_t} = \frac{\sum_{i=1}^{n} \mathrm{A_i} * \mathrm{GWSA_i}}{\sum_{i=1}^{n} \mathrm{A_i}} \quad (2.11)$$

where $\mathrm{GWSA_t}$ is the resulting basin-scale GWSA for month t, A_i is the area of Thiessen polygon corresponding to well i.

Most parts of central and southern India, consisting of the study basins, are composed of Pre-Cenozoic crystalline rocks, consolidated sedimentary formations, and multi-layered basalt flows of the Indian craton (CGWB, 2014b). Moreover, since all three study basins possess a uniform hydrogeological setting (both GRB and KRB are primarily composed of jointed or fractured crystalline aquifer systems and MRB is composed of fractured crystalline or consolidated and permeable sedimentary aquifers) (Bhanja et al., 2016; Dhiman, 2012), similar to previous studies (e.g., (Panda and Wahr, 2016; Rodell et al., 2009), assumption of an average value of specific yields (S_y) was made for each basin (GRB: 0.023, KRB: 0.022, MRB: 0.039) (Bhanja et al., 2016). Unlike the Indo-Gangetic Plain,

consisting of the Indus and Ganges river basins, where the hydrogeology is predominantly unconsolidated sedimentary aquifers (sandy alluvium), and the maximum groundwater table depth is about 1.7 to 2.5 times higher than the study basins (Bhanja et al., 2017b, 2016), the use of distributed specific yields is highly unlikely to improve the observed groundwater storage time series.

2.2.5.5. Groundwater Drought indices (GWDI)

Since the in-situ groundwater is available only four times a year and hence may not give a clear idea of the storage dynamics, the in-situ data was converted to the groundwater drought index. A statistical comparison of the three drought indices viz., GRACE based GWDI ($\mathrm{GWDI_g}$), $\mathrm{GWS_m}$ based GWDI ($\mathrm{GWDI_m}$), and observed GWDI ($\mathrm{GWDI_o}$) was conducted to assess the potential of PCR-GLOBWB to quantify the groundwater drought conditions. Further details of the three types of GWDI used in this chapter are explained below,

$\mathrm{GWS_m}$ based GWDI ($\mathrm{GWDI_m}$): GWDI based on the modeled groundwater ($\mathrm{GWS_m}$) was calculated using the equation,

$$\mathrm{GWDI_{j,k}} = \frac{\mathrm{GWSD_{j,k}} - \mu}{\sigma} \tag{2.12}$$

where $\mathrm{GWDI_{j,k}}$ is the normalized index corresponding to $\mathrm{GWS_m}$ for the j^{th} year and k^{th} month, μ and σ represent the mean and standard deviation of the respective time series, respectively.

Obs-GWS ($\mathrm{GWS_o}$) based GWDI ($\mathrm{GWDI_o}$): GWDI based on the observed groundwater storage was calculated using the in-situ observed GWSA time series and employing the Eq. 2.12.

GRACE-GWS based GWDI ($\mathrm{GWDI_g}$): First, GRACE based GWS ($\mathrm{GWS_g}$) was calculated using the regional water balance,

$$\mathrm{GWSA} = \mathrm{LWSA} - \mathrm{SWSA} - \mathrm{SMSA} \tag{2.13}$$

where LWSA, SWSA, and SMSA are the anomalies of the GRACE-based land water storage ($\mathrm{LWS_g}$), modeled surface water storage ($\mathrm{SWS_m}$), and modeled soil moisture storage ($\mathrm{SMS_m}$), respectively. All the water storage components were used as monthly time series. Due to the insignificant long-term trend in modeled surface water storage ($\mathrm{SWS_m}$) and the absence of snowfall events in the study region, the surface water and snow water storage components are not explicitly shown in the relevant figures. Also, similar to the previous studies (Rodell et

al., 2009), due to the inability of GRACE satellites to detect the changes in biomass, this component was also excluded from Eq. 2.13. The GRACE-based GWDI was then calculated following Eq. 2.12.

A schematic of methodology and the various research components of this chapter are shown in Figure 2.3.

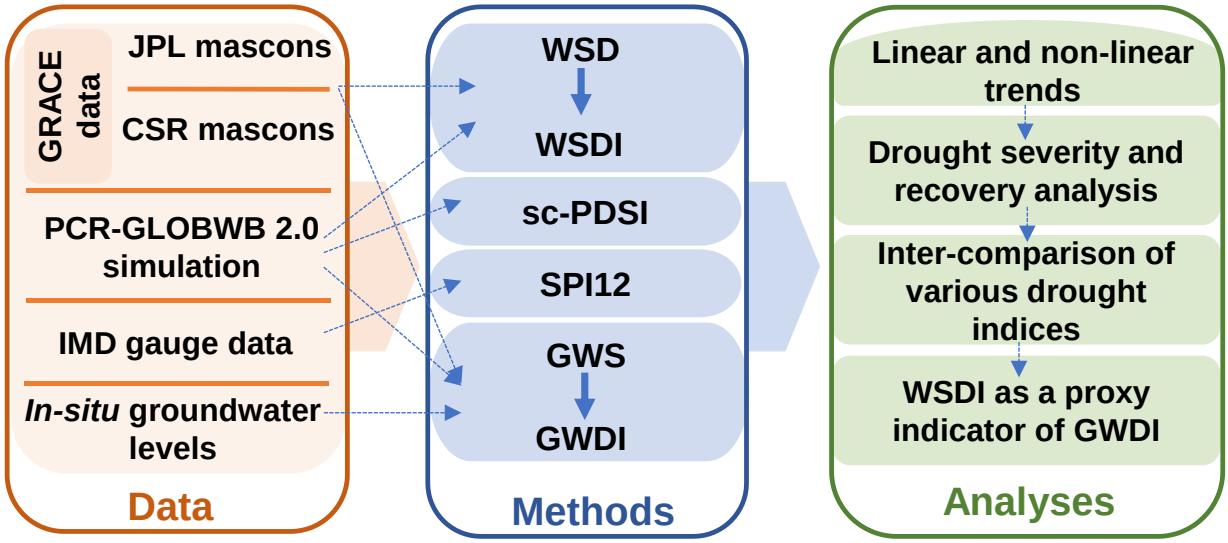

Figure 2.3. Summary of the research flow (Chapter 2). A schematic showing the outline of data sources, data types, methods used, and analysis performed in the study. After (Abhishek and Kinouchi, 2022).

2.3. Results and Discussion

2.3.1. Multidecadal Trends in WSCs

The long-term linear trends in monthly LWS_m from Jan 1980 to Dec 2014 were quantified as 0.56 mm yr^{-1}, 0.46 mm yr^{-1} and 0.26 mm yr^{-1}, which correspond to the trends in an equivalent volume of 6.13 km^3 yr^{-1}, 4.10 km^3 yr^{-1} and 1.29 km^3 yr^{-1} for GRB, KRB, and MRB, respectively. Despite stable linear trends in LWS_m, all three river basins exhibit high inter-annual variability, which can primarily be explained by the precipitation. When compared with the GRACE-based land water storage (LWS_g), the modelled LWS (LWS_m) underestimates both the declining and rising water storage during dry and wet periods, respectively, from Apr 2002 to

Dec 2014, which is consistent with the findings reported by (Scanlon et al., 2018; Xu et al., 2019). Non-linear trends estimated by means of the HP filter reveal that, in general, Krishna river basin (KRB) experienced stable dynamics of $\mathrm{LWS_m}$ and its constituent components ($\mathrm{SMS_m}$, $\mathrm{GWS_m}$) except for the extremely dry years of 1987 and 2003-2004 (Figure 2.4). GRB and MRB revealed almost similar dynamics of the various water storage components (WSCs), albeit with higher amplitudes in MRB. $\mathrm{LWS_m}$ showed a phase lag and amplitude difference from $\mathrm{SMS_m}$and $\mathrm{GWS_m}$, which are attributed to the fact that $\mathrm{LWS_m}$ combines all the WSCs, and hence the slower response of subsurface systems contributes to the existing lag, in particular, that of $\mathrm{GWS_m}$. Precipitation attains a maximum value in Jul (in GRB and KRB) or Aug (in MRB). $\mathrm{SMS_m}$ and $\mathrm{GWS_m}$ lag with a lag of 2-3 months from precipitation because of the natural process of recharge and other inherent vadose zone processes. $\mathrm{SMS_m}$ showed similar dynamics in all three basins despite high variabilities in precipitation, particularly in MRB (Figure 2.4). $\mathrm{LWS_m}$ responds strongly to the precipitation during the monsoon season (Jul-Oct), primarily following the $\mathrm{GWS_m}$ dynamics as ascertained by the deseasonalized WSCs (Figure 2.5). The decline in $\mathrm{GWS_m}$ and hence in $\mathrm{LWS_m}$ during the non-monsoon season (Nov-Jun) can be attributed to the combined impact of groundwater withdrawals for irrigation to the Rabi crops, basinal outflow, and evapotranspiration losses. Moreover, analyses of the deseasonalized and segregated WSCs revealed that the groundwater is the significant contributor to the $\mathrm{LWS_m}$ during both depletion and recovery times with dominant effects of the South Asian summer monsoon.

The climate of all three river basins is dominated by the South Asian summer monsoon, contributing about 80-85% of annual rainfall in the study region. Precipitation in the whole study region shows a seasonal variation due to this monsoon from July to October. The most pronounced fluctuations in the Mahanadi River Basin are followed by the Godavari and Krishna river basins. Groundwater storage (GWS) anomalies attain a minimum value in May/June in all three basins, which is the end of the summer season and the monsoon's onset in the region. The importance of the South Asian summer monsoon in India can be understood by the fact that even minor spatiotemporal variabilities in its annual cycle have led to some severe drought conditions. These climatic variations subsequently derive the dynamics of the surface water storage (and groundwater withdrawal), which further propagate to soil moisture and groundwater storage, and eventually reflect in the land water storage. The comparatively slower response of GW fluctuations to hydrological fluxes (precipitation

and evapotranspiration) than the near-surface WSCs imposes further stress on the replenishable limits of the groundwater withdrawals (Abhishek and Kinouchi, 2021; Rodell et al., 2009).

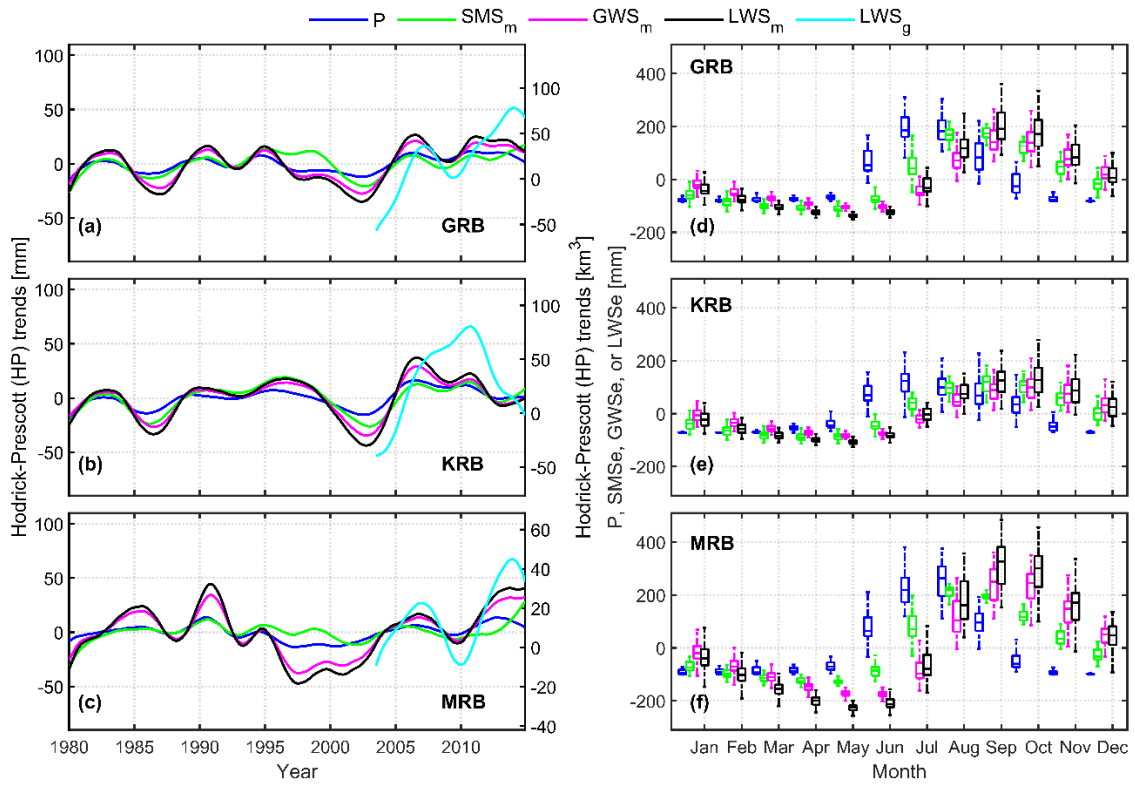

Figure 2.4. Non-linear trends and seasonal variability. (a)-(c) Non-linear (Hodrick-Prescott) trends in the anomaly time series of precipitation (P), modeled soil moisture storage (SMS_m), modeled groundwater storage (GWS_m), and modeled land water storage (LWS_m) from Jan 1980 to Dec 2014 and GRACE-derived LWS (LWS_g) from Apr 2002 to Dec 2014 for GRB (a), KRB (b), and MRB (c). (d)-(f) Box-whisker plots of P, SMS_m, GWS_m, and LWS_m anomalies in GRB (d), KRB (e), and MRB (f) from Jan 1980 to Dec 2014. The values of all the variables are shown in equivalent water depth (mm). The horizontal lines within the boxes represent the median value, the extent of the box signifies the 25th -75th percentile (inter-quartile) range of the respective data, and the lower and upper whisker limits represent the ±1 standard deviation of the individual time series. After (Abhishek and Kinouchi, 2022).

2.3.2. Estimation of Drought Severity and Recovery Time

From Jan 1980 to Dec 2014, Peninsular India has faced significant meteorological and agricultural droughts during 1987, 1997, 2002 (Mallya et al., 2015), 2004, 2009, and 2015. LWSD has signatures of all these droughts, but a distinct behavior was observed in GWSD (e.g., no groundwater deficit condition was detected in 1997 and 2009 in the KRB). Assessment of the intra-annual distribution of the monthly deficit events reveals that July is

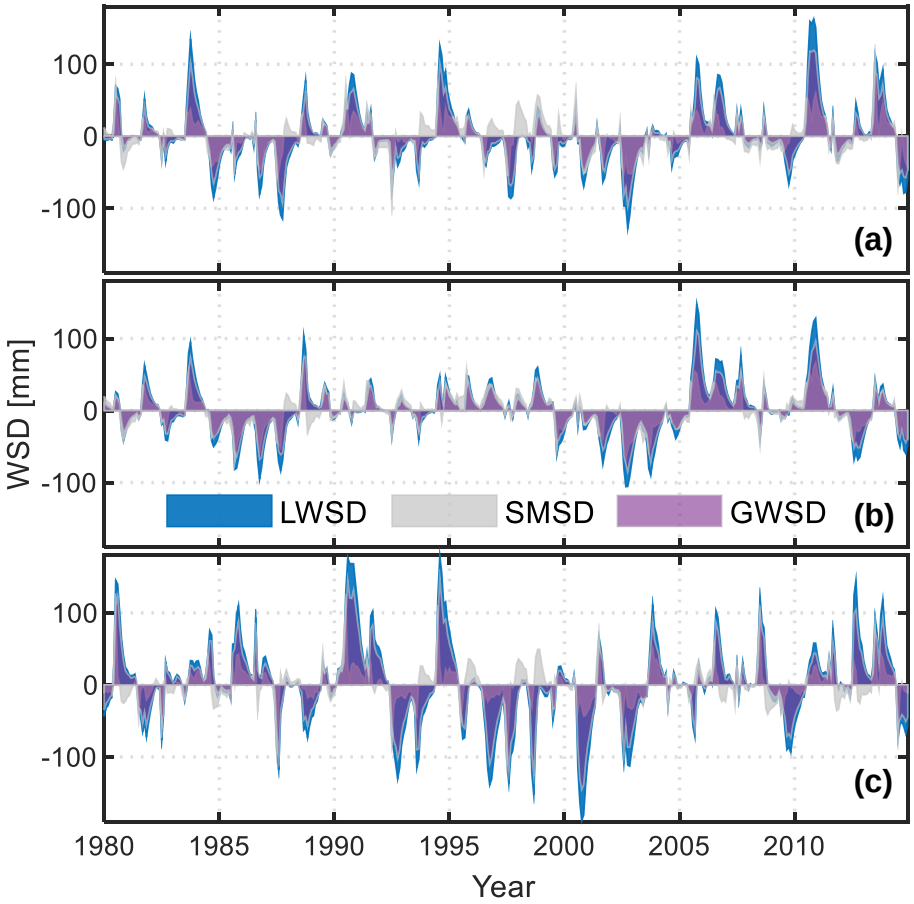

Figure 2.5. Monthly time series of water storage deficits (WSD). Water storage deficits (both depletion and recoveries, i.e., positive and negative storages) in various components ($\mathrm{LWS_m}$, $\mathrm{SMS_m}$ and $\mathrm{GWS_m}$) for GRB (a), KRB (b), and MRB (c). LWSD stands for land water storage deficit, and so on for SMSD and GWSD. This seasonal variability of the water storage deficits was calculated by removing the climatology of the respective component for 35 years from Jan 1980 until Dec 2014 (Eq. 2). After (Abhishek and Kinouchi, 2022).

the most drought-prone month for LWSD for all three basins (Figure 2.6), while for GWSD, there is no fixed pattern. To further quantify the fluctuations in $\mathrm{LWS_m}$ or $\mathrm{GWS_m}$, the monthly water storage deficits (WSD) were calculated for all basins based on Eq. 2.9 (Figure 2.6). A

period showing continuous deficit (negative value of WSD) for equal to or more than three months was classified as a single drought event, while the deficit of one or two months can be explained by the precipitation variability or any other localized activities in the region. Results reveal that all three basins witness a variable number of droughts with varying severity where MRB experienced a comparatively larger number of deficit events (LWSD/GWSD events; 18/15) compared to GRB (12/12) and KRB (13/12) (Figure 2.6). The longest and the most severe LWSD event was quantified in KRB from Aug-99 to Jun-05 (71 months) with a total and average severity of -2220 and -32 mm months and the highest land water storage deficit (LWSD) of -104 mm in Sep-02. Regarding GWSD, GRB experienced the longest and the most severe deficit spanning 84 months (Jul-99 to Jun-06) with total and average severity of -3085 and -36 mm months, and a maximum GWSD of -120 mm in Sep-04 (Figures 2.7 and 2.8). Minimum recovery time analysis estimates the time taken to reach the normal water storage ($\mathrm{LWS_m}$ or $\mathrm{GWS_m}$) conditions in the basin. The fastest recovery corresponds to 7.2/6.3, 7.3/8.17, and 8.4/4.75 months (Oct-02/Sep-04, Sep-02/Dec-04, and Oct-00/Jul-02, respectively, for LWSD/GWSD) (Figure 2.7). The cumulative time needed for the recovery of groundwater storage deficit (GWSD) reaches as high as 161 months (Jul-99 to Jun-06), 185 months (Nov-00 to Jun -05), and 43 months (Apr-09 to Apr-11) for GRB, KRB, and MRB, respectively (Figure 2.7).

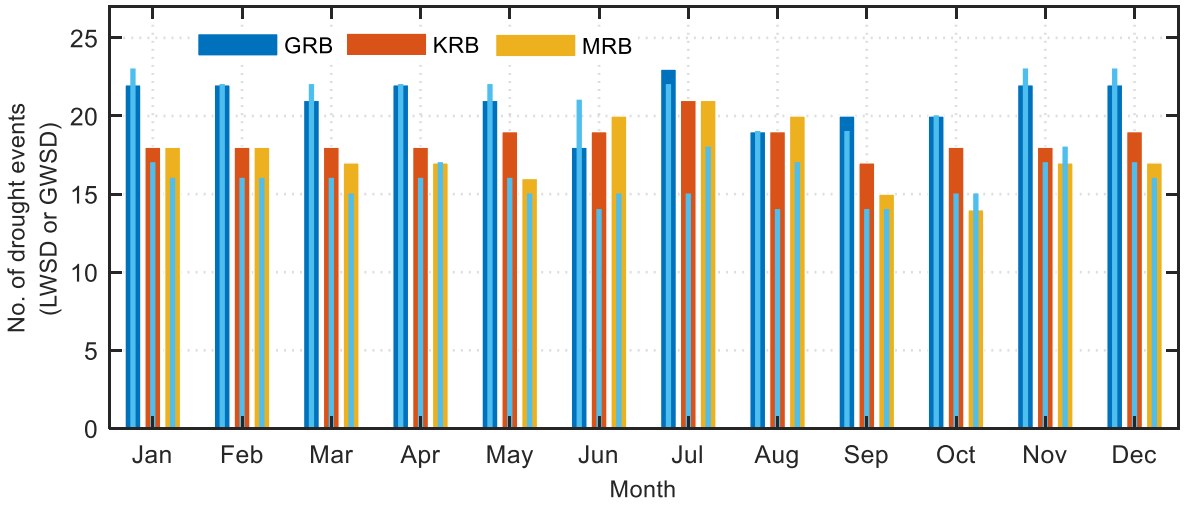

Figure 2.6. Intra-annual distribution of LWSD and GWSD. Intra-annual distribution (i.e., a monthly distribution) of land water storage deficits (LWSD) and groundwater storage deficits (GWSD) in the three river basins from Jan 1980 to Dec 2014. Colored and overlaid sky-blue

bars represent the LWSD (based on $\mathrm{LWS_m}$) and GWSD (based on $\mathrm{GWS_m}$) respectively. After (Abhishek and Kinouchi, 2022).

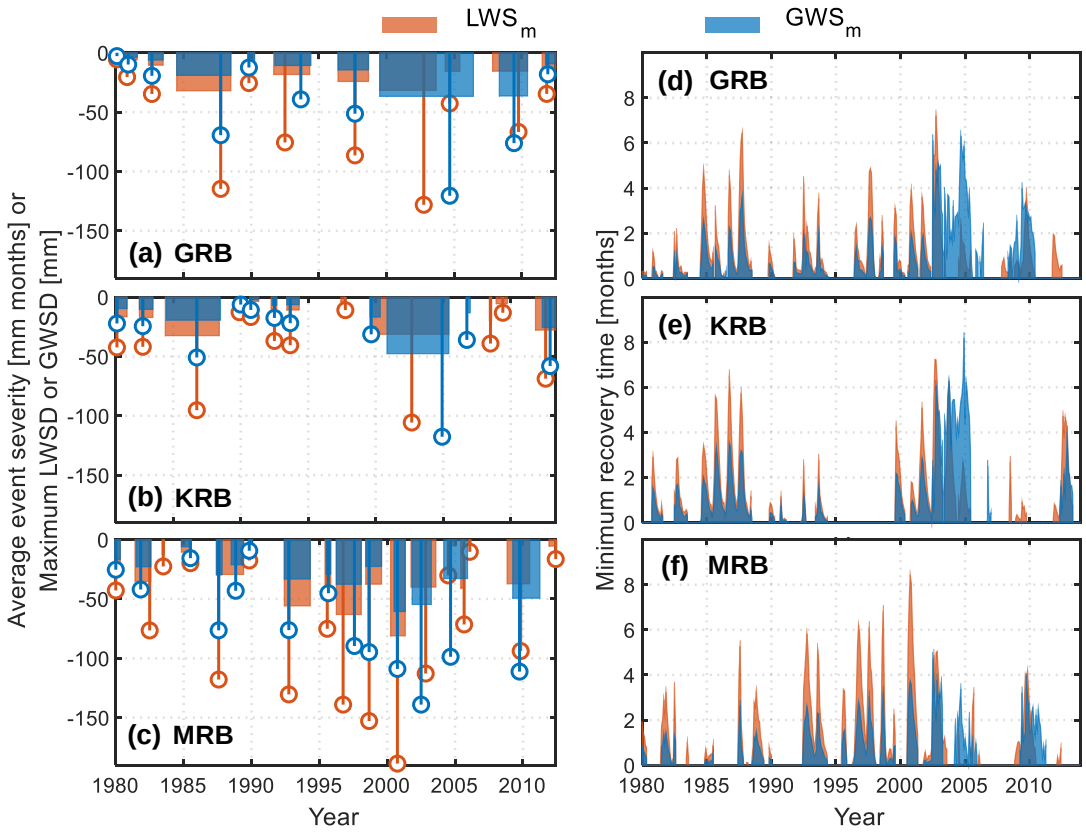

Figure 2.7. Comparison of drought severity and recovery time in $\mathrm{GWS_m}$ and $\mathrm{LWS_m}$. (a)-(c) Average event severity for the drought (deficit) events identified in $\mathrm{LWS_m}$ and $\mathrm{GWS_m}$ for GRB (a), KRB (b), and MRB (c) from Jan 1980 to Dec 2014. Maximum $\mathrm{LWS_m}$ deficits (LWSD) and $\mathrm{GWS_m}$ deficits (GWSD) are also shown by the stem plots. (d)-(f) Minimum recovery time corresponding to the monthly deficits (both LWSD and GWSD) during the study period. After (Abhishek and Kinouchi, 2022).

Occurrence of multi-year groundwater deficits as revealed by the currently employed storage-based approach and the accumulated recovery time of as long as 15 years indicate that the groundwater systems are highly vulnerable to the joint influence of the hydro-meteorological variability (e.g., rainfall) and human influences. Therefore, there is a need for maintaining a

resilient subsurface system that can continue to support local people in the study area even when severe and frequent meteorological droughts occur. Furthermore, the multidecadal analysis enables us to assess the intra-seasonal variations of GW in the region thoroughly. For example, the GWSD continued through the wet season, indicating that although there

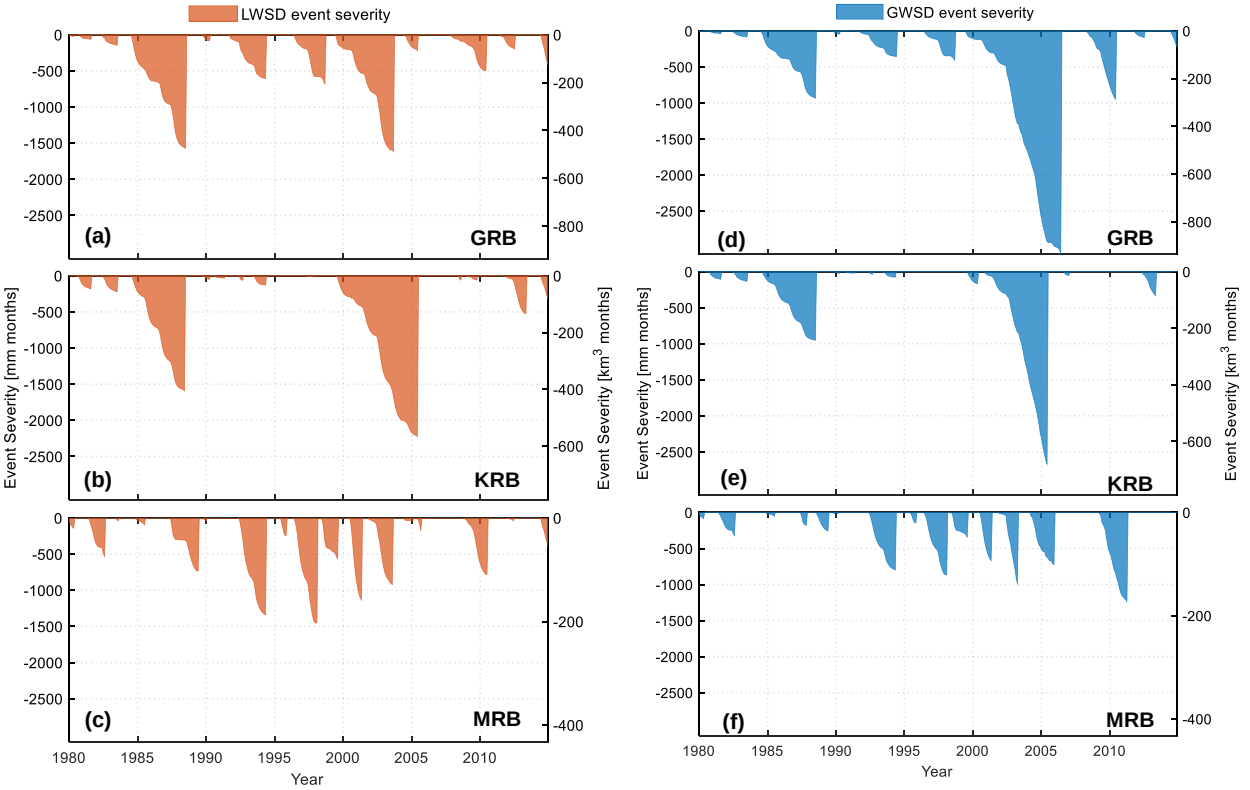

Figure 2.8. LWSD and GWSD events severity. (a)-(c) Severity (S_t) of the drought events identified based on the water storage deficits (WSD) derived from $\mathrm{LWS_m}$ (i.e., LWSD) for the (a) Godavari, (b) Krishna, and (c) Mahanadi river basins. (d)-(f) Severity (S_t) of the drought events identified based on the water storage deficits (WSD) derived from $\mathrm{GWS_m}$ (i.e., GWSD) for the (a) Godavari, (b) Krishna, and (c) Mahanadi river basins. Event Severity (S_t) (mm months or km^3 months) is equivalent to the cumulative $\mathrm{LWS_m}$/$\mathrm{GWS_m}$ deficit during the given drought period. After (Abhishek and Kinouchi, 2022).

may be sufficient surface water, the deficiency in groundwater (GW) is still continuing, albeit invisible. The majority of the water storage deficits do not attain peaks from Apr to Jun even when there is low precipitation, which is because the minimum anomaly of $\mathrm{LWS_m}$ (largest

negative LWSD) is quite stable over the study period, while the maximum anomaly changes a lot from year to year, mainly depending on the amount of net precipitation flux. This storage-based assessment of groundwater droughts offers the potential to develop efficient drought-monitoring and -forecasting systems under sustainable and conjugative water utilities. Moreover, the different patterns of frequency and severity of groundwater droughts among the basins suggest employing the season-independent site-specific drought mitigation approach.

2.3.3. How Well Does WSDI Compare with sc-PDSI and SPI12?

The long-term general behavior of water storage deficit index based on modelled LWS ($\mathrm{WSDI_m}$) agreed well with sc-PDSI and SPI12, classified as per Table 2.2, in all three basins (Figure 2.9). All the indices are linearly correlated (Pearson correlation r>0) and show similar monotonic behavior (Spearman's rho, ρ>0). Both r and ρ are higher between $\mathrm{WSDI_m}$ and sc-PDSI than those between $\mathrm{WSDI_m}$ and SPI12 for all the basins (Tables 2.3 and 2.4). This behavior is because the calculation of sc-PDSI, unlike SPI12, involves both the meteorological and hydrological variables and takes the regional water balance into account while $\mathrm{WSDI_m}$ includes the integrated water storage. The linear correlation, as well as the rank correlation amongst the drought indices, is stronger in the case of the Godavari (GRB) and Krishna (KRB) river basins as compared to the Mahanadi river basin (MRB) primarily attributable to the comparatively smaller basin area of MRB where the lateral fluxes may have induced uncertainties in the estimation of various WSCs, which subsequently propagated in the calculation of the different indices.

Interestingly, all peaks in the severe or extreme drought events (classified as per Table 2.2) based on $\mathrm{WSDI_m}$occurred in Sep-Oct when the study region received the above-average rainfall and witnessed minimal groundwater extraction as a result of the monsoon. This behavior of peak deficits ascertains that the area has suffered from a prolonged deficiency in integrated water storage. Although the monsoon rainfall may have quickly replenished the (near)-surface water deficiency, the water fluxes' cumulative balance could not be attained primarily due to the prolonged persistence of GWSD. On the contrary, the peak deficits of water storage in the events of less severity and small duration occur throughout the year with no characteristic pattern. This behavior can be explained by the individual or combined effects

of localized heterogeneous rainfall events, climatic shifts in particular years, and perturbations due to human activities (groundwater abstractions) in the specific region.

In general, the classification of the drought events with high severity agreed well amongst the three drought indices than the events with less severity (Table 2.4). For example, the longest drought event, which lasted for 71 months in KRB, was classified as a severe drought (D3) by both sc-PDSI and $\mathrm{WSDI_m}$ and as extreme drought (D4) by SPI12 (Table 2.4). Likewise, almost all the major drought events differed in their classification by a maximum of one level among the three indices, and the maximum difference in the levels was two for other drought events. Overall, given the spatiotemporal continuity, the integrated response from natural climate variability or anthropogenic intervention, and a simple but robust approach that is free from any physical model uncertainties, $\mathrm{WSDI_m}$ outperformed the conventional indices, with few instances of minor variations amongst various indices essentially arising from the definition of $\mathrm{WSDI_m}$. A more detailed and explicit discussion of the observed variations among various indices is as below.

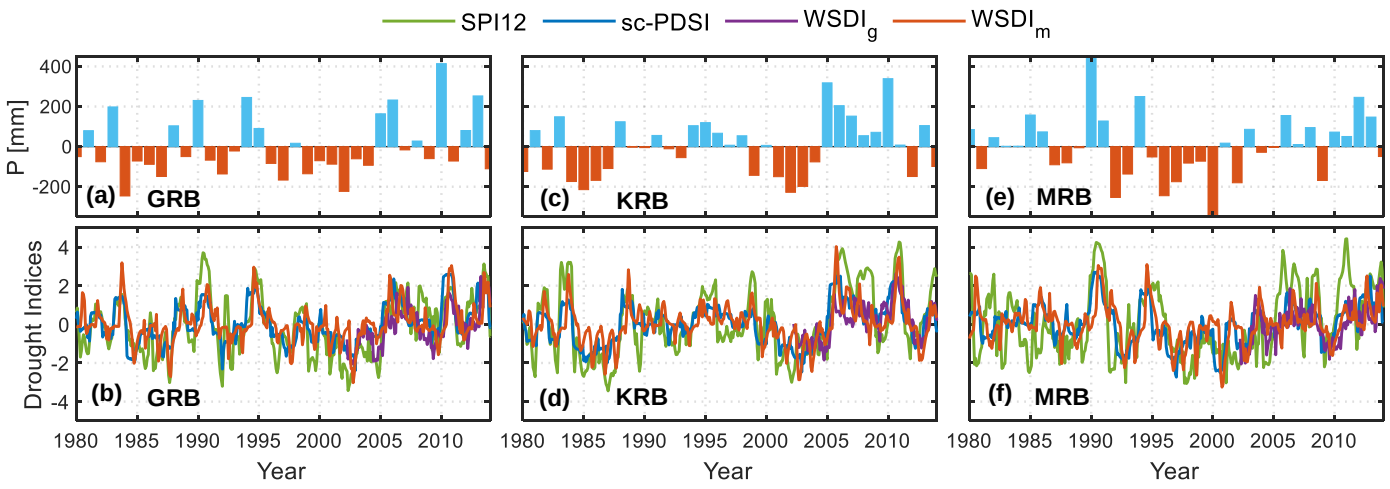

Figure 2.9. Comparison of WSDI with traditional drought indices. Anomaly time series of precipitation and various drought indices (sc-PDSI, SPI12, $\mathrm{WSDI_m}$, and $\mathrm{WSDI_g}$ for GRB (a, b), KRB (c, d), and MRB (e, f). After (Abhishek and Kinouchi, 2022).

Table 2.2. Drought classification criteria. Drought categorization criteria of the drought events based on various drought indices. After (Abhishek and Kinouchi, 2022).

Drought category	Drought condition	SPI12	sc-PDSI	WSDI
D0	No drought	-0.5 < S	-1.0 < P	0 < W
D1	Mild drought	-1.0 < S ≤ -0.5	-2.0 < P ≤ -1.0	-1.0 < W ≤ 0
D2	Moderate drought	-1.5 < S ≤ -1.0	-3.0 < P ≤ -2.0	-2.0 < W ≤ -1.0
D3	Severe drought	-2.0 < S ≤ -1.5	-4.0 < P ≤ -3.0	-3.0 < W ≤ -2.0
D4	Extreme drought	S ≤ -2.0	P ≤ -4.0	W ≤ -3.0

S, P, and W represent SPI12, sc-PDSI, and WSDI, respectively.

Table 2.3. Intercomparison of various drought indices. Pearson correlation of the drought indices of the three study basins. Spearman's rho is also shown in parentheses. After (Abhishek and Kinouchi, 2022).

	Godavari River Basin (GRB)			Krishna River Basin (KRB)			Mahanadi River Basin (MRB)		
Index	sc-PDSI	SPI12	$WSDI_m$	sc-PDSI	SPI12	$WSDI_m$	sc-PDSI	SPI12	$WSDI_m$
sc-PDSI	–			–			–		
SPI12	0.77 (0.79)	–		0.76 (0.77)	–		0.63 (0.59)	–	
$WSDI_m$	0.62 (0.58)	0.59 (0.56)	–	0.69 (0.67)	0.63 (0.60)	–	0.54 (0.49)	0.38 (0.30)	–

$WSDI_m$ does not capture the local short-term drought events that might have occurred due to the climatic variations. For instance, the drought event from Sept-91 to May-94 in the GRB is classified as extreme (D4) based on SPI12, which is based only on precipitation but is classified as moderate (D2) by $WSDI_m$ (Table 2.4). During this period, the rainfall was consistently decreasing compared to the baseline, but the overall deficit in the region could not be much severe, thus making the difference in drought levels identified by two indices. The event severity was maximum for the LWSD events categorized as severe to extreme

(defined as per Table 2.2), with two events in each of the GRB and KRB and three events in the MRB (Table 2.4). The event severity of these events is -1570 mm months and -1614 mm months in the GRB, -1590 mm months, and -2220 mm months in the KRB, and -1340 mm months, -1451 mm months, and -1137 mm months in the MRB (Figures 2.7 and 2.8, Table 2.4).

The drought event in MRB (Apr-00 to May-01) with the severity of -1135.25 mm months is classified as extreme drought (D4) based on $\mathrm{WSDI_m}$ and SPI12 even though the severity is much smaller than other drought events categorized as D3 or D4 in the basins. For $\mathrm{WSDI_m}$, this observation can be explained because the drought category is primarily depending on the minimum water storage conditions and not on the severity of the event. For SPI12 classification, the difference can partially be attributed to the varying scale and shape parameters of gamma distribution with rainfall records and partially to the fact that SPI12 primarily depends on the 12-month averaging precipitation and not on the integrated water resources.

Table 2.4. Comparison of LWSD based WSDI with sc-PDSI and SPI12. Summary of the drought events in the three river basins identified from the time series of LWSD (i.e., $WSDI_m$). The drought category is determined based on Table 2.2. Drought events characterized as D3 or D4 by at least two indices are shown in bold fonts. The drought category based on $WSDI_g$ is also shown in parenthesis for the period from Apr 2002 to Dec 2014. After (Abhishek and Kinouchi, 2022).

Godavari River Basin (GRB)

Duration (months)	Period	Drought Category		
		sc-PDSI	SPI12	WSDI
5	Jan-80 to May-80	D1	D0	D1
11	Oct-80 to Aug-81	D1	D1	D1
14	Jun-82 to Jul-83	D1	D1	D1
49	**Jul-84 to Jul-88**	**D3**	**D3**	**D3**
7	Oct-89 to Apr-90	D0	D0	D1
33	Sep-91 to May-94	D3	D4	D2
28	Jun-96 to Sep-98	D2	D3	D3
51	**Jul-99 to Sep-03**	**D3**	**D4**	**D4**
14	May-04 to Jun-05	D2	D1	D2 (D2)
32	Nov-07 to Jun-10	D1	D2	D2 (D2)
13	Jul-11 to Jul-12	D1	D1	D1 (D2)
7	Jun-14 to Dec-14	D1	D1	D2 (D1)

Krishna River Basin (KRB)

Duration (months)	Period	Drought Category		
		sc-PDSI	SPI12	WSDI
11	Oct-80 to Aug-81	D2	D2	D2
13	Jul-82 to Jul-83	D2	D2	D2
49	**Jun-84 to Jun-88**	**D3**	**D4**	**D3**
6	Nov-89 to Apr-90	D0	D1	D1
9	Sept-90 to May-91	D0	D0	D1
6	Apr-92 to Sep-92	D1	D0	D2
12	Jun-93 to May-94	D1	D0	D2
5	Jun-97 to Oct-97	D0	D0	D1
71	**Aug-99 to Jun-05**	**D3**	**D4**	**D3**
3	Jun-08 to Aug-08	D0	D0	D2 (D1)
11	Dec-08 to Oct-09	D1	D0	D1 (D1)
19	Nov-11 to May-13	D1	D2	D2 (D2)
7	Jun-14 to Dec-14	D0	D1	D2 (D1)

Mahanadi River Basin (MRB)

Duration (months)	Period	Drought Category		
		sc-PDSI	SPI12	WSDI
5	Jan-80 to May-80	D0	D0	D1
15	Jun-81 to Aug-82	D0	D1	D2
3	Jun-83 to Aug-83	D0	D0	D1
9	Nov-84 to Jul-85	D2	D0	D1
25	Jun-87 to Jun-89	D2	D1	D3
3	Nov-89 to Jan-90	D0	D0	D1
24	**Jun-92 to May-94**	**D3**	**D3**	**D3**
6	Jun-95 to Nov-95	D0	D1	D2
23	**Apr-96 to Feb-98**	**D3**	**D4**	**D3**
15	Jun-98 to Aug-99	D2	D2	D3
14	**Apr-00 to May-01**	**D3**	**D4**	**D4**
23	Oct-01 to Aug-03	D2	D2	D2
8	Jul-04 to Feb-05	D2	D1	D1 (D2)
4	Jun-05 to Sep-05	D0	D0	D2 (D1)
3	Jan-06 to Mar-06	D0	D0	D1 (D1)
21	Nov-08 to Jul-10	D2	D2	D2 (D2)
7	Dec-11 to Jun-12	D0	D0	D1 (D1)
7	Jun-14 to Dec-14	D2	D0	D2 (D1)

The larger fluctuation and amplitude with some sharp peaks and troughs in 12-month standardized precipitation index (SPI12) than in self-calibrating Palmer Drought Severity Index (sc-PDSI) and $\mathrm{WSDI_m}$ can be attributed directly to the monthly variations in rainfall. The similar time variations in sc-PDSI and $\mathrm{WSDI_m}$ are mainly attributed to the subsurface hydrological processes with a dampened response, leading to a slight difference in drought categories identified by the two indices. The inherent governing physical mechanisms and algorithms employed in each drought index result in the difference in the identified drought level. In calculating sc-PDSI and SPI12, the water fluxes within a limited soil depth and a single meteorological variable, i.e., precipitation, are respectively used while some critical hydrological components are neglected, leading to the biased evaluation of the hydrological fluxes. On the contrary, the actual drought conditions in a region are derived by more inclusive dynamics of the basin-scale hydrologic system. For the Indian scenario, where the extraction and voluminous use of groundwater are highest in the world with an annual rate of 230 km^3, $\mathrm{WSDI_m}$ seems to be better than the traditional indices in predicting and assessing the severity of drought events. Therefore, $\mathrm{WSDI_m}$ is considered to outperform the conventional indices for manifold reasons: a) it integrates the surface and subsurface water storages and thus portrays a holistic picture of water storage dynamics, b) it includes more straightforward and transparent numerical and statistical computations, c) it represents the near real-time and most accurate measurements over the study region which is not valid in case of indices derived from the data from the limited hydro-meteorological stations, d) it depicts the continuity of the temporal dynamics of the water storage.

Further, $\mathrm{WSDI_g}$ is in good agreement with $\mathrm{WSDI_m}$ from Apr-02 to Dec-14 (Figure 2.9). Statistical comparison between the two indices showed a strong correlation (r = 0.66, 0.74, and 0.62 for GRB, KRB, and MRB, respectively). Moreover, $\mathrm{WSDI_g}$ showed a higher correlation than $\mathrm{WSDI_m}$ with sc-PDSI and SPI12 in all the basins (except for SPI12 in MRB), because GRACE records the real-time data and is free from any atmospheric or model uncertainties in $\mathrm{LWS_m}$ induced by the model's physical structure. A maximum of one level of difference can be seen in the drought category of the two indices ($\mathrm{WSDI_g}$ and $\mathrm{WSDI_m}$) for the drought events post-Apr 2002 (Table 2.4), which can be attributed to the coarse resolution of GRACE data and uncertainties in climate forcing parameters, limited adequacy of the model structure. The qualitative behavior of $\mathrm{WSDI_g}$ and the traditional indices, i.e., sc-PDSI and SPI12, are similar to the results reported by (Z. Sun et al., 2018).

2.3.4. Characterizing GWDI and Potential of WSDI as a Proxy for GWDI

For characterizing the temporal variations of groundwater and validating the model output, three groundwater storage anomaly series, viz., GWS_m (modeled), GWS_g (GRACE-derived), and GWS_o (in-situ observed), were compared in terms of the standard deviation (representing the amplitude of their variations), correlation, and centered root mean square (RMS) difference (Figure 2.10). Both GWS_m and GWS_g have large standard deviations (GWS_g: 81.18, 90.9, and 101.90 mm; GWS_m: 68.04, 54.36, and 103.32 mm) compared to GWS_o (28.91, 38.81, and 40.23 mm) for all three basins. Further, to assess the potential of $GWDI_m$, three normalized groundwater drought indices were inter-compared to quantify the groundwater drought conditions. Qualitatively, all three indices show similar phase variations. $GWDI_m$ compared favorably well with $GWDI_o$ showing a similar seasonal dynamic with maxima and minima occurring in Aug (monsoon season) or Nov (post-monsoon season), and in May (pre-monsoon or summer season), respectively (Figure 2.11). However, sporadically high and sharp amplitude difference is observed probably because of the loss of GW to deep aquifers, short but heavy rainfall events, the influence of direct intrusion of floodwater to the open wells, lateral inflow and outflow to the groundwater, and the response lag compared to the GRACE real-time records (Long et al., 2016b; Panda and Wahr, 2016; Rodell et al., 2007). GWS_o and GWS_g records (with data processing uncertainties and partly biased by the inherent uncertainties in SMS_m) represent the actual groundwater storage, and hence the derived indices are close to each other and smoother than $GWDI_m$. Furthermore, the scatter plots indicate a good agreement between $GWDI_g$ and $GWDI_o$ (almost following the 1:1 line) in all three basins, while $GWDI_m$ shows more diffused plots against $GWDI_o$ (Figure 2.11 (a)-(c) inset). $GWDI_o$ has a strong correlation ($r=0.75–0.80$, $p<0.0001$) with $GWDI_g$ and moderate correlation ($r\sim0.50$, $p<0.001$) with $GWDI_m$, attributed to the reason that the changes in GWS_m estimated by the dynamic equilibrium of the five-module setup of PCR-GLOBWB are not as direct as those captured by GRACE and in-situ observations.

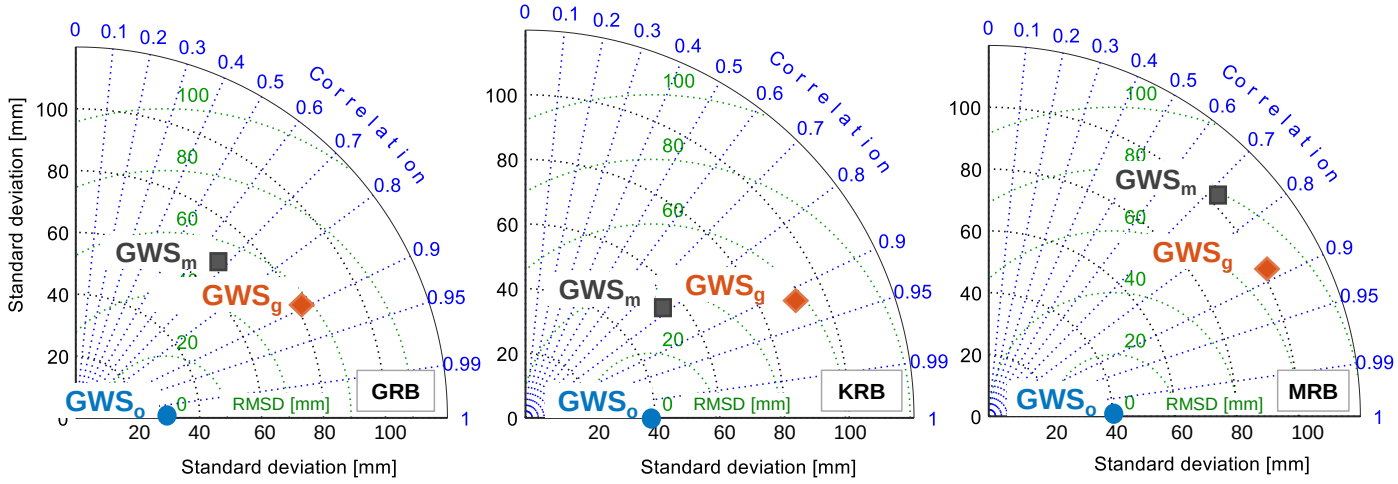

Figure 2.10. Comparison of $\mathrm{GWS_m}$, $\mathrm{GWS_g}$, and $\mathrm{GWS_o}$. Taylor diagram showing the pattern statistics between $\mathrm{GWS_o}$ (taken as reference time series in this study) with $\mathrm{GWS_m}$ and $\mathrm{GWS_g}$ for Godavari, Krishna, and Mahanadi river basins starting from the left. Here, the radial distance (black dotted arcs) denotes the standard deviation of $\mathrm{GWS_m}$ and $\mathrm{GWS_g}$ and is compared with that of $\mathrm{GWS_o}$ on the horizontal axis. The position of the $\mathrm{GWS_m}$ and $\mathrm{GWS_g}$ with respect to $\mathrm{GWS_o}$, as displayed by blue dotted lines, represents the correlation between the two datasets. The centered root mean square difference (RMSD) between any of the two datasets is proportional to the distance between them (measured along the dotted green arcs). After (Abhishek and Kinouchi, 2022).

Lastly, good agreement of $\mathrm{WSDI_g}$ with $\mathrm{GWDI_g}$ (r=0.63–0.70, ρ=0.65–0.69, p<0.0001) and $\mathrm{GWDI_o}$ (r=0.53–0.66, ρ= 0.47–0.71, p<0.0001) highlights the potential of $\mathrm{WSDI_g}$ as a proxy indicator to assess the groundwater drought situation in the region (Figure 2.11). Furthermore, lagged correlation between $\mathrm{WSDI_g}$ and $\mathrm{GWDI_g}$ is maximum with r = 0.82, 0.84, and 0.78 at a lag of one month. Hence, it is inferred that the $\mathrm{WSDI_g}$ can be used to monitor the groundwater (with a lead time of one month, i.e., land water storage (LWS) at i^{th} month can be used to represent GWS at $i+1^{th}$ month) as well as the land water storage-based drought conditions in real-time using the GRACE satellite observations, thus eliminating the need for any complex model simulations.

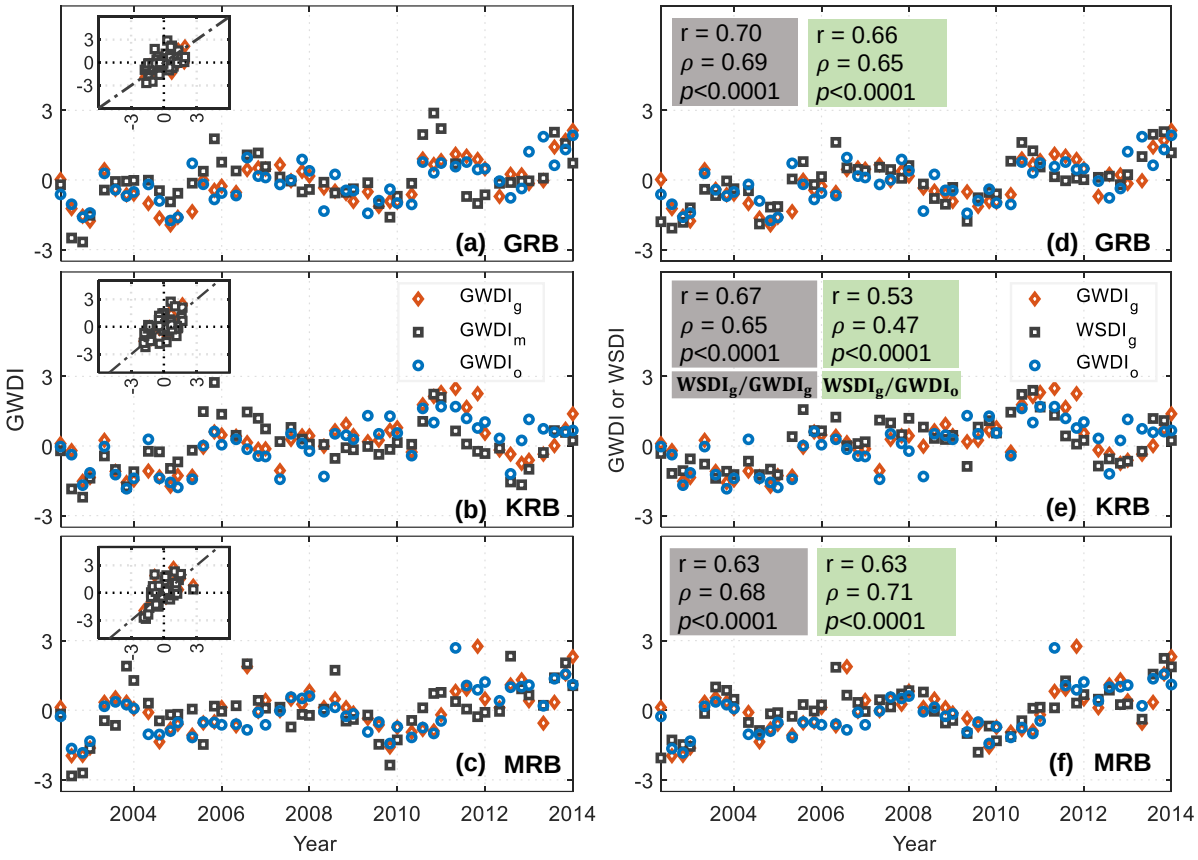

Figure 2.11. Comparison of various GWDIs. (a)-(c) Groundwater drought indices derived from GRACE-based GWSA ($\mathrm{GWDI_g}$), from $\mathrm{GWS_m}$ based GWSA ($\mathrm{GWDI_m}$), and calculated using the in-situ well data ($\mathrm{GWDI_o}$) for the GRB (a), KRB (b), and MRB (c) from May 2002 to Jan 2014. The GWDI time series are denoted four times a year (Jan, May, Aug, and Nov) when the observed GWS records are available. Scatter plots of $\mathrm{GWDI_g}$ and $\mathrm{GWDI_m}$ with $\mathrm{GWDI_o}$ for all three river basins is also shown in the insets. The 1:1 lines are also shown with dashed black lines. (d)-(f) Comparison of $\mathrm{WSDI_g}$ with $\mathrm{GWDI_g}$ and $\mathrm{GWDI_o}$ for the GRB (d), KRB (e), and MRB (f). Pearson correlation coefficient (r), Spearman rho (ρ), and p-values for $\mathrm{WSDI_g}$ and $\mathrm{GWDI_g}$ (grey boxes), and $\mathrm{WSDI_g}$ and $\mathrm{GWDI_o}$ (light green boxes) are also shown for the three river basins. After (Abhishek and Kinouchi, 2022).

2.3.5. Inferences for the Sustainable Groundwater Utilities in the Study Region

The high impact of the South Asian monsoon rainfall on the regional groundwater resources and the recovery time analysis highlights the need for employing a conjunctive water management strategy in the region. In India, similar to other areas of high dependency on

groundwater, the groundwater withdrawals increase during the drought years to meet the various water demands. After drought years, the near-surface components recover quickly by the seasonal increase in the influx (i.e., net precipitation), but the groundwater storage retains the deficits longer. It is believed that the decadal dynamics of the groundwater storage and the analysis of severity and recovery time of various groundwater drought events will help foster the discussion for the sustainable use of the prevailing groundwater in the region. For policy recommendation, constituting a Liaison Committee of multiple ministries and stakeholders for recognition and promoting the sound hydrological cycles and formulation and implementation of revitalization plan will likely lead towards a water-sustainable area because these members are expected to be inefficient while working independently.

To ensure freshwater availability across the country and reduce the farmer's dependency on highly heterogeneous monsoon, India's National Water Development Agency has undertaken the Interlinking of Rivers (ILR) project. Out of the 16 links under the Peninsular Indian region, the Mahanadi Godavari link is the first and critical link of the nine link systems of Mahanadi-Godavari-Krishna-Pennar-Cauvery-Vaigai-Gundar of National Perspective Plan under the ILR project. The southern peninsular component will contribute to an estimated 30 million hectares of irrigation by surface water (Department of Water Resources, n.d.). Apart from aiding various auxiliary sectors like pollution control, navigation, and power generation, the ILR project will reduce the stress on the prevailing groundwater resources and mitigate the impacts of hydrological extremes by ensuring homogeneous accessibility and equity in water distribution.

Various WSC simulations by the global hydrological models have been reported to underestimate the trends (Abhishek and Kinouchi, 2021; Scanlon et al., 2018), and the three basins are revealed to witness frequent water deficit conditions in the recent times. Therefore, in the next Chapter, the more recent dynamics and variability in the various water storage components in the same Peninsular river basins is explicitly analyzed. Moreover, using the basin average aquifer properties (specific yield and specific storage) for calculating the observed groundwater storage might have included some uncertainties which needed to be explicitly dealt with.

Regarding the global hydrological model, it should be calibrated with the ground data, wherever available (e.g., soil moisture (López et al., 2017) discharge data (Sutanudjaja et al., 2014))(López et al., 2017; Sutanudjaja et al., 2014)(López et al., 2017; Sutanudjaja et al., 2014), and the performance should be further analyzed statistically for the study region into consideration. The PCR-GLOBWB model was chosen just for the demonstration purposes of how well we can understand the dynamics and variability of land storage and its constituent components beyond the GRACE period and subsequently assess the capability of land water storage (whether $\mathrm{LWS_g}$ or $\mathrm{LWS_m}$) to depict the near-real-time groundwater situation in the region. Also, the applicability of the model as an auxiliary data source for GRACE-based water storage estimation can further be characterized either using more recent satellite datasets of soil moisture (e.g., SMAP; Soil Moisture Active Passive), land water storage (e.g., Swarm (Richter et al., 2021)), among others. Additionally, the advancements towards hyper-resolution global water resource modeling and improved methods of satellite gravimetry may further enhance our understanding of the various regional and global hydrological systems.

2.4. Conclusions

Herein, the multidecadal (1980-2014) trends (linear and non-linear) in various water storage components (WSCs) were analyzed, dynamics of deseasonalized water storage deficits, and drought characterization in terms of magnitude, duration, severity, and recovery time, with an explicit focus on groundwater.

Key findings of the study are summarized as below:

1. PCR-GLOBWB model is largely suitable for quantifying individual and integrated WSCs in a region and subsequent decadal droughts assessment for the period beyond GRACE records, especially prior to April 2002.
2. Contrary to the near-surface storage components, the commonly invisible groundwater storage (GWS) showed a slow but persistent response (longest deficit period spanning ~6 years) to the seasonal variations of the hydrological fluxes and remained the major contributor to land water storage (LWS).
3. The observed behavior of occurrence of all of the severe to extreme drought events highlights the region's vulnerability to drought conditions even in the monsoon season.

This behavior, combined with the recovery time analysis, will help understand the temporal propagation of groundwater deficits and take precautionary measures to prevent overexploitation.

4. LWS-based water storage deficit index (WSDI) holistically characterizes the drought intensity in a particular region owing to its independence from the geographical area. It enables us to quantify the integrated water deficit below average conditions, unlike the conventional indices where only a few hydro-meteorological components are included, and therefore it is useful in efficient drought monitoring.

5. GRACE based $\mathrm{WSDI_g}$ agrees favorably well (similar dynamics and high correlation (r=0.53–0.70) with the GRACE-based and in-situ observed well-data based groundwater deficit indices ($\mathrm{GWDI_g}$ and $\mathrm{GWDI_o}$, respectively), highlighting the potential of the remotely sensed WSDI as a quick proxy of groundwater with a lead time of one month, thus eliminating the need for the groundwater storage simulations in data-scarce river basins globally, which otherwise is quite complex and may inevitably possess high uncertainties.

In areas like India, where there is a current lack of a real-time integrated drought monitoring framework for reference, the present study will help better understand long-term systemic changes in the hydrological system. This study will provide the blueprint for the comprehensive characterization of drought events using WSDI, and the current approach can subsequently be utilized to understand the basin-scale dynamics of the water resources and subsequent effective and efficient water resources management and policymaking, especially in the data-scarce or data-limited river basins globally.

The multidecadal changes studied in this chapter are retrained until the year 2014, highlighting a need for the more recently emerging assessment of the trends and variability (annual as well as seasonal) in the study regions where the water scarcity is continually growing. Moreover, since the model outputs tend to underestimate the terrestrial water storage trends, only soil moisture (up to a depth of 200 cm) and surface water storage components were further utilized from the model. The potential of the GRACE derived groundwater storage further needs to be examined considering more detailed aquifer properties, such as, discrete specific yield and specific storage correspond to each well, unlike those used as basin averaged (distributed) in this chapter.

Chapter 3

Emerging Trends and Seasonal Variability in Water Storage Components in India

This chapter has been adapted from Abhishek and Kinouchi, 2021.

Abhishek, Kinouchi, T., 2021. Synergetic application of GRACE gravity data, global hydrological model, and in-situ observations to quantify water storage dynamics over Peninsular India during 2002–2017. J. Hydrol. 596, 126069. https://doi.org/10.1016/j.jhydrol.2021.126069

3. Emerging Trends and Seasonal Variability in Water Storage Components in India

3.1. Motivation

A significant number of studies have been conducted to quantify the dynamics of TWS and water fluxes on various spatial and temporal scales (Chen et al., 2019; Richey et al., 2015; Rodell et al., 2018; Scanlon et al., 2018, among others) highlighting the manifold socio-economic problems and deteriorating water availability conditions primarily governed by the global climate change and population growth (Schewe et al., 2014). In particular, the Indian subcontinent is identified as a future global hot spot of water scarcity and food insecurity (Wheeler and Von Braun, 2013) because of the sharp decline in per capita water availability from 5410 m^3 in 1951 to 1614 m^3 in 2011 (UNICEF et al., 2013). Furthermore, projected water requirements for producing 250 million metric ton of food by 2050 and the existing high percentage of agricultural water consumption (~85% of the freshwater resources) (Douglas et al., 2006) underscore the need for investigating water storage dynamics to assist policymakers in adopting sustainable water management strategies. Even minor variations in the annual cycle of the South Asian summer monsoon, which accounts for ~80% of the country's annual rainfall, have caused century-scale drought events (e.g., 2002 and 2009 droughts), costing billions of dollars to the overall economy (Hazra et al., 2013; Webster et al., 1998).

While the groundwater table has been continuously depleting in Northern India, the overexploitation of aquifers has more recently shifted towards the Peninsular and coastal plains and followed by the subsequent water scarcity problems triggered by fluctuating monsoon rainfall (Kumar et al., 2005; Tiwari et al., 2009; Mallya et al., 2015). Currently, the river basins in Peninsular India are moderate to severely non-resilient to the hydro-climatic perturbations, which are likely to increase in the near future amid climate change and increasing human-induced stresses on the water resources (Sharma and Goyal, 2018). Therefore, the basin-scale comprehensive quantification of various water storage components and the subsequent assessment of the controlling factors are imperative for better aquifer management and mitigation strategies for sustained crop production, sustainable ecosystem functioning, and formulation of new water policies and up-gradation or installation of new infrastructure under hydrological extremes (droughts and floods),

ensuring the timely, equitable, and adequate water share among the habitants. There have been a few studies dealing with the GRACE based assessment of the various water storage components followed by validation with the ground data globally, e.g., High Plains Aquifer, USA (Strassberg et al., 2007), Mississippi river basin, USA (Rodell et al., 2007), Bangladesh (Shamsudduha et al., 2012) and in some Indian parts, e.g., Gujarat (Chinnasamy et al., 2013), Gangetic basin (Dasgupta et al., 2014), and north-west India (Long et al., 2016), suggesting the potential of utilizing both satellites- and in-situ data for managing the basin-scale water resources, studies explicitly for basins in Peninsular India, where water scarcity has been increasingly significant, are limited.

In this chapter, a holistic quantification of all water storage (WS) components in Peninsular India was carried out by jointly using the GRACE data, PCR-GLOBWB simulation outputs, and in-situ well data, and subsequently quantified the effects of natural and anthropogenic factors on the TWS trends. However, Since the global hydrological model (i.e., PCR-GLOBWB) has been found to be underestimate the terrestrial water storage trends (Chapter 1), primarily owing to the lack of representation of the deep groundwater storage and inadequate model physics, the use of the model was confined to estimate some of the water storage components, such as, soil moisture storage and surface water storage, only. Apart from the refined data source and more recent tie period selections, unique values of the aquifer properties (i.e., specific yield and specific storage) are used to quantify the in-situ observation-based groundwater storage in this chapter.

Specifically, this chapter seeks to (i) identify trends and dominant patterns in the basin-scale dynamics of various water storage components (TWS, GWS, SMS) by integrating GRACE based satellite data and PCR-GLOBWB 2.0 model simulation during 2002-2017, (ii) assess the water storage deficits in various WS components, (iii) validate the remote sensing estimates of water resources using the in-situ groundwater data, (iv) understand the seasonal variability in various WS components and their interrelation in response to the water influx and (v) assess the role of climate and human interventions on various WS components in the study region and discuss the possible long term implications.

3.2. Materials and methods

Study area

Three major river basins located in Peninsular India, i.e., the Godavari, Krishna, and Mahanadi river basins, which encompass a cumulative area of 709151 km^2 (~21.5% of India's geographical area) and a total population of ~200 million (Census, 2011), were selected for the study (Figure 3.1). The basin boundaries are defined following the Water Resources Information System (India-WRIS, 2012), and CGWB (2017). A summary of the geographical area, annual precipitation, soil characteristics, and the observation wells are shown in Table 3.1.

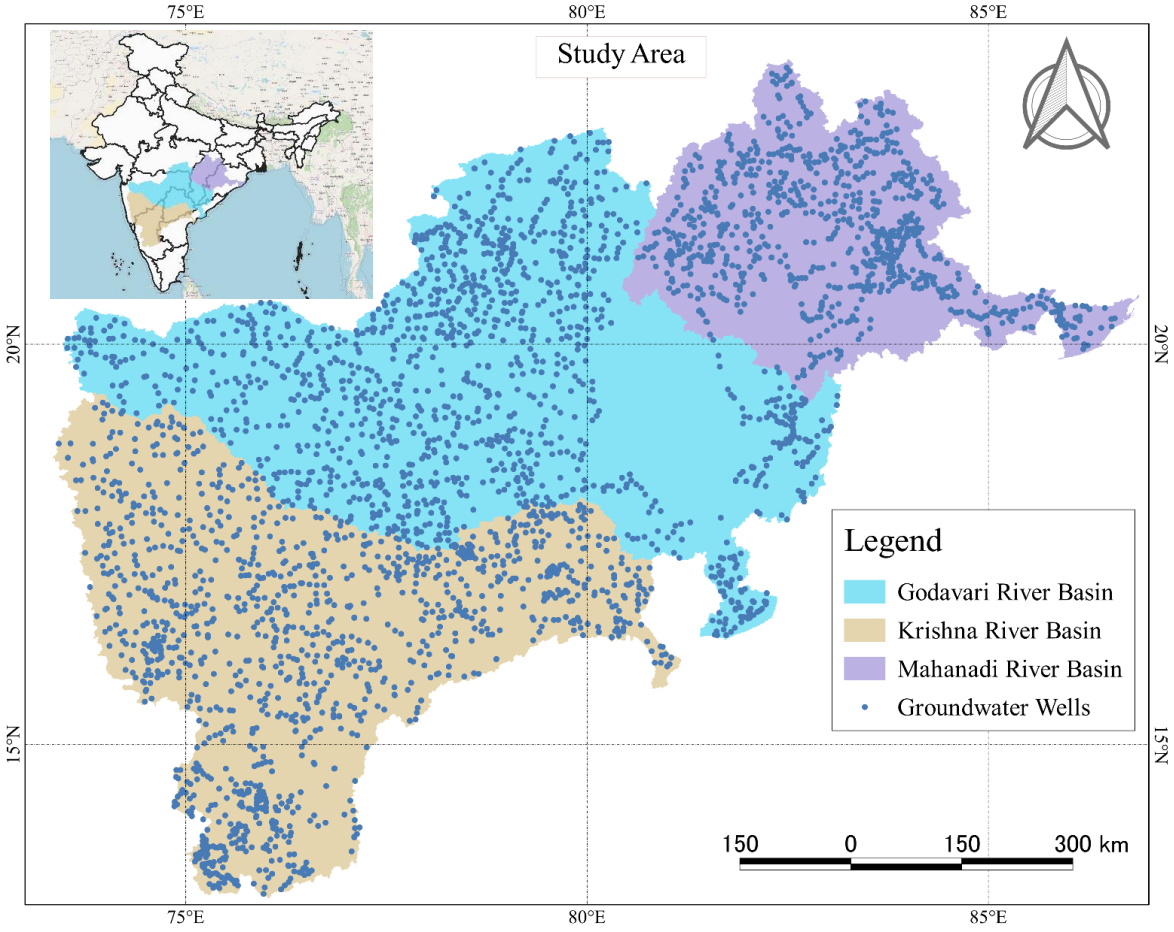

Figure 3.1. Three river basins located in Peninsular India selected for the current study (Chapter 3). The location of each observation well is represented by a solid gray circle. Calculations of all the variables and subsequent mass balance were area-averaged over each river basin. The solid black line represents the political boundaries of the Indian states (inset). After (Abhishek and Kinouchi, 2021).

Table 3.1. Specification of the three selected river basins. The aridity index and climate setting are as per Koppen classification. After (Abhishek et al., 2021).

Basin name	Geographical Area (km^2)	Areal ratio to the total area of India (%)	Mean annual precipitation ($mm\ yr^{-1}$)	Aridity Index	Current category	Climate setting	Areal percentage of the irrigated area (%)	Number of observation wells	Specific yield (S_y)
Godavari	312812	9.5	1255	0.63	Water stressed	SH	12.00	438	0.023
Krishna	254750	7.7	1078	0.47	Water scarce	SA	21.09	521	0.022
Mahanadi	141589	4.3	1452	0.81	Water stressed	H	11.62	144	0.039

Acronyms: H, humid; SH, subhumid; SA, semiarid

3.2.1. Terrestrial water storage (TWS) data

Monthly gravity anomaly data from the GRACE mission from July 2002 to June 2017 was used, which has helped in quantifying the regional scale terrestrial water storage at an unprecedented accuracy of $\pm$10 – 100 mm (Landerer and Swenson, 2012; Swenson and Wahr, 2006). The most recently released gravity anomaly data of Level-06 were obtained from three processing centers, namely, Centre for Space Research (CSR) UT at Austin, and Jet Propulsion Laboratory (JPL) in the form of mass concentration blocks, i.e., mascons (Richard Peltier et al., 2018; Save, 2019), and from GeoForschungsZentrum (GFZ) in the form of Level-2 spherical harmonic (SH) coefficients truncated at degree and order 60 (Dahle et al., 2019). Several corrections and filtering, including C20 replacement (degree 2 coefficients) with satellite laser ranging estimates, de-striping, glacial isostatic adjustment (GIA), geo-center corrections, application of fan filter of 250 km resolution were applied to the GRACE products for getting the basin averaged TWS time series for the study duration. A detailed description of the processing steps can be referred to in the papers by Landerer and Swenson (2012), Richard Peltier et al. (2018), Scanlon et al. (2018, 2016), and Swenson and

Wahr (2006). Measurement and leakage uncertainties in GRACE data were estimated following approaches by Scanlon et al. (2018, 2016).

Basin-scale uncertainties in the TWSA series are calculated as below (Landerer and Swenson, 2012; Scanlon et al., 2018, 2015):

$$\sigma_{\mathrm{mb(lb)}} = {\sqrt{\mathrm{var}}}/{N} \quad (3.1)$$

$$var = \sum_{\mathrm{i=1}}^{\mathrm{n}} \sum_{\mathrm{j=1}}^{\mathrm{n}} w_i \, w_j \, cov\left(\mathrm{x_i x_j}\right) \quad (3.2)$$

$$cov\left(\mathrm{x_i x_j}\right) = \sigma_i \, \sigma_j \exp\left(\frac{-\mathrm{d_{i,j}^2}}{2d_0^2}\right) \quad (3.3)$$

$$d_{i,j} = a \, \frac{\pi}{180} \, \mathrm{A} \sqrt{[long_i - long_j \cos(lat_i)]^2 + [lat_i - lat_j]^2} \quad (3.4)$$

where σ_{mb} and σ_{lb} are the measurement and leakage errors, respectively, N denotes the number of grid cells, subscripts *i* and *j* signify for two different grid cells, var is the error (leakage or measurement) variance of TWSA, *w* is the area weight at each grid cell with respect to the basin average TWSA, cov stands for covariance, σ is the error s. d. of a grid cell, $d_{i,j}$ denotes the distance between the two grid cells, d_0 is decorrelation length (300 km and 100 km for measurement and leakage errors, respectively), *a* is earth's radius (6371 km), $long$ and lat represent longitude and latitude of a grid cell, respectively.

The linear interpolation of the missing monthly values for GRACE TWS followed Xie et al. (2018), along with other post-processing approaches, to deduce TWS anomaly. TWS and all the subsequently derived WS components represent the corresponding long term anomaly series relative to the time mean between July 2002 and June 2017 and not the absolute values (Swenson and Wahr, 2006). Furthermore, to isolate the impact of human interventions on the TWS anomaly (TWSA) trends, GRACE TWSA and PCR-GLOBWB-no human intervention (NHI) model runs were compared for the whole study duration (Scanlon et al., 2018).

3.2.3 Precipitation data

The precipitation data from two sources, one from Tropical Rainfall Measuring Mission (TRMM) archive data (3B43 product, 0.25° × 0.25°, v7) and the other from gauge data measured by India Meteorological Department (IMD), were conjunctively used. TRMM

combines the satellite data with the rain gauge data from the Global Precipitation Climatology Centre (GPCC) (Kummerow et al., 2000). TRMM archive data was further calibrated, validated, and improved with the gauge data taken from the India Meteorological Department (IMD) following Duan and Bastiaanssen (2013) to give the time series of basin averaged monthly precipitation using Thiessen polygon method.

3.2.4. Soil moisture and Groundwater

Due to the unavailability of the continuous and consistent recorded data series of soil moisture storage (SMS) over the study region, the SMS simulated by the PCR-GLOBWB 2.0 model was used, which is a grid-based hydrological model fully integrated with human water use. The model has a computational resolution of 0.1°×0.1° (~10 km at the equator) and daily time step and simulates soil moisture storage and the water exchange between the surface and subsurface systems through precipitation and evapotranspiration for each grid cell in each time step (Sutanudjaja et al., 2018). Human water use is fully integrated into the hydrological model with all the water storage components viz., SMS, GWS, and surface water (SW) routing. Paddy (with 5 cm SW depth) and non-paddy crops are separately parametrized by considering the dynamic balance of hydrological fluxes between surface water and soil moisture incorporating the irrigation water within the region (Wada et al., 2014). The water demands are met by consumptive water use from surface and groundwater resources, followed by the return flow calculations in the model. Temperature and other meteorological forcing data, except for precipitation which was obtained according to section 2.2.2, are obtained from the WFDEI dataset (Sutanudjaja et al., 2018). The daily output of the soil moisture from each grid cell was integrated to give the basin-averaged monthly time series.

In-situ groundwater level data were obtained from the Central Ground Water Board (CGWB), India, for the study period, i.e., July 2002 through June 2017. More than 13,000 groundwater observation wells are operational by CGWB across the country, out of which the data from 1103 wells (India-WRIS, 2012) were found to be reasonable and selected for further use after screening for the temporal continuity and removal of the outliers. The wells having two or more consecutive gaps in the recorded quarterly time series (January, May, August, and November) were eliminated from the further calculations.

The groundwater storage based on the in-situ data for both confined as well as unconfined aquifers was estimated from the following equations (Todd and Mays, 2005):

$$\mathrm{GWS_{obs}} = \begin{cases} \mathrm{h_t} * \mathrm{S_s} * \mathrm{b} - \mathrm{h_m} * \mathrm{S_s} * \mathrm{b} & \text{for confined aquifer} \\ \mathrm{h_t} * \mathrm{S_y} - \mathrm{h_m} * \mathrm{S_y} & \text{for unconfined aquifer} \end{cases} \quad (3.5)$$

where $\mathrm{GWS_{obs}}$ is the groundwater storage (GWS) based on the in-situ data, $\mathrm{h_t}$ and $\mathrm{h_m}$ represent the groundwater level (GWL) at time t, and the long term mean GWL, respectively, $\mathrm{S_s}$ and $\mathrm{S_y}$ denote the specific storage and specific yield of the aquifer, respectively, b is the thickness of the aquifer. Out of 1103 screened wells, 982 wells (89%) were in the confined aquifers, and the remaining 121 were in unconfined aquifers (CGWB, 2017). The specific yield data is provided by CGWB (2012).

3.2.5. Estimation of combined TWS anomaly and regional water balance

The generalized three-cornered hat (GTCH) method was employed to obtain the TWSA time series corresponding to the minimal noise variance (Chen et al., 2019). The combined time series of TWS anomalies were calculated by Eqs. (2) and (3) by choosing the normalized ($\sum_{j=1}^{3} w_j = 1$) time-dependent weights of the individual TWSs corresponding to the three data series:

$$\mathrm{TWSA^t_{combined}} = \sum_{\mathrm{j=1}}^{3} \mathrm{w_j^t\ TWSA_j^t} \quad (3.6)$$

$$\mathrm{w_j} = \frac{\frac{1}{\mathrm{var(r_i)}}}{\sum_{\mathrm{j=1}}^{3} \frac{1}{\mathrm{var(r_i)}}} \quad (3.7)$$

where $\mathrm{w_j^t}$ is the weight corresponding to the jth data series at time t, r_i is the relative uncertainty of three TWSA, and $\mathrm{var(r_i)}$ is the variance of $\mathrm{r_i}$. Considering the climatic conditions and the vegetation cover in the study region, snow water equivalent and canopy water storage were neglected. Therefore, the regional water balance equation becomes,

$$\mathrm{GWSA^t_{est}} = \mathrm{TWSA^t_{combined}} - \mathrm{SWSA^t} - \mathrm{SMSA^t} \quad (3.8)$$

where $\mathrm{GWSA_{est}}$ is the GRACE-based estimate of groundwater storage anomaly, $\mathrm{TWSA_{combined}}$ is the combined terrestrial water storage anomaly from GRACE products as per Eq. 3.6, SWSA, and SMSA are the surface water storage anomaly and the soil moisture storage anomaly, respectively, simulated from the PCR-GLOBWB model. The superscript t

denotes the time. All the water storage components are represented in terms of anomalies which are calculated by subtracting the long-term mean from their respective time series.

Both the GRACE-derived TWS and the model-derived SMS include the effects from the natural as well as anthropogenic factors, thus making the current analysis unbiased, unlike the studies using GLDAS LSMs output for SMS, which include only the climatic factors, and hence neglect the influence of anthropogenic factors on SMS and derived GWS.

All the surface water resources in the region exist either in the form of artificial water tanks (~96% of the total surface water resources) or dammed water for municipal use (India-WRIS, 2012). The PCR-GLOBWB 2.0 model routed these types of surface water using the kinematic wave approximation (Sutanudjaja et al., 2018). Comparing to TWS, an insignificant trend (<0.01 km^3 yr^{-1}) was observed in SWS, according to the output of the PCR-GLOBWB 2.0 model (Figure 3.2). Therefore, SWS was included in the regional water balance (Eq. 3.8) but is not shown in the results. Furthermore, the biomass variations are uncaptured by GRACE owing to its detection limits (Rodell et al., 2009) and hence were not incorporated in the water balance calculations. Details of all the data used for TWS estimation and the subsequent segregation of GW components from TWS are tabulated in Table 3.2.

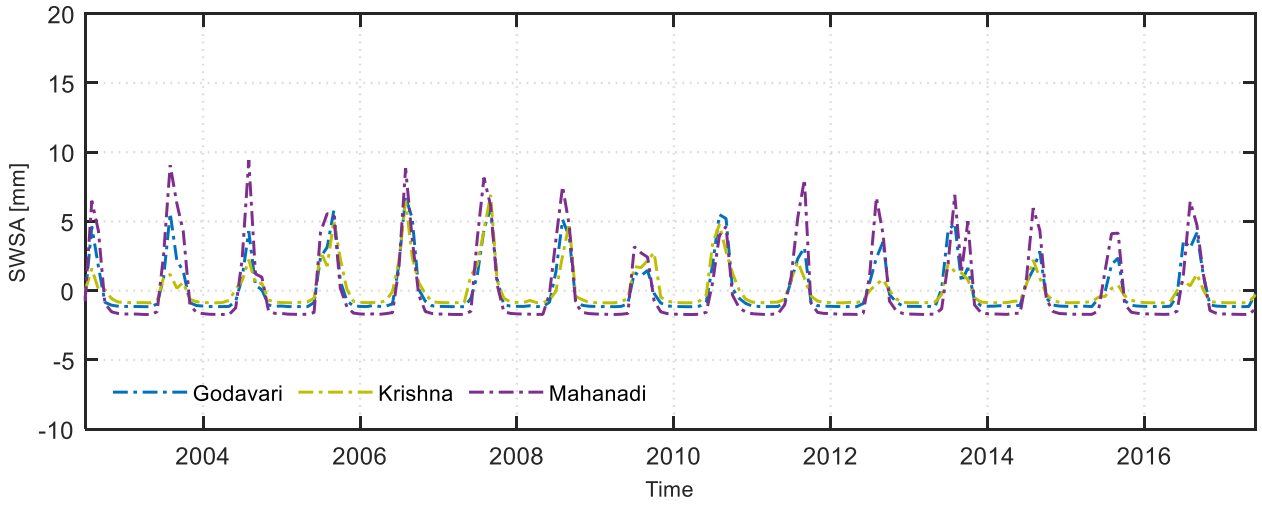

Figure 3.2. Routed surface water storage anomaly (SWSA) simulated by the PCR-GLOBWB model. After (Abhishek and Kinouchi, 2021).

Table 3.2. Summary of the TWS data and auxiliary data used for analyzing regional water balance and the subsequent segregation of GWSA from GRACE based TWSA estimates. After (Abhishek and Kinouchi, 2021).After (Abhishek and Kinouchi, 2021).

Dataset	Data type and version	Data Resolution and time duration	Reference(s)
TWS	CSR- and JPL-Mascon solutions, GFZ Level-2 spherical harmonic (SH); RL06, and PCR-GLOB-NHI	0.25° × 0.25° (CSR-M), 0.5° × 0.5° (JPL-M), 1° × 1° (GFZ-SH); monthly, 07/2002–06/2017, and 0.1°×0.1°, daily, 07/2002–06/2017	Dahle et al. (2019), Wiese et al. (2018), Save (2019), Scanlon et al. (2018), Sutanudjaja et al. (2018)
SMS and SWS	PCR-GLOBWB 2.0	0.1°×0.1°, daily, 07/2002–06/2017;	Sutanudjaja et al. (2018)
ET	GLDAS_NOAHv2.1	0.25° × 0.25°, monthly, 07/2002–06/2017	Li et al. (2018)
Precipitation	TRMM (3B43) archive data (L3, version 7)	0.25 ° ×0.25 °, monthly, 07/2002–06/2017	Duan and Bastiaanssen (2013), Kummerow et al. (2000)
	Data from gauging stations	0.25 ° ×0.25 °, gridded daily rainfall data	India Meteorological Department (IMD)
GW data and aquifer properties	In-situ GW level and specific yield	Quarterly (pre-monsoon, during the monsoon, and twice post-monsoon), 07/2002–06/2017	India-WRIS (2012), Central Ground Water Board, Ministry of Jal Shakti, Department of Water Resources (Central Ground Water Board, 2017)

3.2.6. Error analysis

The error associated with the resulting monthly GWS anomaly time series was derived from Eq. 3.9 using a root mean square of the respective errors in other monthly WS components used in Eq. 3.8 (Voss et al., 2013):

$$\mathrm{E_{GWS}} = \sqrt{(\mathrm{E_{TWS}})^2 + (\mathrm{E_{SMS}})^2 + (\mathrm{E_{SWS}})^2} \quad (3.9)$$

where $\mathrm{E_{TWS}}$, $\mathrm{E_{SMS}}$ and $\mathrm{E_{SWS}}$ are the trend-error (one-sigma) in TWS from GRACE, SMS and SWS from the PCR-GLOBWB model, respectively. $\mathrm{E_{TWS}}$ is estimated as 0.5 mm yr^{-1}, 0.7 mm $yr^{-1,}$ and 0.8 mm yr^{-1} for the Godavari, Krishna, and Mahanadi river basins, respectively, and was calculated by the propagation of monthly error (GRACE measurement errors + leakage errors) in TWS onto the least square estimated trends. Errors in the output of the PCR-GLOBWB model were quantified by the standard deviation of the trends in respective time series computed using methods by Kato et al. (2007), which resulted in an error of 1.6 mm yr^{-1}, 1.4 mm $yr^{-1,}$ and 1.7 mm yr^{-1} in SMS, 0.3 mm yr^{-1}, 0.2 mm yr^{-1} and 0.3 mm yr^{-1} in SWS, and 1.7 mm yr^{-1}, 1.8 mm yr^{-1} and 1.9 mm yr^{-1} in the resulting $\mathrm{E_{GWS}}$ for the Godavari, Krishna, and Mahanadi river basins, respectively. Errors in all the WS components were calculated after removing the long-term annual signals from the individual values. Here one notable thing is the magnification of the grace error as the basin size decreases (highest for the smallest basin, and vice-versa), which is consistent with the observation by Scanlon et al. (2018).

Several statistical techniques were used for comparing the observed GWS anomaly series ($GWSA_{obs}$) with the GRACE-based GWS anomaly series ($GWSA_{est}$), which were obtained from the groundwater storage calculated by Eqs. 3.5 and 3.8, respectively. Root mean square error (RMSE) was used for quantifying the combined effect of imprecision and biasness (Helsel and Hirsch, 2002). RMSE manifests the deviation of a variable from its real value, i.e., the observed values ($GWSA_{obs}$ in this chapter). Skewness and kurtosis were used to for assess the time series distribution of individual water storage components. Skewness and kurtosis represent the data symmetry and the tail-heaviness of the distribution (not the peakedness), respectively (Westfall, 2014). Pearson correlation (r) was used for estimating the linear association of both the time series (Helsel and Hirsch, 2002). Non-parametric rank correlation, i.e., Spearman's rank correlation, was also calculated for determining the statistical dependence of the two data sets, which describes the monotonicity of the

relationship between the two variables. A high correlation for the two variables means a similar rank between the two variables, thus high monotonicity.

A schematic diagram depicting the methodology, multiple data sources, and the analyses conducted in this chapter is shown in Fig. 3.3 below.

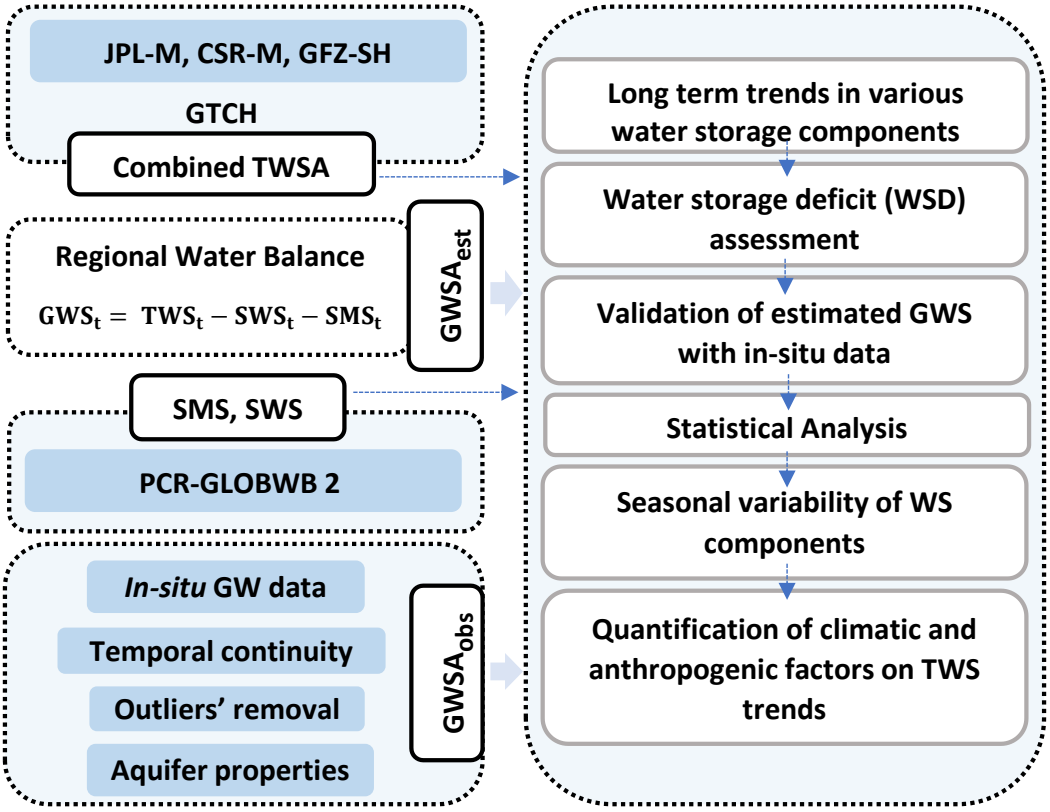

Figure 3.3. A schematic diagram depicting the methodology, various data sources, and the analyses conducted in this Chapter. Subscript t in the water balance equation signifies the time functionality of the water storage components. The acronyms are explained in relevant sections in the chapter. After (Abhishek and Kinouchi, 2021).

3.3. Results and discussion

3.3.1. Terrestrial water storage and water storage deficits

Figs. 3.4(a), 3.5(a), and 3.6(a) show the time series of terrestrial water storage anomaly (TWSA) for the Godavari, Krishna, and Mahanadi river basins, respectively. It is evident that the anomalies of TWS possess seasonal variations and amplitudes larger than surface water and groundwater storage anomalies (SWSA and GWSA, respectively) in all three river basins due to the integration of both the surface water and groundwater storage. Long term linear trends in TWSA were positive (5.21 mm yr^{-1}) in the Godavari and slightly negative in the Krishna and Mahanadi river basins (-1.35 mm yr^{-1} and -0.18 mm yr^{-1}) (Table 3.3). On the contrary to the slightly negative or positive trends of TWSA in the basins (Table 3.3), the per capita water availability in all three basins is projected to be continuously decreased (Table 3.1). An attempt is made to quantify the trends and to analyze how water storage is changing in recent times. For this piecewise analysis, the TWSA series was split before and after the end of the 2009 drought year as detected by the Pettitt test. Thus, TWSA dynamics in two distinct periods were found for all three river basins; the first from July 2002 until June 2010, where TWSA trends were quantified as a mix of positive (the Godavari and Krishna river basins) and negative trend (the Mahanadi River Basin), and the second from July 2010 until June 2017 where TWSA was 'highly decreasing' for all the three basins (Tables 3.3 and 3.4). The time series of TWSA showed a piecewise trend of 1.45 mm yr^{-1}, 10.48 mm yr^{-1} and -5.54 mm yr^{-1} from July 2002 to June 2010 and -10.41 mm yr^{-1}, -30.95 mm yr^{-1} and -18.81 mm yr^{-1} from July 2010 to June 2017 for the Godavari, Krishna, and Mahanadi river basins, respectively (Tables 3.3 and 3.4). The corresponding net volumetric water loss from July 2010 until June 2017 was quantified as 22.79 km^3, 55.19 km^3, and 18.64 km^3 for the three basins, respectively (Table 3.3). In addition to the negative trends in TWS and other water storage (WS) components in the recent period (Table 3.3), the high seasonal fluctuation in response to the variable rainfall in the region imposes a challenge to the policymakers, water managers, and the relevant government agencies to efficiently and equitably meet the freshwater demand under these highly dynamic conditions.

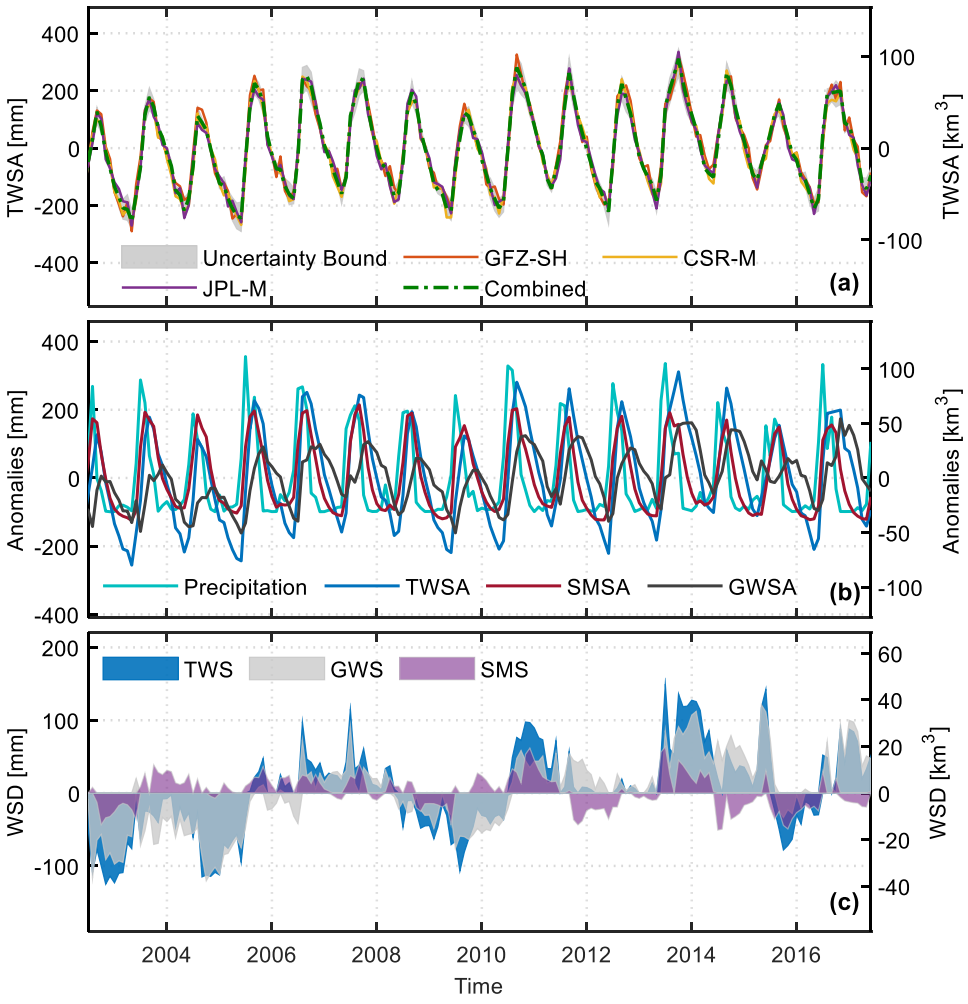

Figure 3.4. Anomalies of monthly water storage and storage deficit for the Godavari River Basin during the period from July 2002 to June 2017: (a) anomalies of monthly terrestrial water storage (TWSA) derived from the three different GRACE solutions (JPL-M, CSR-M, and GFZ-SH), the combined TWSA, and the uncertainty bound, (b) anomalies of precipitation, TWS from GRACE, SMS from PCR-GLOBWB 2.0, and GWS estimated from a regional water balance equation (Eq. (4), SWS is not shown here since the anomaly is negligible (Fig. S1) compared to other components), (c) TWSA, GWSA, and SMSA based water storage deficits (WSD) derived after removing the mean monthly values from the respective time series during July 2002 and June 2017, respectively. The tick marks and the labels on the x-axis are every two years starting from January 2004. The results of all the parameters are shown in terms of equivalent water depth (mm) on the left y-axis and equivalent water volume (km^3) on the right y-axis, which is calculated by multiplying the water depth with the basin area. After (Abhishek and Kinouchi, 2021).

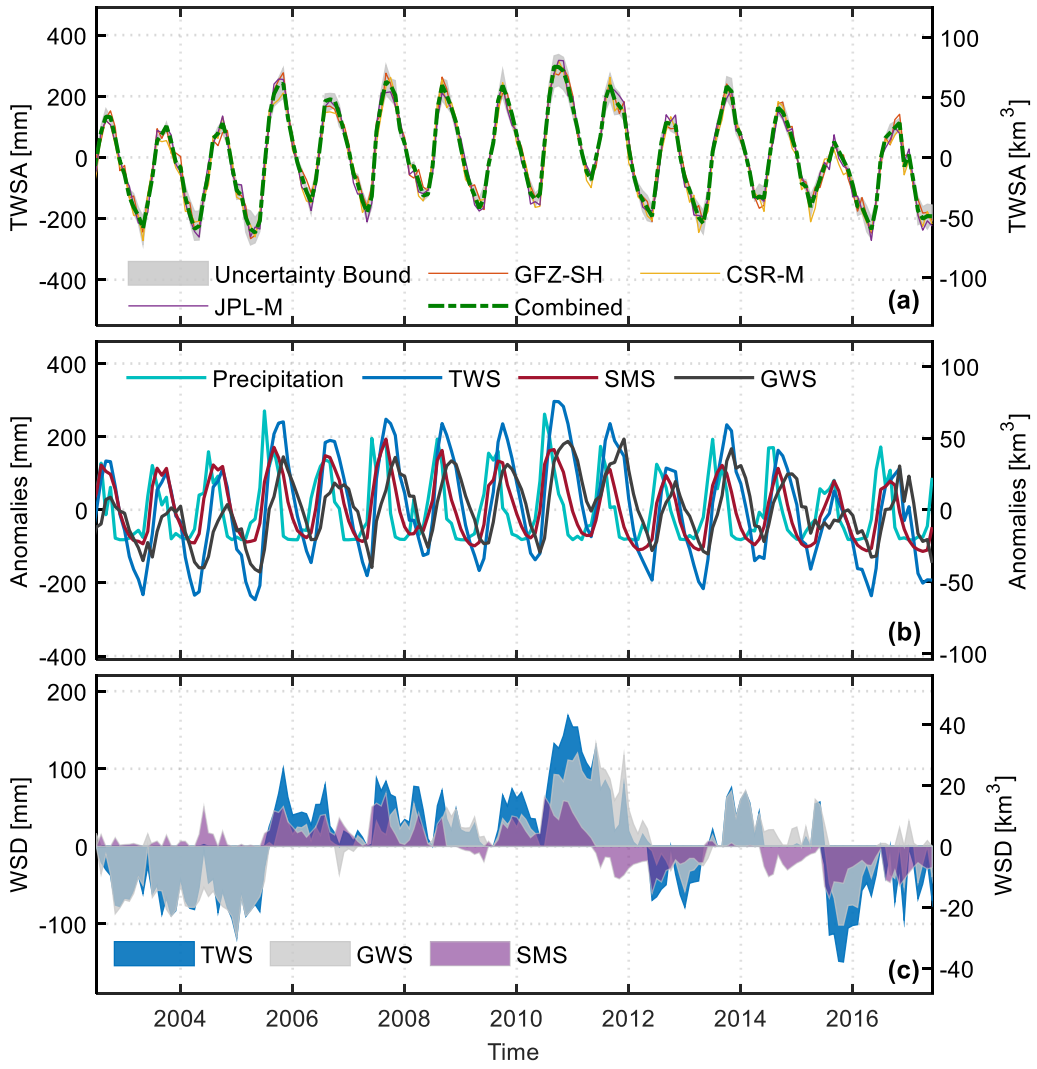

Figure 3.5. Same as Figure 3.4 but for the Krishna River Basin. After (Abhishek and Kinouchi, 2021).

The signatures of water loss were evident in TWSA during the years 2002-2003, 2004-2005, 2009-2011, and 2015-2016 in the Godavari and Mahanadi river basins (Figs. 3.4(a), 3.5(a) and 3.6(a)). However, all the meteorological droughts are well captured in the water storage deficits, except the drought of 2009 in the Krishna river basin, though sometimes with lags and sometimes as a continuous prolonged drought instead of multiple deficits. To further ascertain the water deficit conditions, the monthly water storage deficit (WSD) were calculated (Figs. 3.4(c), 3.5(c), and 3.6(c)) by removing the mean monthly water storage anomaly (TWSA, GWSA, and SMSA) of each basin during the whole study period. TWSA based WSD (TWSA_WSD) revealed the below-average terrestrial water storage during the

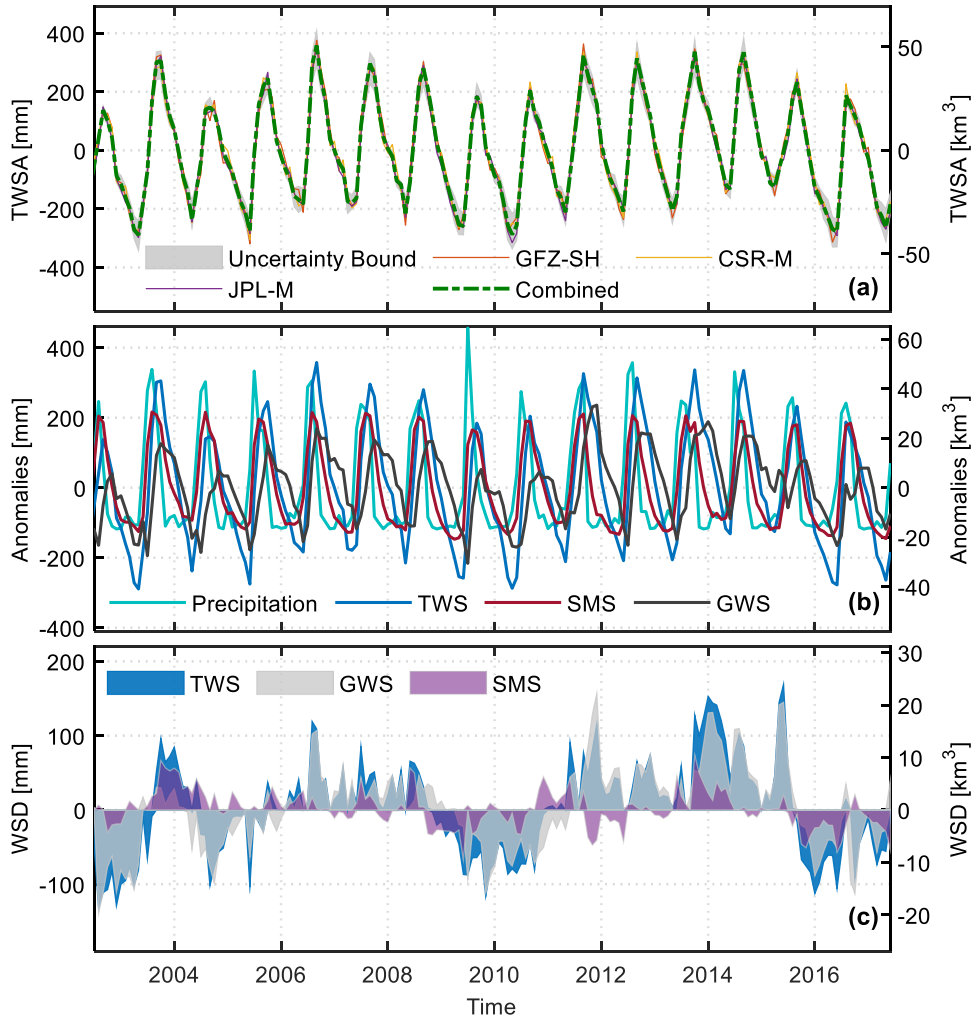

Figure 3.6. Same as Figure 3.4 but for the Mahanadi River Basin. After (Abhishek and Kinouchi, 2021).

four years with a maximum decrease of water equivalent depth of -125.17 mm (Nov 2002), -149.15 mm (Nov 2015), and -132.38 mm (Aug 2002) in the Godavari, Krishna, and Mahanadi river basins, respectively (Figs. 3.4(c), 3.5(c) and 3.6(c)). The corresponding water volume deficit for these river basins was 39.15 km^3, 37.99 km^3, and 18.74 km^3, respectively. Cumulative TWS deficit, i.e., the sum of monthly WSD (negative value only), during the study period was maximum in Mahanadi (-4467.05 mm), followed by Krishna (-4371.21 mm) and Godavari (-4033.12 mm) river basins.

To quantify the water depletion during the drought years and the subsequent recovery volumes, the cumulative water storage deficits were analyzed (WSD) (Fig. 3.7). Cumulative TWS in all three basins captured the downward trend in response to the meteorological drought of years 2002 and 2004 with a continuous prolonged TWS depletion in Godavari and Krishna, but two separate deficit periods in Mahanadi River Basin. A monthly TWS loss rate of ~15 (Jul 2002 to Nov 2005), 14 (Sep 2002 to Jul 2005), and 8 km^3 (Aug 2002 to Jul 2003) was observed in the Godavari, Krishna and Mahanadi River Basins. TWS recovered from Jul 2003 to Jun 2004 (~3 km^3 $month^{-1}$) in Mahanadi river basin when it again started depleting until Nov 2005. Recovery in TWS started from mid to late 2005 in the Krishna and Godavari river basis with a monthly gain rate of ~13 and 9 km^3, respectively. The meteorological drought of the year 2009 started appearing in the Godavari River Basin from May 2008 until June 2010 and resulted in a TWS loss of ~10 km^3 $month^{-1}$, which recovered by late 2011 with ~13 km^3 $month^{-1}$. The Krishna River Basin showed a TWS surplus even after receiving the rainfall deficit of ~20% from the long-term average, which had ultimately resulted in the century-scale drought in the year 2009 (Hazra et al., 2013). It implies that subsurface storage was sufficient in the region to meet various water demands. The water was sustainably used, which resulted in an average monthly recovery of ~13 km^3 from Jul 2005 to March 2012, followed by a stable TWS until Apr 2015. On the contrary, the Mahanadi River Basin experienced two events of average monthly water depletion (~3 and 7 km^3) and recovery (~4 and 7 km^3) each, from Jun 2004 to Aug 2015, which cumulatively had a balance. After showing stable dynamics of TWS during the year 2012, TWS in the Godavari River Basin further recovered by ~30 km^3 $month^{-1}$ until Jun 2017 with a loss rate of ~5 km^3 during Sept 2015- Jun 2016. Cumulative TWS is decreasing in the Krishna River Basin (~12 km^3) and in the Mahanadi River Basin (~5 km^3), but increasing in the Godavari River Basin (~11 km^3) during the year 2016-2017.

3.3.2. Soil moisture variations

Figs. 3.4(b), 3.5(b), and 3.6(b) portray the simulation outputs of soil moisture storage anomalies (SMSA) in the three river basins from the PCR-GLOBWB model, which fully integrates the human water use and the dynamic water balance with compartments of GWS and routes surface water. A quicker response to the climatic factors (precipitation,

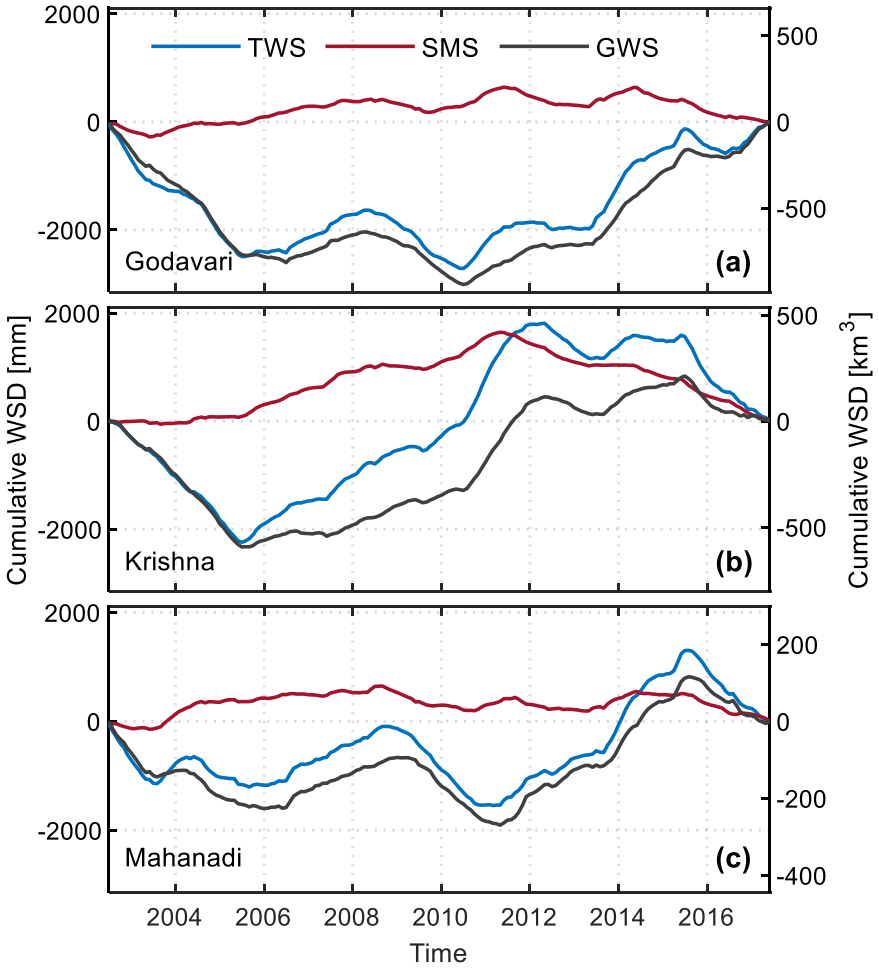

Figure 3.7. Cumulative water storage deficits (WSD) of terrestrial water storage (TWS), soil moisture storage (SMS), and groundwater storage (GWS) for the Godavari (a), Krishna (b), and Mahanadi (c) river basins. Water volume (km^3) is shown on the right y-axis which is equivalent to the water depth (mm) shown on the left y-axis. After (Abhishek and Kinouchi, 2021).

evapotranspiration, and temperature) can be seen in SMSA as compared to GWSA and TWSA. The long-term piecewise trends in the combined time series of SMSA from July 2002 until June 2010 were negative for all basins, viz., the Godavari (-3.57 mm yr^{-1}), Krishna (-0.76 mm yr^{-1}) and Mahanadi (-7.77 mm yr^{-1}) river basins (Table 3.3). SMSA showed a declining trend of -10.06 mm yr^{-1}, -10.76 mm yr^{-1} and -10.51 mm yr^{-1} for the Godavari, Krishna and Mahanadi river basins, respectively, from July 2010 until June 2017. The decrease in SMS in this period accounted for 96.6%, 34.8% and 55.9% of the reduction of TWS (Table 3.3), thus indicating SMS as a significant contributor to TWSA in the Godavari River Basin. Signatures

Table 3.3. Linear trends in the water storage components (TWS, SMS, and GWS) from July 2002 to June 2017, i.e., 180 months. After (Abhishek and Kinouchi, 2021).

Basin Name	TWSA trend	TWSA eq. vol.	SMSA trend	SMSA eq. vol.	GWSA trend	GWSA eq. vol.
	mm yr^{-1}	km^3	mm yr^{-1}	km^3	mm yr^{-1}	km^3
Godavari	5.21	24.47	-2.38	-11.18	7.60	35.67
Krishna	-1.35	-5.18	-4.10	-15.67	2.75	10.52
Mahanadi	-0.18	-0.38	-3.03	-6.45	3.15	6.7

Table 3.4. Piecewise trends (mm yr^{-1}) and equivalent total volume change (km^3) in various components of water storage and net precipitation flux over the three basins from July 2002 until June 2010 (96 months). After (Abhishek and Kinouchi, 2021).

Basin Name	TWSA trend	TWSA eq. vol.	SMSA trend	SMSA eq. vol.	GWSA trend	GWSA eq. vol.
	mm yr^{-1}	km^3	mm yr^{-1}	km^3	mm yr^{-1}	km^3
Godavari	1.45	3.63	-3.57	-8.93	5.02	12.56
Krishna	10.48	21.36	-0.76	-1.55	11.23	22.89
Mahanadi	-5.54	-6.28	-7.77	-8.80	2.24	2.54

of the drought events were also reflected in SMSA but with dampened magnitudes than TWSA, which can be attributed to the apparent reason that the SMSA contributes partially to TWSA. The various water storage components (soil moisture and surface water anomalies, i.e., SMSA and SWSA, respectively) estimated from the PCR-GLOBWB 2.0 model may be affected by uncertainties and error propagation due to model spin-up and initial conditions, model structure and capacity, and forcing parameters.

The Krishna River Basin experienced relatively less frequent deficit events in SMS than the other two basins (Figs. 3.4 to 3.7). Effects of all the meteorological droughts of 2002, 2004,

2009, and 2011 are not evident consistently in all three basins. In response to these droughts, a volumetric water loss of ~7, 3.5 and 2 km^3 $month^{-1}$ was observed in the Godavari, Krishna, and Mahanadi river basins, respectively, from mid-2002 to mid-2003. A stable dynamic (< 1 km^3 $month^{-1}$) is observed in each basin during 2004. Like the terrestrial water storage (TWS), the effect of the 2009 drought appeared in the Godavari basin as early as Jun 2008 and lasted up to late 2009 with a monthly depletion of ~2.5 km^3. Krishna and Mahanadi river basins showed stable and decreasing rates (~2 km^3) in soil moisture storage (SMS) during the drought year 2009. After that, SMS in the Krishna basin continuously recovered until Jun 2011, while Godavari and Mahanadi basins experienced multiple events of losses and recoveries until mid-2014, which cumulatively balanced. SMS in all three basins has been decreasing with ~ 4, 5, 2 km^3 $month^{-1}$, starting from May 2014, Jun 2011, and Sept 2014 in the Godavari, Krishna, and Mahanadi river basins, respectively (Fig. 3.7).

3.3.3. Trends in GWSA and its role during dry years

The anomalies of groundwater storage (GWSA) showed seasonality throughout the study period in all three river basins (Figs. 3.4(b), 3.5(b), and 3.6(b)). This seasonality is summarized by calculating the mean monthly WS components throughout the study period which will be discussed in Section 3.3.5. It is also apparent that GWSA showed a phase lag of 1-3 months throughout the observation period due to the delay in groundwater recharge (Figs. 3.4(b), 3.5(b), 3.6(b)). Smaller amplitudes of GWSA compared to SMS can be attributed to the smaller influence of climatic factors, the limited storage change by groundwater recharge, and the high groundwater withdrawal during the non-monsoon seasons, typically from Oct. to May. GWSA showed a minimal decline in the GRB at the rate of -0.34 mm yr^{-1} (equivalent water volume of 0.74 km^3) and comparatively higher rates of -20.18 mm yr^{-1} (eq. water vol. of 35.98 km^3) and -8.3 mm yr^{-1} (eq. water vol. of 8.23 km^3) in the Krishna and Mahanadi river basins, respectively, during the period from July 2010 to June 2017 (Table 3.4). The loss of GWS in the three basins accounted for 3.29%, 65.2% and 44.1% of the loss in TWS, respectively, making GWS the least contributor to TWS in the GRB and the highest contributor in the KRB.

GWS well captures the meteorological drought signatures in the study region, with largely similar behavior to TWS. The impact of climatic factors (e.g., precipitation) is dampened in

the groundwater storage, which had resulted in the time lag in the onset of deficits (and recoveries) in GWS as compared to SMS or TWS (Figs. 3.4 to 3.7). There is GWS depletion starting from mid-2002 until late 2005 and early 2006 with an approximate volumetric loss rate of 15, 14, and 4 km^3 $month^{-1}$ in the Godavari, Krishna, and Mahanadi river basins, respectively (Fig. 3.7), followed by the recovery. However, GWS could not be recovered fully when it started to decrease again in late 2008 towards early 2011 for the Godavari and Mahanadi river basins. As an exception, the Krishna river basin did not reveal the influence of the drought in the year 2009. The Godavari River Basin experienced a continuous recovery of GWS with a mean rate of ~11 km^3 $month^{-1}$ from Jul 2010, while the Krishna and Mahanadi river basins showed decreasing GWS rates of ~7 km^3 $month^{-1}$ and ~4 km^3 $month^{-1}$, respectively since mid-2015.

Moreover, the time series of monthly GWSA was consistent with the terrestrial water storage (TWS) loss during the water deficit periods (Figs. 3.4 to 3.7). Nevertheless, the inherent phase lag due to the response of the hydrological system was present in GWSA throughout the period. During the period of meteorological droughts, it is likely that the water storage dynamics, in particular the groundwater dynamics, is primarily governed by the anthropogenic influences owing to the increased reliance and hence the withdrawal of GW for domestic- and agricultural- water demands and resulting irrigation for farmlands. In case of meteorological drought years of 2002, 2005, 2009, and 2015 increased GW extraction for meeting high water demand (~61% of irrigation and ~80% of drinking water) during these periods (Siebert et al., 2010) appears to have determined the prominent dry phase centering the drought years and hence govern the interannual variability of TWSA (r = 0.7-0.8). The coinciding of the maximum deficits in GWSA with that of TWSA showed that the GW extractions primarily govern the water storage conditions during these dry years. Groundwater storage deficits (GWSA_WSD) in Figs. 3.4(c), 3.5(c) and 3.6(c) show the below-average groundwater storage during the four drought years with a maximum decrease of water depth of -120.47 mm (Oct 2004), -117.61 mm (Jan 2005) and -139.01 mm (Aug 2002), and the corresponding water volume loss of 37.68 km^3, 29.96 km^3 and 19.68 km^3 in the Godavari, Krishna and Mahanadi river basins, respectively. Moreover, the cumulative negative deficits in GWS_WSD during the study period were -3843.8 mm, -3677.3 mm and -3863.02 mm, which comprised 95.30%, 84.12% and 86.5% of the total deficit based on TWSA (TWS_WSD) for the three basins, respectively. On the other hand, soil moisture storage based WSD (SMS_WSD) made up 37.9%, 40.1%

and 33.6% of the cumulative negative TWS deficits in the three basins. Hence it is concluded that the groundwater plays a significant role in terrestrial water storage and, therefore, in the water availability during the dry periods in all basins.

3.3.4. Comparison of observed and GRACE-derived GWSA

For comparing GWSA estimated from Eq. 3.8 ($GWSA_{est}$) with that from Eq. 3.5 using the in-situ records ($GWSA_{obs}$), the time series of $GWSA_{est}$ and $GWSA_{obs}$ were analyzed at four times a year when the in-situ record of the groundwater wells is available (January, May, August, and November) (Fig. 3.8). For consistency, the precipitation was accumulated in four seasons, i.e., June–August (Monsoon), September–November (post-monsoon), December–January (post-monsoon) and February–May (pre-monsoon) (Fig. 3.8). $GWSA_{obs}$ was compared with $GWSA_{est}$ using various statistical approaches. $GWSA_{est}$ agreed favorably well with $GWSA_{obs}$ in terms of seasonal phase and the amplitude dynamics. The maxima of both series occur in August (monsoon season) or November (post-monsoon season), and the minima occur in May (pre-monsoon or summer season). RMSE between both the time series increases as the basin area decreases, and follows the order, Mahanadi (65.45 mm) > Krishna (54.79 mm) > Godavari (54.74 mm). Similar to the observations in various parts of the world (Long et al., 2016a; Shamsudduha et al., 2012; Strassberg et al., 2007), the GRACE based estimates of GWSA showed a strong linear correlation with the observed GWSA as indicated by Pearson correlation (r) with the highest in the Krishna River Basin (r = 0.91) and the lowest in the Mahanadi River Basin (r = 0.86), which depicts the high potential of the satellite for estimating the basin-scale groundwater storage. The scatter plots and linear fits shown in Fig. 3.9 represent that $GWSA_{est}$ followed a similar gradient to $GWSA_{obs}$ ($GWSA_{est}$: $GWSA_{obs}$ = 1: 0.53 ~ 0.55) for all three basins. The negative values of skewness and high kurtosis values (>2) for all the basins depicted the data asymmetry and the heavier tails in the data series. A strong monotone relationship between $GSWA_{obs}$ and $GSWA_{est,}$ as indicated by Spearman's rank correlation coefficient (ρ > 0.85), implies that the observed GWSA was in phase with the estimated GWSA. Moreover, on an annual scale, $GWSA_{est}$ and $GSWA_{obs}$ agreed well, and both showed no significant decreasing trend since 2002, implying the sustainable use of groundwater resources for various purposes. The assumption of uniform aquifer thickness and physical properties and the uneven distribution of groundwater observation wells (Fig. 3.1) accounts for the difference in the estimated and observed GWSA

(Long et al., 2016). Moreover, the observation wells do not represent the exact GWS in the representative area at any time, which adds errors in the observed time series of GWSA. Overall, the high correlation among both the series provides confidence in the synergetic application of GRACE data, PCR-GLOBWB model simulation and in-situ groundwater data.

Observed GWSA was relatively constant during both the decline and recovery period compared to the estimated GWSA, probably due to the loss of nonrenewable water (deep aquifers) and the response lag compared to the real-time record by GRACE. A few times in monsoon and post-season (e.g., during 2002 and 2005 in the Godavari and Krishna river basins, and during 2002 and 2015 in Mahanadi river basin), comparatively more rise in observed GWSA than in estimated GWSA (Fig. 3.8) can be explained by the local flood impacts on the open wells. After the drought in 2009, the Krishna River Basin showed a high recovery in the estimated GWSA (Fig. 3.8), which can most likely be explained by the non-negative condition of TWSA_WSD in preceding years and continuous recharge of water from soil moisture storage to the deeper aquifers. The higher amplitude variations in the $GWSA_{est}$ may be partially attributed to the propagation of uncertainties in the modeled soil moisture storage either due to the model's physical structure or due to the uncertainties in the forcing variables to the PCR-GLOBWB model (Rodell et al., 2007). Continuously developing the PCR-GLOBWB model and the GRACE(-FO) data with higher accuracy, availability of the soil moisture data from the ground-based sensors, enhanced temporal and spatial continuity in the groundwater data may reduce the amplitude gap between $GWSA_{obs}$ and $GWSA_{est}$ in future studies.

To test the effects of the basin averaged and the distributed aquifer properties on the results, two time series were compared. GWS with those from previous studies (Abhishek and Kinouchi, 2021; Bhanja et al., 2016) using the unique value of Sy for individual well were compared for a common period of May 2002 to November 2014. Both the time series agree well (Pearson correlation, r=0.97-0.99; Spearman's rho, ρ~0.98; p<0.001), and therefore it is inferred that the assumption uniform Sy value does not lead significant uncertainties in the current results of long-term trends and/or subsequently derived normalized drought indices.

3.3.5. Intra annual distribution of water storage fluxes

The average monthly values of WS components and net precipitation (P-ET) were calculated for each river basin for the period from July 2002 to June 2017 (Fig. 3.10). While the mean monthly net precipitation was the largest in July, TWSA exhibits the maximum in September or October. The mean monthly values for constituent components of TWS maximize in August or September for SMSA and in November for GWSA. The magnitude of maximum mean monthly water storage (WS) components was the largest in the terrestrial water (TWSA), followed by soil moisture (SMSA) and the smallest in groundwater (GWSA) anomalies for all three river basins.

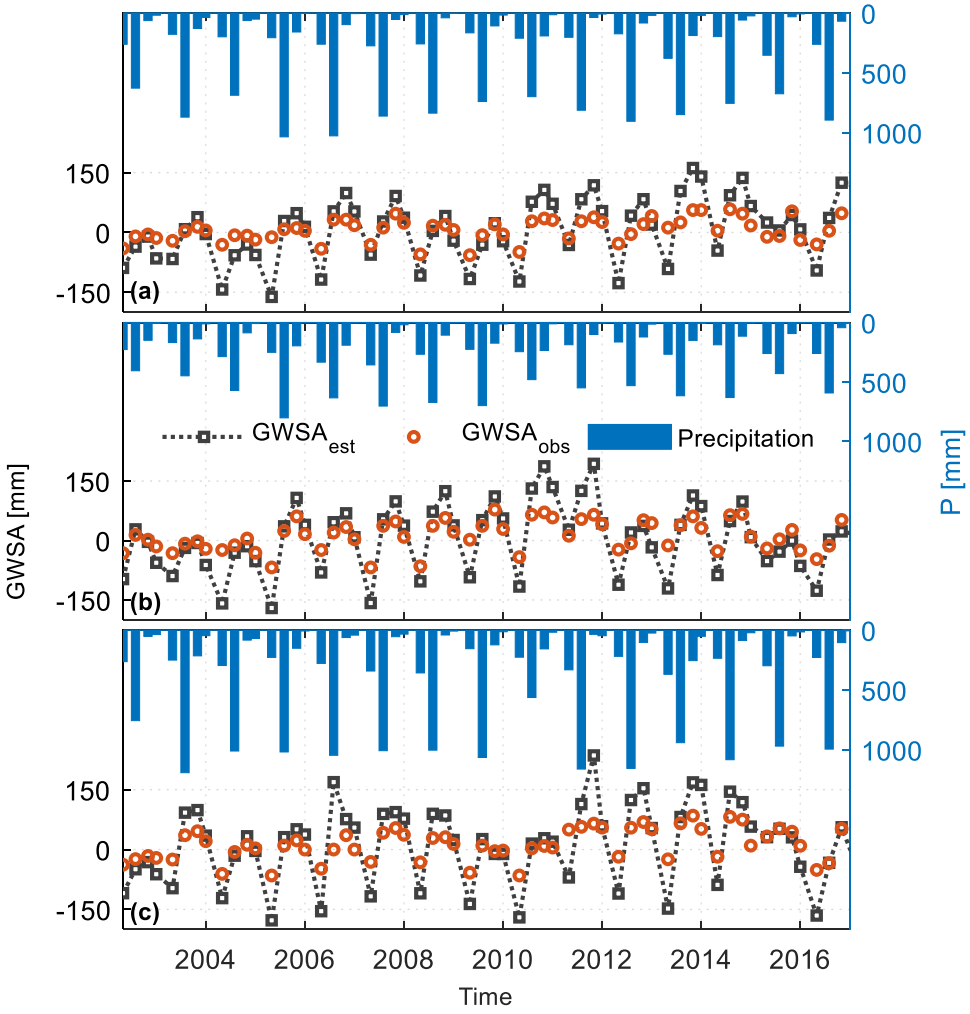

Figure 3.8. Cumulative precipitation during four seasons in a year (December – January, February – May, June – August and September – November), estimated GWSA ($GWSA_{est}$)

and observed GWSA ($GWSA_{obs}$) for the Godavari River Basin (a), the Krishna River Basin (b), and the Mahanadi River Basin (c). Both the observed and estimated GWSA represent the quarterly values when the in-situ record of the groundwater wells is available, i.e., January, May, August, and November. After (Abhishek and Kinouchi, 2021).

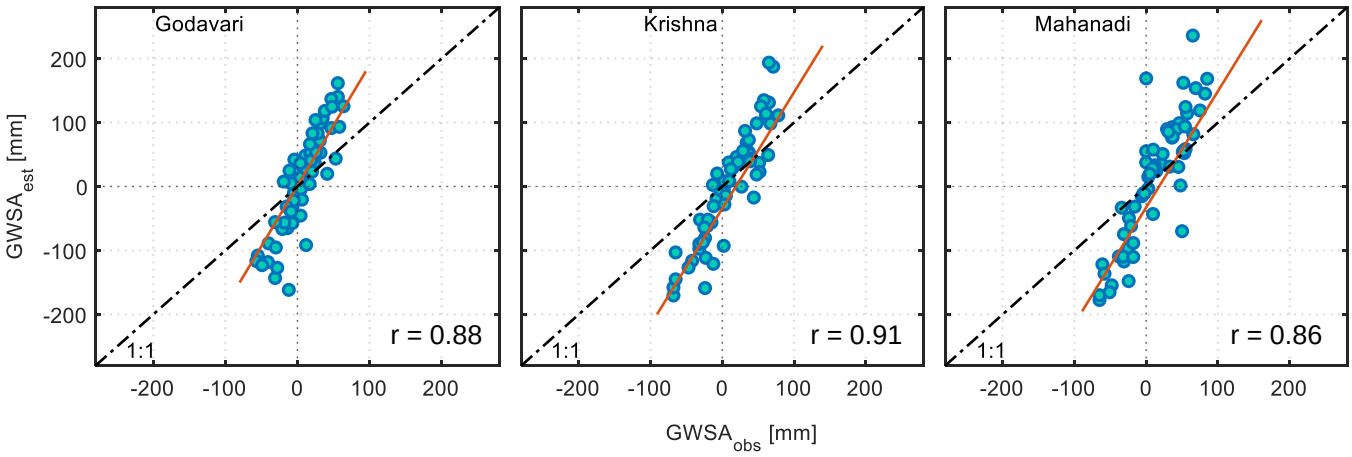

Figure 3.9. Scatter plots of $GWSA_{est}$ (GRACE-derived) and $GWSA_{obs}$ (derived from in-situ data) for the Godavari River Basin (left), the Krishna River Basin (center), and the Mahanadi River Basin (right). The linear fit between $GWSA_{est}$ and $GWSA_{obs}$, and the 1:1 line are shown with the thick coral and dashed black lines, respectively. Correlation coefficients between the $GWSA_{obs}$ and $GWSA_{est}$ are also shown. After (Abhishek and Kinouchi, 2021).

Three notable inferences are drawn for each WS component during the Indian monsoon season:

1) The dominant climatic factor, i.e., net precipitation flux, apparently governs the dynamics of water storage in all three basins during the monsoon season (June-October) since the peaks in mean monthly values of all WS components occurred within a specific range of time lag from the peak of net precipitation flux. Since there is a surplus of available water, the irrigation activities by abstracted GW are likely to be almost absent in this season, thus making the net precipitation flux a major contributor to the variation of SMSA (Fig. 3.10). The gradual decrease in temperature during the monsoon season (Fig. 3.11), leading to reduced evapotranspiration, further facilitates the recovery of WS components (Fig. 3.10). It must be noted here that the

actual timing of the Indian monsoon varies by 1-2 weeks within this study region, which is highly unlikely to affect the current conclusions based on a long decadal assessment.

2) During December to March/April, i.e., the post-monsoon season, TWS declined at a faster rate that is mostly attributed to declining GWS due to climatic and anthropogenic factors. This declining behavior can be explained on one side by the minimal (and highly heterogeneous) precipitation, and increased air temperature and evapotranspiration, and on the other side by the decline of GWS due to more frequent than usual irrigation (irrigation done before the crop harvesting) activities of Rabi crops (Rabi and Kharif are two cropping seasons in India) during these periods. This leads to a continuous decline (with a lag) until the monsoon arrives in May or June.
3) During the pre-monsoon season (March to May), all the WS components reflect the dry environment due to the temperature increase towards the upcoming summer season (Figs. 3.10 and 3.11). After that, the variable pre-monsoon precipitation and minimal or no irrigation activities recover GWS slowly. The recovery of all WS components becomes steep as the monsoon arrives.

3.3.6. Are anthropogenic Interventions the main drivers of water storage trends?

For determining the governing factors of WS dynamics, the trends of TWSA were compared with the irrigation intensity (indicated by the percentage of irrigated areas) in the basin (Table 3.1). The Krishna River Basin, with the highest irrigation intensity of 21.09%, showed the highest declining trend in TWS (-30.95 mm yr^{-1}). On the contrary, inconsistency in the relationship between the trends in TWS and irrigation intensity for the Godavari and Mahanadi river basins indicates other influencing factors (e.g., irrigation with surface water). Therefore, to further quantify and isolate the impact of human interventions (reservoir management and water abstractions), PCR-GLOBWB-no human intervention (NHI) model was run (Scanlon et al., 2018). By the model output, the contribution of the human interventions to the trend in TWSA was quantified as -6.38 mm yr^{-1}, -23.56 mm yr^{-1}, and -8.42 mm yr^{-1}, which were equivalent to 61.29%, 76.12% and 44.76% of the total TWSA trend for the Godavari, Krishna and Mahanadi river basins, respectively. The difference in trend between the GRACE-derived TWSA and that from PCR-GLOBWB-NHI runs was the highest for the Krishna River Basin, thus ascertaining that the GW extractions govern the TWS dynamics in this basin. The second

highest declining rate of TWSA in the Mahanadi River Basin can be explained by the most negative trend of net precipitation flux (Table 3.3). In particular, dry warm climate (low precipitation and high temperatures) and enhanced agricultural activities during the non-monsoon season cumulatively make the water balance negative for the river basin.

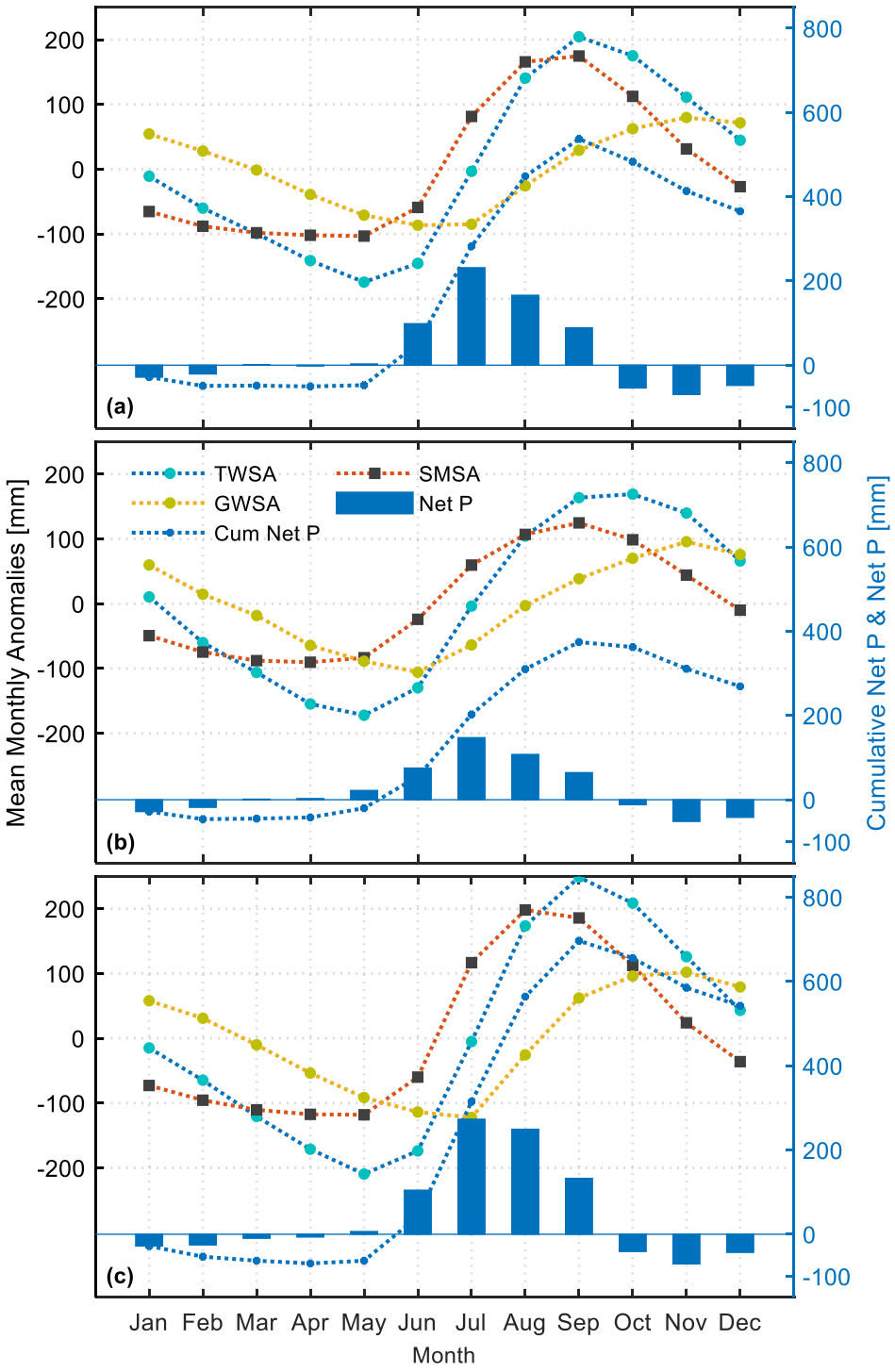

Figure 3.10. Mean monthly WS components (TWSA, SMSA and GWSA), net precipitation flux (P-ET), and cumulative net precipitation flux calculated using the time series of the respective components from July 2002 to June 2017 for (a) the Godavari River Basin, (b) the Krishna River Basin and (c) the Mahanadi River Basin (e.g. value for Jan is the mean value of all Jan values, and so on). After (Abhishek and Kinouchi, 2021).

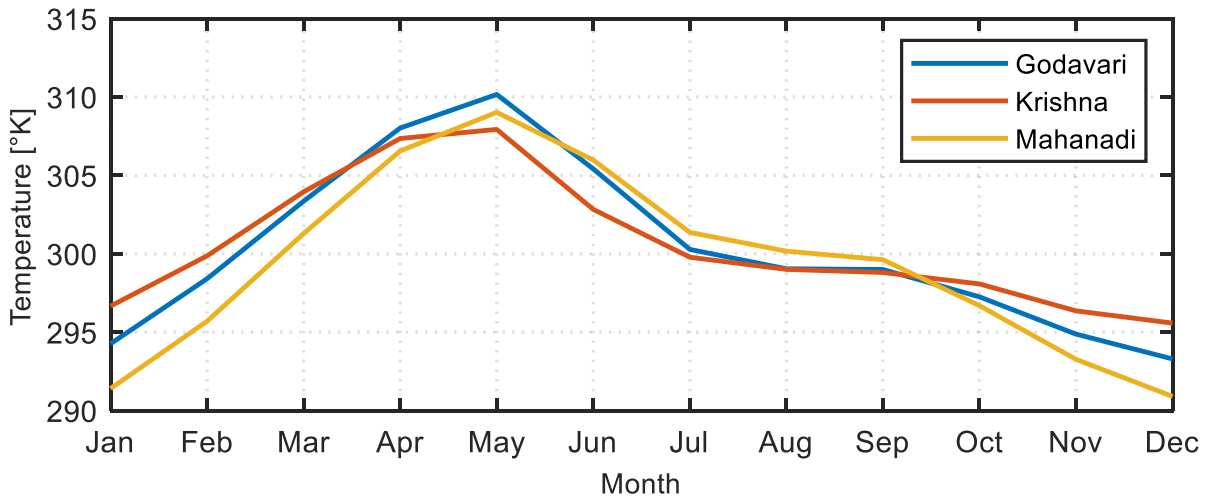

Figure 3.11. Mean monthly temperature from GLDAS Noah (1°×1°, v2.1) for the three basins. After (Abhishek and Kinouchi, 2021)

Furthermore, the trends in climatic variables were estimated to compare with those of TWSA. Since no significant relationship was observed between TWSA and precipitation (r = 0.25–0.32, ρ = 0.18–0.25), the net precipitation fluxes, i.e., P–ET, were estimated because the imbalance of water fluxes induces the change in water storage through the boundary of a system as a result of natural and anthropogenic perturbations. The net precipitation flux showed negative values during the non-monsoon season (October to February) with a transition during the pre-monsoon season (March to May), and positive during the monsoon season (June to September) (Figs. 3.12 and 3.13). The overall trends in annual total net precipitation are negative, i.e., -2.83 mm yr^{-1}, -1.05 mm yr^{-1} and -3.39 mm yr^{-1} for the Godavari, Krishna and Mahanadi river basins, respectively during July 2010 to June 2017, which explains about 27%, 3% and 18% of the total trend of respective TWSA (Table 3.4). The remaining differences in the TWSA were likely due to the underestimation of the water demand by the PCR-GLOBWB 2.0 model because instead of the actual water demand of a region, it considered the water demand and subsequent allocation based on the auxiliary forcing parameters. Moreover, the highest GRACE errors in TWSA estimation for the smallest basin, i.e., Mahanadi, can be one reason for the largest difference in trends (37.24%).

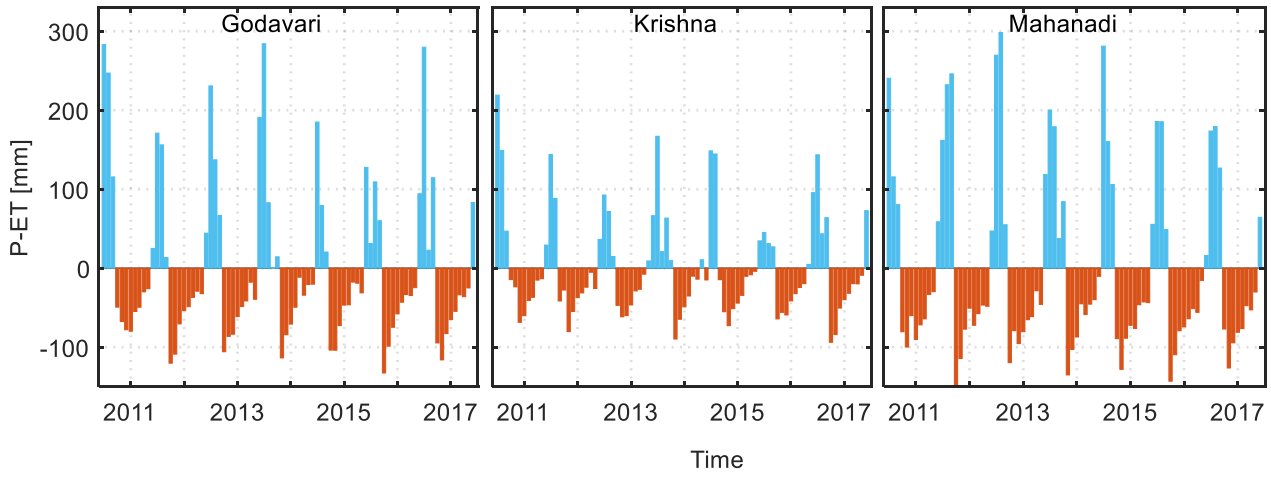

Figure 3.12. Basin-wide anomalies of the net precipitation flux (P-ET) for the three study basins during the period from July 2010 to June 2017. After (Abhishek and Kinouchi, 2021).

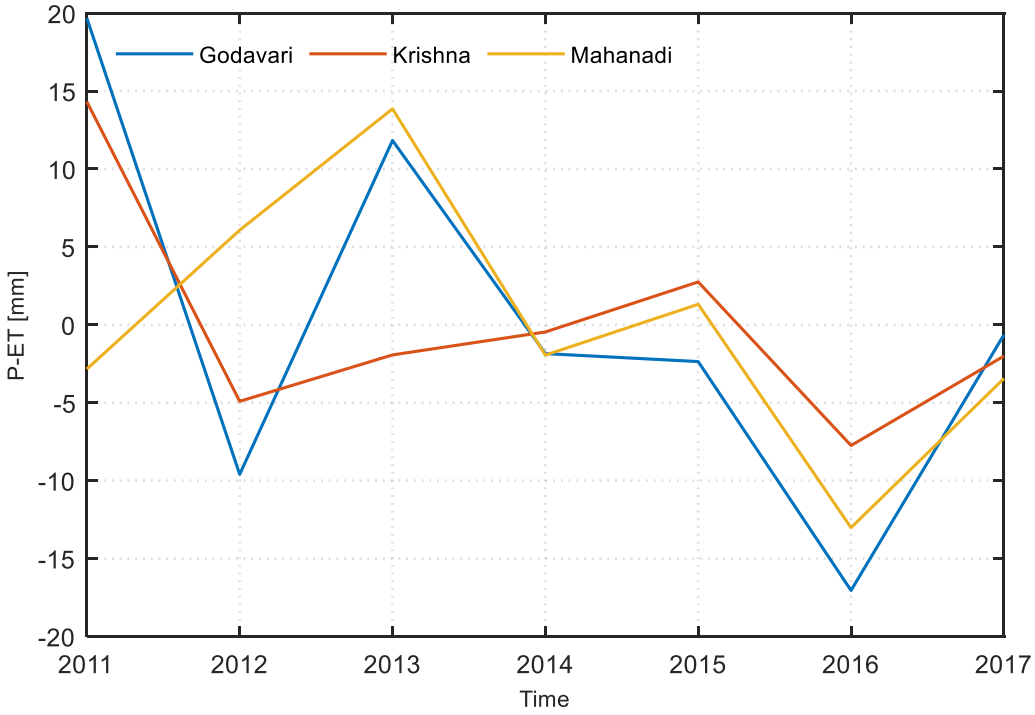

Figure 3.13. Annual P-ET for the three river basins for the duration of July 2010 to June 2017. After (Abhishek and Kinouchi, 2021).

3.4. Conclusion

In this chapter, a basin-scale holistic quantification of the water resources dynamics and long-term trends was carried out under the influence of the human interventions and natural climatic perturbations over the Godavari, Krishna, and Mahanadi river basins located in Peninsular India. The current framework can be applied to various river basins globally for a complete quantification of the different components of water storage based on the GRACE satellite observations, the global hydrology and water resources model PCR-GLOBWB 2.0, and in-situ groundwater observations. The long-term variation of water storage components (July 2002 to June 2017) showed a mixed behavior of either increasing or minimally decreasing (terrestrial water storage; TWS), decreasing (soil moisture storage; SMS) and increasing (groundwater storage; GWS) trends in the study region. However, all the water storage components showed declining trends in recent time (July 2010 to June 2017). The water storage deficit analysis revealed that despite the minimal linear trends during July 2002 to June 2017, all three river basins experienced multiple deficit events in response to the cumulative influence of the rainfall deficits and groundwater abstraction, the former likely due to ENSO impacts on the monsoon rainfall. The relative contribution of 84-95% by the deficit of groundwater storage to total water storage deficit in the region indicates the excessive groundwater withdrawals relative to the replenishment and underscore the need for multilateral cooperation among the states and the various related stakeholders to wisely integrate the groundwater usage with the surface water availability for irrigation in the region. Trends and deficits in various water storage components in recent times highlight the need for revising water allocation strategies (e.g., conjunctive water management plan), irrigation systems and methods (e.g., switching to drip irrigation), and assessment of the governing factors (social, physical, and economic) of crop management practices for sustainable management to ensure optimum and equitable future water supply.

The meteorological drought events are well captured by the time series of TWS and GWS in the region, albeit with the lags in various water storage components. These signatures of drought events representing the integrated as well as disaggregated water availability in various components highlight the potential for efficient irrigation scheduling and effective quantification of the water deficit conditions that are not commonly visible, leading to a timely evolution of the deficit severity and efficient measures of mitigation and adaption. Furthermore, very good agreement ($r = 0.86 – 0.91$, $\rho = 0.85 – 0.91$) of the GRACE-derived

groundwater anomalies with those estimated from in-situ groundwater well data reveal that the GRACE products could potentially be used for quantifying GWS and for subsequent basin-scale hydrological implications. The current study puts forward a blueprint for managing the basin-scale water resources and food security more timely and efficiently

It is believed that the water deficit conditions revealed in this study will foster urgent discussions towards ensuring sustainable water use in the three basins. The proposed framework for quantifying the surface and subsurface water resources dynamics complements the little existing knowledge on the basin-scale water storage. The potential areas of the future work within and beyond the current study region include the use of the currently operational GRACE(-FO) mission (launched on May 22, 2018), which will cover more period compared to GRACE, using the improved land surface models' output or the ground-based soil moisture data (subject to the availability) which will be conjunctively used with the improved PCR-GLOBWB model to eliminate the model related uncertainties. Improvement in the temporal and spatial resolutions of the in-situ groundwater data will represent the GWS with reduced uncertainties. It is also planned to use the artificial neural network (ANN) models based on the various constituent water storage components as predictors to predict terrestrial water storage. The ANN model-based forecasting and hindcasting of TWS will enable us to fill the data gap between GRACE and GRACE(-FO) records and help quantify the water storage dynamics of the region even beyond GRACE(-FO) data records.

Taking forward the caveats of this chapter, all of the prospective work including an up-to-date assessment (up to 2020) of the TWSA dynamics and its role in modulating the hydroclimatic extreme in the Chao Phraya river basin is studied in the next chapter. ANN model is employed to generate the continuous time series followed by developing a novel drought index based on the antecedent water storage condition. The rationale of shifting the focus from Peninsular Indian region to Chao Phraya is the complex water allocation and management of the later basin where there are as 31 ministerial departments and several other governing agencies. Thus, this basin provide better insights into hoe TWSA translates to the extreme water events in context of the heavy human interventions such as reservoir management (which is not significant in Peninsular Indian basins) and groundwater extraction (which is similar to the Indian scenario).

Chapter 4

Water Storage Dynamics and Hydroclimatic Extremes in Chao Phraya River Basin

This chapter has been adapted from Abhishek et al., 2021.

Abhishek, Kinouchi, T., Sayama, T., 2021. A comprehensive assessment of water storage dynamics and hydroclimatic extremes in the Chao Phraya River Basin during 2002–2020. J. Hydrol. 603. https://doi.org/10.1016/j.jhydrol.2021.126868

4. Water Storage Dynamics and Hydroclimatic Extremes in Chao Phraya River Basin

4.1. Introduction

With a contribution of about 66% in the Gross Domestic Product and covering about 30% of the country's geographical area, the Chao Phraya River Basin (CPRB) is the most important basin in Thailand in terms of agriculture, economics, and livelihood in general (Shakti et al., 2020). The basin is home to around 40% of the country's population. Over 45% of the basin is used for agriculture, which depends on the highly heterogeneous rainfall derived primarily from the Asian summer monsoon (Komolafe et al., 2019; ONWRC, 2006). Despite the availability of vast water resources, the high vulnerability to the minor shifts in the monsoon patterns and variable human interventions (i.e., reservoir management and water abstractions) govern the water resource dynamics and agricultural productivity in the basin (Fig. 4.1). Continuously increasing stress on the prevailing water resources is a major challenge in the basin, especially in terms of the water quantity available in the dry periods, which may ultimately disrupt the water demand-supply cycle and limit the crop production (Kinouchi et al., 2018). CPRB has suffered from multiple episodic hydro-climatological extremes in the recent past (e.g., floods of 2006 and 2011 (Promchote et al., 2016), droughts of 2015-2016 (Kinouchi et al., 2018), and the most recent drought in 2019-2020, which had affected a multitude of sectors in the country. The unprecedented floods of 2011, for example, inundated over 20,000 km^2 of farmland, causing over 800 deaths and about 13.6 million affected people, and incurred exorbitant damage of about 45 billion USD; a loss costlier than Hurricane Katrina (Haraguchi and Lall, 2015; Promchote et al., 2016; Shakti et al., 2020; Supharatid, 2015; World Bank 2011). As a result, the country's economy ultimately contracted up to 9%, highlighting the socio-economic impact of the extreme events on national and subsequently on global economies through supply-chain disruptions (Shakti et al., 2020). Although some studies dealing with the specific extreme events, particularly the 2011 flood event, in the basin have been conducted in the past (e.g., Hagiwara et al., 2016; Komolafe et al., 2019; Promchote et al., 2016; Sayama et al., 2017; Tau Chia et al., 2015), a comprehensive study covering both floods and droughts under the integrated impact of both natural and anthropogenic influences and focusing on the various components of the water storage is still lacking. Moreover, an increasing and decreasing trend in monsoon and dry season precipitation (20% each), respectively, and an increase in the peak precipitation

amount in the wet season from past and near-future (2010–2039) to the far-future (2070–2099) period as reported by Supharatid (2015), highlight a possibility of an increase in the water-related extremes in the basin. Therefore, a holistic assessment of the hydro-climatic extremes, their propagation behavior, along with the dynamics of terrestrial water storage (TWS) and its constituent components, is imperative to better understand the hydrological complexity of the basin and for employing an efficient and effective strategy to mitigate the socio-economic impact of these water-related disasters.

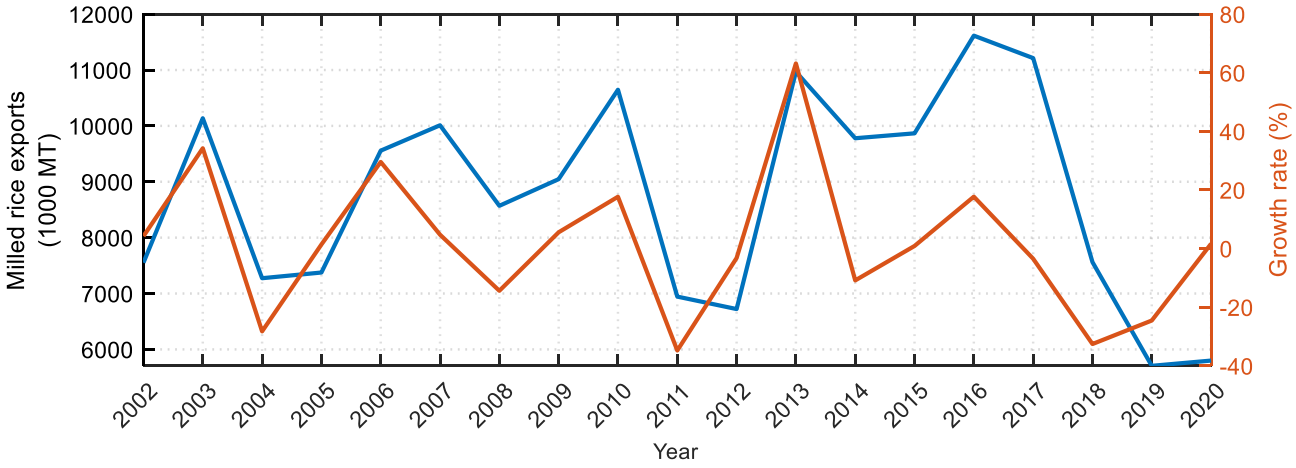

Figure 4.1. An example of the impact of water resources dynamics (primarily driven by the climatic variability and exaggerated by the human interventions in terms of reservoir management and (ground)water abstraction) on the agricultural productivity (milled rice is taken as an example) in Thailand. The graph shows the time series of exports of milled rice by Thailand (left y-axis) and the percentage growth rate (right y-axis) (FAO, 2021). The hydroclimatic extremes have heavily affected agricultural production and export, which subsequently disrupts the global supply-chain network. For example, the growth rate of milled rice within the country experienced a decline of as high as 34.77% during floods of 2011, and 28.24%, 14.39%, 10.85, 32.56%, and 24.54% during the drought years of 2004, 2008, 2014, 2018, and 2019, respectively. After (Abhishek et al., 2021).

Terrestrial water storage, which represents the water storage in soil moisture, surface water, biomass, and groundwater, is a decisive component of the hydrologic cycle in any river basin. Improved quantification of TWS is pivotal in understanding the regional water cycle, which ultimately helps to allocate, govern, and manage the basin-scale water resources efficiently and effectively (Ndehedehe et al., 2016). Although the conventional way of quantifying the various hydrological as well as water storage components includes ground-based data, the

inherent limitations leading to the infrequent data lengths on the fine spatial scales usually impede an accurate, continuous, and integrative assessment for the river basins globally (Abhishek and Kinouchi, 2021; Jing et al., 2020). Nevertheless, the past Gravity Recovery and Climate Experiment (GRACE) and the ongoing GRACE-Follow On (both jointly referred to as GRACE-(FO) hereafter), a tandem satellite mission initially launched in March 2002, enable us to measure the Earth's mass distribution and subsequently quantify the changes in TWS with unprecedented accuracy (Chen et al., 2020; Tapley et al., 2019). Outperforming a variety of remotely sensed data that primarily focus on few components of water storage, GRACE-(FO)-derived TWS has the least uncertainties on a basin size of >100,000 km^2 at the current processing level and thus provides a big picture of the water storage (Famiglietti et al., 2015; Jing et al., 2020). Some studies have used GRACE based TWS for assessing the impact of anthropogenic disturbances (e.g., Scanlon et al., 2012), climate change (e.g., Rodell et al., 2018), and events of droughts (e.g., Liu et al., 2020), and floods (e.g., Chen et al., 2010) in various regions globally. However, no work has been done utilizing the GRACE-(FO) to analyze the dynamics of the terrestrial water storage (TWS) and segregated constituent components in the Chao Phraya River Basin, where frequent floods and droughts have been affecting various human activities. Moreover, the sparse and infrequent measurement of groundwater (GW), in addition to overreliance on GW by registered and unregistered wells, especially during dry periods, potentially limit appropriate monitoring and assessment of GW resources, leading to the continuous unsustainable abstraction, which eventually may lead to significant depletion of the commonly invisible GW. In this Chapter, therefore, GRACE satellite data was jointly used with the land surface models' output to disaggregate the constituent components of TWS, quantify the linkage and interaction among water fluxes (e.g., runoff, evapotranspiration), assess the hydroclimatic extremes that occurred in the basin, and analyze the effect of the policy change for water management essentially among groundwater and surface water.

Due to the climatic shift to a warmer temperature, rapid industrialization and urbanization, and intense agricultural practices, the intensity, frequency, and extent of the hydroclimatic extremes, i.e., droughts and floods, are expected to increase in the near future with relatively severe consequences attributed to the region's high dependency on water resources (Amnuaylojaroen and Chanvichit, 2019; IPCC, 2007; Supharatid, 2015; Tangang et al., 2020). CPRB has likely been shifting from a state of water richness towards water scarcity

conditions, making the basin more vulnerable to minor variations in the hydrological cycle (Kiguchi et al., 2021; Supharatid, 2015). Given the highly variable climate conditions and continually increasing urbanization, and the subsequent extreme hydrological conditions costing billions of dollars to the economy, and a key economic and policymaking role in Southeast Asia (Kiguchi et al., 2021), sound knowledge of the basin-scale hydrologic cycle is crucial. In this chapter, therefore, the terrestrial water storage dynamics in the basin is quantified and an attempt is made to get insights into the ability of the satellite data, jointly used with land surface models and artificial neural networks, to capture the flood and drought events. The variability of TWS and its constituent components and their propagation behavior through the system will enable us to understand the hydrological footprints for supporting sustainable decisions on a necessary adaptation of the human activities (e.g., updating the reservoir rule curves, revising the groundwater pumping regulations) in the basin.

4.2. Materials and methods

4.2.1. Study Area

The Chao Phraya River Basin (Figure 4.2) is primarily an agrarian basin (agricultural lands covering over 90% of the basin) with a geographical area of 160,000 km^2 and a population of ~30 million (ONWRC, 2006; https://fdmt.iwlearn.org/). The southern part of CPRB is a low-lying area with an elevation of as low as 2.5 m above mean sea level (MSL) (Figure 4.2), making it susceptible to large flooding events. The basin's climate is dominated by tropical monsoons with a mean and maximum daily temperature of 27°C and >40°C, respectively. The basin receives an average annual rainfall of 150 cm, varying between 100-200 cm, from the western to eastern parts. About 90% of the rainfall is received in the monsoon season from May to October, which generates an average runoff of 25-45 cm in the basin, 85% of which occurs in July to December (Komolafe et al., 2019; Tau Chia et al., 2015). Due to the absence of ample rainfall after the onset of the dry season, during the first half of the year, i.e., from January to June, natural flows generally remain small, which leads to an intermittent shift of dependence from surface water to groundwater for meeting various water demands in the basin subject to the prevailing water availability and the related policies. The basin's water cycle is affected by human interventions such as reservoir management (water storage and release from Bhumibol and Sirikit reservoirs with capacities of 13.5 and 9.5 billion m^3,

respectively), some minor dam reservoirs (Figure 4.2) and groundwater withdrawals (Abhishek et al., 2021).

Due to the lack of a sufficiently dense and uniform observation network of in-situ data in the basin and the insufficient record length, and intermittent and frequent gaps in the limited ground data, the auxiliary datasets of weather and water storage (WS) components were assessed from various remote sensing products and land surface models. Although the output fields from NASA's Global Land Data Assimilation System (GLDAS) agree favorably well with the other model products and observed data (Rodell et al., 2015), the ensemble mean of the multisource data products for the weather data, depending on the time range of available data, was used to characterize the uncertainty and to avoid implicit biases in a single dataset (Li et al., 2019; Long et al., 2014), as described in detail below.

4.2.2. Weather data

Weather datasets from reanalysis, remote sensing, and observed in-situ records, spanning May 2002 to April 2020 are used. All water budget components used in this analysis are basin averaged monthly time series represented as equivalent water depth (mm). Precipitation (rainfall+snowfall) and evapotranspiration (evaporation+transpiration) are the largest incoming and outgoing water fluxes in any hydrologic system, respectively, and play significant roles in the distribution and availability of water resources in a region (Oki and Kanae, 2006). Traditional in-situ point-based monitoring of both precipitation and evapotranspiration is costly, restricted to local scales, and prone to large uncertainties, especially in the data-limited regions like the CPRB (with a meager rain gauge density of 0.5 rain gauges per 1000 km^2) (Abhishek et al., 2022). Therefore, to get the spatially distributed continuous time series, ancillary data from multiple sources were retrieved (Abhishek et al., 2022).

Precipitation, the main water influx to any region, plays a vital role in regional water balance and hydrological modeling (Chen et al., 2017; Xie et al., 2019). An average of the precipitation data from TRMM 3B43 Version7, i.e., Tropical Rainfall Measuring Mission that is a joint mission by NASA and JAXA, GPCP, ERA5, MERRA-2, and CHIRPS (Chen et al., 2020; Gelaro et al., 2017; Funk et al., 2015; Hersbach et al., 2020; Huffman et al., 2009; Huffman

et al., 2016; TRMM, 2011) was used. The study area does not receive any snowfall; hence this component was excluded from the analysis.

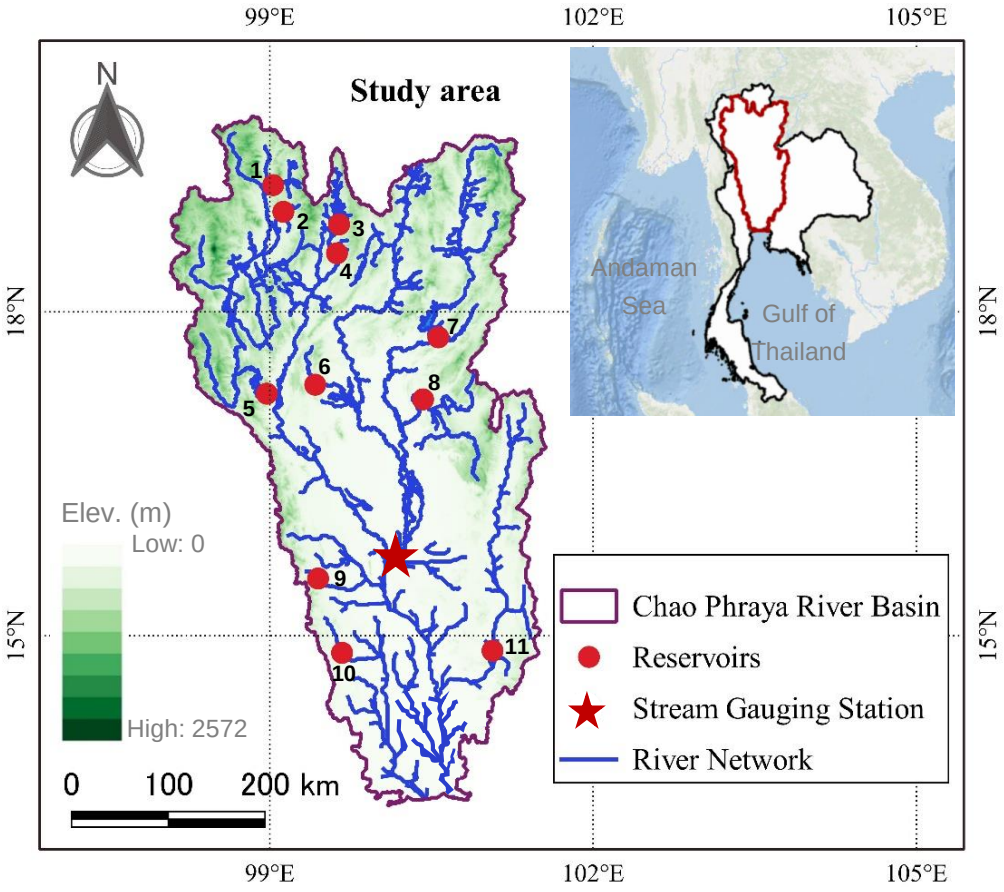

Figure 4.2. Location map of the Chao Phraya River basin. The river network, location of the eleven reservoirs (as per numbering from 1 through 11; Mae Ngat Somboon Chon, Mae Kuang, Kewkhoma, Kiew Lom, Bhumibol, Mae Mok, Sirikit, Kwai Noi, Thap Salao, Kraseao, Pasak Jolasid), stream gauging station at Nakhon Sawan (C2 station), and elevation above mean sea level are also shown. Thailand's national boundary is also represented by the solid black lines in the inset. After (Abhishek et al., 2021).

Evapotranspiration, the major outflux in a region, is an indispensable component and also one of the most scarcely measured variables, which is difficult to ground-reference primarily due to the high non-closure of energy budget and micrometeorological flux measurements footprints (Xie et al., 2019; Zhang et al. 2018). Therefore, the average of evapotranspiration products from three different categories (Land surface model, LSM: GLDAS Noah v2.1

(Beaudoing et al., 2020), satellite: GLEAM v3.5a (Martens et al., 2017), reanalysis: MERRA-2 (Gelaro et al., 2017), was used to get reliable and unbiased estimates of evapotranspiration over the study region. Ensemble mean of the monthly values of basin-wide near-surface air temperature were obtained from the GLDAS Noah archive and MERRA-2 reanalysis dataset (Gelaro et al., 2017).

4.2.3. Water storage components' data

The past GRACE (data availability: April 2002 to June 2017) and current GRACE-FO (data availability: June 2018 to present) satellite data from the three processing centers, namely, Center for Space Research (CSR), GeoforschungsZentrum (GFZ), and Jet Propulsion Laboratory (JPL) were used from Sept 2002 to Aug 2020. A combination of the spherical harmonics (SH) from GFZ and mascons from JPL and CSR was used to derive the combined time series of the basin-averaged terrestrial water storage (TWS) time series (Ferreira et al., 2016; Long et al., 2014).

Spherical harmonics (SH) coefficients, used in TWSA products, are processed for noise reduction at high frequencies (low wavelength) using low-pass filtering (e.g., 300 km Gaussian filtering, truncation at the maximum order and degree 60, de-striping), which would have inevitably led to signal errors (Long et al., 2016a; Sakumura et al., 2014; Swenson and Wahr, 2006). These errors consist of bias (leakage-out; signal loss within specific study area due to the basin function/filtered averaging kernel) and leakage (leakage-in; contamination/gain in the target signal from the surrounding region) errors (Longuevergne et al., 2010; Swenson and Wahr, 2006). To restore true signals, a number of model-dependent (additive (Klees et al., 2007), scaling (Landerer and Swenson, 2012), and multiplicative (Longuevergne et al., 2010); all of which primarily use outputs from the hydrological models (Vishwakarma et al., 2018)) or model-independent (i.e., data-driven (Vishwakarma et al., 2017)) approaches have been employed in globally distributed river basins. Since the data-driven approach outperforms other methods in the CPRB, the same was employed for restoring GRACE signals. Overall, an inter-comparison of filtered GRACE TWSA and ΔS shows strong agreement between all products. Since there is minimal signal loss attributed to the regularization and postfit residual analysis, no signal restoration procedures are required for GRACE Mascon (mass concentration) solutions (Scanlon et al., 2015). No bias between GRACE and GRACE-FO data was assumed following recent studies that reported

negligible intermission biases over the Central United States, Middle East, Europe, Australia (Landerer et al., 2020; Pascolini-Campbell et al., 2021), and ice caps and glaciers (Ciracì et al., 2020; Velicogna et al., 2020)

Uncertainties associated with the post-processing of the GRACE gravity data has been reduced continuously and are at a minimum for the latest GRACE-(FO) data, which has resulted in reasonably good agreement between the various GRACE derived variables and those estimated from other hydrologic models (Chen et al., 2020). All the processing steps for converting the GRACE(-FO) satellite data to basin-averaged monthly TWS and for the subsequent corrections are described in several studies (e.g., Rodell et al., 2018; Scanlon et al., (2018, 2015); Vishwakarma et al., 2017, among others) and are not repeated here.

For the soil moisture storage (SMS), the average of the simulation outputs from the three LSMs from NASA's Global Land Data Assimilation System (GLDAS) model, namely Noah v3.3 (GLDAS v2.1), Variable Infiltration Capacity (VIC), and CLM v2.0 (GLDAS v1) (Li et al., 2019), and one Global Hydrological Water Resource Model (WaterGAP v2.2d, (Müller Schmied et al., 2021; Yin et al., 2021) were used. Observed data of the dam water storage and stream gauge data were obtained from The Royal Irrigation Department (RID), Thailand (http://app.rid.go.th:88/reservoir/rsvmiddle) and National Hydroinformatics Data Center (http://www.thaiwater.net/), respectively. Since the Nakhon Sawan gauge station (Figure 4.2) is the most downstream station where the flow records are not contaminated by the factors such as tidal oscillations, upstream diversion or intake, the runoff data is taken at Nakhon Sawan (C2 station) (Abhishek et al., 2022). The basin-wide river water storage and flood inundation depth data was obtained from Sayama et al. (2015). Groundwater well data (in terms of groundwater table data) used for the qualitative comparison of the remotely sensed groundwater storage derived in this study was obtained from the Department of Groundwater Resources (http://www.dgr.go.th).

The mean monthly runoff recorded at the Nakhon Sawan C2 station (Figure 4.3) ranges from 3.05 mm (February 2020) to 115.67 mm (October 2006), while the seasonal time series record maximum and minimum values in October (44.48 mm) and April (8.05 mm), respectively (Figure 4). The high correlation of the seasonal runoff cycle with one and two months ($r \sim 0.92$ for both) lag with precipitation is attributable to the memory of natural hydrological processes (e.g., baseflow) in the basin. The basin experienced the most severe

flood within the past five decades in 2011, where runoff records show the second largest peak of 109.45 mm in October 2011, followed by 74.17 mm and 66.08 mm in October 2002 and October 2017, respectively. Note, all of which correspond with flood events. Minimal monthly runoff of 3 to 5 mm was observed during the dry season of drought years 2004-05, 2010, 2013, 2015-16, and 2020 (Figure 4.3).

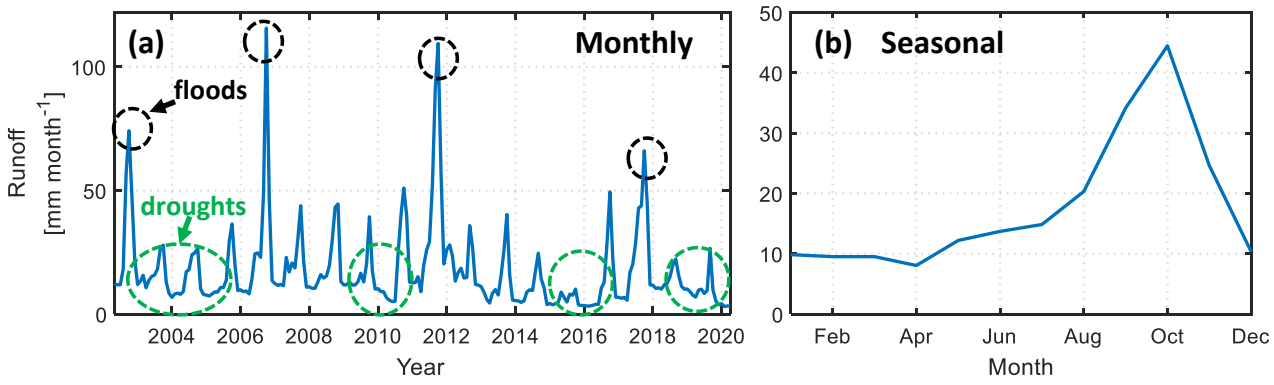

Figure 4.3. (a) Monthly and (b) seasonal time series of the observed runoff recorded at the Nakhon Sawan C2 gauging station. Various flood (black dotted circles) and drought years (dotted green circles) are also shown. A comprehensive assessment of the various hydroclimate extremes in CPRB can be found in the companion study (Abhishek et al., 2022, 2021).

To fulfill the objectives, a continuous monthly time series of basin-wide TWSA was firstly generated using an ANN model coupled with the genetic algorithm and the linear and non-linear decadal trends in various segregated and integrated components of the hydrological cycle and water storage were quantified. Then, various hydroclimatic extremes (droughts and floods) in the basin were evaluated and an empirical analysis of different drought indices was conducted to understand the drought propagation between various water storage components in the basin. Finally, a novel drought potential index (DPI) was proposed to not only explore the long-term trend in the basin's drought potential but also to examine the drought in the wet season considering both the natural variability in precipitation and human influences embedded in the water storage. All the data sources and types, along with the methodology and the various research components considered in this study, are represented in Figure 4.4.

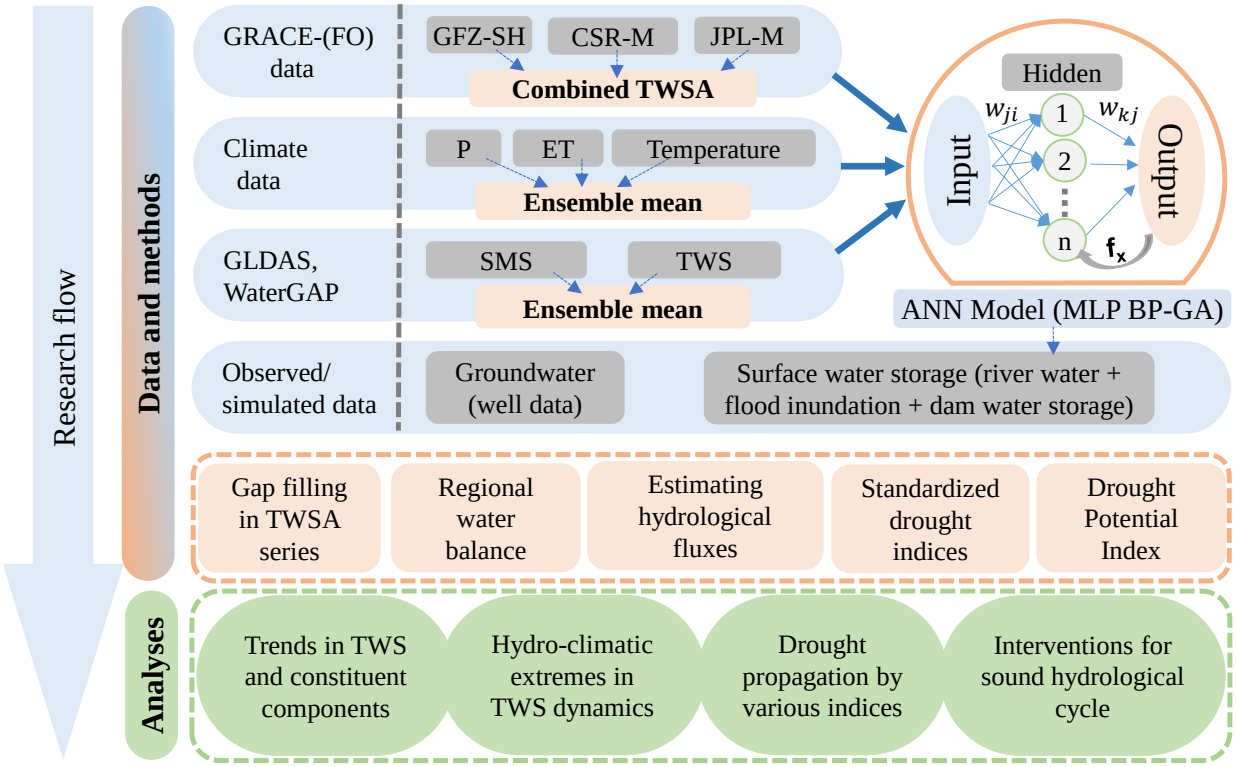

Figure 4.4. A schematic diagram depicting various data sources, methodology, and the analysis carried out in the study (Chapter 4). The three-layered (input, hidden, and output layers) artificial neural network is shown in a simplified manner where various predictors are the input layers, w_{ji} is the weight of the ith input layer for the jth hidden layer, w_{kj} is the weight of jth hidden layer to the output, f_x is the optimization function of the genetic algorithm. After (Abhishek et al., 2021).

4.2.4. Artificial Neural Network

GRACE, operational from 04/2002 to 06/2017, and GRACE-FO, operational from 06/2018 onwards, monitor Earth's gravity at an unprecedented spatiotemporal resolution (Tapley et al., 2004). GRACE products have been revolutionary in understanding terrestrial water storage dynamics, sea-level change, melting of polar ice, and climate change (Rodell et al., 2018; Tapley et al., 2019). GRACE products have frequent gaps, especially post 2011, and an 11-month gap between GRACE and GRACE-FO datasets. For overcoming the data gap of the GRACE-(FO) records, an artificial neural network-based model is hereby proposed

employing the multilayer perceptron (MLP) neural network with backpropagation (BP) and coupled with genetic algorithms (GA) (MLP BP-GA, hereafter) by taking advantage of the availability of the multisource ancillary data products and less complex configuration of ANN compared to the recent complex deep learning models. ANN models have been utilized for a multitude of applications in water resources, such as forecasting streamflow (Tongal and Booij, 2018), flood frequency analysis (Shu and Ouarda, 2007), rainfall-runoff modeling (Nourani, 2017), among others. Owing to their non-parametric nature, ANN methods outperform the forecasting using the conventional hydro-meteorological models, particularly in the complex underlying processes (Shu and Ouarda, 2007; Xie et al., 2019). MLP neural network is one of the most widely used ANN methods for predicting various hydro-meteorological variables and subsequent water resources management (Chitsazan et al., 2015; Long et al., 2014; Seyoum and Milewski, 2017; Xie et al., 2019). The feed-forward network using the hyperbolic tangent activation function, a sigmoidal function with a range of [-1, 1], was used. The tested predictors include the combinations of soil moisture, air temperature, evapotranspiration, and the output is terrestrial water storage. The network has three-layer types, i.e., the input layer, the hidden layer consisting of many neurons (user-defined) defining the weighted sum of the various predictors, and the output layer (Figure 4.4). Due to the less elapsed time in the convergence, a Levenberg-Marquardt backpropagation algorithm was used. Further, a genetic algorithm (with an optimization function to minimize the root mean square error and maximize the Nash-Sutcliffe efficiency (NSE) coefficient) was employed to decide the optimum number of hidden neurons (Maier et al., 2014), which turned out to be 5. The GA thus prevents the MLP BP-GA model from either over-fitting or under-fitting the functional relationship between the predictors and the output.

Mathematically, the ANN technique seeks to learn the functional mapping (f) between a set of predictors or states (x) and the target or output variable (y), when there is a lack of conventional physics-based models. Mathematically, ANN can be represented as below (Abhishek et al., 2021; Long et al., 2014b)

$$y = f(x) + \varepsilon \tag{4.1}$$

where ε is the process noise. The ANN model consists of three components: an input layer (predictors), a hidden layer, and an output layer. A combination of monthly time series of various hydroclimatic (temperature, precipitation, evapotranspiration) and water storage

components (soil moisture storage, surface runoff, TWS from GLDAS) were tested as predictors during model calibration, and the best performing set was further used for model validation and prediction. The hidden layer of the ANN is comprised of hidden neurons whose numbers were optimized with the coupled genetic algorithm and finalized as six, corresponding to the minimum root mean square error and the maximum Nash-Sutcliffe efficiency during model calibration. Each neuron in the hidden layer is the weighted sum of the predictors,

$$a_k = \sum_{i=1}^{P} w_{ki} x_i + w_{ki} \quad (4.2)$$

where, a_k is hidden neuron (k = 1,2,….5), w_{ki} is the weight associated with the input layer i $(= 1,2, \dots P)$ and neuron k, and w_{ki} is the bias term. The weighted sum is then utilized to calculate the output variable (i.e., TWSA) via a transfer function as below,

$$z_k = \Psi(a_k) \quad (4.3)$$

where, z_k is the output, and Ψ is the transfer function. Building upon a previous study (Abhishek et al., 2021), the ANN model was used for gap-filling between GRACE and GRACE-FO and other data gaps due to battery management. The initial 178 values of TWSA (i.e., ~87% of the total 205 available monthly values) from Sept 2002 to Jun 2017 were used for training the model, and the remaining 27 values (i.e., ~13%) from Jun 2018 to Aug 2020 were used for validation purpose. Furthermore, the model performance was evaluated during the training and validation using a number of statistical parameters, including Pearson correlation coefficient (r), normalized root mean square error (NRMSE), and Nash- Sutcliffe efficiency (NSE). Lastly, the TWSA for the eleven missing months (July 2017 to May 2018) was estimated using the trained (and validated) model. Recurring gaps of 1-2 months at every 5-6 months due to the active battery management after 2011 were filled by linear interpolation of the two bounding values (Abhishek and Kinouchi, 2021; Xie et al., 2018). The ANN model set up was carried out using the MATLAB and Statistics Toolbox Release 2019a.

4.2.5. Combined TWSA time series, and regional water balance

A combined terrestrial water storage time series was derived using the three GRACE-(FO) products, namely, CSR-M, GFZ-SH, and JPL-M, using the three-cornered hat (TCH) method, which has recently been utilized in hydrology (Long et al., 2014a). Although the ensemble mean of multiple time series is also used, which considers the uncertainties associated with the individual data series, was adhered to (Ferreira et al., 2016). The combined TWS series

corresponding to the minimal noise variance is generated based on the common signals' removal from the multiple data series (Abhishek and Kinouchi, 2021; Chen et al., 2019; Koot et al., 2006).

Since all of the water storage components are influenced by either climatic impacts or anthropogenic impacts, or a combination of both, the dynamics of each component need to be understood to assess how the water moves through the system (AghaKouchak et al., 2021; Scanlon et al., 2015). Therefore, the individual water storage components of TWS were segregated using the regional water balance to better understand the imbalance between water inputs and outputs. Mathematically,

$$\mathrm{TWS} = \mathrm{SWS} + \mathrm{SMS} + \mathrm{GWS} \quad (4.4)$$

where, SWS, SMS, and GWS are storage components corresponding to the surface water (i.e., the water storage in the dam reservoirs, flood inundation, and rivers), soil moisture, and groundwater. Please note that all of the above water storage components and the climatic variables are basin-averaged monthly time series anomalies relative to the long-term mean of the individual time series and are represented as the equivalent water depth (cm) or as equivalent water volume (km^3). The basin-wide river water storage data was obtained as the difference between catchment water storage and soil moisture following the Green–Ampt (G-A) model for 2002-2011 (Sayama et al., 2015) and was estimated for 2012-2020 using the current MLP BP-GA model with dam water storage, water release from dams, stream gauge data collected at Nakhon Sawan (Fig. 4.2), TWS, and P as predictors. Additionally, the flood inundation depths simulated for 2002-2011 by the rainfall-runoff-inundation (RRI) model (Sayama et al., 2015) and estimated for 2012-2020 using the ANN model were used. Lastly, linear and non-linear trends (extreme-point symmetric mode decomposition method; ESMD) were quantified. Further details of the ESMD method can be found in Chen et al. (2019), Wang and Li (2013), and Wu et al. (2020). ESMD is an improved version of the Hilbert–Huang Transform (HHT) in terms of the extreme-point symmetry, empirical mode decompositions, optimal sifting times, and data-based interpolation (Huang and Shen, 2014; Wang and Li, 2013), and therefore outperform the typical running-mean and least-square approaches.

4.2.6. Water storage deficits

Further, the monthly climatology was removed from all the water storage components to get insights into the dynamics of each component and their contribution to flood and drought events. E.g., the deficits and surplus in the terrestrial water storage were calculated as,

$$\mathrm{TWSD_{j,k}} = \mathrm{TWSA_{j,k}} - \overline{\mathrm{TWSA_k}} \quad (4.5)$$

where TWSD is the terrestrial water storage deficit (or surplus), subscripts j and k represent the year and month, respectively, $\mathrm{TWSA_{j,k}}$ is the terrestrial water storage anomaly for the j^{th} year and k^{th} month, and $\overline{\mathrm{TWSA_k}}$ is the average of monthly TWSA over the period between September 2002 and August 2020. Similarly, the surface water storage deficit (SWSD), soil moisture storage deficit (SMSD), and groundwater storage deficit (GWSD) were calculated.

4.2.7. Uncertainty analysis

Assuming the solution uncertainty as the major contributor (and neglecting the trend and glacial isostatic adjustment uncertainties), the GRACE total uncertainty was calculated as the standard deviation of the estimated trends among different solutions (Li et al., 2019; Scanlon et al., 2018). A similar procedure of standard deviation was used for precipitation, evapotranspiration, soil moisture, and temperature. Since SWS consists of only the observed data, based on the literature (Abolafia-Rosenzweig et al., 2021), a linearly interpolated mean monthly uncertainty of 2.3-28.8% from the highest to the lowest flow in the SWS time series was considered and subsequently propagated to the trends following weighted least square regression (Long et al., 2016). Since all other components except GWS of Eq. 4 were obtained from the independent data sources, one-sigma trend errors in GWS were estimated by propagation through various water storage (WS) components ($\sigma_{\mathrm{GWS}} = \sqrt{(\sigma_{\mathrm{TWS}})^2 + (\sigma_{\mathrm{SWS}})^2 + (\sigma_{\mathrm{SMS}})^2}$; Voss et al. (2013)).

4.2.8. Drought Potential Index (DPI)

Traditionally, drought is defined solely by the deficit (below normal) conditions in climatic (e.g., precipitation), hydrological (e.g., runoff), or agricultural (e.g., soil moisture) variables, occurring primarily due to the natural variabilities that are beyond the control of policymakers (AghaKouchak et al., 2021; Shukla and Wood, 2008). However, in the complex human-nature systems, droughts (termed ‘anthropogenic droughts’, AghaKouchak et al., 2021) evolve due

to the synergistic impact of natural and anthropogenic drivers, which are generally difficult to disentangle (Rodell et al., 2018). In this regard, in addition to analyzing the drought behavior from various standardized indices, a novel Drought Potential Index (DPI) was devised based on the monthly time series of TWSA following the effective water storage-based approach first used by Reager and Famiglietti (2009) for estimating the flood potential. For this aim, firstly, the monthly rates of the minimum required relative storage change, S_{def}^{t}, were calculated as below,

$$S_{def}^{t} = S_{min} - S^{t-1} \tag{4.6}$$

where S_{min} is the minimum TWSA during the wet season in the study period (10.57 cm on Oct 2015), and S^{t-1} is the TWSA of the previous month ($t-1$). To remove the effects of the regional hydrological heterogeneity and the average difference between the storage change and precipitation that may not always result in drought, the normalized drought potential index was then obtained from the monthly drought potential amount (DPA) as follows:

$$DPA^{t} = P_{anom}^{t} - S_{def}^{t} \tag{4.7}$$

$$DPI^{t} = \frac{DPA(t)}{\min(DPA(t))} \tag{4.8}$$

where P_{anom}^{t} is the precipitation anomaly corresponding to the month t, and DPA represents the difference in the deficit of the system's available water storage and precipitation (water that sustains runoff or evapotranspiration owing to the precipitation influx). DPI varies from -1 to 1; the closer it is to 1, the more drought is likely to occur. In the regions like CPRB, where the compounding effects of the natural water variability and human activities are pronounced and crucial for sustainable water management, DPI will enable us to quantitatively characterize the transition for the region to a drought-prone situation, which can evolve even during the wet season.

4.3. Results and discussion

4.3.1. TWS based on GRACE(-FO)

Terrestrial water storage anomalies (TWSA) presented as basin-averaged water depth (mm) or equivalent water volume (km^3) from the three GRACE solutions agreed well in terms of amplitude and dynamics and are highly consistent in terms of the Pearson correlation ($r >$

0.95), and are following 1:1 line as shown in the scatter matrix (Figures 4.5). Some minor discrepancies among TWSA products can be attributed to different processing algorithms and correction and filtering methods used by various data centers. However, all variations are well within the error ranges of the GRACE data with no significant biases, which is consistent with the previous studies. Hence, a combined TWSA series was obtained by the TCH method (Figure 4.6). Since all three TWSA time series from various data processing centers utilize common GRACE and GRACE-FO data, they agree favorably well. For filling the gap in GRACE and GRACE-FO records, the artificial neural network (ANN) BP-GA model was run for various combinations of the predictors' monthly time series. The performance of the ANN model improved as the number of predictors increased while keeping the precipitation (major influx) and soil moisture persistent (previous studies, e.g., Long et al. (2013), Sun et al. (2020) showed that the strong correlation of SMS with GRACE TWSA) (Figure 4.7). All the model runs showed in Fig. 4.7 agree well with the observed TWSA in terms of the seasonal phase. Moreover, the coupled genetic algorithm eliminates the need for the trial and error method for determining the optimum number of the hidden neurons in the model setup. The best performing model during the training (r = 0.96, NRMSE = 0.31, NSE = 0.90) using the five predictors, viz., GLDAS based TWSA, temperature, evapotranspiration, precipitation, and soil moisture storage, was used further for validation and prediction (estimation) phases. The model showed a good agreement in the validation phase with r = 0.94, NRMSE =0.39, and NSE = 0.85 (Fig. 4.6(b)). Good model performance can partially be ascribed to a) small uncertainties in GRACE data, primarily from the short-wavelength signals and subsequent filtering processes which tends to be smaller for large areas, b) ample predictor availability from ancillary data sources, and c) the embedded genetic algorithm avoids underfitting or overfitting in the ANN model. These results indicate that the proposed MLP BP-GA model can be used not only to fill the data gaps between GRACE-(FO) but also to forecast TWSA

ahead of the satellite data subject to the availability of the forecasted time series of various predictors.

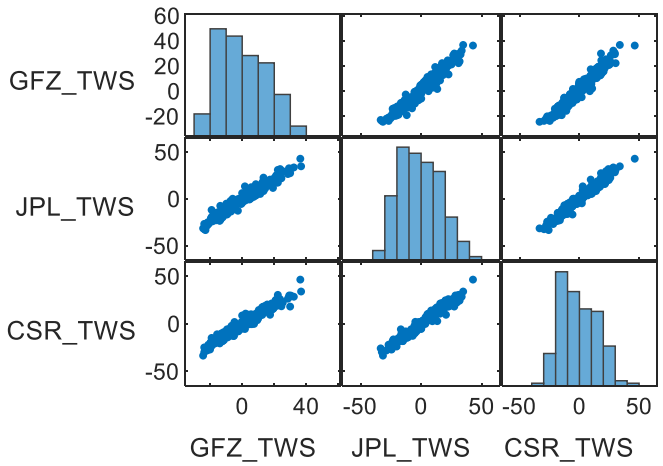

Figure 4.5. Scatter matrix of the three TWSA time series. After (Abhishek et al., 2021).

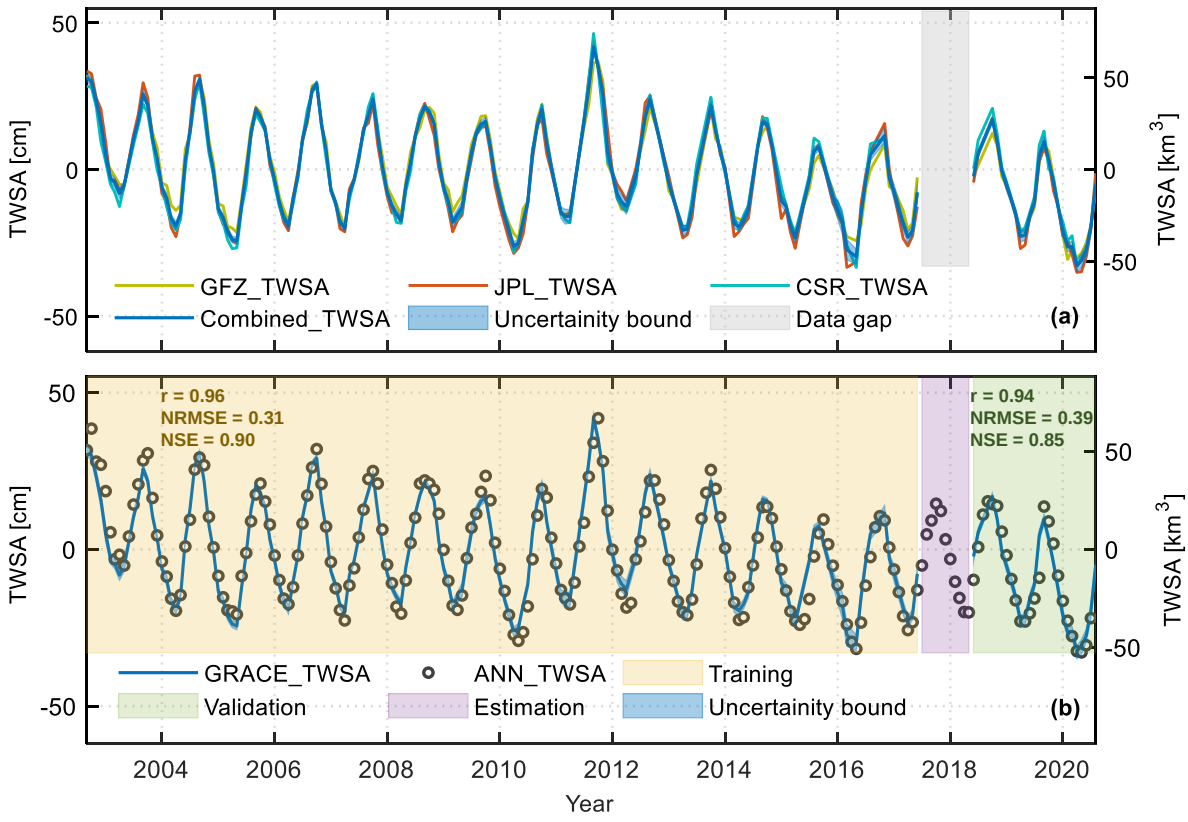

Figure 4.6. Time series of GRACE based and ANN derived TWSA over CPRB. (a) Monthly terrestrial water storage anomaly (TWSA) time series from the three data processing centers. The combined TWSA series and the uncertainty bound are also shown with a blue-colored

solid line and light blue shaded area, respectively. The grey shaded region highlights the data gap of 11 months between GRACE and GERACE-FO records. (b) Monthly TWSA based on GRACE(-FO) data (solid blue line) and the best performed ANN model (black circles) over the period September 2002 through August 2020. The shaded areas also show the various phases of training, validation, and estimation along with the TWSA uncertainty bound. Please note that GRACE_TWSA of Fig. 3(b) is the same as Combined_TWSA of Fig. 3(a). Various performance indicators are also shown for the training and validation phases. After (Abhishek et al., 2021).

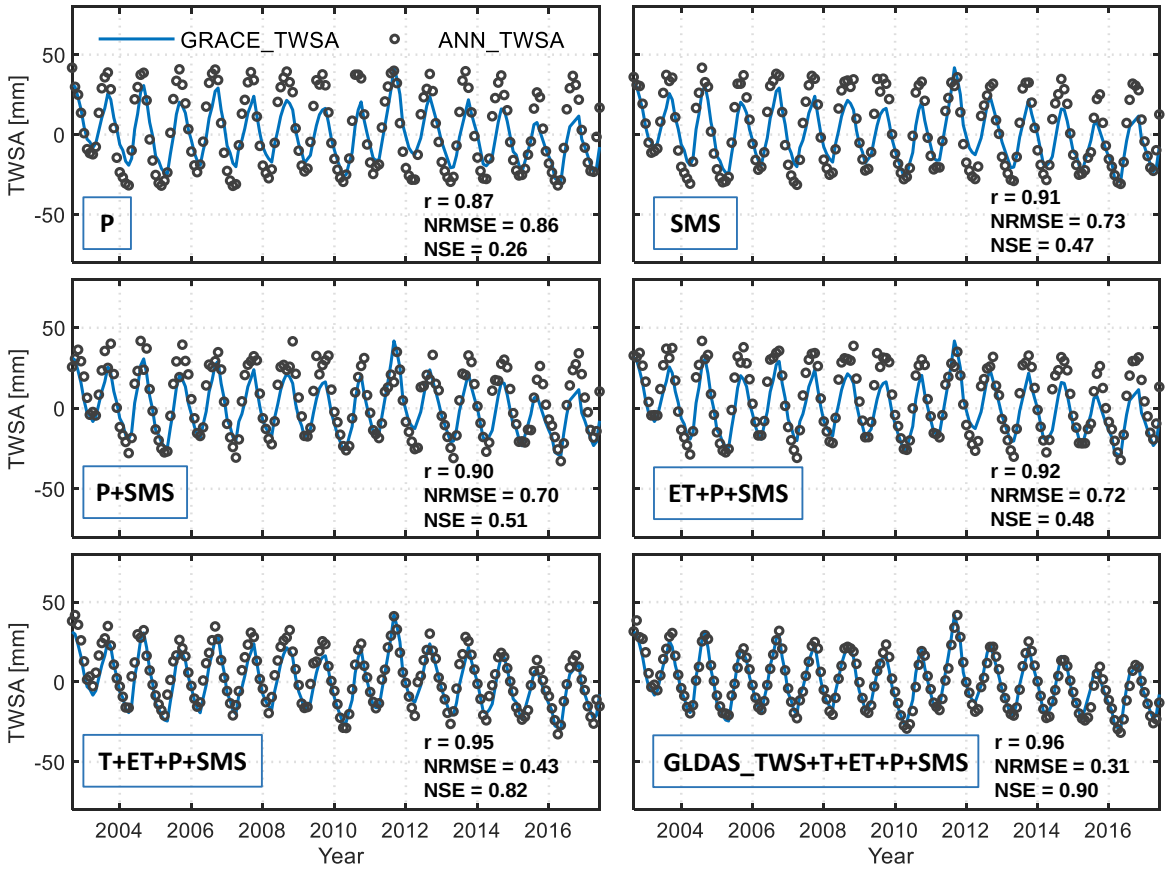

Figure 4.7. Comparison between GRACE-based and ANN-modelled TWSA for various combinations of the predictors during the training phase**.** After (Abhishek et al., 2021).

4.3.2. Hydrological fluxes and water storage dynamics

Figure 4.8(a) shows the monthly anomaly series of the ensemble mean precipitation (P) and evapotranspiration (ET) and the respective spread of the values from various products.

Composite annual cycles of P and ET are shown in Figure 4.9. Two peaks can be observed in precipitation where the first swift peak during May can be attributed to the western monsoon onset, and the second peak during August corresponds to the tropical rainfalls from the South China Sea combined with the western monsoon rainfall in the basin. South winds and northeast monsoon contribute to the marginal rain in the non-monsoon season. The high fluctuations in the monthly precipitation emphasizes the significance of seasonal (monsoon and non-monsoon) and intra-annual precipitation throughout the year (Figure 4.10). The minimum of the precipitation anomaly is relatively constant during the dry season with a deficiency of ~11 cm throughout the study period, which can be explained by the reason that the basin receives only 10% of the precipitation during the dry season, i.e., from November to April (Figures 4.8 and 4.9). Monthly terrestrial water storage anomaly (TWSA) over the Chao Phraya River Basin varies from -31.81 cm (May 2020) to 42.86 cm (Oct 2011), with a similar seasonal dynamic during the study period (Figure 4.8(b)). The basin experienced a decreasing trend of -1.12±0.05 cm yr^{-1} (equivalent to a volumetric trend of -1.79±0.08 km^3 yr^{-1}) in TWSA from Sept 2002 to Aug 2020. Decreasing trends in precipitation (1.5%), increasing air temperature (6.4%, Figure 4.11), increasing evapotranspiration (10.21%; consistent with the global increase in ET by 10±2% as reported by Pascolini-Campbell et al. (2021)), relative to their long-term means, and their seasonal variations have partly contributed to the decrease of TWS.

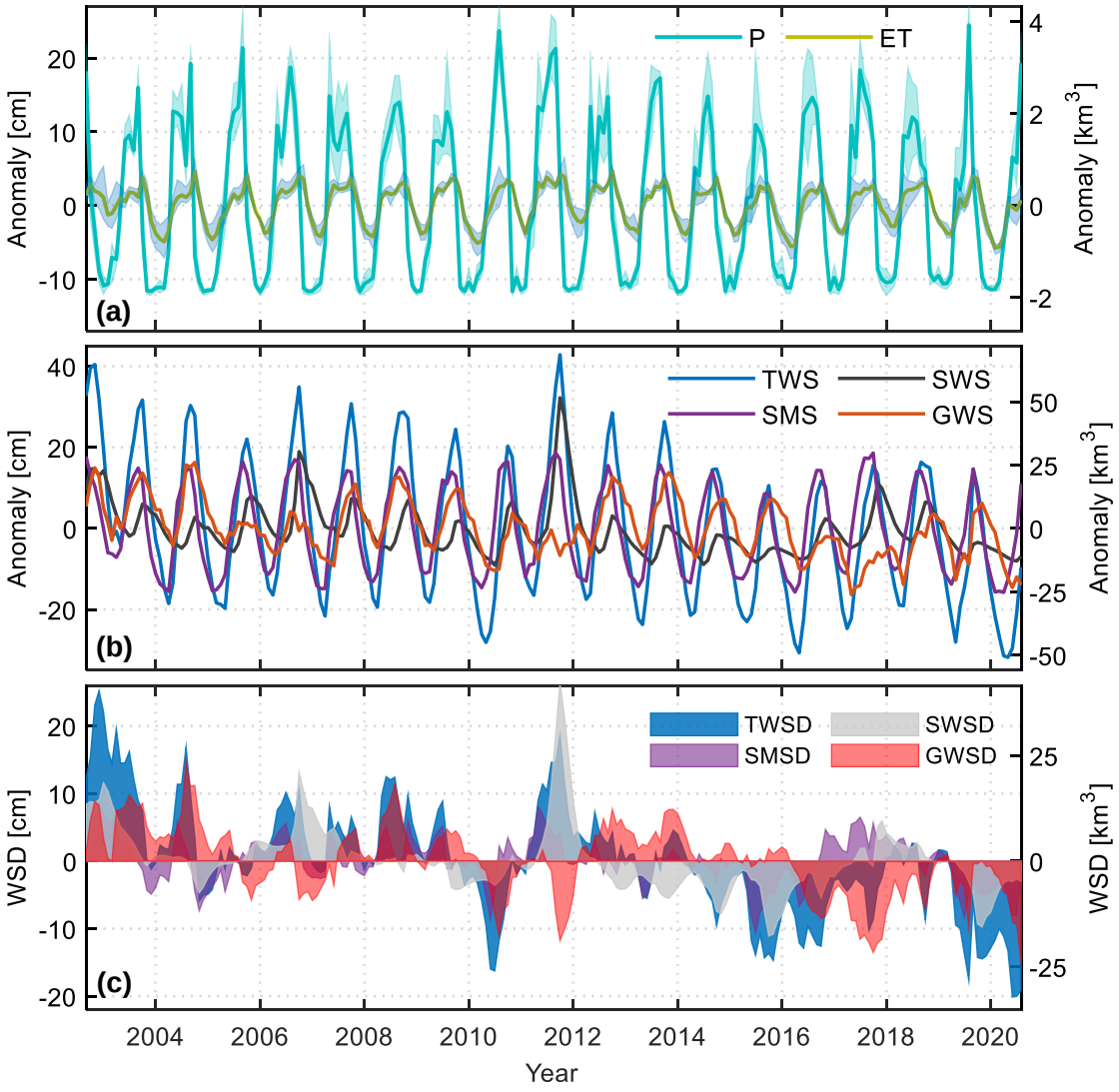

Figure 4.8. Time series of monthly hydrometeorological fluxes, water storage components, and the deseasonalized components. (a) Monthly anomalies of ensemble precipitation (P) and ensemble evapotranspiration (ET) with the range of various datasets shown by shaded areas. (b) Monthly anomalies of terrestrial water storage (TWS), surface water storage (SWS), soil moisture storage (SMS), and groundwater storage (GWS). The monthly anomalies of all the variables are represented as the monthly time series of basin averaged equivalent water depth (cm) or equivalent water volume (km^3) from Sept. 2002 to Aug. 2020. (c) Water storage deficits (both positive and negative, i.e., deficit and surplus) in terrestrial water (TWSD), surface water (SWSD), soil moisture (SMSD), and groundwater (GWSD) storage calculated by removing the monthly climatology from each time series. After (Abhishek et al., 2021).

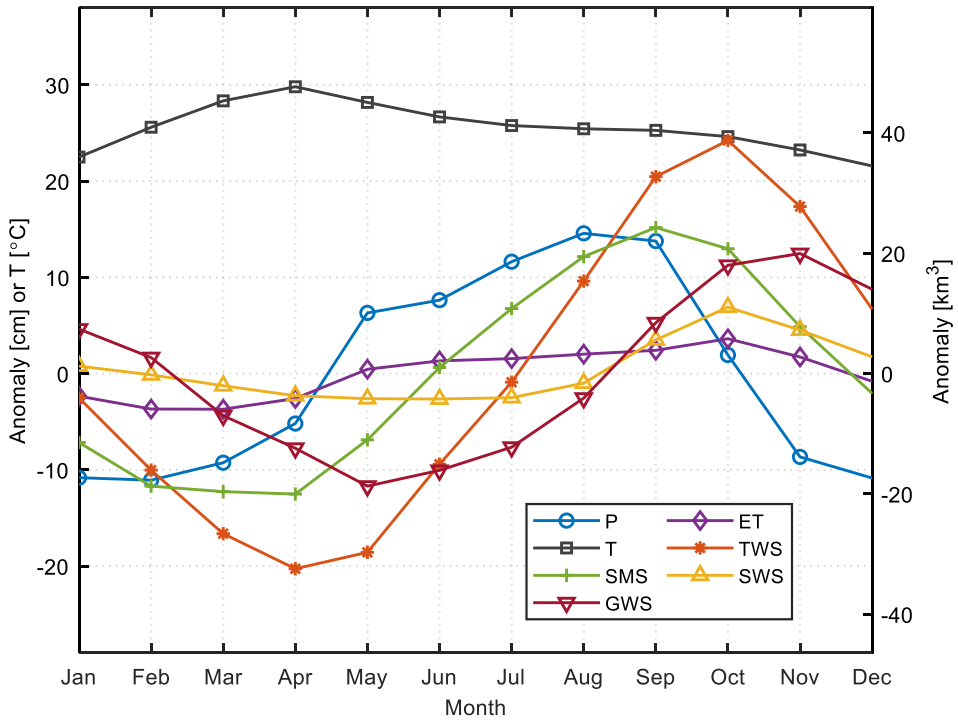

Figure 4.9. Composite annual cycle of various hydrological fluxes and various water storage components in the Chao Phraya river basin from Sept 2002 to Aug 2020. Monthly mean (not anomaly) air temperature (T) is also shown during the study period. After (Abhishek et al., 2021).

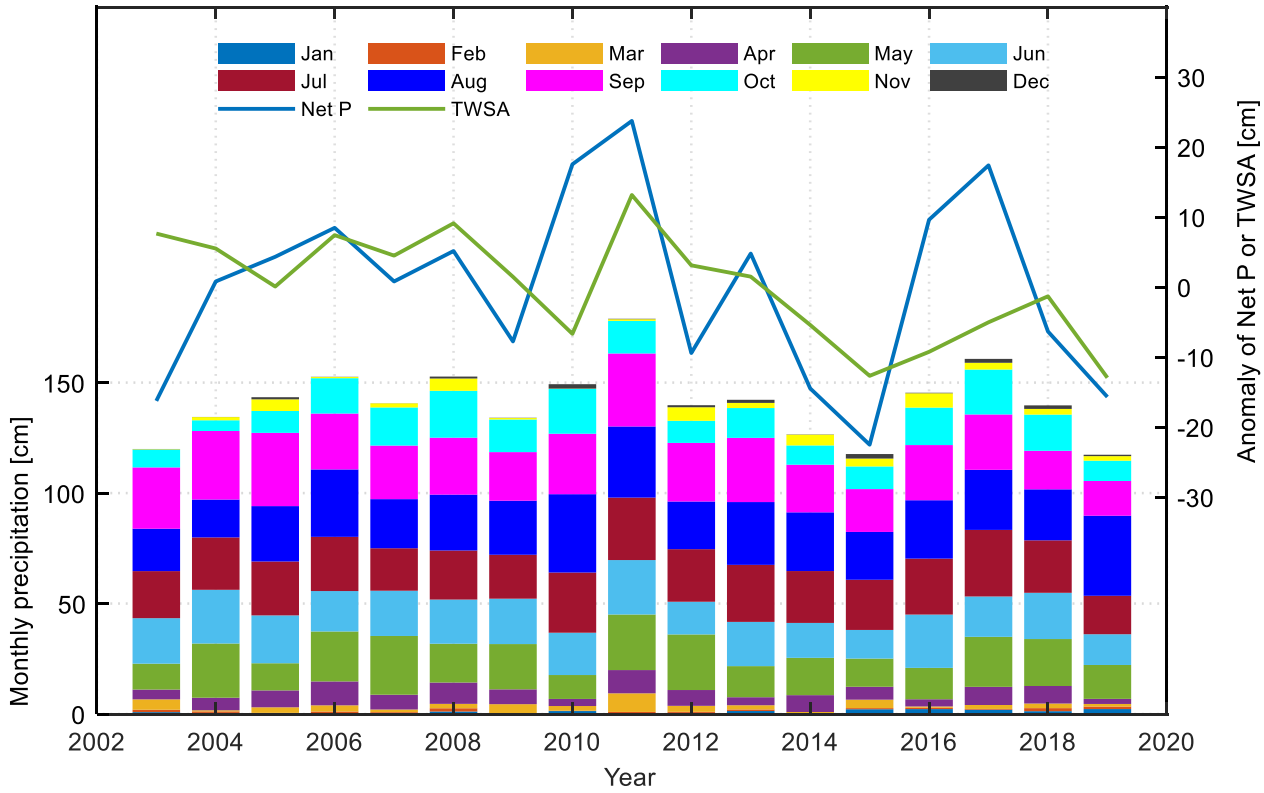

Figure 4.10. The anomaly of annual total net precipitation during monsoon (May to October) and the annual mean anomaly of TWSA with two months' lag time (July to December). Both net precipitation (net P) and TWSA are represented as the basin-wide anomalies of the respective time series. The monthly distribution of precipitation during 2003-2019 is also shown. Years 2002 and 2020 were excluded from this analysis because they did not cover full-year data in the study. After (Abhishek et al., 2021).

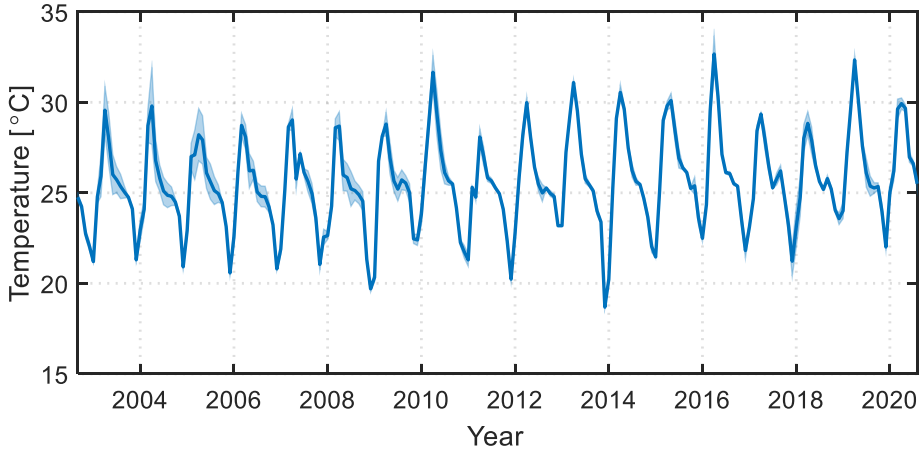

Figure 4.11. Monthly anomaly time series of air temperature. After (Abhishek et al., 2021).

Further, to quantify the effects of the reservoir water management, the water storage in major dam reservoirs was analyzed, which showed similar dynamics and ~15% amplitude of TWSA (Figure 4.12). A time lag of up to two months from TWSA is due to the travel time of the runoff to the reservoirs. Linear decreasing trends (-0.40±0.03 cm yr^{-1} or -0.64±0.05 km^3 yr^{-1}) in total surface water, including dam water storage from eleven dams (Figure 4.2), flood inundation water depth, and river water storage, explains about 36% of TWSA trends in the basin. Soil moisture storage and groundwater storage show the long-term linear trend of decrease at the rate of -0.21±0.02 cm yr^{-1} (-0.34±0.03 km^3 yr^{-1}) and -0.51±.06 cm yr^{-1} (-0.82±0.10 km^3 yr^{-1}), which are about 19% and 45%, respectively, of the total TWSA trend. The soil moisture storage is slightly decreasing (5%) in the region primarily due to the increasing temperature and decreasing precipitation. High fluctuations in SMS are evident during the 2011 flood and 2015 drought years, respectively (Figure 4.8(b)).

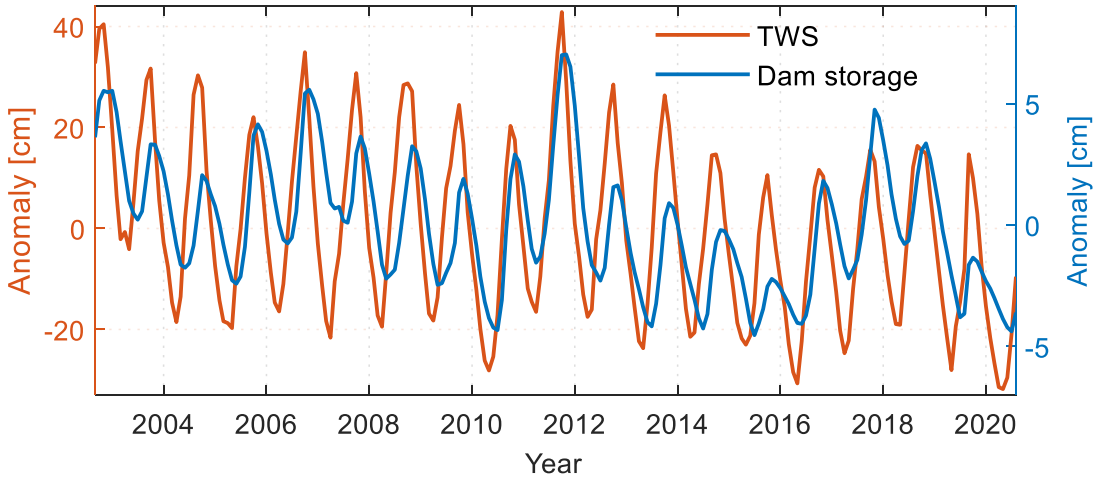

Figure 4.12. Monthly anomalies of the terrestrial water storage (solid coral line) and the total water storage in major dam reservoirs (solid blue line). After (Abhishek et al., 2021).

Further analysis of the residuals of P, ET, and WS components using the ESMD approach (Figure 4.13) reveals the footprints of major flood and drought events in the basin. A convex shape is found in TWS, SMS, and SWS during the period of 2006-2013 due to the water surplus and two major flood events during this period. GWS has been continuously decreasing throughout the study period with much steep decline in recent years (Figure 4.13), which can be explained by the joint influence of long-term droughts, pumping-induced localized declines, and seasonal and inter-annual water table fluctuations. The current findings of highly declining trends in GWS are consistent with the annual groundwater reports by the Department of Groundwater Resources, Thailand, when compared qualitatively with

the basin-wide GW level depth data (decline as much as 50 cm yr^{-1}). The groundwater (GW) level varies from being fairly constant in a few wells to a huge decline of several meters in the majority of wells in recent years (Figure 4.14). Thus, groundwater storage plays a major role in TWS in the basin, albeit the observed behavior needs to be further investigated in the future.

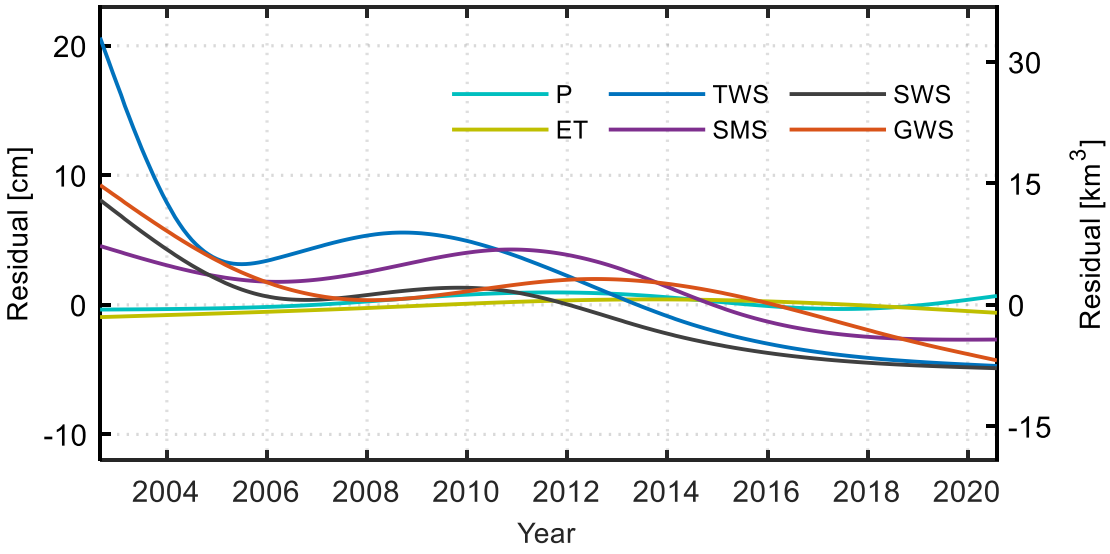

Figure 4.13. Residuals of the various hydrometeorological and water storage components as calculated by the ESMD approach. Time series of the various intrinsic mode functions are not shown for simplicity. An initial sharp decline in TWS and GWS is partly due to the 2002 drought year and partly due to the duration of the particular time series in ESMD. While the residuals in ensemble P and ET do not have significant trends, all the water storage components have declining trends, particularly after 2014. After (Abhishek et al., 2021).

Since the spatiotemporally sufficient groundwater table data, well location data, and the aquifer properties (specific yield, specific storage, and aquifer thickness information) were not available, the groundwater table fluctuations were analyzed by a set of representative 21 wells in the basin (Figure 4.14). The legends in Figure 4.14 correspond to the actual well names available at the Department of Groundwater Resources website (www.dgr.go.th). The y-axis in the figure corresponds to the inverted depth (in meters) of the groundwater table from the surface. Given the aforementioned data unavailability, it was constrained to qualitatively compare the currently estimated groundwater storage (GWS) with the observed groundwater table data. The annual groundwater reports prepared by the Department of

Groundwater Resources (available at http://www.dgr.go.th/th/public-service/329 in the Thai language only) report that the groundwater wells have a basin-wide decline in the groundwater table as large as 50 cm per year during recent years (Figure 4.14(b)). However, the groundwater declines in the regions of Bangkok (Figure 4.14(a)) is heaving a decline of as high as >200 cm per year. The overall declining behavior of GWS is evident in this analysis of long-term GWS dynamics and linear as well as non-linear trends (Figs. 4.8(b) and 4.13).

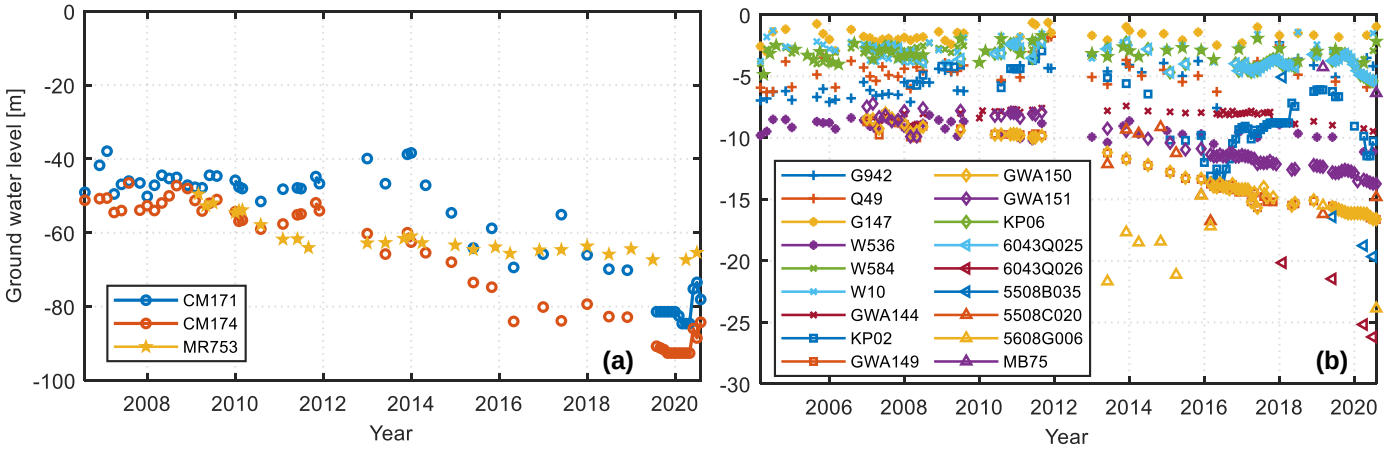

Figure 4.14. Groundwater table variations in the representative 21 wells in the basin. (a) Three wells around the Bangkok region, and (b) the remaining 18 wells located throughout the Chao Phraya River Basin. The exact location of the wells is not shown due to the limited access to the related data. All other wells were also found to be possessing similar data gaps and similar dynamics, and therefore not shown. After (Abhishek et al., 2021).

All the water storage components follow similar temporal dynamics with different annual amplitudes, as revealed by the 18-year composite intra-annual cycle (Figure 4.9). SMS and GWS have a lag of two and three months in minima with precipitation, while their maxima are in a lag of zero and two months, respectively (Fig. 4.9). This lag time behavior can be primarily explained by the synergistic influence of the inherent vadose zone processes (e.g., infiltration, percolation, etc.) and human water abstractions. Instances of variations in the lag months between precipitation and soil moisture storage (SMS) or groundwater storage (GWS) (e.g., 2011, 2015) can mostly be caused by the monthly variations of the precipitation and subsequent changes in water withdrawal and usage behavior, especially during the years of droughts or floods (Fig. 4.8). Since TWS integrates SWS, SMS, and GWS, it attains the maxima and minima in-between these components and with a variable lag time of one to three months (Figs. 4.8 and 4.9). All the water storage components show a dampened

response to precipitation due to the prevailing hydrological processes in the surface and subsurface systems. Smaller amplitudes in the anomalies (Fig. 4.8(b)) and detection of the more acute decreasing trends in the WS components than that of precipitation (Fig. 4.10) during the recent periods also highlight the weakening hydrological cycle in CPRB. To ascertain this situation, storage deficit and surplus in various water storage components were calculated after removing the respective climatology for each month as per Eq. 4.8. Results reveal the prolonged persistence of the GWS deficit (or surplus) conditions as compared to the SMSD (Fig. 4.8(c)). Groundwater storage deficit (GWSD) has continuously been negative from Apr 2014 until recently, while SMSD has experienced a minor recovery phase during 2018. Signatures of major floods and drought events are evident in all the WS components with varying magnitudes and persistence (Fig. 4.8(c)). Monsoon precipitation and water abstractions were the controlling factors of recovery and depletion, respectively, of various water storage components.

4.3.3. Seasonal analysis of net precipitation and TWS change

To further analyze the seasonal variations in net precipitation (P-ET) and TWS, the anomaly of annual total P-ET and annual mean TWSA were compared during the monsoon season (from May to October for precipitation and from July to December for TWS) (Fig. 4.10) and corresponding percentage changes during the study period (Fig. 4.15). An average lag of two months was observed in TWS from precipitation and hence was taken into consideration. TWSA well captures the hydroclimatic extremes in the basin in response to the precipitation heterogeneities. During the monsoon seasons of 2010 and 2011, the basin received an excess of 40.27 and 54.29% net precipitation, which resulted in a 99% increase in the TWS during the severe flood year 2011 (Fig. 4.15). Although the net annual precipitation during the monsoon season in 2011 is comparable to other years, e.g., 2010 and 2017 (Fig. 4.10), the flood of 2011 was amplified by the anomalously high rainfall in the pre-monsoon season in 2011 (bar graphs in Fig. 4.10) along with the frequent tropical storms from the northern Pacific Ocean between June to October in the basin (Thai Meteorological Department, 2011). The flood intensity was further exaggerated by the year-long relatively high soil moisture content along with the elevated sea level height in the Gulf of Thailand, partly constraining the basin's drainage (Promchote et al., 2016; Rakwatin et al., 2013). A large decline in TWS in 2010 can be explained by the larger negative anomaly of GWS in 2010 affected by the smallest non-

monsoon precipitation during Nov-2009 to Apr-2010 (bar graphs in Fig. 4.10) and higher temperature and evapotranspiration in 2010 (Figs. 4.8(a) and 4.11). Such effects of the seasonal variations in precipitation on TWS dynamics can also be seen during 2003-2004. Years 2016 and 2017 also received above-average net rainfall (22.31% and 39.87%), respectively, which led to a positive change of 32.70% in TWS, which was still negative compared to the long-term mean of TWS in the monsoon season (Fig. 4.15). The drought of 2015, along with other drought events, is evident in TWSA (Figs. 4.8(b) and 4.10). The largest deficit in the precipitation was observed during the years 2015 (48.49%), 2019 (34.35%), and 2014 (25.17%), which correspond to the relative TWS deficits of 101.1%, 103.2%, 44.77%, respectively. An opposite behavior is observed during the years of 2003, 2004, 2010 (TWSA showed +56.31%, +39.81%, -54.61% while precipitation -35.93%, -23.90%, and 27.07%, respectively). This inconsistency can most likely be attributed to the antecedent precipitation and water availability (especially surface water), which, in turn, affects the GW withdrawals patterns. This variability in TWS highlights insufficient storage in the system, and hence, employing water conservation practices (e.g., rainwater harvesting) in the basin is of paramount importance. Moreover, since the atmospheric circulation, assessed by the regression analysis of Southern Oscillation Index (SOI) and Niño 3.4, explains only about 12% and 18% variance in TWSA, respectively, (and are weakly correlated with r = 0.34 and -0.42; Fig. 4.16) human abstractions seem to be significant factor governing the water storage dynamics in the region, which needs to be further investigated in future multiscalar studies using various statistical and dynamical models and in-situ data. Moreover, the recent period of continuous deficit in TWS, when combined with the persistent deficiency in the precipitation, may lead to a transition to a drought-prone situation in the basin. Similarly, the likely occurrence of the floods in response to the continuous heavy precipitation, e.g., one experienced in 2011 in the basin, has direct implications on the better reservoir management practices or the irrigation water allocation plans in the basin.

Temporal patterns of depletion and recovery in different storage components, terrestrial water storage (TWS) in particular, help to assess the evolution of the hydro-climatic extremes in the basin and to better manage the prevailing water resources. The depletion and recovery behavior of TWS in the basin in response to the wet and dry cycles, defined according to the 12-month moving average of the net precipitation flux (Fig. 4.17), seems to be primarily controlled by the variable water influx in the system in response to the dry and wet cycles

which in turn affects the human abstractions. A total of 4 and 3 events of multiyear depletion and recovery, respectively, were quantified in the basin. TWS depleted (~48 km^3) from Sept 2002 to May

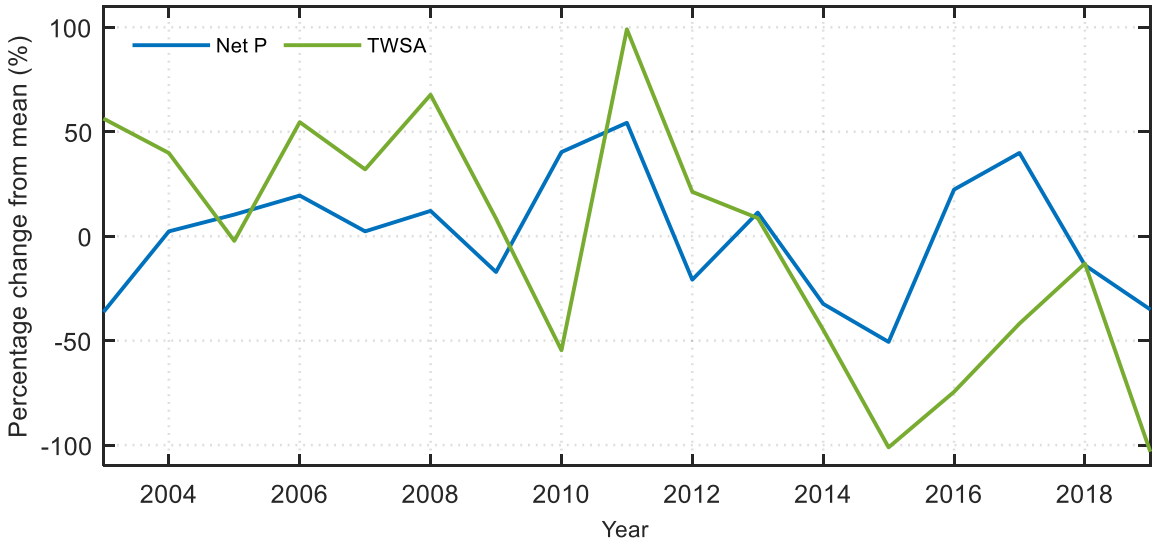

Figure 4.15. Percentage change from the long-term mean of the basin-wide precipitation during May and October and TWS during July and December. After (Abhishek et al., 2021).

2005, followed by a short recovery (~12 km^3) until June 2006, while remaining almost stable until Nov 2008 (Fig. 4.17 and Table 4.1). A deficit in the precipitation flux (-17.14%) combined with the most likely increase in GW pumping during 2009 lead to a depletion of 22 km^3 until May 2010, which was recovered by ~26 km^3 after receiving an excess of cumulative precipitation flux ~95% in the two consecutive years. After the 2011 flood, the basin suffered from the dry phase, with a short wet phase during 2013, until mid-2016, which led to a depletion of ~32 km^3 in the basin. The depletion rate was slowest (-0.63 km^3 $month^{-1}$) due to the stringent irrigation regulations during this period. A slow recovery of ~17 km^3 from Jan 2016 to Oct 2018 was followed by the highest depletion until Aug 2020 with a rate of ~1.8 km^3 $month^{-1}$ (Fig. 4.17). In general, the basin's aquifer system has fast depletion rates due to the less net influx and large dependence on groundwater to supplement the deficit of surface water, especially during drought years, e.g., 2018-2020 (Fig. 4.17 and Table 4.1). Moreover, the steepest decline in TWS in recent times is alarming for another severe drought in the basin if the precipitation remains average or below average in the subsequent year(s).

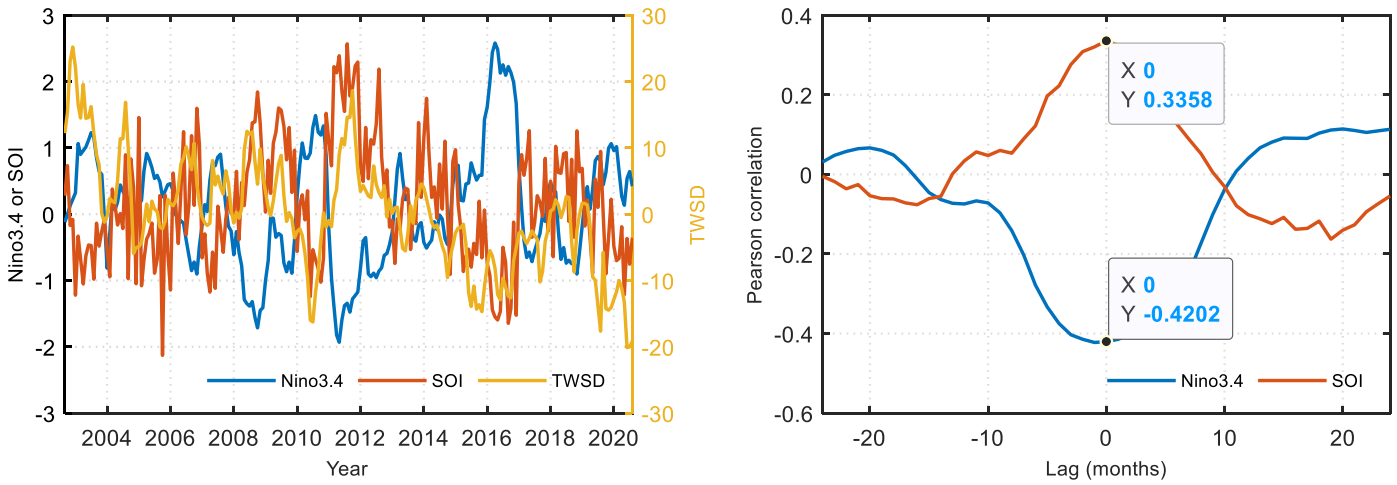

Figure 4.16. Time series of Niño3.4, SOI, and TWSD (left), and lagged correlation of TWSD with Nino3.4 and SOI (right). After (Abhishek et al., 2021).

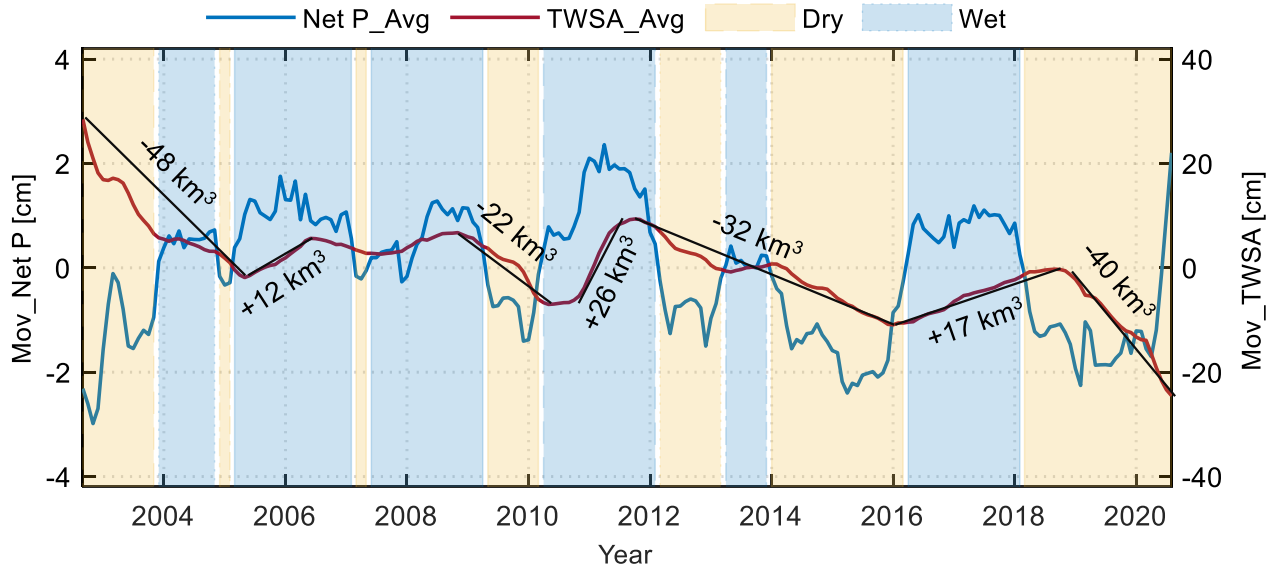

Figure 4.17. 12-month moving averages of the net precipitation and terrestrial water storage (TWSA) from Sept 2002 to Aug 2020. The shaded areas qualitatively characterize the wet and dry cycles as wet, dry, respectively, with respect to the long-term mean net precipitation. The total depletion and recovery of TWSA during the respective periods are also shown with solid black lines with the respective volumetric water loss or gain in km^3. After (Abhishek et al., 2021).

Table 4.1. Multiyear hydro-climatic events in the Chao Phraya river basin. After (Abhishek et al., 2021).

Type of extreme	Interval	Duration (months)	Equivalent water depth (cm)	Volume (km^3)	Volumetric rate of depletion/surplus ($km^3\ month^{-1}$)
Deficits	Sept-02 to May-05	32	-30	-48	-1.5
	Nov-08 to May-10	18	-14	-22	-1.2
	Oct-11 to Jan-16	51	-20	-32	-0.63
	Oct-18 to Aug-20	22	-25	-40	-1.82
Surplus	May-05 to Jun-06	13	-7.5	+12	0.92
	Jun-10 to Oct-11	16	-16	+26	1.6
	Jan-16 to Oct-18	33	-11	+17	0.51

4.3.4. Monthly surplus and deficits in TWS

The monthly deficits and surplus of TWS were investigated to reveal the factors affecting the depletion of TWS in recent periods. Fig. 4.18 depicts the monthly water storage surplus and deficit of TWS relative to monthly climatology during the past 18 years (Sept 2002 to Aug 2020). Total monthly deficit and surplus events are almost equal (107 and 109 events, respectively) in the basin, but the distribution is highly variable during the study period (Figs. 4.8(c) and 4.18). The basin mostly experienced a water storage surplus until Mar 2014 with some short-lasting deficit events, mainly during the dry periods of 2004, 2005, 2007, and 2010 or prolonged until the wet seasons augmented by large seasonal variation in precipitation at some instances (e.g., 2010). During the period from Sept 2002 until March 2014, the maximum duration of continuous deficits was one year from Nov 2009 to Oct 2010, while the surplus events lasted as long as 19 months from Mar 2011 to Oct 2012, centering the flood year of 2011. Since April 2014, the basin was getting dried continuously, with an occurrence of about 63% deficit events during this period, with a minimum of -20 cm in July 2020. Although there has been a peak in rainfall during August 2019, the average during the

year's rainy season was ~34% less than the average of long-term monsoon precipitation, which resulted in ~103% decrease in TWS during the year. There was no distinct annual distribution, except for a slightly higher number of surplus months during monsoon and post-monsoon season, of the monthly deficit or surplus events since the majority of the extreme events are spanning over multiple years.

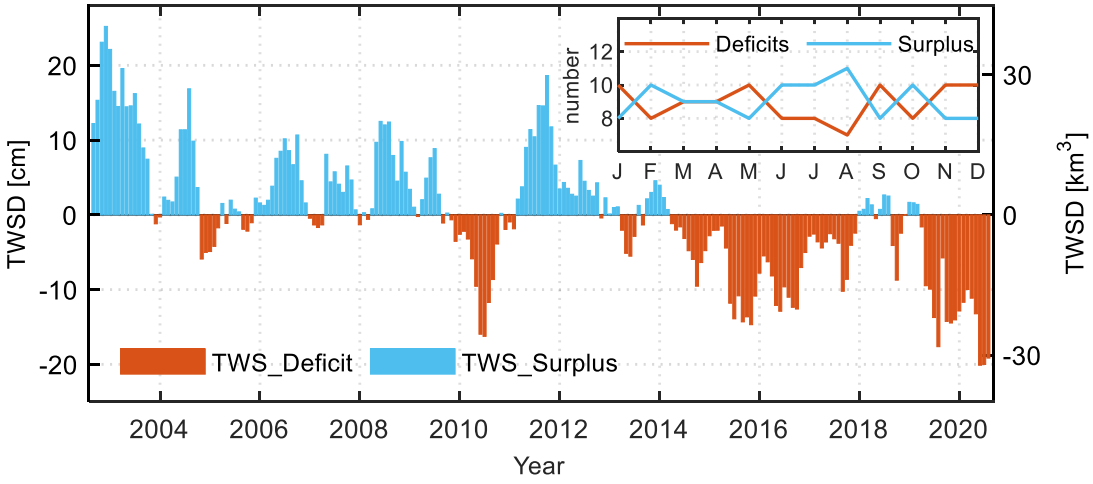

Figure 4.18. Time series of the monthly deficits and surplus in terrestrial water storage (TWS). The annual distribution of the deficit and surplus events (months) is also shown in the inset. After (Abhishek et al., 2021).

4.3.5. Drought propagation behavior

To analyze the behavior of drought evolution and propagation from meteorological to agricultural and the system's total water storage, a number of standardized indices, viz., standardized precipitation index (SPI12) (Scanlon et al., 2015), standardized soil moisture index (SSMI) (Das et al., 2020), and water storage index (WSI) (Z. Sun et al., 2018) were calculated and inter-compared as shown in Fig. 8. SPI and SSMI have a high correlation (r = 0.74) with a lag time of two months. TWSD based normalized WSI has a strong correlation (r = 0.69) and zero-month lag with SSMI but moderate correlation (r = 0.56) and a lag of one month with SPI12. This implies that the meteorological drought takes two months to reach the soil moisture and also to reflect in the water storage drought. The difference in the lag months between SPI12 and SSMI (two months) and that between SPI12 and WSI (one month) can be attributed to the effect of the groundwater storage (possibly more pumping in response to the less precipitation) since TWS is incorporating the GWS along with SMS.

These findings of the drought propagation in CPRB are consistent with those reported by Gevaert et al. (2018) by employing an ensemble of global hydrological models. The drought propagation time and the relative magnitude of the transformation from the meteorological drought to the water storage droughts in the basin can be utilized for engineering design and planning of the early warning systems for floods and droughts and may additionally constrain the hydro climate extremes' variability in future climate scenarios.

All three indices show similar inter-annual dynamics and amplitudes from Sept 2002 to Aug 2020, except for the three instances in 2004, 2011, and 2017 (Fig. 4.19, during which periods WSI showed a weak correlation with SPI and SSMI. From Apr 2004 to November 2004, WSI kept highly increasing compared to SPI and SSMI, while during Jan 2017 to Jan 2018, WSI kept sporadically decreasing, unlike SPI and SSMI, which were increasing during the period. In 2011, a long duration of high SPI, relatively small positive values of SSMI, and a shorter peak in WSI can be seen. This behavior can most likely be explained by the variations in the release of the water from the two major reservoirs in the basin, namely, Sirikit (capacity: 9.5 billion m^3) and Bhumibol (capacity: 13.5 billion m^3) dams, along with alterations in the groundwater abstraction during the extreme drought (e.g., 2017-2018) or flood (e.g., 2011) events.

4.3.6. Drought Analysis using DPI

To further ascertain the water storage deficit trends, the basin's drought potential was assessed by the new drought potential index based on the concept of the effective water storage availability in the basin at a given time. The normalized Drought Potential Index (DPI), being the direct indicator of the basin's water storage deficiency, represents the integrated drought potential in the basin. The dry season (Nov to Apr) is the main period of drought in the basin, as illustrated by the DPI dynamics in Fig. 4.20. While DPI attains a minimum value of -0.94 during the peak flood of 2011 when TWSA is maximum (42.86 cm) (both values for Oct 2011), it attains a maximum value of 1 in May 2016, although the minimum TWSA occurred in May 2020 (-31.81 cm). This difference can be explained by the fact that unlike TWS, which is the integrated water storage estimate at any month, DPI reveals the excess water (minimum required relative storage change) that sustains runoff or evapotranspiration on the basin (Figs. 4.20 and 4.21). Thus, DPI helps to gain insights into the tendency of the basin to experience droughts that could not be analyzed merely by monthly TWSA series. An

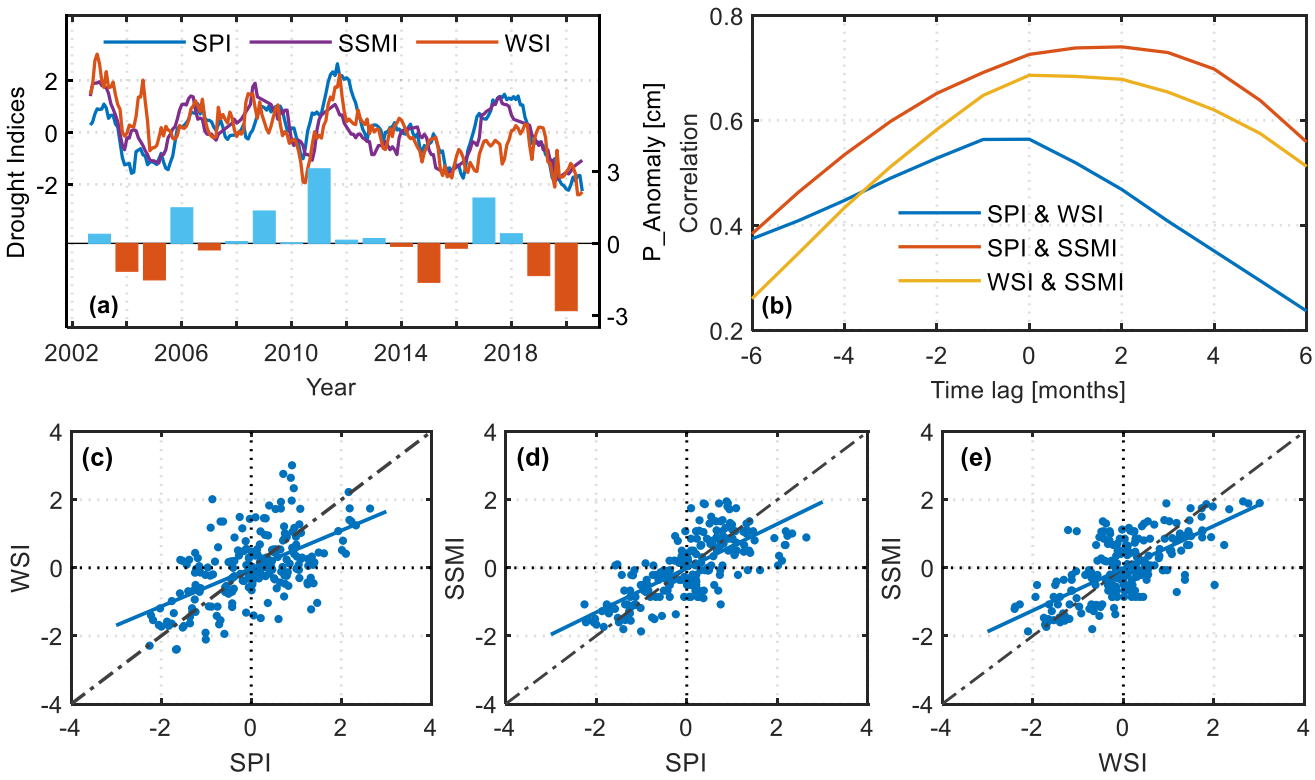

Figure 4.19. (a) Various drought indices (standardized precipitation index, standardized soil moisture index, and the water storage index) along with the yearly precipitation anomaly, (b) correlation among various indices with monthly lag, and (c-e) the scatter plots of all indices. After (Abhishek et al., 2021).

increasing trend of DPI highlights the greater drought potential in the Chao Phraya River Basin from Sept 2002 to Aug 2020. Also, the continuous higher values of DPI (including both maxima and minima) in recent years indicate the most likely occurrence of a drought event and indicate the possible transition of the basin towards a drought-prone region.

During the dry season, the storage in the dam reservoir is substantially important, even if TWSA is low. For example, in 2015, CPRB experienced an extremely severe drought, and farmers were forced to stop irrigation. In this year, both TWSA and dam storage were very low not only in the dry season but also in the wet season (Fig. 4.12). In 2018, although the minimum level of TWSA is similar to 2015, no serious drought occurred because the dam storage was larger due to excess rainfall in 2017 (Fig. 4.12). Since 2019, drought conditions are continuing, as illustrated by TWS and dam storage in Fig. 4.12. From Fig. 4.20, both 2015 and 2019 show relatively larger DPI minima (slightly below 0), which have never happened

in previous years. So, it is inferred that, apart from the general tendency of the basin to experience a drought in the long term and prevailing drought situation in dry periods, DPI is also useful for identifying elevated drought potential in the wet season, which otherwise could not be captured in other standardized indices.

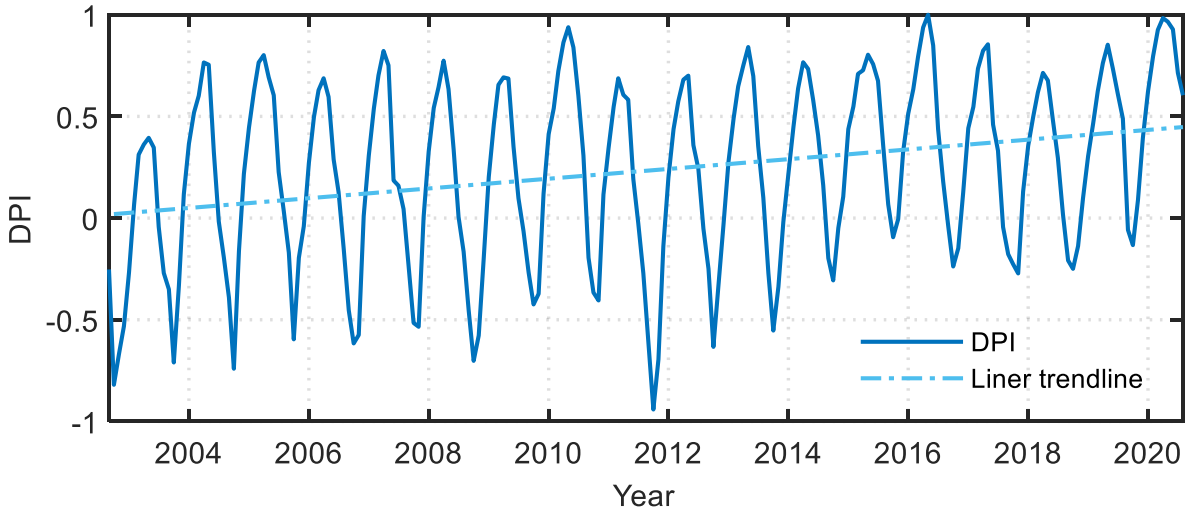

Figure 4.20. The drought potential index (DPI) evaluated for each month from Sept 2002 to Aug 2020. The linear trend line of DPI is also shown by the dash-dotted line. After (Abhishek et al., 2021).

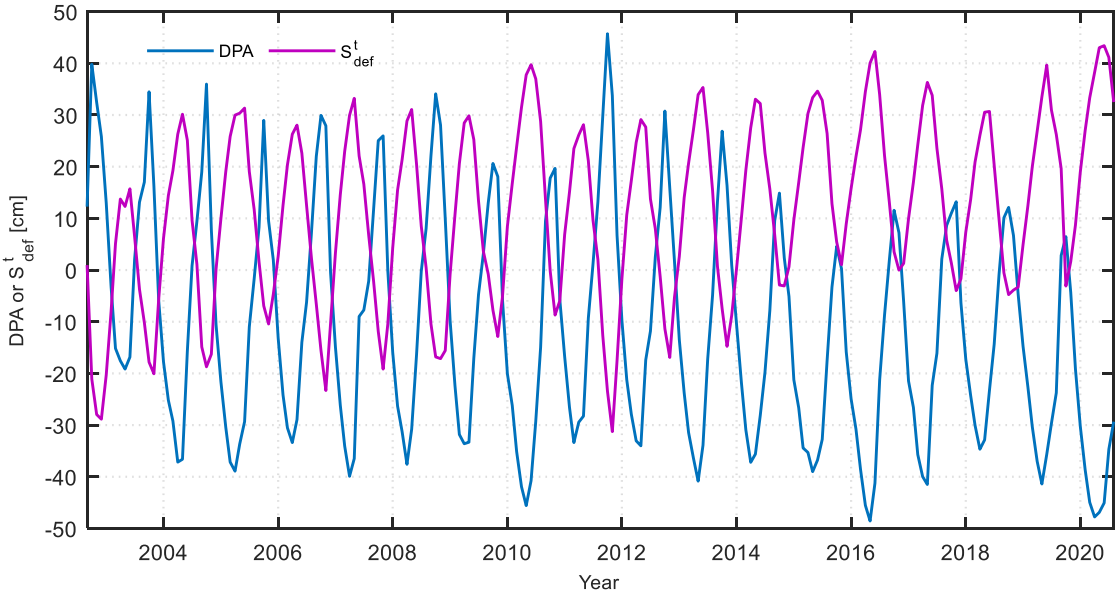

Figure 4.21. Monthly rates of the minimum required relative storage change (S^t_{def}) and monthly drought potential amount (DPA). After (Abhishek et al., 2021).

The normalized drought potential index (DPI) accounts for the regional hydrological variability by removing the typical difference between water storage and precipitation anomaly and thus presents a basin-wide holistic estimate of the prevailing drought conditions. The high storage deficit (i.e., large negative deficit value) combined with the high negative precipitation anomaly indicates the high probability of the drought. DPI is also unaffected by the short-lasting high fluctuations in the precipitation, e.g., torrential rain, and rather presents the effect of the persistent precipitation trend on the regional scale. Since it represents the tendency of the basin for the likelihood of hydroclimatic extremes based on the preceding water storage conditions, it can support the forecasting of droughts at a much accurate level when combined with the precipitation projections.

The GRACE(-FO) derived DPI is highly reliable for the long-term assessment of the water deficit situation in the basin rather than the short-term analysis. Droughts with higher DPI are evident in the inter-annual profiles of precipitation and TWSA, which enables DPI to assess the severe droughts more accurately than the mild droughts. Since the proposed DPI is capable of recording the regional event of hydroclimatic extremes along with the annual variability, it will be valuable for the improved basin-scale drought predictions. A continuous deficit in the precipitation may lead to higher DPI and should be confirmed with the monthly TWS deficits in the study region because DPI considers the water storage based on the precipitation for calculating the monthly drought potential amount. Also, the longer the GRACE-(FO) based TWSA data is, the better is the DPI's performance in representing the prevailing hydrological characteristics of the basin.

4.3.7. Institutional interventions for sustainable water utilities

Decreasing trends in various water storage components, especially groundwater, seem to be triggered during the drought years partly by the variable precipitation and partly by the integrated impact of less recharge and high water demand leading to the amplified pumping (Figure 4.22). Further, the increasing tendency of the basin to experience prolonged droughts (and floods) due to the highly variable precipitation may impose threats to the food production, health, and livelihood of the people and the economy. As groundwater levels are going down, there is a strong likelihood to shift the reliance on the deeper wells, which may further affect several processes. Firstly, digging deeper wells may not alleviate water scarcity due to the poor GW quality in deep aquifers. Secondly, it might enhance the water availability gap

between the various economic classes of society (Jasechko and Perrone, 2021). Thirdly, it may exaggerate the existing land subsidence issues in and around highly urbanized cities (e.g., Bangkok) (Babel et al., 2006) and may further extend to other developing areas. Therefore, to ensure the equitable share and reliability of the groundwater-based water supply, a multifaceted strategy for efficient management, inclusive governance, and effective policymaking for groundwater sustainability is imperative in the basin. Despite the limited change in net precipitation during the study period (Fig. 4.22), which is the natural source of groundwater recharge, the continuous depletion of GWS seems primarily driven by the enhanced pumping highlighting the over-reliance on the groundwater (GW) attributed to the limited surface availability in drier seasons and the shifted water use policy. The over-abstraction situation is further ascertained by the highly decreasing GW table in the basin as compared with the declining GW table data, as shown in Fig. 4.14.

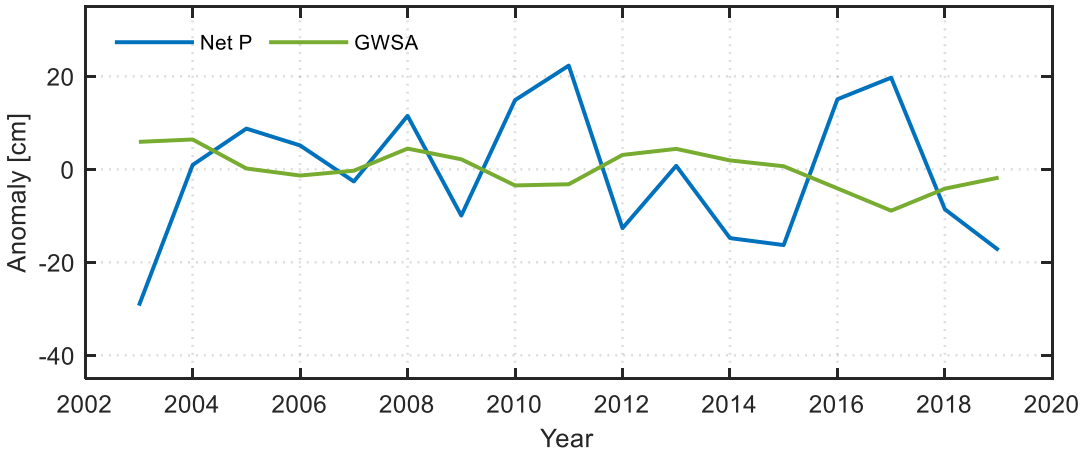

Figure 4.22. The anomaly of annual total net precipitation and the annual mean anomaly of GWSA during 2003-2019.

Amid a transition from a historical center of rice production to the current water-scarce conditions, the prevailing complex institutional environment of the Chao Phraya River Basin, with different agencies having different roles at various administrative levels and in multiple stages of water resources development, storage, and distribution, needs to be understood because, in this critical phase, every small change in the hydrological situation can heavily impact the socio-economic conditions of the basin (https://fdmt.iwlearn.org/). For example,

had there been ample time and accurate assessment of the flood in 2011, an early monsoon release of water, albeit uncommon, from the Bhumibol and Sirikit Reservoirs would have enabled storing about one billion cubic meter floodwater in these reservoirs during the flooding event as pointed out by Komori et al. (2012). Alarming deforestation rates due to urbanization and farmland exploitation have lowered the soil's water-retaining capacity and, therefore, increases the risk of soil erosion, flash floods, and landslides (https://fdmt.iwlearn.org/). The resulting low infiltration/percolation and subsequent pollution to near-surface water resources might have intensified the overreliance on groundwater for irrigation, ultimately leading to the decreasing terrestrial water storage trends in the basin. To maintain sustainable water utilities against the observed weakening hydrological cycle in the region, the promotion of institutional interventions to ensure sound hydrological cycles is of paramount importance. In addition to the ongoing groundwater recharge projects (http://www.dgr.go.th), water conservation practices focused on the demand side such as switching from more water intense (e.g., rice) to less water-intensive and commercial crops and/or upgrading the irrigation systems to more efficient ones should be promoted to ensure the uninterrupted and efficient water-supply in future.

The large declining trends of TWS and its constituent components as revealed in the current assessment indicate an imbalance in withdrawals and replenishment rates in various water storage components and underscore the need to either revising the existing multilateral cooperation among various stakeholders or effective and efficient policymaking regulating the new settlements and water allocation strategies especially in the regions with existing complex water management. Despite the presence of a dense network of flood control and water storing measures (e.g., dikes, reservoirs, etc.), the multiple drought and flood events experienced in CPRB highlight the need for revising the approach for managing the hydroclimatic extremes while giving the associated risks of the ecosystem degradations a due consideration. Analyses of individual water storage components, enhanced drought potential by DPI, and drought propagation behavior by various standardized indices in this study, are expected to provide a new perspective for revising the overlapping water management strategies among a plethora of government agencies in the basin.

4.4. Conclusion

Driven from the high vulnerability of the Chao Phraya River Basin to water-related disasters (i.e., floods and droughts), an attempt has been made to quantify the water storage dynamics by integrating the GRACE-(FO) based terrestrial water storage (TWS), global and local hydrological datasets, and multiple drought indices. Major findings of the study are summarized as below,

1) Reasonably good performance of the proposed model (training, r = 0.96, NSE = 0.90; validation, r = 0.94, NSE = 0.85) indicates its potential not only for filling the data gap between GRACE and GRACE-FO records but also for filling the intermittent data gaps in GRACE-(FO) occurring due to the battery management. Moreover, the genetic algorithm, when coupled with the ANN model (ANN BP-GA), eliminates the need for the trial and error method, prevalent to determine hidden layers in ANN models.
2) Effects of all the drought and flood events in CPRB are evident in the TWSA series, with high fluctuations during the major flood event of 2011 and drought events of 2015 and 2019, which is still continuing. TWSA has multiyear depletion and recovery events from 2002 to 2020 with surplus water storage until March 2014. This framework of quantifying various hydro-climatic extremes using multisource data products can be adopted to various data-scarce regions globally.
3) Groundwater storage is the dominant component (45%) of declining TWS trends, followed by surface water storage (36%) and soil moisture storage (19%). These trends, especially in GWS, provide a quantitative evaluation of groundwater resources in the region which otherwise, due to the limited in-situ data (pumping, GW table, aquifer properties, etc.), impedes the holistic assessment of the water beneath our feet. Results of the current study may provide an observational constraint and basis for employing early water management initiatives not only in the CPRB but in other regions, e.g., India, where there is overreliance, though often unreported (due to lack of documentation or stringent measures, among other reasons), on groundwater resources.
4) Detection of the decreasing trend in groundwater storage, which is probably more acute than the decrease (change) in precipitation, through the application of GRACE and other auxiliary multisource products highlights the need for swift policy change to

reduce the water demand (e.g., encouraging less water-intense crops), decrease the dependence on groundwater, and increase the implementation of the new groundwater recharge projects in the basin and provides a blueprint for similar studies in the data-scarce basin to get insights of the commonly invisible groundwater.

5) The lag time between various standardized indices helped to understand the drought propagation through various components of the system, which will help in efficiently employing the early warning measures of the water management in the likelihood of water-related extremes in the region.
6) The highest deficit in the available water storage and the precipitation during the wet season, as revealed by the drought potential index (DPI), indicate the early signs of the region's transition to a drought-prone situation. The crux of DPI is that it incorporates combined effects of the climate variability and human activities (water management, policymaking, etc.) and can be applied to holistically quantify the potential of the development of the anthropogenic droughts in coupled human-nature systems globally with implications for both short- and long-term water resources planning and management, water governance, and policymaking. DPI can also be effectively utilized for identifying droughts during wet seasons, employing the optimal adaptation measures, and multilateral water management policymaking and efficient water allocation strategies in the data-scarce river basins globally.

The CPRB has been under a continuously increasing water stress since April 2014, as revealed by the water storage deficit analysis and the increasing trend in the proposed DPI. The current framework, when jointly used with precipitation and evapotranspiration forecasting and the adaptive reservoir operation rule curves (Kompor et al., 2020), can help in developing the early warning systems for floods and droughts that will efficiently sustain the basin's socio-economic activities. To this end, the relative biases in various components of the water cycle, i.e., precipitation, evapotranspiration, runoff and change in storage, are imperative yet challenging to quantify. Since there are not any real ground truthing for most of these variables, except runoff from the gauge stations at the basin outlets, we must adhere to alternative strategies, e.g., multisource mean, to reduce the systematic biases implicit to any single data product. Since the runoff data is available in the Chao Phraya river basin, the non-closure error of the water balance is studied followed by providing the corrected variables in the next chapter for further use in the hydrological applications.

Chapter 5

Water Budget Closure in the Upper Chao Phraya River Basin

This chapter has been adapted from Abhishek et al., 2022.

Abhishek; Kinouchi, T.; Abolafia-Rosenzweig, R.; Ito, M. Water Budget Closure in the Upper Chao Phraya River Basin, Thailand Using Multisource Data. Remote Sens. 2022, 14, 173. https://doi.org/10.3390/rs14010173

5. Water Budget Closure in the Upper Chao Phraya River Basin

5.1. Motivation

The terrestrial water cycle governs water and food security, hydrologic extremes, and ecosystem health (Pan et al., 2012). Continually increasing human activities are altering the global and regional terrestrial water balance directly (e.g., water abstraction and infrastructure development) and indirectly (e.g., deforestation and increasing atmospheric greenhouse gases alter hydroclimate) (Abhishek and Kinouchi, 2021; Abolafia-Rosenzweig et al., 2021). Amid this integrated complexity between the natural water cycle and human activities, it is imperative to quantify water cycle components and their governing factors towards effective management, efficient water allocation, sustainable and strategic planning, and policymaking, especially for socioeconomically sensitive hydrologic systems (Abhishek et al., 2021; NSIT, 2007; Rodell et al., 2015; Rosenzweig et al., 2008; Zhang et al., 2018). Basin-scale assessments of the terrestrial water budget quantify hydrologic dynamics on various temporal scales (e.g., annual, seasonal, monthly) and uncertainties for each water budget component [9]. These assessments provide knowledge of the mean state and variability of the water budget, which is fundamental to understanding the regional climate system and characterizing memories, pathways, and feedbacks between key energy, water, and biogeochemical cycles (Pan et al., 2012; Zhang et al., 2018)

Although ground-based observations (i.e., in-situ data) of water budget components are often considered true, long-term assessments solely based on these data remain challenging due to inherent limitations regarding their spatiotemporal heterogeneity, sampling errors, high costs of installation and maintenance, and intermittent data gaps, especially in data-scarce (ungauged) or data-limited regions (Abhishek and Kinouchi, 2021; Penatti et al., 2015; Sheffield et al., 2009; Zhang et al., 2018). To overcome this, multisource strategies, i.e., combinations of ancillary datasets from remote sensing observations, reanalysis models, and offline land surface models, have proven crucial to monitoring water storage and fluxes in a changing world (Pan et al., 2012; Rodell et al., 2018; Sheffield et al., 2009). Although multisource data can provide spatially continuous estimates of the terrestrial water budget, they have several drawbacks. For instance, remote sensing data is subject to sensor and signal processing uncertainties, and models typically lack the fully dynamic coupling of human impacts on the water budget and propagate uncertainties associated with metrological forcing

data and parameterizations (Abolafia-Rosenzweig et al., 2021; Pan et al., 2012; Scanlon et al., 2018; Sheffield et al., 2009). These error sources in quantifying constituent water budget components result in a water budget imbalance, i.e., residual error, which does not satisfy the physical mass balance constraint (Pan et al., 2012).

Further, multisource strategies may provide conflicting information if proper attributions of closure errors are not considered. Several deterministic (e.g., weighted average corresponding to error variance; (Rodell et al., 2015; Zhang et al., 2018)) and probabilistic (Abolafia-Rosenzweig et al., 2021) approaches have computed estimates of water budget components from multisource datasets while carefully accounting for uncertainties that are used to force water budget closure. Since each dataset contains unique information, the ensemble approach proposed by Abolafia-Rosenzweig et al. 2021 was adhered to probabilistically quantify the terrestrial water budget while enforcing closure on each unique realization. Enforcing water budget closure across multiple unique realizations from unique combinations of datasets (up to 72 realizations) reduces the risk of unknown bias cancellation (i.e., inaccurate datasets providing minimal water budget residuals).

River basin management, the backbone of many economies, relies on understanding historical and projected fluctuations of water budget components: precipitation (P), evapotranspiration (ET), streamflow (Q), and change in terrestrial water storage (ΔS) (FAO, 2011; Turral et al., 2008). Thus, long-term records of basin-scale water budgets and associated uncertainties for each constituent component are of paramount importance. We provide a water budget assessment over the upper Chao Phraya River Basin (CPRB), Thailand. The CPRB, historically known as “Thailand’s rice bowl”, inhabits about 40% of the country’s population and contributes to about 2/3rd of the country’s GDP, thus affecting the nation’s overall socioeconomic development and water and food security (Abhishek et al., 2021). The CPRB is vulnerable to hydrological extremes and has suffered flood and drought events in the past (e.g., 2004, 2007, 2011, 2015), which cost Thailand more than one billion US dollars and severely disrupted industrial production of global supply chains in surrounding countries (Abhishek et al., 2021). Moreover, the basin has an increased potential for severe drought, as revealed by the recently developed Drought Potential Index (DPI) (Abhishek et al., 2021). Further, the CPRB has experienced up to a 73% increase in water withdrawal from 33.1 km^3 in 1990 to 57.3 km^3 in 2007 against an annual aquifer recharge of 41.9 km^3 (5-6% of the total precipitation) (FAO, 2011), which is projected to decrease in the near future due to natural and anthropogenic perturbations (e.g., climate change and increasing water

demands) (Supharatid, 2015). Notwithstanding the importance of understanding hydrologic dynamics in the CPRB, previous global (e.g., (Abolafia-Rosenzweig et al., 2021; Pan et al., 2012; Rodell et al., 2015; Sahoo et al., 2011; Zhang et al., 2018)) or regional (e.g., humid to arid regions in the South Central United State (Long et al., 2014a), nine major US river basins (Gao et al., 2010), Mississippi River basin (Sheffield et al., 2009), 16 large drainage basins in Canada (S. Wang et al., 2014), Mackenzie River basin (Szeto et al., 2008), Upper Paraguay River Basin (Penatti et al., 2015), Xingu basin (Panday et al., 2015), Rufiji basin (Armanios and Fisher, 2014), Amazon basin (Azarderakhsh et al., 2011)) terrestrial water budget assessments do not consider the CPRB or put forward the bulk estimate of water budget components of the larger region. Furthermore, limited studies have applied closure techniques to attain the physical constraint of mass balance in their respective study regions. Thus, this chapter advances the state of hydrologic science through a novel water budget assessment of a valuable but understudied and vulnerable region. The comprehensive understanding of CPRB's hydrologic dynamics and uncertainties/biases in constituent water budget components can inform water resources management, particularly for irrigation planning (water withdrawals and allocation strategies), flood and drought mitigation, drainage system design, and groundwater recharge estimation in the region (Abhishek et al., 2021; S. Wang et al., 2014).

This chapter is motivated to fill the aforementioned gaps in previous research by addressing the following questions over CPRB, 1) how much do state-of-the-art multisource data vary among themselves, and how well does an ensemble mean represent the regional water balance? 2) what is the direction and magnitude of relative biases in various water budget components that contribute to the imbalance in water budget closure? 3) what is the seasonal and annual variability of corrected components? These questions are answered by reconciling various hydrologic data products through the application of three water budget closure techniques proposed by Abolafia-Rosenzweig et al. 2021. The long-term implications of corrected water cycle components are further discussed in the context of CPRB water management as a pathway for future research.

5.2. Materials and Methods

Since the Nakhon Sawan gauge station (Fig. 5.1) is the most downstream station where the flow records are not contaminated by the factors such as tidal oscillations, upstream diversion or intake, the target study area is limited to the upper CPRB in this study. All other reanalysis

and remote sensing data were selected and retrieved as per the spatiotemporal availability of individual datasets.

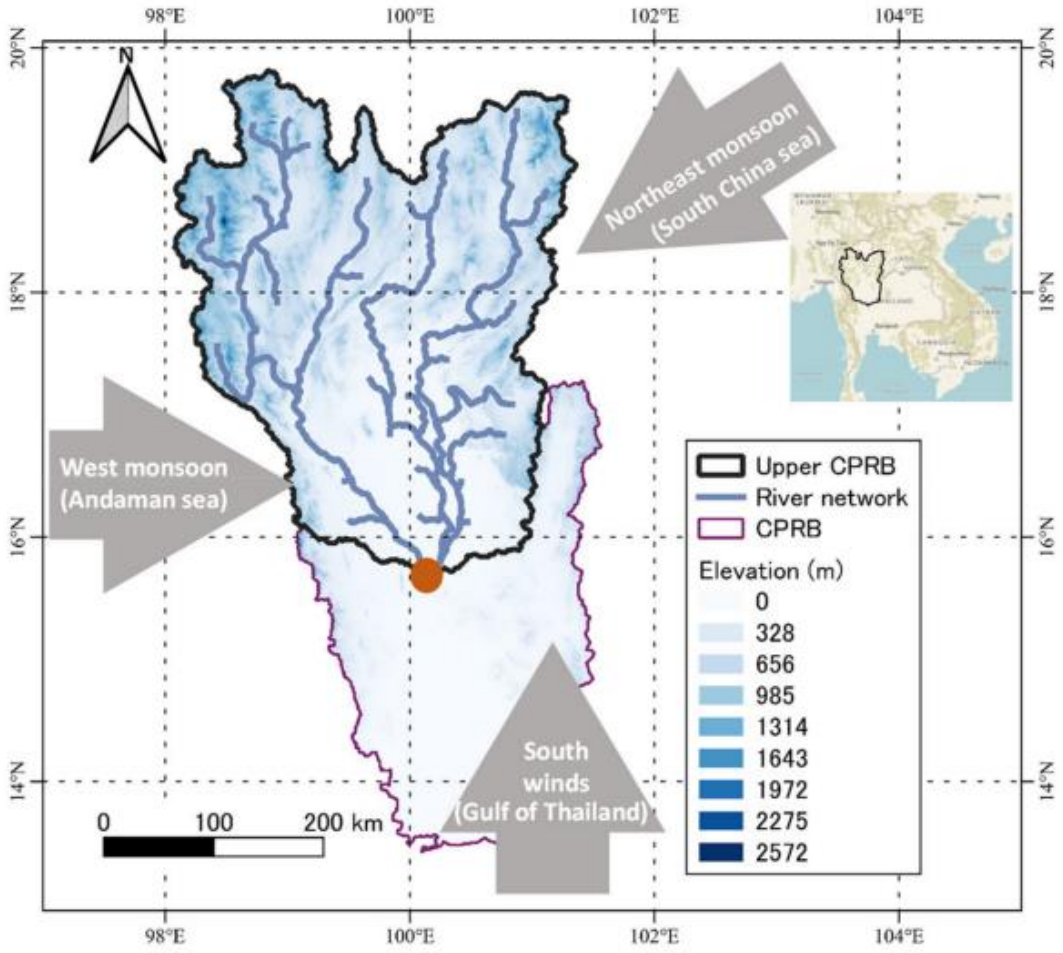

Figure 5.1. Location map of the Upper Chao Phraya River basin. Stream gauging station at Nakhon Sawan (C2 station) is shown as the orange-filled circle. Various mechanisms (west monsoon from the Andaman sea during May to October, South winds from the Gulf of Thailand during February to April, Northeast monsoon during November to January, and tropical cyclones originating from the South China sea) governing the climate of the basin are also shown. After (Abhishek et al, 2022).

5.2.1. Study area

The upper CPRB is an agrarian river basin located in northern Thailand (Fig. 5.1 inset) consisting of four sub-basins: the Ping, Wang, Yom, and Nan River basins, with a total catchment area of ~102,600 km^2 (~20% of the country's land area). The basin's climate is

primarily governed by alterations between northeast monsoons, south-west monsoons, southern winds, and intermittent tropical cyclones. The upper CPRB receives an annual rainfall of 1100 mm and has a mean annual runoff of about 26 km^3, which is 12.2% of the country's annual runoff (FAO, 2011). The basin's water cycle is affected by human interventions such as reservoir management (water storage and release from Bhumibol and Sirikit reservoirs with capacities of 13.5 and 9.5 billion m^3, respectively) and groundwater withdrawals (Abhishek et al., 2021). The research framework illustrating different datasets used, methods employed, and analyses carried out in this study is summarized in Fig. 5.2 below.

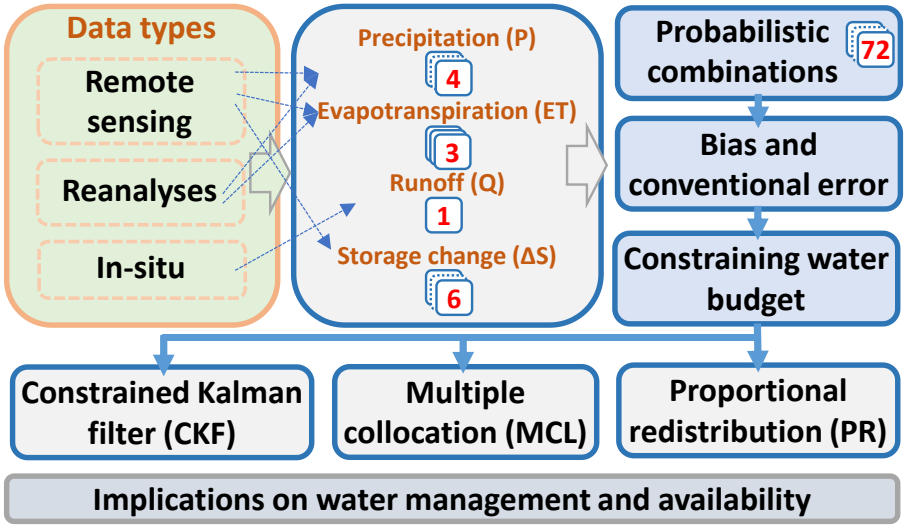

Figure 5.2. Schematic showing the multisource data used, research flow adopted, methods employed, and major analyses conducted in the current study. The 72 combinations were obtained by a permutation of the available products (4(P)x3(ET)x1(Q)x6(ΔS))=72). Bias and conventional errors were assessed as the standard deviation from the ensemble mean or by the predefined values based on the literature, respectively, followed by the application of three water budget constraining techniques. After (Abhishek et al, 2022). Readers are reminded that all the data sources in this schematic correspond to the basin averaged time series for the upper Chao Phraya river basin.

5.2.2. Water budget closure

Considering the landmass as a one-dimensional column and neglecting the lateral fluxes, the terrestrial water budget at the basin scale for a given month can be written as,

$$r = P - ET - Q - \Delta S \neq 0 \quad (5.1)$$

where r is the residual error. ΔS is calculated as the central difference of terrestrial water storage anomalies (TWSA) (i.e., $\Delta S_t = (TWSA_{t+1} - TWSA_{t-1})/2$) of the monthly TWSA from the GRACE and GRACE-FO. Similar to previous studies (Gao et al., 2010; Tang et al., 2010; Zhang et al., 2018), VIC-derived ΔS is found to agree more with this ΔS than that calculated using forward or backward difference. To be consistent with the other data products, TWSA is first linearly interpolated to daily values before performing monthly ΔS calculations (Rodell et al., 2015). Since multisource datasets contain unique information, probabilistically generated combinations (4(P)x3(ET)x1(Q)x6(ΔS) =72 in total) of unique datasets are used following (Abolafia-Rosenzweig et al., 2021). The mathematical representation of enforcing the water balance closure is notated in eq. 5.2:

$$r' = (P + \varepsilon_P) - (ET + \varepsilon_{ET}) - (Q + \varepsilon_Q) - (\Delta S + \varepsilon_{\Delta S}) = 0 \quad (5.2)$$

where r' is the water budget closure error after correcting all the individual components against their respective errors (ε). Initial and enforced water budget, Eqs. 5.1 and 5.2, respectively, can be rewritten in the form as,

$$\begin{cases} r = Gx \neq 0\ ; \forall\ G = [1\ -1\ -1\ -1], x = [P\ ET\ Q\ \Delta S]^T & \text{initial water budget} \\ r' = Gx' = 0\ ; \forall\ G = [1\ -1\ -1\ -1],\ x' = [P'\ ET'\ Q'\ \Delta S']^T & \text{enforced water budget} \end{cases} \quad (5.3)$$

where x' is the corrected variable (P', ET', Q', and $\Delta S'$).

5.2.3. Enforcing water budget closure

Three available closure techniques, namely Constrained Kalman filter (CKF) (Pan et al., 2012), Multiple collocation (MCL) (Pan et al., 2015), and Proportional redistribution (PR) (Abolafia-Rosenzweig et al., 2021), are applied here to enforce water budget closure in upper CPRB. Since the true value of any variable (P, ET, and ∆S) is unknown, the ensemble means across all datasets for respective variables are assumed to represent true values (Zhang et al., 2018). For Q, since the gage type and stage-discharge relationship were not available, runoff volume and associated uncertainties are assumed to be inversely proportional, as reported in an observational study (Shiklomanov et al., 2006). A time series of uncertainty

linearly varying from 2.3% to 28.8% [2], corresponding from highest to the lowest flow (Q) was used.

Constrained Kalman filter (CKF)

Assuming that errors in all water budget components follow zero-mean Gaussian distributions and are non-correlated among various estimates, the error covariance for an estimate can be represented as,

$$\varepsilon_{xx} = \overline{(x' - x_t)(x' - x_t)^T} \tag{5.4}$$

where x' and x_t are the state estimates, and its true values, respectively. Water budget closure constraints (i.e., ε) that assume non-correlated errors (Rodell et al., 2015) take the form,

$$\varepsilon_{xx} = \begin{bmatrix} \varepsilon_{P-P} & \varepsilon_{P-ET} & \varepsilon_{P-Q} & \varepsilon_{P-\Delta S} \\ \varepsilon_{ET-P} & \varepsilon_{ET-ET} & \varepsilon_{ET-Q} & \varepsilon_{ET-\Delta S} \\ \varepsilon_{Q-P} & \varepsilon_{Q-ET} & \varepsilon_{Q-Q} & \varepsilon_{Q-\Delta S} \\ \varepsilon_{\Delta S-P} & \varepsilon_{\Delta S-ET} & \varepsilon_{\Delta S-Q} & \varepsilon_{\Delta S-\Delta S} \end{bmatrix} = \begin{bmatrix} \varepsilon_{P-P} & 0 & 0 & 0 \\ 0 & \varepsilon_{ET-ET} & 0 & 0 \\ 0 & 0 & \varepsilon_{Q-Q} & 0 \\ 0 & 0 & 0 & \varepsilon_{\Delta S-\Delta S} \end{bmatrix} \tag{5.5}$$

Eq. 5 was further solved for ε_{xx} and Kalman gain in accordance with Pan and Wood (Pan and Wood, 2006) and Pan et al. (Pan et al., 2012).

Multiple collocation (MCL)

Assuming all the N (=4,3,1, and 6 for P, ET, Q, and ∆S, respectively) sets of estimates (with n monthly values in each estimate; n = 216 here) of a variable are unbiased, the distance between any two estimates (x_i and x_j), measured as root mean squared (RMS) distance can be written as,

$$d_{ij} = \sqrt{\frac{1}{n}\sum_{k=1}^{n}(x_{i,k} - x_{j,k})^2}\,;\ \forall\ i = 1{:}\,N \tag{5.6}$$

Considering the errors of all estimates are uncorrelated (i.e., two errors are orthogonal), the Pythagorean Theorem in Hilbert space becomes,

$$d_{it}^2 + d_{jt}^2 = d_{ij}^2\ ;\ \forall\ i \neq j \tag{5.7}$$

where, subscript t denotes the true value of a water budget component which, in the current study, is assumed equal to the ensemble mean for P, ET, ∆S. The Pythagorean constraints for any system (e.g., N =3) can be written by eq. (8) in vector form (Pan et al., 2015),

$$\begin{bmatrix} 1 & 1 & 0 \\ 1 & 0 & 1 \\ 0 & 1 & 1 \end{bmatrix} \begin{bmatrix} d_{1t}^2 \\ d_{2t}^2 \\ d_{3t}^2 \end{bmatrix} = \begin{bmatrix} d_{12}^2 \\ d_{13}^2 \\ d_{23}^2 \end{bmatrix} \tag{5.8}$$

where, for example, d_{23}^2 is the mean squared distance between estimates 2 and 3. Moreover, since there is no exact solution for over-constrained (N>3; ∆S in the current study) systems,

MCL uses a least-squares solution to minimize Pythagorean distances of the constraints to reach the best 'compromise' (Pan et al., 2015). Water budget closure error is then redistributed to the various components proportional to their relative distance (not the magnitude like in PR; explained below) from the true value (ensemble mean).

Proportional redistribution (PR)

PR is the simplest method assuming that the relative errors for any given water budget component at a given time step are proportional to its relative magnitude (Abolafia-Rosenzweig et al., 2021),

$$x_i' = x_i - r(G)\left(\frac{|x_i|}{\sum_{j=1}^{4} x_j}\right) \tag{5.9}$$

where i corresponds to the i^{th} element, and other parameters have values as explained earlier.

5.2.4. Data used

Datasets of water budget components are from reanalysis, remote sensing, and observed in-situ records, spanning May 2002 to April 2020 (Tables 5.1 and 5.2). All water budget components used in this analysis are basin averaged monthly time series represented as equivalent water depth (mm). Data products showing favorably similar inter-annual and seasonal dynamics are used for calculating the coefficient of variation (CV = standard deviation/ensemble mean).

Precipitation and evapotranspiration

Precipitation (rainfall+snowfall) and evapotranspiration (evaporation+transpiration) are the largest incoming and outgoing water fluxes in any hydrologic system, respectively, and play significant roles in the distribution and availability of water resources in a region (Oki and Kanae, 2006). Traditional in-situ point-based monitoring of both P and ET is costly, restricted to local scales, and prone to large uncertainties, especially in the data-limited regions like the upper CPRB (with a meager rain gauge density of 0.5 rain gauges per 1000 km^2). Therefore, to get the spatially distributed continuous time series, data from multiple sources were retrieved. A detailed list of various gridded datasets used for precipitation and evapotranspiration, their sources, and spatiotemporal resolutions are shown in Table 5.1.

Terrestrial water storage

Various datasets for terrestrial water storage (TWS) and their salient features are listed in Table 5.2. Spherical harmonics (SH) coefficients, used in TWSA products, are processed for

noise reduction at high frequencies (low wavelength) using low-pass filtering (e.g., 300 km Gaussian filtering, truncation at the maximum order and degree 60, de-striping), which would have inevitably led to signal errors (Long et al., 2016a; Sakumura et al., 2014; Swenson and Wahr, 2006). These errors consist of bias (leakage-out; signal loss within specific study area due to the basin function/filtered averaging kernel) and leakage (leakage-in; contamination/gain in the target signal from the surrounding region) errors (Longuevergne et al., 2010; Swenson and Wahr, 2006). To restore true signals, a number of model-dependent (additive (Klees et al., 2007), scaling (Landerer and Swenson, 2012), and multiplicative (Longuevergne et al., 2010); all of which primarily use outputs from the hydrological models (Vishwakarma et al., 2018)) or model-independent (i.e., data-driven (Vishwakarma et al., 2017)) approaches have been employed in globally distributed river basins. Since the data-driven approach outperforms other methods in the upper CPRB, the same was employed for restoring GRACE signals. Overall, an inter-comparison of filtered GRACE TWSA and ΔS shows strong agreement between all products. The variance (scatter RMS varying from 12.5 to 19.5 mm) among different GRACE products range within error bounds of the GRACE data with no significant biases, which is consistent with previous studies (Abolafia-Rosenzweig et al., 2021; Sakumura et al., 2014). Since there is minimal signal loss attributed to the regularization and postfit residual analysis, no signal restoration procedures are required for GRACE Mascon (mass concentration) solutions (Scanlon et al., 2015). No bias was assumed between GRACE and GRACE-FO data following recent studies that reported negligible intermission biases over the Central United States, Middle East, Europe, Australia (Landerer et al., 2020; Pascolini-Campbell et al., 2021), and ice caps and glaciers (Ciracì et al., 2020; Velicogna et al., 2020). Finally, the ANN-MLP/GA method (details provided in the section 4.2.4) was employed to fill the data gaps in the GRACE/FO time series arising from both the intermittent maintenance operations and the 11 months data gaps between the two missions.

Table 5.1. Summary of precipitation and evapotranspiration datasets spanning May 2002 to April 2020 (except for TRMM data which is for May 2002 to Dec 2019). After (Abhishek et al, 2022).

Variable	Dataset	Spatial resolution and frequency	References	Remarks
Precipitation	TRMM (TMPA) 3B42 V7	0.25°x0.25° Daily	(G J Huffman et al., 2019)	Derived by the multi-channel microwave and IR observations from satellites, followed by rescaling based on gauge observations, summing (and applying a factor of three) 3-hourly valid retrievals in a grid cell.
	GPM IMERG	0.1°x0.1° Monthly	(G.J. Huffman et al., 2019)	Intercalibrates and merges the satellite microwave precipitation estimates with microwave-calibrated IR satellite estimates and gauge data using the quasi-Lagrangian time interpolation.
	CHIRPS-2.0	0.05°x0.05° Daily	(Funk et al., 2015)	Incorporates satellite data from NASA and NOAA, and in-situ station data followed by the removal of systematic bias based on IR CCD observations.
	GPCP	2.5°x2.5°	(Adler et al.,	Integration of various rain gauge stations, satellite data sets
	PERSIANN-CDR	0.25°x0.25° Daily	(Hsu et al., 1997)	Uses the ANN algorithms on GridSat-B1 IR satellite data, ANN training using the NCEP stage IV precipitation data (hourly), and finally bias adjusted using the GPCP monthly product version 2.2.
Evapotranspiration	GLDAS NOAH v2.1	0.25°x0.25° Monthly	(Beaudoing et al., 2020)	Temporal averaging of 3-hourly GLDAS-2.1 Noah output (Princeton meteorological forcing input data) to produce monthly data followed by the post-processing with the MOD44W MODIS land mask.
	GLEAM v3.5a	0.25°x0.25° Daily	(Martens et al., 2017)	Uses PT equation with an updated water balance module and updated evaporative stress functions. Extracts maximum information from different components of terrestrial ET (evaporation from bare land and open water, interception, sublimation, transpiration) from the satellite databases.
	MERRA-2	0.5°x0.625° Daily	(Reichle et al., 2017)	Jointly uses the atmospheric general circulation model, atmospheric assimilation system (including modern hyperspectral radiance and microwave observations), an interactive aerosol scheme, and the observed precipitation at the land surface.

Table 5.2. Summary of terrestrial water storage (TWS) datasets used in this study from May 2002 to April 2020. After (Abhishek et al, 2022).

Variable	Dataset	Spatial resolution and frequency	References	Remarks
Terrestrial water storage	CSR Mascons RL06M v02	0.25° × 0.25° Monthly	(Save et al., 2016), (Save, 2020)	Corrected for representation on ellipsoidal Earth applied separately to land and ocean to minimize signal leakage. ΔC_{30} coefficient was replaced with a more accurate estimate from SLR for computing GRACE-FO mascons.
	JPL Mascons RL06M v02	0.5° × 0.5° Monthly	(Wiese et al., 2018), (Watkins et al., 2015)	Coastline Resolution Improvement (CRI) filter applied, which leads to reduced leakage errors across coastlines. Realistic geophysical information is introduced during the solution inversion to intrinsically remove correlated error.
	GFZ Spherical Harmonics RL06 Level-2	1° × 1° Monthly	(Dahle et al., 2018), (Dahle and Murböck, 2019)	A number of modifications in the static gravity background field, time-variable gravity background field, atmospheric mass variability models, model for planetary ephemerides, parameterization of the accelerometers, processing of GPS constellation have been incorporated compared to the previous versions.
	COST G Spherical Harmonics RL02	1° × 1° Monthly	(Meyer et al., 2020a), (Meyer et al., 2020b), (Jean et al., 2018)	A harmonization and quality control of the individual input solution level is performed, followed by application of variance component estimation. The resulting COST-G combined gravity fields are validated by assessing their signal and noise content in the spectral and spatial domain.
	CNES GRGS Spherical Harmonics RL05	1° × 1° Monthly	Lemoine et al. 2019	Latest version of L1B measurements, new model of ocean tides (FES2014b), and IGS orbits and clocks are used instead of GRGS ones are used. The normal matrices are first diagonalized, ordered by decreasing order of the Eigenvalues, and only the best-defined sets of linear combinations of the SH are solved, unlike other SH solutions, which use simple Cholesky inversion.
	GSFC Mascons RL06v1.0	0.5° × 0.5° Monthly	(Loomis et al., 2019)	GSFC monthly regularization matrices are determined by analyzing the geographical binning of the inter-satellite range-acceleration pre-fit residuals. The 1-arc-degree equal-area values have been placed on an equal angle 0.5°x0.5° grid. Land values are determined with a least-squares estimator that conserves mass over each region.

5.3. Results and discussion

5.3.1. Variability among influx and outflux data products and observations

Precipitation: Although all precipitation products have similar dynamics in both monthly and seasonal time series (Figs. 5.3 (a)-(b)) and are highly correlated ($r \geq 0.9$ except for PERSIANN-CDR), there are substantial deviations in magnitude (as high as 150 mm in July). Despite the adjustments with GPCP data (Ashouri et al., 2015), PERSIANN-CDR, in general, underestimates (average ~110 mm per month, equivalent to ~35%, during the rainy season) precipitation relative to the ensemble mean; meanwhile, other products fluctuate between overestimation or underestimation. PERSIANN-CDR tends to underestimate heavy precipitation (≥ 20 mm d^{-1}) events and therefore results in the dampened monthly and seasonal cycles, and hence was excluded from further analysis. Deviations among data products, even within the same category (satellite-related, reanalysis, gauge-based), depends on a multitude of factors such as location, topography, climate (e.g., arid and semi-arid regions possess higher discrepancies among various products than in humid regions; (Cattani et al., 2016)), physical inadequacies (e.g., including few cloud-related parameters, or few gauge observations) of various retrieval algorithms (e.g., in PERSIANN-CDR case), interpolation processes, and bias adjustments (Q. Sun et al., 2018). Incorporation of few but overlapping gauge data in sparsely gauged basins, like the upper CPRB, can also result in a smaller spread among various precipitation products, possibly due to limited uncertainties in gridding and undercatch correction procedures (Pan et al., 2012). Consistent with the tropical climate regime, GPM, TRMM, CHIRPS, and GPCP show precipitation patterns with reasonably consistent distributions (maximum seasonal variation of 86 mm in July) and hence were considered for further analysis (Fig. 5.3). The average rainy season CV is 10.5% (maximum of 15.7% in July) and non-rainy season CV is 32.4% (May to October); the latter is due to the near-zero precipitation values from all four products. The first precipitation peak in May is from the onset of the western monsoon season (May-October) and tropical rainfalls from the South China Sea. The second peak in August-September (variable among products) corresponds with monsoon rainfall and tropical storms in the basin, and the dry season rainfall is attributable to southern winds and the northeastern monsoon (Fig. 5.1).

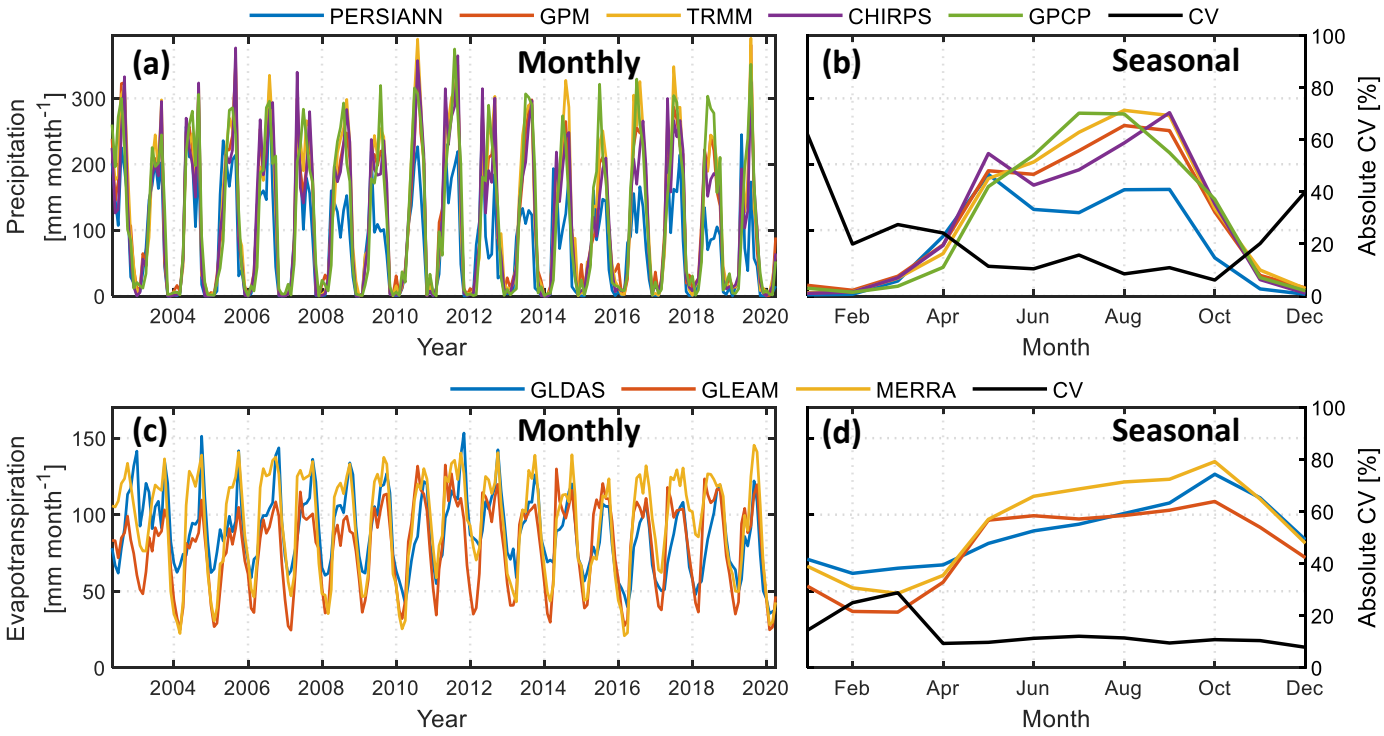

Figure 5.3. (a) Monthly and (b) mean seasonal time series of various precipitation products for the period from May 2002 to April 2020. The coefficient of variation (CV) from the ensemble mean is also shown with a black colored line, (c) monthly, and (d) seasonal time series of various evapotranspiration products. All the values are represented as the basin averaged equivalent water depth in mm. After (Abhishek et al, 2022).

Evapotranspiration: ET products reveal complex monthly and seasonal time series over the basin due to high spatiotemporal variability in soil moisture, meteorological conditions, and other phenological factors (Guan et al., 2015; Zhang et al., 2018). Despite similar dynamics in annual and seasonal cycles, the three ET products possess a widespread (i.e., less agreement) relative to the precipitation products (Fig. 5.3), which is consistent with previous water budget assessments. Seasonal dynamics of all three ET products have more stable behavior than P (Figs. 3(c)-(d)), attributable to the humid climate and intense irrigation (by surface water and groundwater in both wet and dry seasons), which reduces ET's dependence on soil moister availability. (Miralles et al., 2011). GLEAM underestimates ET, whereas GLDAS provides overestimates, especially during the dry period. Underestimation by GLEAM is likely attributable to inadequate representation of the evaporation from water bodies in the region and underestimation of canopy interception, vegetation optical depth,

and the water extent in the rainforests. Overestimation by MERRA in the tropical CPRB is consistent with the Climate Data Record (CDR) (Zhang et al., 2018). Average dry and wet seasonal ET variations are comparable with the CV of 13.4% and 10.8%, respectively.

Observed runoff: The mean monthly runoff recorded at the Nakhon Sawan C2 station (Fig. 5.1) ranges from 3.05 mm (February 2020) to 115.67 mm (October 2006), while the seasonal time series record maximum and minimum values in October (44.48 mm) and April (8.05 mm), respectively (Fig. 5.4). The high correlation of the seasonal runoff cycle with one and two months (r~0.92 for both) lag with precipitation is attributable to the memory of natural hydrological processes (e.g., baseflow) in the basin. The basin experienced the most severe flood within the past five decades in 2011, where runoff records show the second largest peak of 109.45 mm in October 2011, followed by 74.17 mm and 66.08 mm in October 2002 and October 2017, respectively. Note, all of which correspond with flood events. Minimal monthly runoff of 3 to 5 mm was observed during the dry season of drought years 2004-05, 2010, 2013, 2015-16, and 2020 (Fig. 5.4).

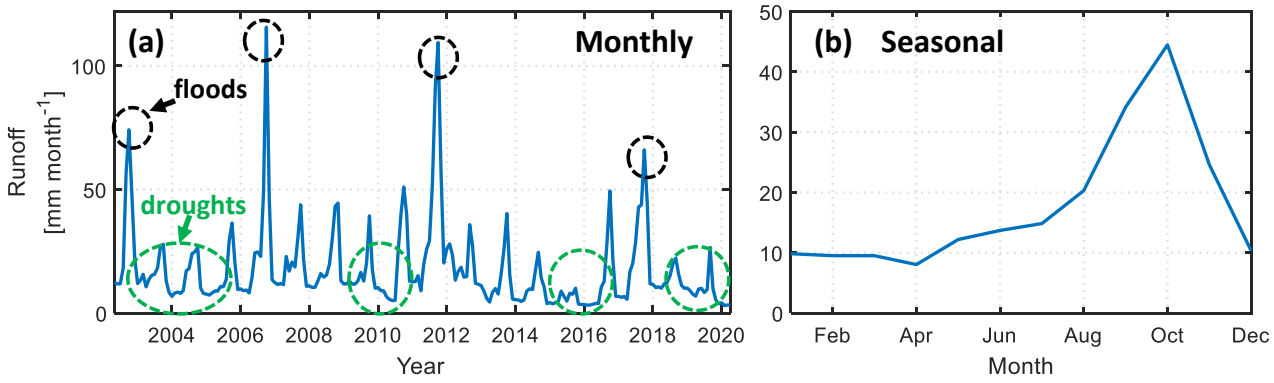

Figure 5.4. Same as figure 4.3. (a) Monthly and (b) seasonal time series of the observed runoff recorded at the Nakhon Sawan C2 gauging station. Various flood (black dotted circles) and drought years (dotted green circles) are also shown. A comprehensive assessment of the various hydroclimate extremes in CPRB can be found in the companion study (Abhishek et al., 2021). After (Abhishek et al, 2022).

5.3.2. Generating continuous TWSA time series

Since all six terrestrial water storage anomaly (TWSA) time series from various data processing centers utilize common GRACE and GRACE-FO data, they agree favorably in terms of amplitude and dynamics for both the monthly and seasonal time series (Figs. 5.5(a)-

(b)). The ANN model performed reasonably well ($r \geq 0.95$, NRMSE=0.24-0.37, and $NSE \geq 0.89$) for all six TWSA time series during both calibration and validation phases (Table 5.1) which can be ascribed to a) small uncertainties in GRACE data, primarily from the short-wavelength signals and subsequent filtering processes which tends to be smaller for large areas, b) ample predictor availability from ancillary data sources, and c) the embedded genetic algorithm avoids underfitting or overfitting in the ANN model. The current ANN model is used for data gap filling between GRACE and GRACE-FO TWSA time series (11 values) and for filling intermittent data gaps (23 values) occurring approximately every six months starting from 2011; the latter of which has been filled by linear interpolation of the two or more bounding values in previous studies. This linear interpolation may induce uncertainties by a) underestimating the actual (positive/negative peak) TWS if the data gap happens to be in the peak of the wet or dry season, or b) overestimation or underestimation in case of the high short-term fluctuations in the TWS. Furthermore, these instances of overestimation or underestimation might lead to inappropriate inferences in the river basins like CPRB, which is highly vulnerable to floods and droughts. Therefore, we have attempted to quantify various water budget components as accurately as possible. Moreover, the long-term linear trends of TWSA in the upper CPRB are consistent with those for the whole CPRB depicting that along with the highly urbanized southern reaches of the basins, e.g., near Bangkok, even upper reaches will also be likely at the verge of facing water scarcity situations in the near future.

A number of floods (e.g., 2011) and droughts (e.g., 2015, 2016) experienced in the basin are evident in the TWSA time series (Abhishek et al., 2021). Subsequently derived ΔS agrees well with a minimal scatter of <20% (Figs. 5.5(c)-(d)). Some minor discrepancies among TWSA products can be attributed to different processing algorithms and correction and filtering methods used by various data centers. However, all variations are well within the error ranges of the GRACE data with no significant biases, which is consistent with the previous studies (Abolafia-Rosenzweig et al., 2021; Sakumura et al., 2014).

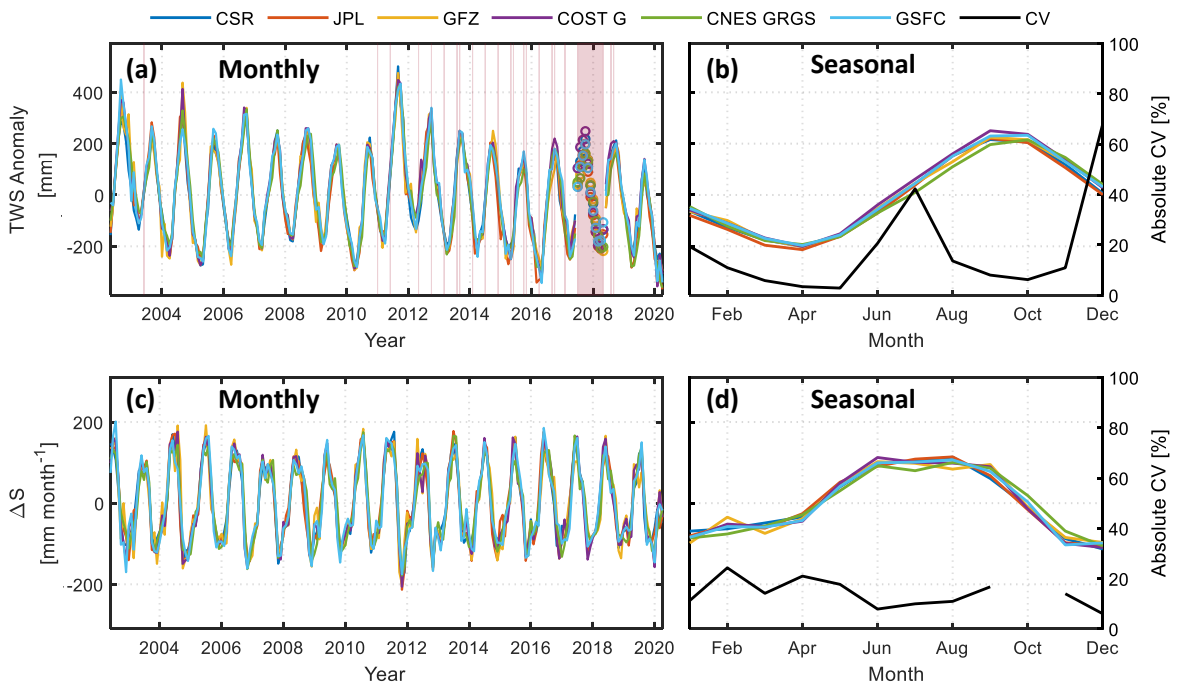

Figure 5.5. Same as Figure 5.3 but for terrestrial water storage anomaly (TWSA) and storage change (ΔS). TWSA during May 2002 to June 2017 and June 2018 to April 2020 is from the various GRACE data products, and during July 2017 to May 2018 (and during the missing 21 months as listed in Table 5.3) is the output from the ANN model. The shaded region represents the months of missing values (a total of 32 values). Since the value of ΔS is almost zero in October, leading to a very high CV value (>100%), the exact value is not shown in Fig. 5.5 (d) for simplicity. After (Abhishek et al, 2022).

Table 5.3. Performance indicators (r, NRMSE, and NSE) for all six TWSA products during training and validation phases. After (Abhishek et al, 2022).

TWSA product	Training (164 values; 04/2002-06/2017)*			Validation (25 values; 06/2018-10/2020)**		
	r	NRMSE	NSE	r	NRMSE	NSE
CSR	0.97	0.27	0.93	0.97	0.32	0.92
JPL	0.97	0.24	0.94	0.96	0.26	0.93
GFZ	0.94	0.32	0.89	0.91	0.37	0.82
COST-G	0.96	0.28	0.92	0.95	0.35	0.90
CNES GRGS	0.96	0.29	0.91	0.97	0.28	0.92
GSFC	0.95	0.30	0.90	0.96	0.28	0.90

*21 values (Jun-02, Jul-02, Jun-03, Jan-11, Jun-11, May-12, Oct-12, Mar-13, Aug-13, Sep-13, Feb-14, Jul-14, Dec-14, May-15, Jun-15, Oct-15, Nov-15, Apr-16, Sep-16, Oct-16, Feb-17) were missing during 04/2002-06/2017. **2 values (Aug-18, Sept-18) were missing during 06/2018-10/2020.

5.3.3. Raw ensembles of the water budget and residual error

Seasonal variations of water budget components (shown in Fig. 5.6)—excluding estimates from model products (e.g., GLDAS) which neglect anthropogenic activities—possess embedded effects of both natural and human-induced climate variability (e.g., reservoirs management, groundwater abstraction, irrigation, etc.) and has strong seasonality. Generally, precipitation (P) controls the other water cycle components during the rainy season (May to October) since the anthropogenic activities are minimal during this period, with an opposite situation in the dry season (November to April) (Fig. 5.6). P attains a minimum of ~7-10 mm (December-February) and a maximum of 267.73 mm (September). Evapotranspiration (ET) has a minimum of ~50 mm (February-March) and continually increases from May to October from the onset of the monsoon season with a maximum of 123.24 mm (October). ΔS is primarily driven by the net precipitation (P-ET) and shows a minimum of -105 mm in December and a maximum of 103 mm during June to August. Maxima and minima of all the water budget components have the lag behavior varying between one to three months from each other.

The mean monthly residual error averaged across all combinations of water budgets is 14.37 mm month^{-1} for the basin and is consistent with the previously reported tendency for positive residuals in lower latitude basins (Abolafia-Rosenzweig et al., 2021). The mean monthly error accounts for about 15% (consistent with Rodell *et al.* (Rodell et al., 2015)) and 16% of the ensemble mean of monthly P and ET, respectively. An increasing trend of 0.03 mm month^{-1} in residual errors may partly be attributed to increased human interventions. Specifically, the CPRB has hosted a 10% increase in the area equipped for irrigation from 5830x10^3 ha to 6415x10^3 ha from 2002 to 2020 in Thailand; (FAO-AQUASTAT, 2020), which is expected to drive increasingly negative biases in model-based ET due to missing irrigation information. Although overall variations of the residual error in the basin are minimal (mean of the % variation = -0.02%), the residual error is more frequently positive than negative and generally possesses relatively high fluctuations from April to November (Fig. 5.6). The tendency of the

residual error to be positive can be mainly explained by either wet biases in precipitation or by dry biases in the ET and ΔS (or a combination of these factors).

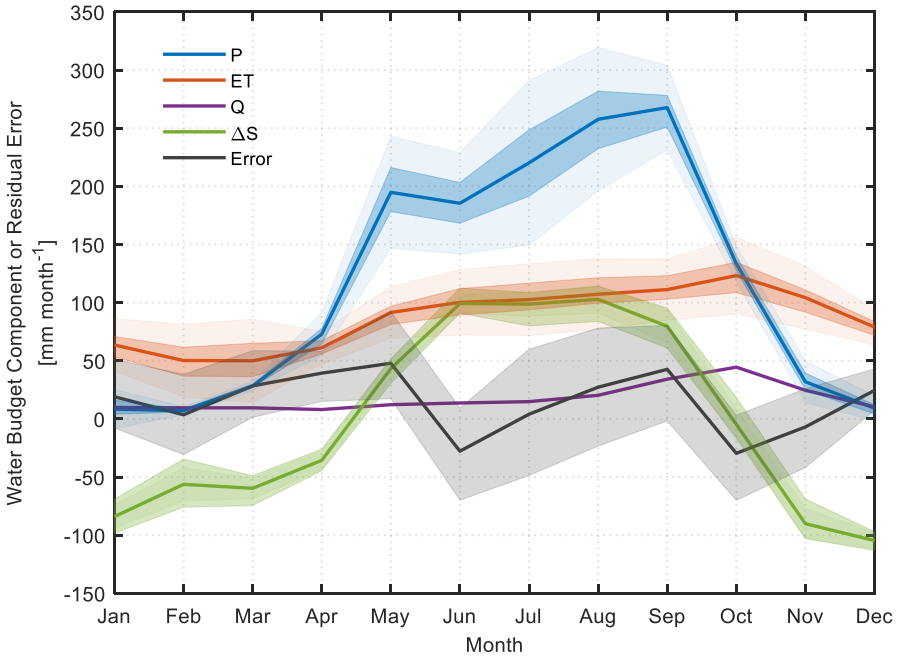

Figure 5.6. Seasonal variations of the water budget components (P, ET, Q, ΔS) and the residual error. The solid colored lines represent the ensemble mean of either the data products used in this study (for P, ET, Q, ΔS) or the mean of residuals from 72 combinations (for residual error). The darker shaded regions represent the range of the values of the respective variable (for P, ET, Q, ΔS) and the error range corresponding to the different combinations of data products (for residual error) used in water budget. The lighter shaded regions (for P, ET, ΔS) represent the 95% confidence interval. After (Abhishek et al, 2022).

Since ground-truthing for most of the water budget variables is unavailable in data-limited/data-scarce river basins such as the upper CPRB, a set of data products having large errors in different directions (e.g., underestimated P, overestimated ET, Q, and ΔS in case of positive residuals) may erroneously lead to minimal or even near-zero residuals in the water balance resulting in misleading interpretation and implications. Therefore, three water balance closure techniques of varying mathematical complexity are applied to attain the physical water balance constraint for each unique realization of the water budget. Since an independent and uncorrelated a priori bias in various datasets cannot be known, we assume corrected values as ‘true’; note that the development of more robust and advanced techniques may lead to more realistic results.

5.3.4. Comparison of three water budget closure techniques

All three closure techniques perform similarly across water balance components without presenting unidirectional characteristics (Fig. 5.7). The proportional redistribution (PR) method generally provides the lowest and highest closure constraints (eq. 9) for P, ET and Q in case of wet and dry biases, respectively (Fig. 5.7). ΔS closure constraints are persistently positive during the dry season. P closure constraints are typically negative (indicating a wet bias in P), while those for ET, Q and ΔS have opposite signs during respective time periods. Although closure constraints are minimal during October-November in P, other components (Q, ET, and ΔS) have dry biases attributed to the negative residual during these months. Since Q is observed in-situ, it generally possesses low constraint values except for the month of October (corresponding to the highest Q), particularly from the PR approach.

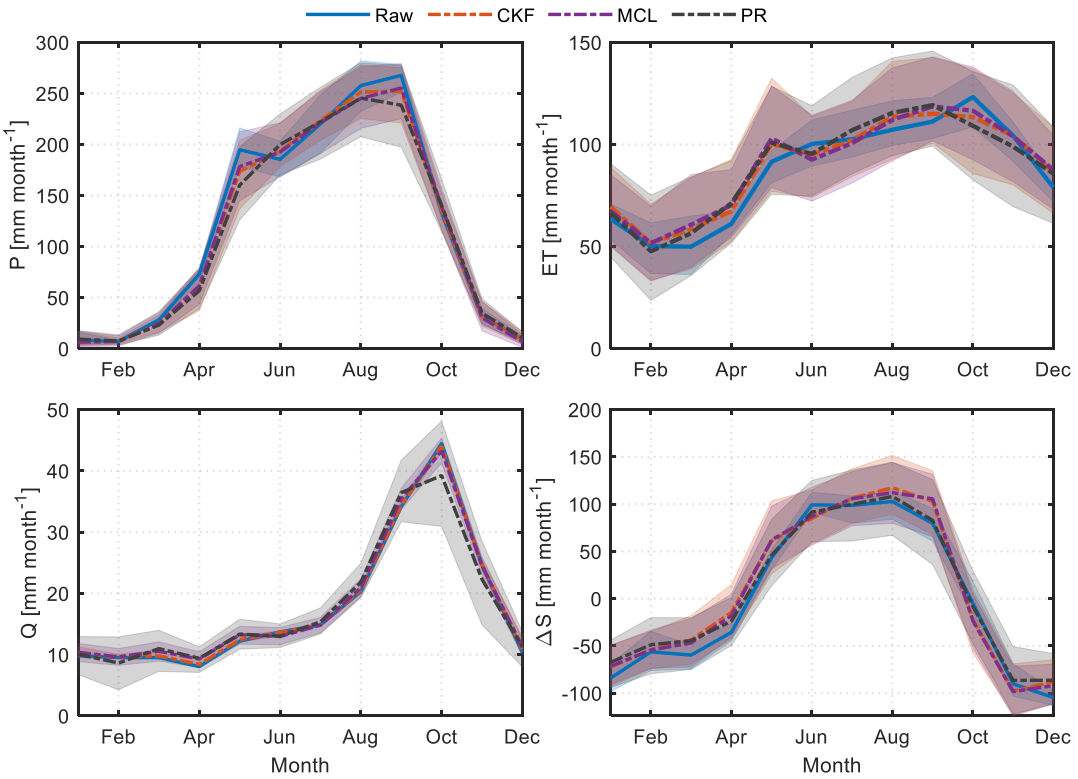

Figure 5.7. Seasonal variations of the corrected water budget components (P, ET, Q, ΔS) using three different methods, namely, Constrained Kalman filter (CKF), Multiple collocation (MCL), Proportional redistribution (PR). Raw data in terms of the ensemble mean of the various data products are also shown for the inter-comparison. The residual water budget error using the corrected components is zero. After (Abhishek et al, 2022).

Despite the mixed behavior of closure constraints in seasonal time series, the mean annual variability of various components reveals wet biases in P and Q and dry biases in ET and ΔS (Fig. 5.8). The absolute magnitude of these biases follows the order of variability as ΔS>P>ET>Q. One notable inference is that negative (positive) closure constraints for P do not necessarily imply positive (negative) constraints in the remaining components on annual scales. All components may have similar constraints (same sign/direction: positive or negative) but with different magnitudes, as revealed in the annual time series (e.g., the year 2012; Fig. 5.8). Wet bias (overestimation) of P or dry bias (underestimation) of ET, especially in the rainy season, may lead to misinterpretation of regional flood and drought potential and projections. Similarly, accurate assessments of Q and ΔS may inform dam reservoir operations (water release amount and timing) and agricultural water management (e.g., partitioning and dependence on surface water and groundwater extraction).

5.3.5. Long-term variations and trends in corrected water budget components

Long-term annual means of various water storage components (precipitation: P, evapotranspiration: ET, and runoff: Q) are calculated from 2003 to 2019 and compared them other global studies. Long term means of P, ET, and Q for the upper CPRB are 1355 mm yr^{-1} (global mean 811 mm yr^{-1}), 1086 mm yr^{-1} (1.8 to 3.3 times larger than global estimates based on various methods (Rodell et al., 2015)), and 210 mm yr^{-1} (global mean of 366 mm yr^{-1}), respectively. Uncertainties of all the water budget components are decreased after applying closure constraints (shaded areas in Fig. 5.8). Corresponding uncertainties for corrected P (σ_P), Q (σ_Q), ET (σ_{ET}), and ΔS ($\sigma_{\Delta S}$), calculated as the standard deviation across data products (Pascolini-Campbell et al., 2020), are 10.4, 4.7, 9.12, and 2.6 mm $month^{-1}$, respectively. Intercomparison of the annual trends in raw and corrected components reveal that P have highest change (raw vs corrected trends: -1.85 to -4.67 mm yr^{-1}) followed by ET (-1.94 to -1.09 mm yr^{-1}) and Q (-4.38 to -4.25 mm yr^{-1}). Corrected long term linear trends reveal a 1.0% decrease in P, 8.6% increase in ET, and 13% decrease in Q. ET/Q has an increasingly significant trend, which suggests that P is increasingly partitioned in ET rather than Q (i.e., decreasing runoff efficiency). Increases in ET can be associated with the joint impact of ENSO events with increasing temperature and irrigation in the region (Abhishek et al., 2021). This result agrees with the premise of intensification of the water cycle in a warming climate (Pascolini-Campbell et al., 2021). Although the majority of deforestation in CPRB

occurred in the late 20th century (especially in the 1970s and 1980s), ongoing dynamic and heterogeneous land use land cover changes in the basin may partially influence ET trends. The observed increase in ET/Q indicates a potential overreliance on groundwater in future if the current trend persists. Further human influences of irrigation and reservoir management

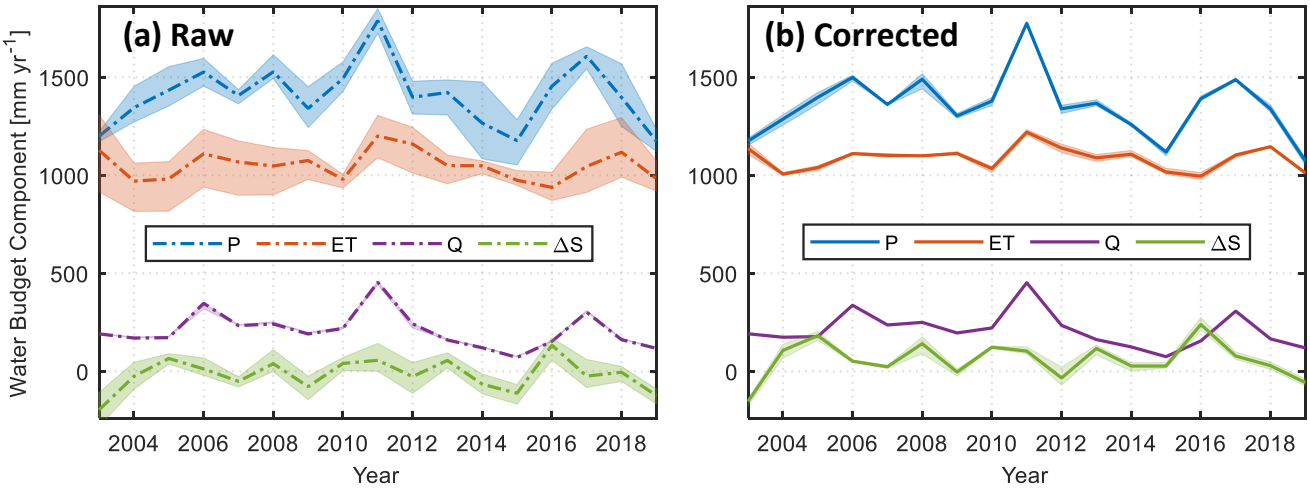

Figure 5.8. (a) Mean annual variability of the raw products (dash-dotted lines), and their variation (shaded areas). (b) the ensemble mean of the corrected water storage components (solid lines), and the corresponding variation using the three closure techniques (shaded areas). All the components are represented as the annual average of the basin-wide equivalent water depth in mm. After (Abhishek et al, 2022).

may be implicated in our water budget closure assessment. For example, corrected ET is larger than raw ET. This computed underestimate is consistent with expected biases from ET products that do not fully account for irrigation. Additionally, the long-term average of ΔS is persistently positive, even in some drought years (e.g., 2015) (Fig. 5.8). This may be partially attributable to dam reservoir operations in the region that maintains water in CPRB or to the relative redistribution of biases among other water budget variables (P, ET, and Q); the latter of which can simply be a mathematical artifact and should be investigated further. Moreover, the effect, though likely negligible as compared to the water stored in the system at a given point in time, along with the interdependency between multisource data, should also be considered in future work. These observationally-based signals of human interventions with the water cycle are important to consider for risk mitigation associated with extreme hydrologic events and agricultural water management in the basin. Thus future water budget assessments over CPRB can benefit from the use of higher spatial and temporal resolution

data with longer records followed by downscaling/reconstruction (e.g. (Richter et al., 2021)). Continuously increasing density of rain gauges, ET flux towers, and groundwater monitoring will further assist in understanding the complex interactions of human-induced changes and climate variability on regional hydrology.

5.4. Conclusions

In this chapter, relative biases in water budget components are quantified to better understand regional earth system processes and water dynamics in the upper Chao Phraya River Basin (CPRB) from May 2002 to April 2020. The basin is highly vulnerable to hydroclimatic extremes, plays a key role in the policymaking in Thailand and subsequently in neighboring countries, and possesses a complex existing water governance framework with a multitude of institutions (as many as 31 ministerial departments, among other national and autonomous agencies; (FAO, 2011; Kiguchi et al., 2021)). The major findings of our study are summarized below,

- Various data products, which are based on remote sensing, reanalysis, and in-situ observations, have similar seasonal and annual dynamics, and the variations across products can be attributed to the different retrieval algorithms, model inadequacies, and other biases. The ANN model has the potential to fill data gaps between the GRACE and GRACE-FO TWS time series (11 months missing values) and for the sporadically missing values due to battery management practices (a total of 21 missing values during the study period); the latter of which is otherwise filled by using the linear interpolation of the bounding values and thus may underestimate the terrestrial water storage (TWS) especially during the peak of the dry or wet season.
- Generally, precipitation (P) tends to have wet bias while evapotranspiration (ET), runoff (Q), and storage change (ΔS) have dry biases. Seasonal time series of the closure constraints of various water budget components reveal a mixed behavior, while the absolute mean annual variability follows the order as ΔS>P>ET>Q. Interestingly, a negative (or positive) closure constraint in P does not necessarily imply a positive (or negative) constraint in the remaining components on an annual scale. Knowledge of wet or dry biases of individual components of the water cycle has potential implications for water resources, climate, and agriculture in the basin. For example, correction of an overestimation (underestimation) implicit to P (ET) in the rainy season may avert inaccurate flood (drought) projections.

- The magnitude and sign of closure constraints on various water budget components using the three closure techniques and the resultant partitioning of the water cycle when combined with long term trends in various hydrological and water storage components in our companion study (Abhishek et al., 2021) can be effectively used to inform water management especially for mitigation of the adverse effects of drought and floods and for water availability in the basin.
- Although the currently employed water balance closure techniques utilize the unique information from the available scatter of various data products for any given component, the derived combination, though physically consistent, may not be most accurate. This could happen because of similar biases (e.g., dry bias in both P and ET), biases with opposite directions, correlation among various components arising from geophysical variabilities, or simply due to the mathematical artifact (even negative runoff values in Wong et al., 2021; magnitude shift of about >100 mm even in the seasonal time series in Abolafia-Rosenzweig et al., 2021). However, the results may serve as the basis for the starting point of getting insights into water availability and other hydrological applications for guiding potential users.

This assessment provides insights into relative uncertainties of observed and modeled water budget components for the study period and may be utilized for enabling efficient water management and related policymaking. Results may be useful for further segregating the impacts of natural and anthropogenic factors on hindcasted or forecasted water budget components and subsequent potential adaptation measures. The improved understanding of regional water cycle dynamics is of utmost importance and has potential in benchmarking regional hydroclimate models for better understanding, quantification, and predicting the distribution and variability of the terrestrial water cycle and ultimately leading to reduced water budget imbalance.

The closed water budget/balance achieved through the multisource ensemble strategy and various mathematical techniques in this chapter will enables us to refine the hydrological models. To understand this, say, we are simulating runoff using the precipitation and evapotranspiration, along with other land use and climate forcing, as the input. If the simulated runoff using the corrected variables matches with the observed runoff better than that from the uncorrected variables, it provides confidence in the adopted closure techniques which may further evolve.

Chapter 6

Summary and Way Forward

6. Summary and Way Forward

The increasing stress on terrestrial systems has threatened nearly 2/3rd of the prevailing habitats, with over five billion people living in the regions prone to water scarcity of varying levels. This number is most likely to increase due to climate change, population growth, and human activities like groundwater extractions, water impoundments and diversions, urbanization, and land use cover changes. Apart from compromising food production and reduced freshwater availability, unsustainable water usage and subsequent depleting water storage can ultimately affect the economy with a more pronounced and severe impact on the developing agrarian countries like India and Thailand. Therefore, a long-term basin-scale assessment of water storage dynamics and water-related extremes is imperative for understanding the systematic changes in the hydrological system and ensuring timely and equitable water share. This thesis is devoted to addressing the above by jointly assimilating the Gravity Recovery and Climate Experiment (GRACE) gravity data, a global hydrological model (GHM), i.e., PCR-GLOBWB model outputs, auxiliary weather datasets from remote sensing and reanalysis products, and in-situ observations for three Peninsular Indian river basins, namely, Godavari, Krishna, and Mahanadi river basins and Chao Phraya river basin in Thailand.

Quantification of the land water storage (LWS, comprised of biomass, snow cover, surface water, canopy water, and soil moisture and groundwater) and groundwater storage (GWS) deficits (i.e., below normal conditions) in Peninsular India for 35 years from January 1980 to December 2014 shows that the study basins experienced high interannual variations despite the minimal linear LWS trends (0.26–0.56 mm yr^{-1}). GWS showed a slow but persistent response (longest deficit spanning ~6 years) to the seasonal variations in the hydrological fluxes and remained the major contributor to LWS and primarily governed the water availability during dry years. The GHM showed potential to analyze LWS and its segregated components beyond GRACE data records and the LWS-based index served as a better drought indicator than traditional drought indices. GRACE-LWS emerged as a proxy indicator of real-time groundwater monitoring without relying upon the intermittent in situ observations. The GHM underestimating both the increasing and decreasing water storage trends and decreasing trends in the recent time highlighted the need for more detailed quantification of the water storage dynamics covering the most recent periods, e.g., starting from GRACE data

records in 2002. Decadal trends of terrestrial water storage (TWS; the equivalent of LWS except for water in ice sheets of Greenland and Antarctic) and its constituent components in three basins reveal a stable annual cycle and minimal trends during the period from July 2002 to June 2010, and declining trends (largest for Krishna basin) of TWS, SMS, and GWS during the period from July 2010 to June 2017. GRACE-derived GWS anomalies and those obtained from the in-situ data are in good agreement depicting the profound applicability of satellite observation in quantifying basin-wide water resources.

Further, the developed artificial neural network method coupled with the genetic algorithms ensures the continuity in and between the two GRACE missions. Long-term analysis for the Chao Phraya River Basin, with more complex human interventions, e.g., reservoir management, than the Indian basins, revealed a linear trend of −1.12 cm yr^{-1} (equivalent to a volumetric trend of −1.79 km^3 yr^{-1}). GWS is a significant contributor (45%) to TWS with a linear trend of −0.51 cm yr^{-1} (-0.82 km^3 yr^{-1}) followed by surface water storage (i.e., cumulative of the water storage in the reservoirs, flood inundation, and rivers) (36%) and soil moisture storage (19%) during 2002–2020. The variations in precipitation primarily trigger the hydroclimatic extremes detected in TWSA during the monsoon season (May to October) and are further amplified by the subsequent water storage and abstraction. All the flood and drought events are well recorded in TWSA, albeit with a lag time of up to two months from precipitation. The basin's increasing potential for severe drought, as assessed by the effective water storage-based novel drought potential index (DPI), underscored the need for multifaceted water management essentially focused on the demand side rather than the supply side in the basin. Lastly, a physically consistent zero water budget residual was enforced with three different mathematical techniques, and the seasonal and annual variations of the closure constraints (i.e., wet or dry biases) were studied for the inferences of likely over(under)estimation of various water budget components.

The proposed framework for observation-based assessment of the various water cycle components and the water budget closure in this thesis puts forward a blueprint for effectively and efficiently managing the basin-scale water resources and food security and developing the early warning systems for droughts and floods in the data-scarce river basins globally. Future research should focus on disentangling the human-induced and the climate-driven signals in the TWS for an advanced understanding of the earth system processes and

adapting and prioritizing the mitigation strategies, especially in the basins vulnerable to the hydroclimate extremes. This segregation of various constituent signals of the water storage should be carried out on multiple spatial (e.g., grid-based, basin-averaged, regional, zonal averaged, etc.) and temporal (monthly, seasonal, annual) scales. Since the variability of the human water usage or diversion play crucial role in the global transboundary river basins where upstream activities primarily governs the freshwater availability and ecological functionality in the downstream basins in other countries, such basins could be a prime focus of the future studies in this direction.

7. Acknowledgments and data availability

The datasets utilized in this thesis are open access and are available from http://grace.jpl.nasa.gov (JPL GRACE RL06 Mascon solutions supported by NASA MEaSUREs program), http://www2.csr.utexas.edu/grace (CSR GRACE RL06 Mascon solutions), https://isdc.gfz-potsdam.de/grace-isdc/ (GFZ GRACE RL06 SH products), www.imd.gov.in (IMD; precipitation data), TRMM (3B43, precipitation data), http://www.india-wris.nrsc.gov.in (India-WRIS; groundwater well data), CGWB (aquifer properties), and http://www.globalhydrology.nl/models/pcr-globwb-2-0/ (PCR GLOBWB 2.0). All other data sources are duly cited in the respective chapters of this thesis.

8. References

Abhishek, Kinouchi, T., 2022. Multidecadal Land Water and Groundwater Drought Evaluation in Peninsular India. Remote Sens. 14, 1486. https://doi.org/10.3390/rs14061486

Abhishek, Kinouchi, T., 2021. Synergetic application of GRACE gravity data, global hydrological model, and in-situ observations to quantify water storage dynamics over Peninsular India during 2002–2017. J. Hydrol. 596, 126069. https://doi.org/10.1016/j.jhydrol.2021.126069

Abhishek, Kinouchi, T., Abolafia-Rosenzweig, R., Ito, M., 2022. Water Budget Closure in the Upper Chao Phraya River Basin, Thailand Using Multisource Data. Remote Sens. 14. https://doi.org/10.3390/rs14010173

Abhishek, Kinouchi, T., Sayama, T., 2021. A comprehensive assessment of water storage dynamics and hydroclimatic extremes in the Chao Phraya River Basin during 2002–2020. J. Hydrol. 603. https://doi.org/10.1016/j.jhydrol.2021.126868

Abolafia-Rosenzweig, R., Pan, M., Zeng, J.L., Livneh, B., 2021. Remotely sensed ensembles of the terrestrial water budget over major global river basins: An assessment of three closure techniques. Remote Sens. Environ. 252. https://doi.org/10.1016/j.rse.2020.112191

Adler, R.F., Huffman, G.J., Chang, A., Ferraro, R., Xie, P.P., Janowiak, J., Rudolf, B., Schneider, U., Curtis, S., Bolvin, D., Gruber, A., Susskind, J., Arkin, P., Nelkin, E., 2003. The version-2 global precipitation climatology project (GPCP) monthly precipitation analysis (1979-present). J. Hydrometeorol. 4. https://doi.org/10.1175/1525-7541(2003)004<1147:TVGPCP>2.0.CO;2

AghaKouchak, A., Mirchi, A., Madani, K., Di Baldassarre, G., Nazemi, A., Alborzi, A., Anjileli, H., Azarderakhsh, M., Chiang, F., Hassanzadeh, E., Huning, L.S., Mallakpour, I., Martinez, A., Mazdiyasni, O., Moftakhari, H., Norouzi, H., Sadegh, M., Sadeqi, D., Van Loon, A.F., Wanders, N., 2021. Anthropogenic Drought: Definition, Challenges and Opportunities. Rev. Geophys. https://doi.org/10.1029/2019rg000683

Alcamo, J., Döll, P., Henrichs, T., Kaspar, F., Lehner, B., Rösch, T., Siebert, S., 2003. Development and testing of the WaterGAP 2 global model of water use and availability. Hydrol. Sci. J. 48. https://doi.org/10.1623/hysj.48.3.317.45290

Alley, W.M., 1984. The Palmer Drought Severity Index: limitations and assumptions. J. Clim. Appl. Meteorol. https://doi.org/10.1175/1520-0450(1984)023<1100:TPDSIL>2.0.CO;2

Amnuaylojaroen, T., Chanvichit, P., 2019. Projection of near-future climate change and agricultural drought in Mainland Southeast Asia under RCP8.5. Clim. Change 155. https://doi.org/10.1007/s10584-019-02442-5

Andrew, R., Guan, H., Batelaan, O., 2017. Estimation of GRACE water storage components by temporal decomposition. J. Hydrol. https://doi.org/10.1016/j.jhydrol.2017.06.016

Armanios, D.E., Fisher, J.B., 2014. Measuring water availability with limited ground data: Assessing the feasibility of an entirely remote-sensing-based hydrologic budget of the Rufiji Basin, Tanzania, using TRMM, GRACE, MODIS, SRB, and AIRS. Hydrol. Process. 28. https://doi.org/10.1002/hyp.9611

Ashouri, H., Hsu, K.L., Sorooshian, S., Braithwaite, D.K., Knapp, K.R., Cecil, L.D., Nelson, B.R., Prat, O.P., 2015. PERSIANN-CDR: Daily precipitation climate data record from multisatellite observations for hydrological and climate studies. Bull. Am. Meteorol. Soc. 96. https://doi.org/10.1175/BAMS-D-13-00068.1

Azarderakhsh, M., Rossow, W.B., Papa, F., Norouzi, H., Khanbilvardi, R., 2011. Diagnosing water variations within the Amazon basin using satellite data. J. Geophys. Res. Atmos. 116. https://doi.org/10.1029/2011JD015997

Babel, M.S., Das Gupta, A., Donna, N., Domingo, S., 2006. Land Subsidence: A Consequence of Groundwater Over-Exploitation in Bangkok, Thailand. Int. Rev. Environ. Strateg. Spec. Featur. Groundw. Manag. Policy 6.

Barnett, T.P., Adam, J.C., Lettenmaier, D.P., 2005. Potential impacts of a warming climate on water availability in snow-dominated regions. Nature. https://doi.org/10.1038/nature04141

Beaudoing, H., Rodell, M., NASA/GSFC/HSL, 2020. GLDAS Noah Land Surface Model L4 monthly 0.25 x 0.25 degree V2.1, Greenbelt, Maryland, USA, Goddard Earth Sciences Data and Information Services Center (GES DISC).

Bhanja, S.N., Mukherjee, A., 2019. In situ and satellite-based estimates of usable groundwater storage across India: Implications for drinking water supply and food security. Adv. Water Resour. 126. https://doi.org/10.1016/j.advwatres.2019.02.001

Bhanja, S.N., Mukherjee, A., Rodell, M., Wada, Y., Chattopadhyay, S., Velicogna, I., Pangaluru, K., Famiglietti, J.S., 2017a. Groundwater rejuvenation in parts of India influenced by water-policy change implementation. Sci. Rep. https://doi.org/10.1038/s41598-017-07058-2

Bhanja, S.N., Mukherjee, A., Saha, D., Velicogna, I., Famiglietti, J.S., 2016. Validation of GRACE based groundwater storage anomaly using in-situ groundwater level measurements in India. J. Hydrol. 543. https://doi.org/10.1016/j.jhydrol.2016.10.042

Bhanja, S.N., Rodell, M., Li, B., Saha, D., Mukherjee, A., 2017b. Spatio-temporal variability of groundwater storage in India. J. Hydrol. 544. https://doi.org/10.1016/j.jhydrol.2016.11.052

Bloomfield, J.P., Marchant, B.P., 2013. Analysis of groundwater drought building on the standardised precipitation index approach. Hydrol. Earth Syst. Sci. https://doi.org/10.5194/hess-17-4769-2013

Bloomfield, J.P., Marchant, B.P., Bricker, S.H., Morgan, R.B., 2015. Regional analysis of groundwater droughts using hydrograph classification. Hydrol. Earth Syst. Sci. https://doi.org/10.5194/hess-19-4327-2015

Bonan, G.B., Oleson, K.W., Vertenstein, M., Levis, S., Zeng, X., Dai, Y., Dickinson, R.E., Yang, Z.L., 2002. The land surface climatology of the community land model coupled to the NCAR community climate model. J. Clim. https://doi.org/10.1175/1520-0442(2002)015<3123:TLSCOT>2.0.CO;2

Cao, Y., Nan, Z., Cheng, G., 2015. GRACE gravity satellite observations of terrestrial water storage changes for drought characterization in the arid land of northwestern China. Remote Sens. https://doi.org/10.3390/rs70101021

Cattani, E., Merino, A., Levizzani, V., 2016. Evaluation of monthly satellite-derived precipitation products over East Africa. J. Hydrometeorol. 17. https://doi.org/10.1175/JHM-D-15-0042.1

Census of India, G., 2011. Report of the Technical Group on Population Projections, 2019 [WWW Document].

Central Ground Water Board, 2017. Ground water year book-India 2016-17. Minist. Water Resour. Gov. India.

CGWB, 2017. Central Ground Water Board, CGWB. Ground Water Year Book—India 2016-17. G. o. I. Ministry of Water Resources, p. 90.

CGWB, 2014a. DYNAMIC GROUND WATER Dynamic Ground Water Resources of India.

CGWB, 2014b. Central Ground Water Board (CGWB), G.o.I., Ministry of Water Resources. Ground Water Year Book – India 2013–14, 76pp.

Chen, H., Zhang, W., Nie, N., Guo, Y., 2019. Long-term groundwater storage variations estimated in the Songhua River Basin by using GRACE products, land surface models, and in-situ observations. Sci. Total Environ. https://doi.org/10.1016/j.scitotenv.2018.08.352

Chen, J., Li, J., Zhang, Z., Ni, S., 2014. Long-term groundwater variations in Northwest India from satellite gravity measurements. Glob. Planet. Change. https://doi.org/10.1016/j.gloplacha.2014.02.007

Chen, J., Tapley, B., Rodell, M., Seo, K.W., Wilson, C., Scanlon, B.R., Pokhrel, Y., 2020. Basin-Scale River Runoff Estimation From GRACE Gravity Satellites, Climate Models, and In Situ Observations: A Case Study in the Amazon Basin. Water Resour. Res. https://doi.org/10.1029/2020WR028032

Chen, J.L., Wilson, C.R., Tapley, B.D., 2010. The 2009 exceptional Amazon flood and interannual terrestrial water storage change observed by GRACE. Water Resour. Res. https://doi.org/10.1029/2010WR009383

CHEN, P.Y., POPOVICH, P.M., 2011. CORRELATION: PARAMETRIC AND NONPARAMETRIC MEASURES, in: Correlation. https://doi.org/10.4135/9781412983808.n1

Chen, X., Long, D., Hong, Y., Zeng, C., Yan, D., 2017. Improved modeling of snow and glacier melting by a progressive two-stage calibration strategy with GRACE and multisource data: How snow and glacier meltwater contributes to the runoff of the Upper Brahmaputra River basin? Water Resour. Res. https://doi.org/10.1002/2016WR019656

Cheng, M., Fang, F., Kinouchi, T., Navon, I.M., Pain, C.C., 2020. Long lead-time daily and monthly streamflow forecasting using machine learning methods. J. Hydrol. 590. https://doi.org/10.1016/j.jhydrol.2020.125376

Cheng, M., Tapley, B.D., Ries, J.C., 2013. Deceleration in the Earth's oblateness. J. Geophys. Res. Solid Earth. https://doi.org/10.1002/jgrb.50058

Chindarkar, N., Grafton, R.Q., 2019. India's depleting groundwater: When science meets policy. Asia Pacific Policy Stud. https://doi.org/10.1002/app5.269

Chinnasamy, P., Hubbart, J.A., Agoramoorthy, G., 2013. Using remote sensing data to improve groundwater supply estimations in Gujarat, India. Earth Interact. https://doi.org/10.1175/2012EI000456.1

Chitsazan, N., Nadiri, A.A., Tsai, F.T.C., 2015. Prediction and structural uncertainty analyses of artificial neural networks using hierarchical Bayesian model averaging. J. Hydrol. https://doi.org/10.1016/j.jhydrol.2015.06.007

Ciracì, E., Velicogna, I., Swenson, S., 2020. Continuity of the Mass Loss of the World's Glaciers and Ice Caps From the GRACE and GRACE Follow-On Missions. Geophys. Res. Lett. 47. https://doi.org/10.1029/2019GL086926

Creutzfeldt, B., Ferré, T., Troch, P., Merz, B., Wziontek, H., Güntner, A., 2012. Total water storage dynamics in response to climate variability and extremes: Inference from long-term terrestrial gravity measurement. J. Geophys. Res. Atmos. https://doi.org/10.1029/2011JD016472

CWC, C.W.C., 2019. Water and Related Statistics. Water Planning and Project Wing. New Delhi: Central Water Commission [WWW Document].

Dahle, C., Flechtner, F., Murböck, M., Michalak, G., Neumayer, H. Abrykosov, O., Reinhold, A., König, R., 2018. GRACE 327-743 (Gravity Recovery and Climate Experiment), GFZ Level-

2 Processing Standards Document for Level-2 Product Release 06 (Rev. 1.0, October 26, 2018), (Scientific Technical Report STR - Data; 18/04), Potsdam: GFZ German Research Centre for Geosci [WWW Document]. https://doi.org/http://doi.org/10.2312/GFZ.b103-18048

Dahle, C., Murböck, M., 2019. Post-processed GRACE/GRACE-FO Geopotential GSM Coefficients GFZ RL06 (Level-2B Product). V. 0002. GFZ Data Services [WWW Document]. https://doi.org/https://doi.org/10.5880/GFZ.GRAVIS_06_L2B

Dahle, C., Murböck, M., Flechtner, F., Dobslaw, H., Michalak, G., Neumayer, K.H., Abrykosov, O., Reinhold, A., König, R., Sulzbach, R., Förste, C., 2019. The GFZ GRACE RL06 monthly gravity field time series: Processing details and quality assessment. Remote Sens. https://doi.org/10.3390/rs11182116

Dai, A., 2013. Increasing drought under global warming in observations and models. Nat. Clim. Chang. https://doi.org/10.1038/nclimate1633

Dai, A., 2011. Drought under global warming: A review. Wiley Interdiscip. Rev. Clim. Chang. https://doi.org/10.1002/wcc.81

Dai, A., Trenberth, K.E., Qian, T., 2004. A global dataset of Palmer Drought Severity Index for 1870-2002: Relationship with soil moisture and effects of surface warming. J. Hydrometeorol. 5. https://doi.org/10.1175/JHM-386.1

Das, P.K., Chandra, S., Das, D.K., Midya, S.K., Paul, A., Bandyopadhyay, S., Dadhwal, V.K., 2020. Understanding the interactions between meteorological and soil moisture drought over Indian region. J. Earth Syst. Sci. 129. https://doi.org/10.1007/s12040-020-01460-7

Dasgupta, S., Das, I.C., Subramanian, S.K., Dadhwal, V.K., 2014. Space-based gravity data analysis for groundwater storage estimation in the Gangetic plain, India. Curr. Sci. https://doi.org/10.18520/cs/v107/i5/832-844

Davis, J.C., 2002. Statistics and Data Analysis in Geology. (3rd edition), Wiley, New York.

Department of Water Resources, M. of J.S. (MoJS), n.d. Department of Water Resources, River Development & Ganga Rejuvenation, Government of India. [WWW Document].

Dhiman, S.., 2012. Aquifer systems of India. Ministry of Water Resources, Government of India.

Döll, P., Kaspar, F., Lehner, B., 2003. A global hydrological model for deriving water availability indicators: Model tuning and validation. J. Hydrol. 270. https://doi.org/10.1016/S0022-1694(02)00283-4

Döll, P., Müller Schmied, H., Schuh, C., Portmann, F.T., Eicker, A., 2014. Global-scale assessment of groundwater depletion and related groundwater abstractions: Combining hydrological modeling with information from well observations and GRACE satellites. Water Resour. Res. https://doi.org/10.1002/2014WR015595

Douglas, E.M., Niyogi, D., Frolking, S., Yeluripati, J.B., Pielke, R.A., Niyogi, N., Vörösmarty, C.J., Mohanty, U.C., 2006. Changes in moisture and energy fluxes due to agricultural land use and irrigation in the Indian Monsoon Belt. Geophys. Res. Lett. https://doi.org/10.1029/2006GL026550

Du, L., Tian, Q., Yu, T., Meng, Q., Jancso, T., Udvardy, P., Huang, Y., 2013. A comprehensive drought monitoring method integrating MODIS and TRMM data. Int. J. Appl. Earth Obs. Geoinf. https://doi.org/10.1016/j.jag.2012.09.010

Duan, Z., Bastiaanssen, W.G.M., 2013. First results from Version 7 TRMM 3B43 precipitation product in combination with a new downscaling-calibration procedure. Remote Sens. Environ. https://doi.org/10.1016/j.rse.2012.12.002

Famiglietti, J.S., 2014. The global groundwater crisis. Nat. Clim. Chang. https://doi.org/10.1038/nclimate2425

Famiglietti, J.S., Cazenave, A., Eicker, A., Reager, J.T., Rodell, M., Velicogna, I., 2015. Satellites provide the big picture. Science (80-.). https://doi.org/10.1126/science.aac9238

Famiglietti, J.S., Lo, M., Ho, S.L., Bethune, J., Anderson, K.J., Syed, T.H., Swenson, S.C., De Linage, C.R., Rodell, M., 2011. Satellites measure recent rates of groundwater depletion in California's Central Valley. Geophys. Res. Lett. https://doi.org/10.1029/2010GL046442

Famiglietti, J.S., Rodell, M., 2013. Water in the balance. Science (80-.). https://doi.org/10.1126/science.1236460

FAO-AQUASTAT, 2020. Global Information System on Water and Agriculture: Water resources [WWW Document]. URL http://www.fao.org/aquastat/en/overview/methodology/water-use%0Ahttp://www.fao.org/aquastat/en/overview/methodology/water-resources/ (accessed 7.20.21).

FAO, 2011. AQUASTAT Country Profile – Thailand. Food and Agriculture Organization of the United Nations (FAO). Rome, Italy. https://doi.org/http://www.fao.org/3/ca0408en/CA0408EN.pdf

Felfelani, F., Wada, Y., Longuevergne, L., Pokhrel, Y.N., 2017. Natural and human-induced terrestrial water storage change: A global analysis using hydrological models and GRACE. J. Hydrol. 553. https://doi.org/10.1016/j.jhydrol.2017.07.048

Ferreira, V.G., Montecino, H.D.C., Yakubu, C.I., Heck, B., 2016. Uncertainties of the Gravity Recovery and Climate Experiment time-variable gravity-field solutions based on three-cornered hat method. J. Appl. Remote Sens. https://doi.org/10.1117/1.jrs.10.015015

Funk, C., Peterson, P., Landsfeld, M., Pedreros, D., Verdin, J., Shukla, S., Husak, G., Rowland, J., Harrison, L., Hoell, A., Michaelsen, J., 2015. The climate hazards infrared precipitation with stations - A new environmental record for monitoring extremes. Sci. Data 2. https://doi.org/10.1038/sdata.2015.66

Gao, H., Tang, Q.H., Ferguson, C.R., Wood, E.F., Lettenmaier, D.P., 2010. Estimating the water budget of major US river basins via remote sensing. Int. J. Remote Sens. 31. https://doi.org/10.1080/01431161.2010.483488

Gelaro, R., McCarty, W., Suárez, M.J., Todling, R., Molod, A., Takacs, L., Randles, C.A., Darmenov, A., Bosilovich, M.G., Reichle, R., Wargan, K., Coy, L., Cullather, R., Draper, C., Akella, S., Buchard, V., Conaty, A., da Silva, A.M., Gu, W., Kim, G.K., Koster, R., Lucchesi, R., Merkova, D., Nielsen, J.E., Partyka, G., Pawson, S., Putman, W., Rienecker, M., Schubert, S.D., Sienkiewicz, M., Zhao, B., 2017. The modern-era retrospective analysis for research and applications, version 2 (MERRA-2). J. Clim. 30. https://doi.org/10.1175/JCLI-D-16-0758.1

Gevaert, A.I., Veldkamp, T.I.E., Ward, P.J., 2018. The effect of climate type on timescales of drought propagation in an ensemble of global hydrological models. Hydrol. Earth Syst. Sci. https://doi.org/10.5194/hess-22-4649-2018

GoI, 2017. Ground Water Year Book India 2016-17. Central Ground Water Board, Ministry of Water Resources. Faridabad: Government of India.

Guan, K., Pan, M., Li, H., Wolf, A., Wu, J., Medvigy, D., Caylor, K.K., Sheffield, J., Wood, E.F., Malhi, Y., Liang, M., Kimball, J.S., Saleska, S.R., Berry, J., Joiner, J., Lyapustin, A.I., 2015. Photosynthetic seasonality of global tropical forests constrained by hydroclimate. Nat.

Geosci. 8. https://doi.org/10.1038/ngeo2382
Hagiwara, Y., Kuribayashi, D., Sawano, H., 2016. Enhancement of flood countermeasures of Japanese-affiliated firms based on the lessons learned from the 2011 Thai flood. J. Disaster Res. https://doi.org/10.20965/jdr.2016.p1176
Haraguchi, M., Lall, U., 2015. Flood risks and impacts: A case study of Thailand's floods in 2011 and research questions for supply chain decision making. Int. J. Disaster Risk Reduct. 14. https://doi.org/10.1016/j.ijdrr.2014.09.005
Hazra, A., Taraphdar, S., Halder, M., Pokhrel, S., Chaudhari, H.S., Salunke, K., Mukhopadhyay, P., Rao, S.A., 2013. Indian summer monsoon drought 2009: Role of aerosol and cloud microphysics. Atmos. Sci. Lett. https://doi.org/10.1002/asl2.437
Heim, R.R., 2002. A review of twentieth-century drought indices used in the United States. Bull. Am. Meteorol. Soc. https://doi.org/10.1175/1520-0477(2002)083<1149:AROTDI>2.3.CO;2
Helsel, D.R., Hirsch, R.M., 2002. Statistical Methods in Water Resources. Techniques of Water Resource Investigations. US Geol. Surv.
Hodrick, R.J., Prescott, E.C., 1997. Postwar U.S. Business Cycles: An Empirical Investigation. J. Money, Credit Bank. https://doi.org/10.2307/2953682
Hsu, K.L., Gao, X., Sorooshian, S., Gupta, H. V., 1997. Precipitation estimation from remotely sensed information using artificial neural networks. J. Appl. Meteorol. 36. https://doi.org/10.1175/1520-0450(1997)036<1176:PEFRSI>2.0.CO;2
Huang, N.E., Shen, S.S.P., 2014. Hilbert Huang Transform and Its Applications, Interdisciplinary Mathematical Sciences.
Huffman, G.J., Adler, R.F., Bolvin, D.T., Gu, G., 2009. Improving the global precipitation record: GPCP Version 2.1. Geophys. Res. Lett. https://doi.org/10.1029/2009GL040000
Huffman, G.J., Stocker, E.F., Bolvin, D.T., Nelkin, E.J., Jackson, T., 2019. GPM IMERG Final Precipitation L3 Half Hourly 0.1 degree x 0.1 degree V06, Greenbelt, MD, Goddard Earth Sciences Data and Information Services Center (GES DISC) [WWW Document]. Goddard Earth Sci. Data Inf. Serv. Cent. (GES DISC). URL 10.5067/GPM/IMERG/3B-MONTH/06 (accessed 7.15.21).
Huffman, G J, Stocker, E.F., Bolvin, D.T., Nelkin, E.J., Tan, J., 2019. GPM IMERG Final Precipitation L3 1 day 0.1 degree x 0.1 degree V06, Edited by Andrey Savtchenko, Greenbelt, MD, Goddard Earth Sciences Data and Information Services Center (GES DISC). Aaaa.
India-WRIS, 2012. River Basin Atlas of India, RRSC-West, NRSC, ISRO, Jodhpur, India [WWW Document]. Gov. India Minist. Water Resour.
Jacobi, J., Perrone, D., Duncan, L.L., Hornberger, G., 2013. A tool for calculating the palmer drought indices. Water Resour. Res. https://doi.org/10.1002/wrcr.20342
Jasechko, S., Perrone, D., 2021. Global groundwater wells at risk of running dry. Science (80-.). 372. https://doi.org/10.1126/science.abc2755
Jean, Y., Meyer, U., Jäggi, A., 2018. Combination of GRACE monthly gravity field solutions from different processing strategies. J. Geod. 92. https://doi.org/10.1007/s00190-018-1123-5
Jing, W., Zhao, X., Yao, L., Jiang, H., Xu, J., Yang, J., Li, Y., 2020. Variations in terrestrial water storage in the Lancang-Mekong river basin from GRACE solutions and land surface model. J. Hydrol. https://doi.org/10.1016/j.jhydrol.2019.124258
Kato, H., Rodell, M., Beyrich, F., Cleugh, H., van Gorsel, E., Liu, H., Meyers, T.P., 2007.

Sensitivity of land surface simulations to model physics, land characteristics, and forcings, at four CEOP sites. J. Meteorol. Soc. Japan. https://doi.org/10.2151/jmsj.85A.187

Kiguchi, M., Takata, K., Hanasaki, N., Archevarahuprok, B., Champathong, A., Ikoma, E., Jaikaeo, C., Kaewrueng, S., Kanae, S., Kazama, S., Kuraji, K., Matsumoto, K., Nakamura, S., Nguyen-Le, D., Noda, K., Piamsa-Nga, N., Raksapatcharawong, M., Rangsiwanichpong, P., Ritphring, S., Shirakawa, H., Somphong, C., Srisutham, M., Suanburi, D., Suanpaga, W., Tebakari, T., Trisurat, Y., Udo, K., Wongsa, S., Yamada, T., Yoshida, K., Kiatiwat, T., Oki, T., 2021. A review of climate-change impact and adaptation studies for the water sector in Thailand. Environ. Res. Lett. https://doi.org/10.1088/1748-9326/abce80

Kinouchi, T., Yamamoto, G., Komsai, A., Liengcharernsit, W., 2018. Quantification of seasonal precipitation over the upper Chao Phraya River Basin in the past fifty years based on monsoon and El Niño/Southern Oscillation related climate indices. Water (Switzerland). https://doi.org/10.3390/w10060800

Klees, R., Zapreeva, E.A., Winsemius, H.C., Savenije, H.H.G., 2007. The bias in GRACE estimates of continental water storage variations. Hydrol. Earth Syst. Sci. 11. https://doi.org/10.5194/hess-11-1227-2007

Komolafe, A.A., Herath, S., Avtar, R., 2019. Establishment of detailed loss functions for the urban flood risk assessment in Chao Phraya River basin, Thailand. Geomatics, Nat. Hazards Risk. https://doi.org/10.1080/19475705.2018.1539038

Komori, D., Nakamura, S., Kiguchi, M., Nishijima, A., Yamazaki, D., Suzuki, S., Kawasaki, A., Oki, K., Oki, T., 2012. Characteristics of the 2011 Chao Phraya River flood in Central Thailand. Hydrol. Res. Lett. 6. https://doi.org/10.3178/hrl.6.41

Kompor, W., Yoshikawa, S., Kanae, S., 2020. Use of seasonal streamflow forecasts for flood mitigation with adaptive reservoir operation: A case study of the Chao Phraya river basin, Thailand, in 2011. Water (Switzerland) 12. https://doi.org/10.3390/w12113210

Koot, L., de Viron, O., Dehant, V., 2006. Atmospheric angular momentum Time-series: Characterization of their internal noise and creation of a combined series. J. Geod. https://doi.org/10.1007/s00190-005-0019-3

Kumar, R., Singh, R.D., Sharma, K.D., 2005. Water resources of India. Curr. Sci. https://doi.org/10.1002/047147844x.wr243

Kummerow, C., Simpson, J., Thiele, O., Barnes, W., Chang, A.T.C., Stocker, E., Adler, R.F., Hou, A., Kakar, R., Wentz, F., Ashcroft, P., Kozu, T., Hong, Y., Okamoto, K., Iguchi, T., Kuroiwa, H., Im, E., Haddad, Z., Huffman, G., Ferrier, B., Olson, W.S., Zipser, E., Smith, E.A., Wilheit, T.T., North, G., Krishnamurti, T., Nakamura, K., 2000. The status of the tropical rainfall measuring mission (TRMM) after two years in orbit. J. Appl. Meteorol. https://doi.org/10.1175/1520-0450(2001)040<1965:tsottr>2.0.co;2

Landerer, F.W., Flechtner, F.M., Save, H., Webb, F.H., Bandikova, T., Bertiger, W.I., Bettadpur, S. V., Byun, S.H., Dahle, C., Dobslaw, H., Fahnestock, E., Harvey, N., Kang, Z., Kruizinga, G.L.H., Loomis, B.D., McCullough, C., Murböck, M., Nagel, P., Paik, M., Pie, N., Poole, S., Strekalov, D., Tamisiea, M.E., Wang, F., Watkins, M.M., Wen, H.Y., Wiese, D.N., Yuan, D.N., 2020. Extending the Global Mass Change Data Record: GRACE Follow-On Instrument and Science Data Performance. Geophys. Res. Lett. 47. https://doi.org/10.1029/2020GL088306

Landerer, F.W., Swenson, S.C., 2012. Accuracy of scaled GRACE terrestrial water storage estimates. Water Resour. Res. https://doi.org/10.1029/2011WR011453

Li, B., Rodell, M., 2015. Evaluation of a model-based groundwater drought indicator in the conterminous U.S. J. Hydrol. https://doi.org/10.1016/j.jhydrol.2014.09.027

Li, B., Rodell, M., Kumar, S., Beaudoing, H.K., Getirana, A., Zaitchik, B.F., de Goncalves, L.G., Cossetin, C., Bhanja, S., Mukherjee, A., Tian, S., Tangdamrongsub, N., Long, D., Nanteza, J., Lee, J., Policelli, F., Goni, I.B., Daira, D., Bila, M., de Lannoy, G., Mocko, D., Steele-Dunne, S.C., Save, H., Bettadpur, S., 2019. Global GRACE Data Assimilation for Groundwater and Drought Monitoring: Advances and Challenges. Water Resour. Res. https://doi.org/10.1029/2018WR024618

Liu, X., Feng, X., Ciais, P., Fu, B., Hu, B., Sun, Z., 2020. GRACE satellite-based drought index indicating increased impact of drought over major basins in China during 2002–2017. Agric. For. Meteorol. https://doi.org/10.1016/j.agrformet.2020.108057

Long, D., Chen, X., Scanlon, B.R., Wada, Y., Hong, Y., Singh, V.P., Chen, Y., Wang, C., Han, Z., Yang, W., 2016a. Have GRACE satellites overestimated groundwater depletion in the Northwest India Aquifer? Sci. Rep. https://doi.org/10.1038/srep24398

Long, D., Chen, X., Scanlon, B.R., Wada, Y., Hong, Y., Singh, V.P., Chen, Y., Wang, C., Han, Z., Yang, W., 2016b. Have GRACE satellites overestimated groundwater depletion in the Northwest India Aquifer? Sci. Rep. https://doi.org/10.1038/srep24398

Long, D., Longuevergne, L., Scanlon, B.R., 2014a. Uncertainty in evapotranspiration from land surface modeling, remote sensing, and GRACE satellites. Water Resour. Res. https://doi.org/10.1002/2013WR014581

Long, D., Shen, Y., Sun, A., Hong, Y., Longuevergne, L., Yang, Y., Li, B., Chen, L., 2014b. Drought and flood monitoring for a large karst plateau in Southwest China using extended GRACE data. Remote Sens. Environ. https://doi.org/10.1016/j.rse.2014.08.006

Long, D., Yang, Y., Wada, Y., Hong, Y., Liang, W., Chen, Y., Yong, B., Hou, A., Wei, J., Chen, L., 2015. Deriving scaling factors using a global hydrological model to restore GRACE total water storage changes for China's Yangtze River Basin. Remote Sens. Environ. https://doi.org/10.1016/j.rse.2015.07.003

Longuevergne, L., Scanlon, B.R., Wilson, C.R., 2010. GRACE hydrological estimates for small basins: Evaluating processing approaches on the High Plains aquifer, USA. Water Resour. Res. 46. https://doi.org/10.1029/2009WR008564

Loomis, B.D., Luthcke, S.B., Sabaka, T.J., 2019. Regularization and error characterization of GRACE mascons. J. Geod. 93. https://doi.org/10.1007/s00190-019-01252-y

López, P.L., Sutanudjaja, E.H., Schellekens, J., Sterk, G., Bierkens, M.F.P., 2017. Calibration of a large-scale hydrological model using satellite-based soil moisture and evapotranspiration products. Hydrol. Earth Syst. Sci. https://doi.org/10.5194/hess-21-3125-2017

Maier, H.R., Kapelan, Z., Kasprzyk, J., Kollat, J., Matott, L.S., Cunha, M.C., Dandy, G.C., Gibbs, M.S., Keedwell, E., Marchi, A., Ostfeld, A., Savic, D., Solomatine, D.P., Vrugt, J.A., Zecchin, A.C., Minsker, B.S., Barbour, E.J., Kuczera, G., Pasha, F., Castelletti, A., Giuliani, M., Reed, P.M., 2014. Evolutionary algorithms and other metaheuristics in water resources: Current status, research challenges and future directions. Environ. Model. Softw. 62. https://doi.org/10.1016/j.envsoft.2014.09.013

Mallya, G., Mishra, V., Niyogi, D., Tripathi, S., Govindaraju, R.S., 2015. Trends and variability of droughts over the Indian monsoon region. Weather Clim. Extrem. https://doi.org/10.1016/j.wace.2016.01.002

Martens, B., Miralles, D.G., Lievens, H., Van Der Schalie, R., De Jeu, R.A.M., Fernández-Prieto, D., Beck, H.E., Dorigo, W.A., Verhoest, N.E.C., 2017. GLEAM v3: Satellite-based land evaporation and root-zone soil moisture. Geosci. Model Dev. 10. https://doi.org/10.5194/gmd-10-1903-2017

Mckee, T.B., Doesken, N.J., Kleist, J., 1993. The relationship of drought frequency and duration to time scales. [WWW Document]. Eighth Conf. Appl. Climatol.

Meyer, U., Jaeggi, A., Dahle, Christoph; Flechtner, F., Kvas, Andreas; Behzadpour, Saniya; Mayer-Gürr, Torsten; Lemoine, Jean-Michel; Bourgogne, S., 2020a. International Combination Service for Time-variable Gravity Fields (COST-G) Monthly GRACE Series. V. 01. GFZ Data Services. https://doi.org/https://doi.org/10.5880/ICGEM.COST-G.001

Meyer, U., Lasser, M., Jaeggi, A., Dahle, Christoph; Flechtner, F., Kvas, Andreas; Behzadpour, Saniya; Mayer-Gürr, Torsten; Lemoine, Jean-Michel; Koch, I., Flury, Jakob; Bourgogne, S., 2020b. International Combination Service for Time-variable Gravity Fields (COST-G) Monthly GRACE-FO Series. V. 01. GFZ Data Services. [WWW Document]. https://doi.org/https://doi.org/10.5880/ICGEM.COST-G.002

Miralles, D.G., De Jeu, R.A.M., Gash, J.H., Holmes, T.R.H., Dolman, A.J., 2011. Magnitude and variability of land evaporation and its components at the global scale. Hydrol. Earth Syst. Sci. 15. https://doi.org/10.5194/hess-15-967-2011

Mishra, A.K., Singh, V.P., 2010. A review of drought concepts. J. Hydrol. https://doi.org/10.1016/j.jhydrol.2010.07.012

Mishra, A.K., Singh, V.P., 2009. Analysis of drought severity-area-frequency curves using a general circulation model and scenario uncertainty. J. Geophys. Res. Atmos. https://doi.org/10.1029/2008JD010986

Mishra, A.K., Singh, V.P., Desai, V.R., 2009. Drought characterization: A probabilistic approach. Stoch. Environ. Res. Risk Assess. https://doi.org/10.1007/s00477-007-0194-2

Molle, F., 2007. Scales and power in river basin management: The Chao Phraya River in Thailand. Geogr. J. 173. https://doi.org/10.1111/j.1475-4959.2007.00255.x

Müller Schmied, H., Caceres, D., Eisner, S., Flörke, M., Herbert, C., Niemann, C., Asali Peiris, T., Popat, E., Theodor Portmann, F., Reinecke, R., Schumacher, M., Shadkam, S., Telteu, C.E., Trautmann, T., Döll, P., 2021. The global water resources and use model WaterGAP v2.2d: Model description and evaluation. Geosci. Model Dev. 14. https://doi.org/10.5194/gmd-14-1037-2021

Ndehedehe, C., Awange, J., Agutu, N., Kuhn, M., Heck, B., 2016. Understanding changes in terrestrial water storage over West Africa between 2002 and 2014. Adv. Water Resour. https://doi.org/10.1016/j.advwatres.2015.12.009

Niemeyer, S., 2008. New drought indices. Options Méditerranéennes. https://doi.org/10.1017/CBO9781107415324.004

Nourani, V., 2017. An Emotional ANN (EANN) approach to modeling rainfall-runoff process. J. Hydrol. https://doi.org/10.1016/j.jhydrol.2016.11.033

NSIT, 2007. NASA Earth Science Implementation Plan for Energy and Water Cycle Research Predicting Energy and Water Cycle Consequences of Earth System Variability and Change. NASA energy water cycle study Sci. Integr. team 89. https://doi.org/http://news.cisc.gmu.edu/doc/NEWS_implementation.pdf

Oki, T., Kanae, S., 2006. Global hydrological cycles and world water resources. Science (80-.).

313, 1068–1072. https://doi.org/10.1126/science.1128845
Pai, D.S., Sridhar, L., Rajeevan, M., Sreejith, O.P., Satbhai, N.S., Mukhopadhyay, B., 2014. Development of a new high spatial resolution (0.25° × 0.25°) long period (1901-2010) daily gridded rainfall data set over India and its comparison with existing data sets over the region. Mausam 65.
Pan, M., Fisher, C.K., Chaney, N.W., Zhan, W., Crow, W.T., Aires, F., Entekhabi, D., Wood, E.F., 2015. Triple collocation: Beyond three estimates and separation of structural/non-structural errors. Remote Sens. Environ. 171. https://doi.org/10.1016/j.rse.2015.10.028
Pan, M., Sahoo, A.K., Troy, T.J., Vinukollu, R.K., Sheffield, J., Wood, A.E.F., 2012. Multisource estimation of long-term terrestrial water budget for major global river basins. J. Clim. 25. https://doi.org/10.1175/JCLI-D-11-00300.1
Pan, M., Wood, E.F., 2006. Data assimilation for estimating the terrestrial water budget using a constrained ensemble Kalman filter. J. Hydrometeorol. 7. https://doi.org/10.1175/JHM495.1
Panda, D.K., Wahr, J., 2016. Spatiotemporal evolution of water storage changes in India from the updated GRACE-derived gravity records. Water Resour. Res. https://doi.org/10.1002/2015WR017797
Panday, P.K., Coe, M.T., Macedo, M.N., Lefebvre, P., Castanho, A.D. d. A., 2015. Deforestation offsets water balance changes due to climate variability in the Xingu River in eastern Amazonia. J. Hydrol. 523. https://doi.org/10.1016/j.jhydrol.2015.02.018
Papa, F., Frappart, F., Malbeteau, Y., Shamsudduha, M., Vuruputur, V., Sekhar, M., Ramillien, G., Prigent, C., Aires, F., Pandey, R.K., Bala, S., Calmant, S., 2015. Satellite-derived surface and sub-surface water storage in the Ganges-Brahmaputra River Basin. J. Hydrol. Reg. Stud. https://doi.org/10.1016/j.ejrh.2015.03.004
Pascolini-Campbell, M., Reager, J.T., Chandanpurkar, H.A., Rodell, M., 2021. A 10 per cent increase in global land evapotranspiration from 2003 to 2019. Nature 593. https://doi.org/10.1038/s41586-021-03503-5
Pascolini-Campbell, M.A., Reager, J.T., Fisher, J.B., 2020. GRACE-based Mass Conservation as a Validation Target for Basin-Scale Evapotranspiration in the Contiguous United States. Water Resour. Res. 56. https://doi.org/10.1029/2019WR026594
Penatti, N.C., Almeida, T.I.R. de, Ferreira, L.G., Arantes, A.E., Coe, M.T., 2015. Satellite-based hydrological dynamics of the world's largest continuous wetland. Remote Sens. Environ. 170. https://doi.org/10.1016/j.rse.2015.08.031
Promchote, P., Wang, S.Y.S., Johnson, P.G., 2016. The 2011 great flood in Thailand: Climate diagnostics and implications from climate change. J. Clim. 29. https://doi.org/10.1175/JCLI-D-15-0310.1
Rakwatin, P., Sansena, T., Marjang, N., Rungsipanich, A., 2013. Using multi-temporal remote-sensing data to estimate 2011 flood area and volume over Chao Phraya River basin, Thailand. Remote Sens. Lett. 4. https://doi.org/10.1080/2150704X.2012.723833
Ramillien, G., Famiglietti, J.S., Wahr, J., 2008. Detection of continental hydrology and glaciology Signals from GRACE: A review. Surv. Geophys. https://doi.org/10.1007/s10712-008-9048-9
Ravn, M.O., Uhlig, H., 2002. On adjusting the Hodrick-Prescott filter for the frequency of observations. Rev. Econ. Stat. https://doi.org/10.1162/003465302317411604
Reager, J.T., Famiglietti, J.S., 2009. Global terrestrial water storage capacity and flood potential using GRACE. Geophys. Res. Lett. https://doi.org/10.1029/2009GL040826

Reichle, R.H., Draper, C.S., Liu, Q., Girotto, M., Mahanama, S.P.P., Koster, R.D., De Lannoy, G.J.M., 2017. Assessment of MERRA-2 land surface hydrology estimates. J. Clim. 30. https://doi.org/10.1175/JCLI-D-16-0720.1

Richard Peltier, W., Argus, D.F., Drummond, R., 2018. Comment on "An Assessment of the ICE-6G_C (VM5a) Glacial Isostatic Adjustment Model" by Purcell et al. J. Geophys. Res. Solid Earth. https://doi.org/10.1002/2016JB013844

Richey, A.S., Thomas, B.F., Lo, M.H., Reager, J.T., Famiglietti, J.S., Voss, K., Swenson, S., Rodell, M., 2015. Quantifying renewable groundwater stress with GRACE. Water Resour. Res. https://doi.org/10.1002/2015WR017349

Richter, H.M.P., Lück, C., Klos, A., Sideris, M.G., Rangelova, E., Kusche, J., 2021. Reconstructing GRACE-type time-variable gravity from the Swarm satellites. Sci. Rep. 11. https://doi.org/10.1038/s41598-020-80752-w

Rodell, M., Beaudoing, H.K., L'Ecuyer, T.S., Olson, W.S., Famiglietti, J.S., Houser, P.R., Adler, R., Bosilovich, M.G., Clayson, C.A., Chambers, D., Clark, E., Fetzer, E.J., Gao, X., Gu, G., Hilburn, K., Huffman, G.J., Lettenmaier, D.P., Liu, W.T., Robertson, F.R., Schlosser, C.A., Sheffield, J., Wood, E.F., 2015. The observed state of the water cycle in the early twenty-first century. J. Clim. 28. https://doi.org/10.1175/JCLI-D-14-00555.1

Rodell, M., Chen, J., Kato, H., Famiglietti, J.S., Nigro, J., Wilson, C.R., 2007. Estimating groundwater storage changes in the Mississippi River basin (USA) using GRACE. Hydrogeol. J. https://doi.org/10.1007/s10040-006-0103-7

Rodell, M., Famiglietti, J.S., Wiese, D.N., Reager, J.T., Beaudoing, H.K., Landerer, F.W., Lo, M.H., 2018. Emerging trends in global freshwater availability. Nature. https://doi.org/10.1038/s41586-018-0123-1

Rodell, M., Houser, P.R., Jambor, U., Gottschalck, J., Mitchell, K., Meng, C.J., Arsenault, K., Cosgrove, B., Radakovich, J., Bosilovich, M., Entin, J.K., Walker, J.P., Lohmann, D., Toll, D., 2004. The Global Land Data Assimilation System. Bull. Am. Meteorol. Soc. 85. https://doi.org/10.1175/BAMS-85-3-381

Rodell, M., Velicogna, I., Famiglietti, J.S., 2009. Satellite-based estimates of groundwater depletion in India. Nature. https://doi.org/10.1038/nature08238

Rosenzweig, C., Karoly, D., Vicarelli, M., Neofotis, P., Wu, Q., Casassa, G., Menzel, A., Root, T.L., Estrella, N., Seguin, B., Tryjanowski, P., Liu, C., Rawlins, S., Imeson, A., 2008. Attributing physical and biological impacts to anthropogenic climate change. Nature 453. https://doi.org/10.1038/nature06937

Sahoo, A.K., Pan, M., Troy, T.J., Vinukollu, R.K., Sheffield, J., Wood, E.F., 2011. Reconciling the global terrestrial water budget using satellite remote sensing. Remote Sens. Environ. 115. https://doi.org/10.1016/j.rse.2011.03.009

Sakumura, C., 2013. An ensemble solution for the Earth's time-varying gravitational field from the NASA/DLR GRACE mission, MSE Thesis, University of Texas at Austin.

Sakumura, C., Bettadpur, S., Bruinsma, S., 2014. Ensemble prediction and intercomparison analysis of GRACE time-variable gravity field models. Geophys. Res. Lett. https://doi.org/10.1002/2013GL058632

Samra, J.S., 2004. Review and Analysis of Drought Monitoring, Declaration and Management in India [WWW Document]. URL https://www.preventionweb.net/files/1868_VL102135.pdf

Satish Kumar, K., Venkata Rathnam, E., Sridhar, V., 2020. Tracking seasonal and monthly

drought with GRACE-based terrestrial water storage assessments over major river basins in South India. Sci. Total Environ. https://doi.org/10.1016/j.scitotenv.2020.142994

Save, H., 2020. CSR GRACE and GRACE-FO RL06 Mascon Solutions v02. https://doi.org/doi: 10.15781/cgq9-nh24

Save, H., Bettadpur, S., Tapley, B.D., 2016. High-resolution CSR GRACE RL05 mascons. J. Geophys. Res. Solid Earth. https://doi.org/10.1002/2016JB013007

Sayama, T., Tatebe, Y., Iwami, Y., Tanaka, S., 2015. Hydrologic sensitivity of flood runoff and inundation: 2011 Thailand floods in the Chao Phraya River basin. Nat. Hazards Earth Syst. Sci. 15. https://doi.org/10.5194/nhess-15-1617-2015

Sayama, T., Tatebe, Y., Tanaka, S., 2017. An emergency response-type rainfall-runoff-inundation simulation for 2011 Thailand floods. J. Flood Risk Manag. https://doi.org/10.1111/jfr3.12147

Scanlon, Bridget R., Faunt, C.C., Longuevergne, L., Reedy, R.C., Alley, W.M., McGuire, V.L., McMahon, P.B., 2012. Groundwater depletion and sustainability of irrigation in the US High Plains and Central Valley. Proc. Natl. Acad. Sci. U. S. A. https://doi.org/10.1073/pnas.1200311109

Scanlon, B. R., Longuevergne, L., Long, D., 2012. Ground referencing GRACE satellite estimates of groundwater storage changes in the California Central Valley, USA. Water Resour. Res. https://doi.org/10.1029/2011WR011312

Scanlon, B.R., Zhang, Z., Reedy, R.C., Pool, D.R., Save, H., Long, D., Chen, J., Wolock, D.M., Conway, B.D., Winester, D., 2015. Hydrologic implications of GRACE satellite data in the Colorado River Basin. Water Resour. Res. https://doi.org/10.1002/2015WR018090

Scanlon, B.R., Zhang, Z., Save, H., Sun, A.Y., Schmied, H.M., Van Beek, L.P.H., Wiese, D.N., Wada, Y., Long, D., Reedy, R.C., Longuevergne, L., Döll, P., Bierkens, M.F.P., 2018. Global models underestimate large decadal declining and rising water storage trends relative to GRACE satellite data. Proc. Natl. Acad. Sci. U. S. A. https://doi.org/10.1073/pnas.1704665115

Scanlon, B.R., Zhang, Z., Save, H., Wiese, D.N., Landerer, F.W., Long, D., Longuevergne, L., Chen, J., 2016. Global evaluation of new GRACE mascon products for hydrologic applications. Water Resour. Res. https://doi.org/10.1002/2016WR019494

Schewe, J., Heinke, J., Gerten, D., Haddeland, I., Arnell, N.W., Clark, D.B., Dankers, R., Eisner, S., Fekete, B.M., Colón-González, F.J., Gosling, S.N., Kim, H., Liu, X., Masaki, Y., Portmann, F.T., Satoh, Y., Stacke, T., Tang, Q., Wada, Y., Wisser, D., Albrecht, T., Frieler, K., Piontek, F., Warszawski, L., Kabat, P., 2014. Multimodel assessment of water scarcity under climate change. Proc. Natl. Acad. Sci. U. S. A. https://doi.org/10.1073/pnas.1222460110

Schreiner-McGraw, A.P., Ajami, H., 2021. Delayed response of groundwater to multi-year meteorological droughts in the absence of anthropogenic management. J. Hydrol. 603. https://doi.org/10.1016/j.jhydrol.2021.126917

Seyoum, W.M., Milewski, A.M., 2017. Improved methods for estimating local terrestrial water dynamics from GRACE in the Northern High Plains. Adv. Water Resour. https://doi.org/10.1016/j.advwatres.2017.10.021

Shah, T., 2009. Climate change and groundwater: India's opportunities for mitigation and adaptation. Environ. Res. Lett. https://doi.org/10.1088/1748-9326/4/3/035005

Shamsudduha, M., Taylor, R.G., Longuevergne, L., 2012. Monitoring groundwater storage changes in the highly seasonal humid tropics: Validation of GRACE measurements in the

Bengal Basin. Water Resour. Res. https://doi.org/10.1029/2011WR010993
Sharma, A., Goyal, M.K., 2018. Assessment of ecosystem resilience to hydroclimatic disturbances in India. Glob. Chang. Biol. https://doi.org/10.1111/gcb.13874
Sheffield, J., Ferguson, C.R., Troy, T.J., Wood, E.F., McCabe, M.F., 2009. Closing the terrestrial water budget from satellite remote sensing. Geophys. Res. Lett. 36. https://doi.org/10.1029/2009GL037338
Shiklomanov, A.I., Yakovleva, T.I., Lammers, R.B., Karasev, I.P., Vörösmarty, C.J., Linder, E., 2006. Cold region river discharge uncertainty-estimates from large Russian rivers. J. Hydrol. 326. https://doi.org/10.1016/j.jhydrol.2005.10.037
Shu, C., Ouarda, T.B.M.J., 2007. Flood frequency analysis at ungauged sites using artificial neural networks in canonical correlation analysis physiographic space. Water Resour. Res. https://doi.org/10.1029/2006WR005142
Shukla, S., Wood, A.W., 2008. Use of a standardized runoff index for characterizing hydrologic drought. Geophys. Res. Lett. 35. https://doi.org/10.1029/2007GL032487
Siebert, S., Burke, J., Faures, J.M., Frenken, K., Hoogeveen, J., Döll, P., Portmann, F.T., 2010. Groundwater use for irrigation - A global inventory. Hydrol. Earth Syst. Sci. https://doi.org/10.5194/hess-14-1863-2010
Sinha, D., Syed, T.H., Famiglietti, J.S., Reager, J.T., Thomas, R.C., 2017. Characterizing drought in India using GRACE observations of terrestrial water storage deficit. J. Hydrometeorol. https://doi.org/10.1175/JHM-D-16-0047.1
Sperna Weiland, F.C., Vrugt, J.A., van Beek, R.L.P.H., Weerts, A.H., Bierkens, M.F.P., 2015. Significant uncertainty in global scale hydrological modeling from precipitation data errors. J. Hydrol. https://doi.org/10.1016/j.jhydrol.2015.08.061
Strassberg, G., Scanlon, B.R., Rodell, M., 2007. Comparison of seasonal terrestrial water storage variations from GRACE with groundwater-level measurements from the High Plains Aquifer (USA). Geophys. Res. Lett. https://doi.org/10.1029/2007GL030139
Suhag, R., 2016. Overview of Groundwater in India.
Sun, Q., Miao, C., Duan, Q., Ashouri, H., Sorooshian, S., Hsu, K.L., 2018. A Review of Global Precipitation Data Sets: Data Sources, Estimation, and Intercomparisons. Rev. Geophys. 56. https://doi.org/10.1002/2017RG000574
Sun, A.Y., 2013. Predicting groundwater level changes using GRACE data. Water Resour. Res. https://doi.org/10.1002/wrcr.20421
Sun, Z., Zhu, X., Pan, Y., Zhang, J., Liu, X., 2018. Drought evaluation using the GRACE terrestrial water storage deficit over the Yangtze River Basin, China. Sci. Total Environ. https://doi.org/10.1016/j.scitotenv.2018.03.292
Supharatid, S., 2015. Skill of precipitation projectionin the Chao Phraya river Basinby multi-model ensemble CMIP3-CMIP5. Weather Clim. Extrem. 12. https://doi.org/10.1016/j.wace.2016.03.001
Sutanudjaja, E.H., Van Beek, L.P.H., De Jong, S.M., Van Geer, F.C., Bierkens, M.F.P., 2014. Calibrating a large-extent high-resolution coupled groundwater-land surface model using soil moisture and discharge data. Water Resour. Res. https://doi.org/10.1002/2013WR013807
Sutanudjaja, E.H., Van Beek, R., Wanders, N., Wada, Y., Bosmans, J.H.C., Drost, N., Van Der Ent, R.J., De Graaf, I.E.M., Hoch, J.M., De Jong, K., Karssenberg, D., López López, P., Peßenteiner, S., Schmitz, O., Straatsma, M.W., Vannametee, E., Wisser, D., Bierkens,

M.F.P., 2018. PCR-GLOBWB 2: A 5 arcmin global hydrological and water resources model. Geosci. Model Dev. https://doi.org/10.5194/gmd-11-2429-2018

Swenson, S., Wahr, J., 2006. Post-processing removal of correlated errors in GRACE data. Geophys. Res. Lett. https://doi.org/10.1029/2005GL025285

Szeto, K.K., Tran, H., MacKay, M.D., Crawford, R., Stewart, R.E., 2008. The MAGS water and energy budget study. J. Hydrometeorol. 9. https://doi.org/10.1175/2007JHM810.1

Tang, Q., Gao, H., Yeh, P., Oki, T., Su, F., Lettenmaier, D.P., 2010. Dynamics of terrestrial water storage change from satellite and surface observations and modeling. J. Hydrometeorol. 11. https://doi.org/10.1175/2009JHM1152.1

Tangang, F., Chung, J.X., Juneng, L., Supari, Salimun, E., Ngai, S.T., Jamaluddin, A.F., Mohd, M.S.F., Cruz, F., Narisma, G., Santisirisomboon, J., Ngo-Duc, T., Van Tan, P., Singhruck, P., Gunawan, D., Aldrian, E., Sopaheluwakan, A., Grigory, N., Remedio, A.R.C., Sein, D. V., Hein-Griggs, D., McGregor, J.L., Yang, H., Sasaki, H., Kumar, P., 2020. Projected future changes in rainfall in Southeast Asia based on CORDEX–SEA multi-model simulations. Clim. Dyn. 55. https://doi.org/10.1007/s00382-020-05322-2

Tangdamrongsub, N., Steele-Dunne, S.C., Gunter, B.C., Ditmar, P.G., Sutanudjaja, E.H., Sun, Y., Xia, T., Wang, Z., 2017. Improving estimates of water resources in a semi-arid region by assimilating GRACE data into the PCR-GLOBWB hydrological model. Hydrol. Earth Syst. Sci. https://doi.org/10.5194/hess-21-2053-2017

Tapley, B.D., Bettadpur, S., Ries, J.C., Thompson, P.F., Watkins, M.M., 2004. GRACE measurements of mass variability in the Earth system. Science (80-.). https://doi.org/10.1126/science.1099192

Tapley, B.D., Watkins, M.M., Flechtner, F., Reigber, C., Bettadpur, S., Rodell, M., Sasgen, I., Famiglietti, J.S., Landerer, F.W., Chambers, D.P., Reager, J.T., Gardner, A.S., Save, H., Ivins, E.R., Swenson, S.C., Boening, C., Dahle, C., Wiese, D.N., Dobslaw, H., Tamisiea, M.E., Velicogna, I., 2019. Contributions of GRACE to understanding climate change. Nat. Clim. Chang. https://doi.org/10.1038/s41558-019-0456-2

Tau Chia, C., Yasuhiro, M., Hiroaki, I., 2015. Simulation of Modeling Approach for Flood Condition and Proposed Flood Protection at Midstream of Chao Phraya River Basin, Thailand. Am. J. Environ. Prot. https://doi.org/10.12691/env-3-3-4

Taylor, R.G., Scanlon, B., Döll, P., Rodell, M., Van Beek, R., Wada, Y., Longuevergne, L., Leblanc, M., Famiglietti, J.S., Edmunds, M., Konikow, L., Green, T.R., Chen, J., Taniguchi, M., Bierkens, M.F.P., Macdonald, A., Fan, Y., Maxwell, R.M., Yechieli, Y., Gurdak, J.J., Allen, D.M., Shamsudduha, M., Hiscock, K., Yeh, P.J.F., Holman, I., Treidel, H., 2013. Ground water and climate change. Nat. Clim. Chang. https://doi.org/10.1038/nclimate1744

Telteu, C.E., Müller Schmied, H., Thiery, W., Leng, G., Burek, P., Liu, X., Boulange, J.E.S., Andersen, L.S., Grillakis, M., Gosling, S.N., Satoh, Y., Rakovec, O., Stacke, T., Chang, J., Wanders, N., Shah, H.L., Trautmann, T., Mao, G., Hanasaki, N., Koutroulis, A., Pokhrel, Y., Samaniego, L., Wada, Y., Mishra, V., Liu, J., Döll, P., Zhao, F., Gädeke, A., Rabin, S.S., Herz, F., 2021. Understanding each other's models An introduction and a standard representation of 16 global water models to support intercomparison, improvement, and communication. Geosci. Model Dev. https://doi.org/10.5194/gmd-14-3843-2021

Thomas, A.C., Reager, J.T., Famiglietti, J.S., Rodell, M., 2014. A GRACE-based water storage deficit approach for hydrological drought characterization. Geophys. Res. Lett.

https://doi.org/10.1002/2014GL059323
Thomas, B.F., Famiglietti, J.S., Landerer, F.W., Wiese, D.N., Molotch, N.P., Argus, D.F., 2017. GRACE Groundwater Drought Index: Evaluation of California Central Valley groundwater drought. Remote Sens. Environ. https://doi.org/10.1016/j.rse.2017.06.026
Tiwari, V.M., Wahr, J., Swenson, S., 2009. Dwindling groundwater resources in northern India, from satellite gravity observations. Geophys. Res. Lett. https://doi.org/10.1029/2009GL039401
Tongal, H., Booij, M.J., 2018. Simulation and forecasting of streamflows using machine learning models coupled with base flow separation. J. Hydrol. https://doi.org/10.1016/j.jhydrol.2018.07.004
Trenberth, K.E., Dai, A., Van Der Schrier, G., Jones, P.D., Barichivich, J., Briffa, K.R., Sheffield, J., 2014. Global warming and changes in drought. Nat. Clim. Chang. https://doi.org/10.1038/nclimate2067
Tripathi, P., Rabara, R.C., Shulaev, V., Shen, Q.J., Rushton, P.J., 2015. Understanding water-stress responses in soybean using hydroponics system—A systems biology perspective. Front. Plant Sci. https://doi.org/10.3389/fpls.2015.01145
Turral, H., Burke, J., Faurès, J.-M., 2008. FAO Water Report 36 : Climate change, water and food security.
Velicogna, I., Mohajerani, Y., Geruo, A., Landerer, F., Mouginot, J., Noel, B., Rignot, E., Sutterley, T., van den Broeke, M., van Wessem, M., Wiese, D., 2020. Continuity of Ice Sheet Mass Loss in Greenland and Antarctica From the GRACE and GRACE Follow-On Missions. Geophys. Res. Lett. 47. https://doi.org/10.1029/2020GL087291
Vishwakarma, B.D., Devaraju, B., Sneeuw, N., 2018. What is the spatial resolution of GRACE satellite products for hydrology? Remote Sens. 10. https://doi.org/10.3390/rs10060852
Vishwakarma, B.D., Horwath, M., Devaraju, B., Groh, A., Sneeuw, N., 2017. A Data-Driven Approach for Repairing the Hydrological Catchment Signal Damage Due to Filtering of GRACE Products. Water Resour. Res. 53. https://doi.org/10.1002/2017WR021150
Vörösmarty, C.J., McIntyre, P.B., Gessner, M.O., Dudgeon, D., Prusevich, A., Green, P., Glidden, S., Bunn, S.E., Sullivan, C.A., Liermann, C.R., Davies, P.M., 2010. Global threats to human water security and river biodiversity. Nature. https://doi.org/10.1038/nature09440
Voss, K.A., Famiglietti, J.S., Lo, M., De Linage, C., Rodell, M., Swenson, S.C., 2013. Groundwater depletion in the Middle East from GRACE with implications for transboundary water management in the Tigris-Euphrates-Western Iran region. Water Resour. Res. https://doi.org/10.1002/wrcr.20078
Wada, Y., Van Beek, L.P.H., Viviroli, D., Drr, H.H., Weingartner, R., Bierkens, M.F.P., 2011. Global monthly water stress: 2. Water demand and severity of water stress. Water Resour. Res. https://doi.org/10.1029/2010WR009792
Wada, Y., Wisser, D., Bierkens, M.F.P., 2014. Global modeling of withdrawal, allocation and consumptive use of surface water and groundwater resources. Earth Syst. Dyn. https://doi.org/10.5194/esd-5-15-2014
Wang, J., Jiang, D., Huang, Y., Wang, H., 2014. Drought analysis of the Haihe river basin based on GRACE terrestrial water storage. Sci. World J. https://doi.org/10.1155/2014/578372
Wang, Q., Zheng, W., Yin, W., Kang, G., Zhang, G., Zhang, D., 2021. Improving the accuracy of water storage anomaly trends based on a new statistical correction hydrological model

weighting method. Remote Sens. 13. https://doi.org/10.3390/rs13183583
Wang, S., Huang, J., Li, J., Rivera, A., McKenney, D.W., Sheffield, J., 2014. Assessment of water budget for sixteen large drainage basins in Canada. J. Hydrol. 512. https://doi.org/10.1016/j.jhydrol.2014.02.058
Watkins, M.M., Wiese, D.N., Yuan, D.N., Boening, C., Landerer, F.W., 2015. Improved methods for observing Earth's time variable mass distribution with GRACE using spherical cap mascons. J. Geophys. Res. Solid Earth. https://doi.org/10.1002/2014JB011547
Webster, P.J., Magaña, V.O., Palmer, T.N., Shukla, J., Tomas, R.A., Yanai, M., Yasunari, T., 1998. Monsoons: Processes, predictability, and the prospects for prediction. J. Geophys. Res. Ocean. https://doi.org/10.1029/97jc02719
Westfall, P.H., 2014. Kurtosis as Peakedness, 1905–2014. R.I.P. Am. Stat. https://doi.org/10.1080/00031305.2014.917055
Weedon, G.P., Gomes, S., Viterbo, P., Shuttleworth, W.J., Blyth, E., Österle, H. , Adam, J.C., Bellouin, N., Boucher, O. & Best, M. (2011). Creation of the WATCH Forcing Data and Its Use to Assess Global and Regional Reference Crop Evaporation over Land during the Twentieth Century. Journal of Hydrometeorology: Vol 12, No 5. https://doi.org/10.1175/2011JHM1369.1
Wheeler, T., Von Braun, J., 2013. Climate change impacts on global food security. Science (80-.). https://doi.org/10.1126/science.1239402
Wiese, D.N., Yuan, D.-N., Boening, C., Landerer, F.W., Watkins, M.M., 2018. JPL GRACE Mascon Ocean, Ice, and Hydrology Equivalent Water Height Release 06 Coastal Resolution Improvement (CRI) Filtered Version 1.0. Ver. 1.0. PO.DAAC, CA, USA [WWW Document]. https://doi.org/http://dx.doi.org/10.5067/TEMSC-3MJC6
Wilhite, D.A., Svoboda, M.D., Hayes, M.J., 2007. Understanding the complex impacts of drought: A key to enhancing drought mitigation and preparedness. Water Resour. Manag. https://doi.org/10.1007/s11269-006-9076-5
WMO, W.M.O., 2012. Standardized Precipitation Index User Guide (M. Svoboda, M. Hayes and D. Wood). (WMO-No. 1090), Geneva [WWW Document].
Wong, J.S., Zhang, X., Gharari, S., Shrestha, R.R., Wheater, H.S., Famiglietti, J.S., 2021. Assessing water balance closure using multiple data assimilation– and remote sensing–based datasets for canada. J. Hydrometeorol. 22. https://doi.org/10.1175/JHM-D-20-0131.1
Worldbank, 2012. India Groundwater: a Valuable but Diminishing Resource [WWW Document]. URL http://www.worldbank.org/en/news/feature/2012/03/06/india-groundwater-critical-diminishing
Wu, K., Li, L., Zhang, N., 2020. Application of ESMD method to the runoff process in the Arid and semi-Arid area, in: IOP Conference Series: Earth and Environmental Science. https://doi.org/10.1088/1755-1315/558/4/042047
Xie, J., Xu, Y.P., Gao, C., Xuan, W., Bai, Z., 2019. Total Basin Discharge From GRACE and Water Balance Method for the Yarlung Tsangpo River Basin, Southwestern China. J. Geophys. Res. Atmos. https://doi.org/10.1029/2018JD030025
Xie, Y., Huang, S., Liu, S., Leng, G., Peng, J., Huang, Q., Li, P., 2018. GRACE-based terrestrialwater storage in Northwest China: Changes and causes. Remote Sens. https://doi.org/10.3390/rs10071163
Xu, L., Chen, N., Zhang, X., Chen, Z., 2019. Spatiotemporal Changes in China's Terrestrial Water

Storage From GRACE Satellites and Its Possible Drivers. J. Geophys. Res. Atmos. 124. https://doi.org/10.1029/2019JD031147

Yi, H., Wen, L., 2016. Satellite gravity measurement monitoring terrestrial water storage change and drought in the continental United States. Sci. Rep. https://doi.org/10.1038/srep19909

Yin, Z., Xu, Y., Zhu, X., Zhao, J., Yang, Y., Li, J., 2021. Variations of groundwater storage in different basins of China over recent decades. J. Hydrol. 598. https://doi.org/10.1016/j.jhydrol.2021.126282

Yirdaw, S.Z., Snelgrove, K.R., Agboma, C.O., 2008. GRACE satellite observations of terrestrial moisture changes for drought characterization in the Canadian Prairie. J. Hydrol. https://doi.org/10.1016/j.jhydrol.2008.04.004

Zargar, A., Sadiq, R., Naser, B., Khan, F.I., 2011. A review of drought indices. Environ. Rev. https://doi.org/10.1139/a11-013

Zaveri, E., Grogan, D.S., Fisher-Vanden, K., Frolking, S., Lammers, R.B., Wrenn, D.H., Prusevich, A., Nicholas, R.E., 2016. Invisible water, visible impact: Groundwater use and Indian agriculture under climate change. Environ. Res. Lett. https://doi.org/10.1088/1748-9326/11/8/084005

Zhang, Y., Pan, M., Sheffield, J., Siemann, A.L., Fisher, C.K., Liang, M., Beck, H.E., Wanders, N., MacCracken, R.F., Houser, P.R., Zhou, T., Lettenmaier, D.P., Pinker, R.T., Bytheway, J., Kummerow, C.D., Wood, E.F., 2018. A Climate Data Record (CDR) for the global terrestrial water budget: 1984-2010. Hydrol. Earth Syst. Sci. https://doi.org/10.5194/hess-22-241-2018